UNIVERSITE BRETAGNE LOIRE

UNIVERSITÉ DE NANTES

# Thèse de Doctorat

Omar Mohammed ABDULKAREEM

*Mémoire présenté en vue de l'obtention du*
***grade de Docteur de l'Université de Nantes***
*sous le sceau de l'Université Bretagne Loire*

**École doctorale: Sciences pour l'ingénieur-SPI**

**Discipline: Sciences pour l'ingénieur**
**Spécialité: Génie Civil**
**Unité de recherche: Génie Civil et Mécanique UMR CNRS 6183**

**Soutenue le 08/12/2017**

# Microstructure and Durability Properties of Environmentally Friendly Ultra-High Performance Concrete (UHPC)

## JURY

| | | |
|---|---|---|
| Président du jury | **Jean Michel TORRENTI** | Ingénieur HDR, IFSTTAR |
| Rapporteurs : | **Emmanuel DENARIE** | Maître d'enseignement et de recherche, EPF Lausanne |
| | **André LECOMTE** | Professeur des Université, Université de Lorraine |
| Co-encadrants : | **Amor BEN FRAJ** | Chargé de recherche, Cerema |
| | **Marwen BOUASKER** | Maître de Conférence, Université d'Orléans |
| Invité(s) : | **Rachida IDIR** | Chargée de recherche, Cerema |
| | **Laurent FROUIN** | Chercheur industriel, ECOCEM |
| Directeur de Thèse : | **Abdelhafid KHELIDJ** | Professeur des Universités, Université de Nantes |

L’Université Bretagne Loire

# Abstract

This thesis deals with microstructural and durability performances of -environmentally friendly Ultra-High Performance Concrete (UHPC) by integrating high volumes of Blast Furnace Slag (BFS) with and without activation. Three substitution rates of cement by slag are explored (30%, 50% and 80%). Results show that for a slag content of 30% the hydration reaction is accelerated by heterogeneous nucleation, which increases the amount of produced hydrates and thus improves the compressive strength. However, for high BFS content (50 and 80%), the dilution effect prevails on heterogeneous nucleation, which results in less formed portlandite and hydrates. As a result, the compressive strength decreases, in particular at early age. At 90 days, the volume of capillary pores decreases greatly and the global pores network becomes finer when cement is substituted by BFS. This results in decreasing gas permeability (30-61%) and chloride diffusion (up to 4 times). Results show also that all tested UHPCs have quite the same $CO_2$ depths after an exposure duration of 1 year. Indeed, the decrease of porosity due to slag incorporation, is balanced by the decrease of pH which promotes $CO_2$ diffusion.

The chemical activation accelerates the hydration, improves the packing density and the mechanical properties of UHPC with high BFS content at early age. However, these properties do not reach that of reference UHPC (0% BFS). The thermal activation promotes the reactivity of the mineral admixtures and refines the microstructure of blended UHPCs. This results in improving their mechanical and durability properties.

From an environmental viewpoint and considering FU 1, the partial substitution of cement with BFS reduces the environmental impacts of UHPC. Indeed, despite the application of thermal activation on $UHPC_3$ (50% BFS) with a purpose of satisfying the same compressive strength of reference UHPC, the Global Warming Potential (GWP) is lower for the former compared to that in the latter.

# Résumé

Cette thèse traite de l'effet de l'incorporation des laitiers des hauts fourneaux (LHF) sur la microstructure et la durabilité des bétons à Ultra Haute Performance (BUHP) avec et sans activation. Trois taux de substitution du ciment par des LHF sont explorés (30%, 50% et 80%). Les résultats montrent qu'une teneur de 30% de laitier accélère la réaction d'hydratation par la nucléation hétérogène, ce qui augmente le taux d'hydrates formées et améliore ainsi la résistance à la compression. Cependant, pour des taux élevés de LHF (50 et 80%), l'effet de dilution prévaut sur celui de nucléation hétérogène, engendrant une diminution du taux de portlandite et d'hydrates formées. Cela diminue la résistance à la compression, particulièrement au jeune âge. A 90 jours, la réaction des LHF induit une diminution de la porosité capillaire et le réseau poreux devient plus fin. Ainsi, la perméabilité au gaz et la diffusion des ions chlore diminuent significativement. Les résultats montrent aussi que tous les bétons testés ont une profondeur de carbonatation similaire, après une année d'exposition au $CO_2$. En effet, la diminution de la porosité due à l'ajout des LHF est équilibrée par la diminution du pH qui favorise la diffusion de $CO_2$. Pour ce qui concerne l'activation, les résultats montrent que l'activation chimique des BUHP à fort dosage en LHF accélère l'hydratation et améliore les propriétés microstructurales et mécaniques du béton au jeune âge. Toutefois, les propriétés restent moindres que celles du béton de référence (0% LHF). Le traitement thermique active les additions minérales et permet une densification de la microstructure. Cela induit une amélioration des propriétés mécaniques et de durabilité.

D'un point de vue environnemental et en considérant l'UF 1, la substitution partielle du ciment par des LHF réduit les impacts environnementaux du BUHP. En effet, malgré l'application d'une activation thermique au BUHP3 (50% LHF) afin d'atteindre la même résistance à la compression que le BUHP de référence, l'indicateur dégagement de CO2 du premier reste plus faible que celui du dernier.

# Table of Contents

# Chapter 3. UHPC properties: BFS content and activation methods



# Part 2. Experimental program

# Chapter 4. Testing methods

# Chapter 5. Mixture design and early age investigations



# Chapter 6. Microstructural properties of UHPCs



# Chapter 7. Mechanical properties of UHPCs

# Chapter 8. Durability properties of UHPCs



# Chapter 9. Life cycle assessment of UHPCs

# Abbreviations and symbols

**AAS:** Alkali activated slag;

**AFm, AFt:** Sulfoaluminate phases;

**$Al_2O_3$:** Alumina;

**ASC:** Activated slag cement;

**BFS:** Blast furnace slag;

**CaO:** Lime;

**$C_3A$:** Tri-calcium aluminate;

**CH ($Ca(OH)_2$):** Portlandite (Calcium hydroxide);

**C/S:** Lime to silica ratio=BI=Basicity index;

**C-S-A-H:** Calcium aluminosilicate hydrate;

**C-S-H:** Calcium silicate hydrates;

**$C_6H_6H$:** Xonotlite;

**$C_2S$:** Di-calcium silicate;

**$C_3S$:** Tri-calcium silicate;

**CSI:** Council for sustainable development-cement sustainability initiative;

**$D_{app}$:** Apparent **c**oefficient chloride diffusion;

**FU 1:** First functional unit;

**FU 2:** Second functional unit;

**FU 3:** Third functional unit;

**GGBFS:** Ground granulated blast furnace slag;

**GWP:** Global warming potential;

**HPC:** High performance concrete;

**ITZ:** Interfacial transition zone;

**$K_2O$:** Potassium oxide;

**KOH:** Potassium hydroxide;

**$[KOH]_1$:** First concentration of potassium hydroxide;

**$[KOH]_2$:** Second concentration of potassium hydroxide;

**$[KOH]_3$:** Third concentration of potassium hydroxide;

**MgO:** Magnesia;

**MS:** Silica modulus=$SiO_2/Na_2O$;

**$Na_2O$:** Sodium oxide;

**$[Na_2O]_{eq}$:** Equivalent sodium oxide;

**NaOH:** Sodium hydroxide;

**NSC:** Normal strength concrete;

**OPC:** Ordinary Portland cement;

**RPC:** Reactive powder concrete;

**SCMs:** Supplementary cementing materials;

**SF:** Silica fume;

**$SiO_2$:** Silica;

**SP:** Superplasticizer;

**UHPC:** Ultra-high performance concrete;

**$UHPC_1$:** Ultra-high performance concrete with 0% BFS (Reference mixture);

**$UHPC_2$:** Ultra-high performance concrete with 30% BFS;

**$UHPC_3$:** Ultra-high performance concrete with 50% BFS;

**$UHPC_4$:** Ultra-high performance concrete with 80% BFS;

**$UHPC_4$-$[KOH]_3$:** Ultra-high performance concrete with 80% BFS and chemically activated;

**UHPFRC:** Ultra-high performance fibred reinforced concrete;

**w/b:** Water to binder ratio;

**w/c:** Water to cement ratio;

**w/f:** Water to fines ratio;

**$X_d$:** Depth of chloride diffusion.

# Acknowledgment

This doctoral thesis is the outcome of my work carried out at the Center for Studies and Expertise on Risks, Environment, Mobility and Development (Cerema) which is a public administrative institution under the joint supervision of the French Ministry for Ecology, Sustainable Development and Energy, and the French Ministry of Transport, Equality of Territories and Rurality.

Giving the opportunity to endeavor this doctoral study and financial support from The **Iraqi Ministry of Higher Education and Scientific Research** and **University of Mosul**, are gratefully acknowledged.

This thesis was undertaken under the principle supervisor **Prof. Abdelhafid KHELIDJ** at University of Nantes. I wish to extend my deepest thanks to him for his positive attitude that made much easier the development of this research.

With respect to the personal appreciations, my second and widest gratitude is for my co-supervisor **Amor BEN FRAJ** at Cerema for his detailed and constructive comments, and for his important guidance throughout my candidature. Thank you for all the countless times, patiently giving guidance and insight throughout the thesis.

I am also grateful to my second co-supervisor **Marwen BOUASKER** at University of Orléans, his input throughout this research either through chance meetings, invaluable comments and innovative ideas were so helpful.

I like to thank the members of jury who are Prof. **Emmanuel DENARIÉ** from EPFL, Prof. **André LECOMTE** from University of Loraine, Mr. **Laurent FROUIN** from Ecocem Materials, and Prof. **Jean-Michel TORRENTI** from IFSTTAR. Thank you for your interesting questions and invaluable comments.

I have to acknowledge the support provided by Mrs. **Rachida IDIR** at Cerema for her wide knowledge and interesting discussions and her help for Life Cycle Assessment (LCA) part in my thesis.

Cerema employers and technicians also deserve my thanks, especially Mr. **Alexandre PAVOINE**, **Jérome CARRIAT**, **Samantha DUCLEROIR, Véronique QUEYBART** and all fellows for their help provided at laboratory with a positive attitude. Besides, I cannot forget Mrs. **Marta CHOINSKA** at GeM and Mr. **Lahcen KHOUCHAF** at Ecole de Mines de Douai for their helps, respectively in permeability and microstructure tests. Mrs **Maryse RADIN** at department of civil engineering in IUT of Saint-Nazaire has been acknowledged deeply for her assistance in the administrative affairs.

To my parents, and sisters, thank you. Your loving support and care along my study has been a key factor in my every achievement. I am further grateful for my father Prof. **Mohammed ABDULKAREEM** at university of Mosul for his high encouragement and worthy remarks throughout my PhD.

Finally, I owe my loving thanks to my wife **Marwah**, and my little daughters **Dima** and **Mina** who has been there for me throughout my PhD. I have to say that the largest support and understanding came from them during the hard period of the PhD.

# Introduction

## Généralités

En tant que matériau de construction, le béton est le matériau composite le plus utilisé dans le monde, deux fois plus comparé aux autres matériaux de construction, selon le World Business Council for Sustainable Development-Cement Sustainability initiative (CSI), à cause du coût et de la disponibilité de ses constituants, sa multi-fonctionalité, sa durabilité et son adaptabilité. C'est aussi, derrière l'eau, le matériau de loin le plus utilisé dans le monde, avec plus de 5 milliards de mètres cubes de béton produits annuellement [Aysha et al., 2014 ; Aïtcin and Mindess, 2011].

Pendant longtemps, l'industrie du béton et les fabricants ont produit et spécifié un béton universel, dont la résistance à la compression est généralement comprise entre 15 et 25 MPa, c'est-à-dire suffisamment performant pour être employé en toutes circonstances. Au cours des années 1970, des spécifications ont été imposées sur les bétons aux résistances élevées (40 à 50 MPa) pour leur utilisation dans la construction des éléments de grande hauteur, offrant davantage de possibilités architecturales et plus d'espace de location. Au fil des années, le béton à haute résistance a été appelé béton à haute performance (BHP) car on a réalisé que ces bétons ont plus qu'une simple résistance. L'acceptation des BHP est lente, mais elle progresse constamment et cette progression continuera car les concepteurs et les propriétaires réaliseront la valeur et la durabilité de ce béton [Aïtcin, 2008].

Bien sûr, les BHP ne sont pas une panacée qui arrêtera le développement de tous les autres types de béton. L'intérêt pour la production de béton à très haute résistance a augmenté au cours des dernières années, en particulier dans les industries du béton préfabriqué et précontraint, les constructeurs de structures en béton de grande hauteur pourraient également bénéficier d'un béton plus résistant en réduisant considérablement le volume. Toutefois le béton à très haute résistance ne peut être utilisé pour la plupart des constructions coulées sur place et une attention particulière s'impose [Aïtcin, 2008 ; Maroliya, 2012].

Par ailleurs, la réalisation de béton très performant est un réel challenge en raison du manque de granulats de bonne qualité dans de nombreuses parties du monde [Ahmad et al., 2015]. Le développement du béton ultra-hautes performances (BUHP), qui est l'une des avancées les plus significatives dans le développement du béton dans les années 1990, représente l'une des avancées majeures des technologies du béton au cours des dernières décennies du siècle dernier. Les origines de ce matériau remontent à la France lorsque les idées de Bache ont été reprises en 1994 par l'entrepreneur français Bouygues (Richard et Cheyrezy) et se sont développées davantage. Coopérant avec Lafarge, un nouveau

mélange a été mis au point : "Béton à Poudres Réactives", qui continue d'exister sous la forme de "Ductal". Une première application consistait à remplacer les poutres en acier par des BFUP dans les tours de refroidissement d'une centrale électrique de Cattenom en France. Les poutres en acier ont dû être remplacées parce qu'elles se corrodaient dans l'environnement extrêmement agressif à l'intérieur des tours de refroidissement. Un point important à noter ici est que ce n'est pas la haute résistance des BFUP qui fût décisive dans ce cas, mais plutôt la durabilité du matériau en relation avec la très longue durée de vie prévue sans entretien ni réparation. Il a été réalisé que le matériau peut être spécifié pour ses autres propriétés et pas seulement pour sa grande résistance qui a conduit à remplacer le terme « béton à très haute résistance » par « béton à ultra haute performance » [Fehling et al. 2014]. Le BUHP est un matériau très compact et dense qui présente une fluidité attrayante, d'excellentes propriétés mécaniques et une durabilité exceptionnelle [Zhao and Sun, 2014]. Le BUHP pourrait montrer une résistance à la compression de 150 à 810 MPa, environ 3 à 16 fois celle du béton conventionnel.

En raison de la très haute résistance à la compression, les structures BUHP ne pèsent que le tiers ou la moitié des structures en béton conventionnel, sous la même charge. Cette réduction de poids a un avantage dans la production de structures plus fines, l'augmentation de la surface utile dans les immeubles de grande hauteur et la réduction des coûts globaux. L'élimination des armatures en acier réduit les coûts de main-d'œuvre et offre une plus grande liberté architecturale, permettant des formes et des formes d'éléments de structure presque illimitées pour les architectes et les concepteurs. Les tendances récentes de la construction de ponts à travées multiples et de gratte-ciels à grande hauteur imposent l'utilisation de la technologie BUHP en raison de sa sécurité, de sa facilité d'entretien, de sa durabilité et de ses avantages économiques. La construction de nouvelles et anciennes structures en béton utilisant la technologie BUHP peut améliorer leur durée de vie au-delà de 100 ans, avec des exigences minimales de maintenance et de faibles coûts de cycle de vie [Wang et al., 2015 ; Yi et al., 2012].

Néanmoins, étant donné que le développement durable est un enjeu stratégique majeur et que diverses industries se sont efforcées de réaliser des économies d'énergie, le coût élevé des matériaux, la forte consommation d'énergie et les émissions de $CO_2$ de BUHP sont des faiblesses. Une teneur élevée en liant d'environ 800-1000 kg / $m^3$ affecte non seulement les coûts de production, mais également une forte chaleur d'hydratation, entraînant des problèmes de retrait. Des caractéristiques de retrait accrues et des microfissures à haute sensibilité peuvent réduire la performance à long terme. Du point de vue de la durabilité, le BUHP contient trois fois plus de ciment par $m^3$ que le béton ordinaire, utilisant ainsi trois fois plus d'énergie et produisant trois fois plus de $CO_2$. Comme on le sait, le secteur des matériaux de construction est le troisième secteur industriel émetteur de $CO_2$ au monde,

ainsi que dans l'Union européenne. Selon le World Business CSI, la production de ciment a augmenté de 74% entre 1990 et 2011 et représente 7% des émissions anthropiques totales de $CO_2$ [Aysha et al., 2014 ; Wang et al., 2015 ; Yu et al., 2015 ; Yiğiter et al., 2012 ; Courtial et al., 2013 ; Yu et al., 2014].

De plus, il n'est pas satisfaisant de dire que la consommations énergétique d'1 $m^3$ de béton est négligeable, car à 6,4 milliards de fois une faible quantité d'énergie n'est plus négligeable. Dans l'Union européenne, environ 40% de la consommation totale d'énergie est attribuée au secteur du bâtiment et de la construction. Les émissions de $CO_2$ sont principalement liées à la décarbonatation du calcaire, à la consommation de combustible et à la consommation d'électricité, résultant des processus de calcination et de broyage dans la production de ciment [Aïtcin, 2008 ; Randl et al., 2014 ; Proske et al., 2014].

L'un des principaux défis en matière de durabilité pour les prochaines décennies est la conception et la production de béton avec moins de ciment-clinker et des émissions de $CO_2$ plus faibles que les traditionnelles. De cette façon, la réduction des émissions de $CO_2$ est réalisée avec quelques avantages de base de réduire la consommation de matières premières naturelles, l'énergie thermique et électrique. Cette technologie met l'accent sur la réduction de la consommation de ressources non renouvelable couplé à l'utilisation de matériaux de recyclage ; fonctionnalité améliorée d'une structure grâce à l'amélioration de la durée de vie et de la durabilité. Les ressources naturelles sont en train de s'épuiser dans le monde entier en même temps que de nouveaux produits sont générés par diverses industries qui pourraient avoir un avenir prometteur dans l'industrie de la construction en substitution partielle ou totale du ciment ou des granulats. Par conséquent, la manière de produire efficacement des BFUP, basée sur le point de vue des matériaux, nécessite encore des investigations supplémentaires [Yu et al., 2015 ; Yu et al., 2014 ; Khokhar et al., 2010 ; Voo, 2010 ; Ambily et al., 2015].

La solution la plus judicieuse consiste à remplacer de grandes quantités de ciment par des produits industriels tels que les cendres volantes, les fumées de silice, les latiers de hauts fourneaux (LHF), les cendres volantes rejetées, la poudre de verre recyclée et les cendres de riz en tant que matériaux de substitution. L'incorporation de ces matériaux dans les BUHP répond non seulement aux exigences économiques, mais apporte également d'autres avantages tels que l'abaissement du retrait et l'amélioration de la durabilité du matériau. Plus important encore, la substitution contribue au recyclage des déchets industriels et à la réduction de la consommation de ciment, ce qui réduit les émissions de $CO_2$ et rend le matériau respectueux de l'environnement. La pratique de l'utilisation des coproduits industriels est en augmentation, le pourcentage moyen mondial de clinker dans le ciment ayant diminué de 85% en 2003 à 77% en 2010, et il devrait encore diminuer à 71% à l'avenir. Aux États-Unis, les coproduits industriels sont généralement ajoutés au béton plutôt

qu'au mélange de clinker, et actuellement plus de 60% des bétons prêts à l'emploi utilisent des coproduits industriels [Zhao and Sun, 2014 ; Ambily et al., 2015 ; Juenger and Siddique, 2015].

Le laitier de hauts fourneaux (LHF) est utilisé depuis de nombreuses années comme matériau cimentaire de substitution dans la technologie du béton. L'utilisation du LHF dans cette zone présente des avantages environnementaux et économiques importants puisque sa production nécessite moins d'énergie que la production de ciment Portland. Et il n'y a pas d'émission de $CO_2$ dans l'atmosphère pendant ce processus. Si une tonne de laitier remplace une tonne de clinker, environ 800 kg d'émissions de $CO_2$ peuvent être "économisés". D'un autre côté, en raison du système cimentaire complexe de BUHP (quantité d'eau extrêmement faible et teneur en superplastifiant relativement élevée), l'influence de différents adjuvants minéraux sur la cinétique d'hydratation et les propriétés au jeune âge des BUHP doit encore être clarifiée. Comme communément connu, le LHF est un matériau cimentaire hydraulique latent. Lorsqu'il est utilisé conjointement avec le ciment Portland, la dissolution du LHF est favorisée car l'hydratation au jeune âge du ciment, ce qui augmente l'alcalinité de la solution de pores. Bien que le taux de réaction avec l'eau soit faible, les ciments LHF présentent l'inconvénient d'une résistance initiale plus faible et d'un temps de prise plus long, qui pourraient néanmoins être modifiés par certaines approches. Prévoir le comportement au jeune âge des matériaux cimentaires devient une tâche difficile dans la science et la pratique concrètes. Cela résulte du fait que de nombreuses propriétés des structures en béton sont sensibles aux conditions de cure du matériau. Par conséquent, la connaissance de ces caractéristiques a beaucoup de potentiel pour améliorer la qualité de la construction et donc la durabilité [Yu et al., 2015 ; Aydın and Baradan, 2014 ; Ben Haha et al., 2011 ; Gebregziabiher et al., 2015 ; Wu et al., 1990 ; Mounanga et al., 2006].

En raison de la faiblesse des propriétés au jeune âge, le LHF peut être activé par plusieurs méthodes telles que l'activation mécanique, chimique et thermique. Les systèmes LHF activées présentent souvent un développement rapide de la résistance et, en utilisant les activateurs adéquats, ils peuvent conduire à un durcissement rapide, une bonne durabilité et une grande résistance aux attaques chimiques. L'effet de l'activation dépend fortement de la nature physico-chimique du LHF, de la nature et de la quantité des activateurs et de l'état de polymérisation. Comprendre l'hydratation et le développement de la microstructure est la clé pour comprendre la performance des matériaux à base de LHF. Les questions concernant l'influence de différentes méthodes d'activation, par exemple chimique, thermique, et leur combinaison sur le processus d'hydratation et la résistance mécanique sont d'un grand intérêt car elles ont un impact majeur sur l'applicabilité de tout matériau de construction [Ben Haha et al. 2011].

## Objectifs

Le LHF est considéré comme une solution prometteuse pour surmonter les principaux problèmes de BUHP en réduisant la consommation de ciment afin de réduire les coûts des matériaux et de diminuer les impacts négatifs (chaleur d'hydratation, retrait et empreinte environnementale). Ce travail de recherche vise à concevoir des BUHP plus durables, intégrant le laitier de haut fourneau (LHF) et à évaluer leurs propriétés au jeune âge et à long terme, en relation avec le développement de la microstructure. Pour remédier à la faible réactivité des LHF au jeune âge, des activations chimiques et thermiques seront appliquées et leurs effets sur les propriétés microstructurales, mécaniques et de durabilité seront discutés. La dernière partie de ce travail de recherche est consacrée à l'évaluation de l'empreinte environnementale des BUHP développés, pour différentes unités fonctionnelles.

Il est important de rappeler que l'objectif final de cette thèse n'est pas de donner des recommandations aux concepteurs, mais de participer à la compréhension du comportement des BUHP à plus faible empreinte environnementale (en présence de LHF), notamment dans un environnement agressif.

# General Introduction

## Overview

As a building material, concrete is the most used man-made material in the world, utilized at double the rate of all other building materials, according to the World Business Council for Sustainable Development-Cement Sustainability Initiative (CSI) because of the economic and widespread availability of its constituents, its versatility, its durability and its adaptability. It is also, next to water, by far the most widely used material in the world, with over 5 billion cubic metres of concrete produced annually [Aïtcin and Mindess, 2011; Aysha et al., 2014].

For a long time, the concrete industry and designers have produced and specified a universal concrete, good enough to be used under any circumstances, whose compressive strength was usually between 15 and 25 MPa. During the 1970s, concrete having a higher strength (40 to 50 MPa) began to be specified for columns in high-rise buildings, because slender columns offered more architectural possibilities and more renting space. Over the years, the name of these initial high-strength concretes has been changed to High-Performance Concrete (HPC) because it was realized that these concretes have more than simply a high strength. These concretes started to be used outdoors and faced more severe environments such as off-shore platforms, bridges, roads, etc. The acceptance of HPC is slow but it is progressing constantly and this progression will continue because designers and owners will realize the value and durability of this concrete [Aïtcin, 2008].

Of course, HPCs are not a panacea that will stop the development of all other kinds of concrete. Interest in the production of very high-strength concrete has been increasing over the past several years, particularly in the precast and pre-stressed concrete industries, builders of high rise concrete structures also could benefit from higher strength concrete by large reduction in dead load. Although the very high strength concrete is used for most cast in place, the construction could not be applicable. Reasoning behind, it requires special care of each aspect of strength development and preventative measures [Aïtcin, 2008; Maroliya, 2012]. Nevertheless, it has been a challenging task to produce a very high-performance concrete due to the lack of good quality coarse aggregates in many parts of the world [Ahmad et al., 2015]. As a result of the remarkable advances in the concrete technology in recent decades, one of the major breakthroughs of the 1990s was the development of the Ultra-High Performance Concrete (UHPC) which is the most significant leap forward in the development of concrete in the past quarter-century [Fehling et al., 2014].

Ultra-High Performance Fibre Reinforced Concretes (UHPFRC) were originally developed with focus on the optimization of their matrix (which can be called Ultra High-Performance Concrete (UHPC), although it is closer to a micro mortar), with a special attention to the increase of the compressive strength, above 200 MPa, by optimization of the packing of

grains with ultrafines and dramatic decrease of the water/binder ratio (w/b). This very dense but brittle matrix, with a dramatic decrease of the intrinsic permeability to liquids and gases, was subsequently reinforced by a fibrous mix and lead to a technological breakthrough applied at the industrial scale from the end of the 80's in Denmark and end of the 90's first in Canada, France, Australia and Japan. UHPFRC are characterized by a high compressive resp. tensile strength: above 150 resp. 10 MPa, and deflection or tensile strain-hardening depending on their fibrous mix. In France, Bache's ideas were taken up in 1994 by the French contractors Bouygues (Richard and Cheyrezy) and developed further. Cooperating with Lafarge, a new mixture was devised: "Reactive Powder Concrete", which continues to exist in the form of "Ductal". One early application involved replacing steel beams by UHPC ones in the cooling towers of a power station at Cattenom in France. The steel beams had to be replaced because they were corroding in the extremely aggressive environment inside the cooling towers. One important point to note here is that it was not the high strength of the UHPC that was decisive in this case, but rather the durability of the material in connection with the anticipated very long service life without maintenance or repairs. It was the realization that the material can be specified for its other understanding properties and not just for its high strength that led to the term "ultra-high strength concrete" being replaced by "ultra-high performance concrete" [Fehling et al., 2014].

Due to ultra-high compressive strength, UHPC structures weigh only one-third or one-half of the corresponding conventional concrete structures under the same load. This weight reduction has benefit in producing extra slender structures, increasing usable floor space in high-rise buildings and reducing overall costs. Elimination of steel reinforcement bars reduces labour costs and provides greater architectural freedom, allowing nearly limitless structural member shapes and forms for architects and designers. The recent construction trends of building super-span bridges and mega-height high-rises mandate the use of UHPC because of its outstanding safety, serviceability, durability, and economical advantages. The construction using UHPC can improve their service life beyond 100 years with minimal maintenance requirements and low life cycle costs [Yi et al., 2012; Wang et al., 2015].

Nevertheless, as the sustainable development is currently a pressing global issue and various industries have strived to achieve energy savings, the high material cost, high energy consumption and $CO_2$ emission for UHPC are the certain weaknesses that restrict its wider application. High binder content of about 800–1000 kg/m$^3$ affects not only the production costs, but also high heat of hydration, causing shrinkage problems. Increased shrinkage characteristics and high sensitive microcracking may reduce the early-age and hardened performance. From the sustainability point of view, UHPC contains three times more cement per m$^3$ than ordinary concrete, thus using three times more energy and producing three times more $CO_2$. As commonly known, the sector of building materials is the third largest $CO_2$

emitting industrial sector world-wide, as well as in the European Union. Cement production increased by 74% between 1990 and 2011, according to the World Business CSI, and it is said to represent 7% of the total anthropogenic $CO_2$ emissions [Yiğiter et al., 2012; Courtial et al., 2013; Aysha et al., 2014; Yu et al., 2014; Wang et al., 2015; Yu et al., 2015].

Also it is not satisfactory to say that the energy content of 1 $m^3$ of concrete is negligible, because at 6.4 billion times a small energy content, it is no longer negligible. In the European Union about 40% of total energy consumption is attributed to the building and construction sector. The $CO_2$-emissions are mainly related to the decarbonation of the limestone, the fuel consumption and the electricity consumption, as a result of the calcination and grinding processes in the cement production [Aïtcin, 2008; Proske et al., 2014; Randl et al., 2014].

One of the key sustainability challenges for the next decades is to design and produce concrete with less cement-clinker content and inducing lower $CO_2$ emissions than traditional one. In this way, reduction of $CO_2$ emissions is being achieved with some basic benefits of decreasing the consumption of natural raw materials, thermal and electric energy. This technology focuses on the reduction of none-renewable resources consumption couple with the use of recycle material; enhanced functionality of a structure through enhancement of service life and durability. Natural resources are depleting worldwide at the same time new by products are being generated by various industries which could have a promising future in construction industry as partial or full substitute of either cement or aggregates. Hence, how to efficiently produce UHPC, based on materials point of view, still needs further investigation [Khokhar et al., 2010; Voo, 2010; Yu et al., 2014; Ambily et al., 2015; Yu et al., 2015].

The most sensible solution is to replace large portions of cement with industrial by-products having long term availability such as fly ash, silica fume, blast-furnace slag, reject fly ash, recycled glass powder, limestone filler, and rice husk ash as supplementary cementitious materials (SCMs) in order to produce new “ECO” UHPC. The incorporation of these materials into UHPC not only achieves the economic requirement, but also brings other advantages such as lowering the shrinkage and improving the durability of the material. More importantly, the substitution contributes to the recycling of industrial waste and the reduction of cement consumption, which reduces $CO_2$ emission and makes the material environmentally friendly. The practice of using SCMs is increasing, with the world average percent clinker in cement having decreased from 85% in 2003 to 77% in 2010, and it is projected to further decrease to 71% in the future. In the U.S., SCMs are usually added to concrete rather than blended with clinker, and currently more than 60% of ready-mixed concrete uses SCMs [Zhao and Sun, 2014; Ambily et al., 2015; Juenger and Siddique, 2015].

Ground granulated blast furnace slag (GGBFS) has been used for many years as a supplementary cementitious material in concrete technology. Utilisation of GGBFS in this

area has significant environmental and economic benefits since its production requires less energy than the production of Portland cement. And there is no $CO_2$ emission to the atmosphere during this process. If one ton of slag replaces one ton of clinker, about 800 kg of $CO_2$ emissions can be “saved”. From another side, due to the complex cementitious system of UHPC (extremely low water amount and relatively high superplasticizer content), the influence of different mineral admixtures on the hydration kinetics and early-age properties of UHPC still needs further clarification. As commonly known, GGBFS is a latent hydraulic cementitious material. When used in conjunction with Portland cement, the dissolution of GGBFS is promoted as early cement hydration raises the alkalinity of the pore solution. Although the rate of the reaction with water is low, GGBFS cements have the disadvantage of lower early strength and longer setting time, which nevertheless could be modified by certain approaches. Predicting the early-age behaviour of cementitious materials has becoming a challenging task in concrete science and practice. This results from the fact that many properties of concrete structures are sensitive to the early-age characteristics of the material. Therefore, knowledge of these characteristics has much potential to improve construction quality and hence durability [Wu et al., 1990; Mounanga et al., 2006; Ben Haha et al., 2011; Aydın and Baradan, 2014; Gebregziabiher et al., 2015; Yu et al., 2015].

Because of low early-age strength has been observed using GGBFS, it can be activated by several methods such as mechanical, chemical, and thermal activations. Activated slag systems often exhibit a rapid strength development, and using the adequate activators can lead to rapid setting, good durability and high resistance to chemical attack. The effect of activation strongly depends on the physico–chemical nature of the GGBFS, the nature and quantity of the activators and the curing condition. Understanding the hydration and development of the microstructure is the key to understand the performance of slags. Questions regarding the influence of different methods of activation for example chemical, thermal, and combination of them on the hydration process and mechanical strength are of great interest as they have a major impact on the applicability of any construction material [Ben Haha et al., 2011].

## Research objective

Ground granulated blast furnace slag (GGBFS) is considered as a feasible solution to overcome the main problems in UHPC by reducing consumption of cement in order to lower the material costs, decrease the negative impacts (heat of hydration, shrinkage, and environmental footprint), and to enhance the durability. This research work aims at developing environmentally friendly UHPC mixtures with massive use of GGBFS to replace clinker, and linking the physico-chemical processes associated to hydration of clinker and

reaction of BFS and SCMs to the evolution of the microstructure, mechanical performances, and durability properties. To remedy the low reactivity of BFS at early age, chemical and/or thermal activations will be applied and their effects on microstructural, mechanical and durability properties will be discussed. The last part of this research work is dedicated to assess the environmental footprint of developed UHPCs and perform with these proposed mixtures a life-cycle analysis for three different functional units including a full scale structure. It is important to remind that the final objective of this thesis is not to give recommendations for designers but to participate in the comprehension of environmentally friendly UHPC's behaviour (in presence of BFS) particularly in aggressive environments.

## References


[Ahmad et al., 2015] S. Ahmad, A. Zubair, M. Maslehuddin, Effect of key mixture parameters on flow and mechanical properties of reactive powder concrete. Constr. Build. Mater. 99 (2015) 73-81.

[Aïtcin, 2008] P.C. Aïtcin, Binders for Durable and sustainable Concrete-Series of Modern Concrete Technology 16, 1st Edition, Taylor and Francis Group, 2008.

[Aïtcin and Mindess, 2011] P.C. Aïtcin, S. Mindess, Sustainable of Concrete-Series of Modern Concrete Technology 17, 1st Edition, CRC Press, 2011.

[Ambily et al., 2015] P.S. Ambily, C. Umarani, K. Ravisankar, P.R. Prem, B.H. Bharatkumar, N.R. Iyer. Studies on ultra high performance concrete incorporating copper slag as fine aggregate. Constr. Build. Mater. 77 (2015) 233-240.

[Aydın and Baradan, 2014] S. Aydın, B. Baradan, Effect of activator type and content on properties of alkali-activated slag mortars. Compo. Par. 57 (2014) 166-172.

[Aysha et al., 2014] H. Aysha, T. Hemalatha, N. Arunachalam, A.R. Murthy, N.R. Iyer, Assessment of embodied energy in the production of ultra high performance concrete (UHPC). Int. Jour. Stud. Res. Tech. Manag. 2 (3) (2014) 113-120.

[Ben Haha et al., 2011] M. Ben Haha, B. Lothenbach, G. Le Saout, F. Winnefeld, Influence of slag chemistry on the hydration of alkali-activated blast-furnace slag-Part I: Effect of MgO. Cem. Conr. Res. 41 (2011) 955-963.

[Courtial et al., 2013] M. Courtial, M.-N.D. Noirfontaine, F. Dunstetter, M.S-. Frehel, P. Mounanga, K. Cherkaoui, A. Khelidj. Effect of polycarboxylate and crushed quartz in UHPC: Microstructural investigation. Constr. Build. Mater. 44 (2013) 699-705.

[Fehling et al., 2014] E. Fehling, M. Schmidt, J. Walraven, T. Leutbecher, S. Fröhlich, Ultra-high performance concrete UHPC: Fundamentals-Design-Examples, Wilhelm Ernst & Sohn, 10245 Berlin, Germany, 2014.

[Gebregziabiher et al., 2015] B.S. Gebregziabiher, R. Thomas, S. Peethamparan, Very early-age reaction kinetics and microstructural development in alkali-activated slag. Cem. Conr. Comp. 55 (2015) 91-102.

[Juenger and Siddique, 2015] M.C.G. Juenger, R. Siddique, Recent advances in understanding the role of supplementary cementitious materials in concrete. Cem. Concr. Comp. 78 (2015) 71-80.

[Khokhar et al., 2010] M.I.A. Khokhar, E. Roziere, P. Turcry, F. Grondin, A. Loukili, Mix design of concrete with high content of mineral additions: optimisation to improve early age strength. Cem. Concr. Comp. 32 (2010) 377-385.

[Maroliya, 2012] M.K. Maroliya, A state of art- on development of reactive powder concrete, Int. Jour. Inn. Res. Deve. 1(8) (2012) 493-503.

[Mounanga et al., 2006] P. Mounanga, V. Baroghel-Bouny, A. Loukili, A. Khelidj, Autogenous deformations of cement pastes: part I. temperature effects at early age and micro–macro correlations. Cem. Concr. Res. 36 (2006) 110-122.

[Proske et al., 2014] N. Proske, S. Hainer, M. Rezvani, C.-A. Graubner. Eco-friendly concretes with reduced water and cement content – mix design principles and application in practice. Constr. Build. Mater. 67 (2014) 413-421.

[Randl et al., 2014] N. Randl, T. Steiner, S. Ofner, E. Baumgartner, T. Mészöly. Development of UHPC mixtures from an ecological point of view. Constr. Build. Mater. 67 (2014) 373-378.

[Voo, 2010] Y.L. Voo, Ultra-high performance 'ductile' concrete technology toward sustainable construction. Int. Jour. Sus. Cons. Eng. Tech. 1(2) (2010) 105-126.

[Wang et al., 2015] D. Wang, C. Shi, Z. Wu, J. Xiao, Z. Huang, Z. Fang, A review on ultra high performance concrete: Part II. Hydration, microstructure and properties. Constr. Build. Mat. 96 (2015) 368-377.

[Yi et al., 2012] N.H. Yi, J.H.J. Kim, T.S. Han, Y.G. Cho, J.H. Lee, Blast-resistant characteristics of ultra-high strength concrete and reactive powder concrete. Constr. Build. Mat. 28 (2012) 694–707.

[Yiğiter et al., 2012] H. Yiğiter, S. Aydın, H. Yazıcı, M.Y. Yardımcı, "Mechanical performance of low cement reactive powder concrete (LCRPC). Comp. Par. 43 (2012) 2907–2914.

[Wu et al., 1990] X. Wu, W. Jiang, D.M. Roy, Early activation and properties of slag cement. Cem. Concr. Res. 20 (1990) 961-974.

[Yu et al., 2014] R. Yu, P. Spiesz, H.J.H. Brouwers, Mix design and properties assessment of Ultra-High Performance Fibre Reinforced Concrete (UHPFRC). Cem. Concr. Res. 56 (2014) 29-39.

[Yu et al., 2015] R. Yu, P. Spiesz, H.J.H. Brouwers, Development of an eco-friendly Ultra-High Performance Concrete (UHPC) with efficient cement and mineral admixtures uses. Cem. Concr. Comp. 55 (2015) 383-394.

# Résumé de la partie Bibliographique

Les bétons à ultra haute performance (BUHP) est le résultat d'une réduction séquentielle et/ou d'une élimination des inconvénients du béton conventionnel. Grâce à l'ingénierie microstructurale, le contrôle des propriétés microscopique et macroscopique des constituants d'une matrice de BUHP a produit un matériau de qualité supérieure grâce à l'optimisation de plusieurs propriétés telles que l'homogénéité mécanique, la densité maximale et le compactage dense des particules. Ainsi, pendant la production, la conception d'un BUHP commence par un choix judicieux et une proportion appropriée de matières premières en plus du contrôle de la qualité afin de produire un matériau qui pourra satisfaire les exigences structurelles. Les bétons de type BUHP forment un modèle spécifique de matériaux cimentaires riche en particules minérales fines (ciment Portland, fumée de silice, quartz broyé, sable de quartz et fibres d'acier). La granulométrie de ces fines minérales est de l'ordre de 0,02 à 600 µm avec un très faible rapport massique d'eau/liant (E/L) généralement compris entre 0,13 et 0,28 et une teneur en superplastifiant élevée permettant de réduire d'une manière significative l'eau de gâchage.

Le chapitre 1, montre que les constituants qui forment les BUHP présentent des propriétés physico-chimiques et des distributions granulométriques très variées dans le but d'atteindre un rapport eau/fines le plus faible possible ainsi qu'un faible besoin en superplastifiant. En conséquence, la porosité de la matrice cimentaire est fortement réduite par un effet de remplissage des pores capillaires et la microstructure obtenue est plus riche par les produits d'hydratation. Cette réduction importante de la porosité est à l'origine de la résistance mécanique élevée des BUHP.

La réaction des laitiers de haut fourneau dans un mélange varié de liants est un processus très complexe qui mérite une attention particulière. Contrairement au béton ordinaire, le comportement des bétons à base de laitier de haut fourneau n'est pas suffisamment maîtrisé. Dans le deuxième chapitre, l'origine et la composition minéralogique des laitiers seront présentées. Le comportement chimique des laitiers dans une matrice cimentaire sera également décrit en fonction de la composition de la matrice. Enfin, les méthodes d'activation connues seront présentées (activations chimique et thermique).

Le dernier chapitre présente les propriétés des BUHP. La microstructure sera décrite à travers les résultats de plusieurs essais utilisés dans la littérature tels que l'analyse des phases minérales par diffraction des rayons X (DRX) ainsi que l'analyse thermogravimétrique (ATG). La distribution porale sera également décrite. Les propriétés mécaniques seront ensuite présentées et confrontées aux propriétés microscopiques de la matrice afin d'expliquer la haute résistance mécanique de BUHP. Ce dernier chapitre sera clôturé par une synthèse sur

la durabilité des BUHP et leurs résistances aux agressions environnementales telles que le gel-dégel, la carbonatation ainsi que l’attaque des ions chlorure.

# Part 1. Literatures review

# Chapter 1. UHPC mixture composition

## Table of Contents



## List of figures



## List of tables

# 1. Introduction

The ultra-high performance concrete (UHPC) is the findings of sequential reduction or getting rid of cons of conventional concrete [Zdeb, 2013]. Through microstructural engineering the control of the micro and macro properties of UHPC mixture constituents produced superior material with a view to ensure mechanical homogeneity, maximum density and dense particle packing [Abbas et al., 2015]. Thereby, during production, a design of UHPC mixture starts with careful choice and appropriate proportion of raw materials beside the quality control in order to fulfil these considerations and exhibit a desired structural functioning.

UHPC form a certain pattern of cementitious compounds, including fine mineral particles (Portland cement, silica fume, crushed quartz, quartz sand and steel fibres) in the range of (0.02-600) µm, with very low water-to-cement mass ratio (w/c between 0.13 and 0.28), and high content of high range water-reducing superplasticizer. The typical composition of UHPC with the range of each component is illustrated in Fig. 1 in according to the literature survey [Richard and Cheyrezy, 1995; Menefy, 2007; Ahlborn et al., 2008; Mounanga et al., 2012; Ahmad et al., 2015]:


***Figure 1: Materials proportions of typical UHPC mixture [Mounanga et al., 2012; Menefy, 2007; Richard et Cheyrezy, 1995; Ahlborn et al., 2008; Ahmad et al., 2015]***

This mixture of constituents with quite various physico-chemical properties and particle size distributions, has main purposes including, attain a highest water/fines ratio (w/f) and also low requirements of water and superplasticizer, droves to a prominently dense structure, and high strength of UHPC. Another factors sharing in the high strength are the tight packing of the merged ultra-fine particles (grain size < 125 µm) jointly, and the fraction of them has to be high. As a result, the porosity of the cement matrix is reduced by filling the capillary and microstructure pores in the cement matrix with extra hydration phases [Mounanga et al., 2012; Fehling et al., 2014; Korpa et al., 2014]. Fig. 2 shows the mix compositions (by

volume) of fine-and coarse-grained UHPC compared to another types of concrete [Fehling et al., 2014]:

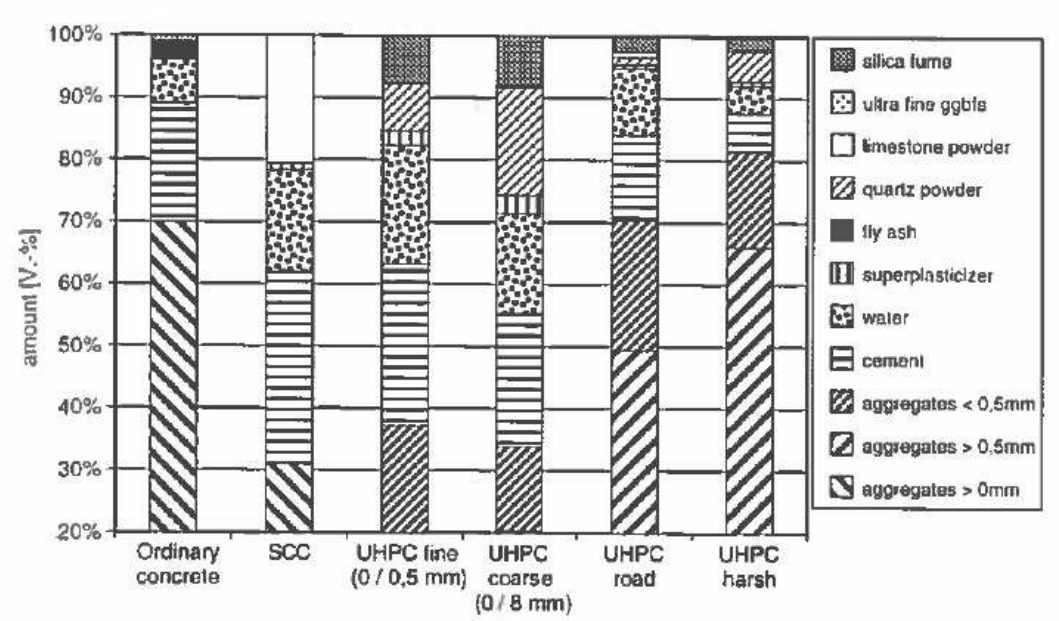


***Figure 2: Comparison of the mix compositions for normal-strength, high-strength and various UHPCs [Fehling et al., 2014]***

## 2. Major principles in UHPC

Strength and durability of UHPC are based on the search of a minimal porosity. This property can be obtained by optimizing the following parameters:

### 2.1. Homogeneity

UHPC mix design depends on decreasing the size of the maximum grain [Zdeb, 2013]. Heterogeneity-regarding problems in the traditional concrete due to the aggregates, which constitute a granular skeleton, are practically diminished in UHPC for the following reasons [Richard et Cheyrezy, 1995]:

(i) Replacement of coarse aggregates with fine sand, (600 µm max);

(ii) Enhancement of mechanical properties of the paste;

(iii) Lowering the aggregate-to-matrix ratio.

The substitution of the coarse aggregates by a reactive fine sand having similar particles in terms of moduli and size achieves two effects:

- The first effect is meso-effect related to aggregate size. The use of fine sand in UHPC instead of coarse aggregate reduces the size of the microcracks of mechanical, thermal or chemical source. As a result, the strengths make better and the Young's modulus of the cement paste grows up 55-75 GPa. Subsequently, the homogeneity and the ultimate load-carrying capacity of the combined material increase by

enhancing the stress transfer between the paste and the aggregate. Thereby, this component (i.e. fine sand) represents an efficient constituent of the matrix. Besides that, the existence of a large amount of binder causes expansion of distance between the aggregate particles and decreases the aggregate-to-matrix ratio [Richard et Cheyrezy, 1995; Sadrekarimi, 2004; Aïtcin, 2008; Price, 2009; Courtial et al., 2013; Zdeb, 2013].

- Macro-effect is the second effect of substituting the coarse aggregate by fine sand, which is related to reduction of aggregate quantity. In UHPC, the aggregates cannot form a rigid structure because the volume of the paste is larger than the voids index of non-compacted aggregate by at least 20%. Contrary, in the traditional concrete, the aggregates form a rigid structure of adjoining granular elements that closed a main part of paste shrinkage and increased porosity [Richard et Cheyrezy, 1995].

## 2.2. Compactness

Pozzolanic mineral additives are used to increase the powders packing density through the physical filling effect on the one hand and through the production of additional calcium silicate hydrates material with a much finer intrinsic porosity on the other. Accordingly, high density is the second principle employed in UHPC due to the presence of four granular components: sand, cement, crushed quartz and silica fume. When these solid fractions mixed simultaneously, the (w/f) affects the granularity. This ratio is an indicator of the quality of the grading of the different ultrafine particles (< 125 µm grain size) and the residual pores between the particles, which must be filled by water, and hence it leads to maximise the density of granular packing and minimise each of the interparticle voids, the mixing water content and the porosity. Thus, the selective optimal grain-size distributions of all solid fractions is significant because of two benefits; developed strength and workability. The particle size of UHPC ingredients is shown in Table 1 [Ahmad et al., 2015; Fehling et al., 2014; Korpa et al., 2014; Sadrekarimi, 2004; Kang, 2010]:

***Table 1: Particle size of UHPC ingredients [Kang, 2010 ; Ahmad et al., 2015]***

| Material | Silica fume | Crushed quartz | Cement | Quartz sand |
|---|---|---|---|---|
| Particle size (µm) | 0.1-0.3 | 10-15 | 10-100 | 150-600 |
| |  |  |  |  |

The vacuum process or press moulding of the UHPC mixture is considered as another suggestion in the prime stage of binder setting to decrease the porosity by bringing out the air from the mixture [Zdeb, 2013].

### 2.3. Microstructure

With regard to UHPC, having compressive strength around 150-200 MPa, the evident outcomes of hydration on porosity in the absence of any following treatment are the disappearance of capillary porosity due to low w/c and the formation of an interfacial transition zone (ITZ) made of calcium silicate hydrates (C-S-H) resulting from the pozzolanic reaction of the silica fume (ITZ) [Courtial et al., 2013].

With a view to develop the performance of UHPC and achieve this performance faster, a thermal treatment can be applied. The roots of this strategy returned to 1994 when intensive researches have been carried out in France and Canada to improve the microstructure of UHPC [Habashi, 2011; Courtial et al., 2013]. Two procedures of hydrothermal treatment are adopted. These procedures, in addition to alterations that occurred at lower temperatures, are responsible of the emergence of crystalline forms of C-S-H.

The First procedure is the low pressure steam curing at about 90°C for 48 hrs, which accelerates the hydration of cement and causes the reaction of silica fume with the calcium hydroxide $Ca(OH)_2$ in the cement. The second procedure is the autoclaving process that is carried out at 250°C. The effect exceeds the rate of reaction of the setting to the production of new mineral phases hence the decreasing of the C-S-H inter-layer spacing, in conjunction with a growing of the C-S-H crystallinity. Consequently, the amorphous cement hydration products transform to crystalline products such as xonotlite ($C_6S_6H$) [Menefy, 2007; Aïtcin, 2008; Zdeb, 2013; Fehling et al., 2014].

### 2.4. Ductility

Enforcement of above principles, the produced UHPC should have very high compressive strength but the same ductility of ordinary concrete. During an uniaxial compression test of UHPC, a linear elastic behavior displays and lengthens-until shortly before accessing its ultimate strength and also before the generation of microcracks, indicating the transition to brittle mode [Fehling et al., 2014].

Recently, the utilization of small metal fibres (µm size) in UHPC led to acquire both of high strength and high ductility. Ultra high performance fibre-reinforced concrete (i.e. UHPC containing fibres) was more progressed for attaining high toughness, ductility, and energy absorption that was got due to the incorporation of fibres. The achievement of these properties is based on the properties of fibres themselves; fibres content, geometry, orientation, stiffness, and the bond between fibres and matrix. The behaviour of the stress-

strain relationship is affected significantly by these properties [Fehling et al., 2014; Korpa et al., 2014].

Short fibres control the appearance and extension of microcracks that associate with an increased tensile strength while long fibres control the larger of cracks which display in the concrete at higher loads.

## 3. Constituent materials of UHPC

Based on the previously mentioned principles of UHPC composition, a breakdown of the essential ingredients of a typical UHPC with their characteristics are given below:

### 3.1. Cement

It is a major binder in the UHPC, at a higher volume rate (about 30%), compared to Normal Strength Concrete (NSC) or High Performance Concrete (HPC). For 1 $m^3$ of UHPC mixture, the cement content ranges between 800 kg and 1000 kg. The suitable choice of the binder type, i.e. its class, mineralogical and chemical composition and, also its specific surface area is very significant [Ahlborn et al., 2008; Yazıcı et al., 2010; Zdeb, 2013; Zdeb, 2015].

Accordingly, the low-alkali Portland cement CEM I of strength classes 42.5 R and 52.5 R according to DIN EN 196, has beneficial effects in terms of high strength potential, low water requirements, limit chemical shrinkage, and also prevention of an alkali-silica reaction. Thus, it is recommended for the manufacture of UHPC [Yazıcı et al., 2010; Fehling et al., 2014; Zdeb, 2015].

Chemically, the optimum cement which was recommended by Richard and Cheyrezy [Richard and Cheyrezy, 1995], has a high amount of $C_2S$ and $C_3S$ (di- & tri-calcium silicate) with very low $C_3A$ (tri-calcium aluminate). Indeed, these compounds (i.e. $C_3S$ and $C_2S$) are mostly in charge of strength of the hydrated cement paste even at the early ages as well as the w/c can be decreased when the Blaine fineness decreased too, around 3000-4500 $cm^2/g$. Furthermore, with thermal curing, the risk of generation of secondary ettringite can be reduced. Thereby, unhydrated cement grains occur in the matrix and act as particle packing material [Zdeb, 2013; Menefy, 2007; Ahlborn et al., 2008; Lee et Chisholm, 2005; Müller et Haist, 2012].

Although $C_3A$ has a minor role as a binding tool, and for development of early strength, it is considered as unfavourable compound for its negative impacts after hydration, aside from its high content, which can decrease the efficiency of superplasticizer, also it can cause durability problems in the long term [Zdeb, 2013; Menefy, 2007; Müller et Haist, 2012].

Hence, the main recommended characteristics of cement, used in UHPC are as following [Richard and Cheyrezy, 1995; Zdeb, 2015]:

(i) Low $C_3A$ content;

(ii) Low alkaline ions content;

(iii) High silica modulus, which supplies best rheological and mechanical properties of the UHPC however its slowly in setting rate.

### 3.2. Silica fume

Basically, more than 85% of silica fume is silicon dioxide in noncrystalline (amorphorous) form. It consists of very fine spherical particles with an average diameter of about 0.1 µm, about 100 times smaller than average cement particles as shown on Fig. 3 [Kosmatka et al., 2003]. Also it has specific area of circa 10000-25000 $m^2$/kg, which is 6-10 times the specific area of a Portland cement. For the color of this material, it is either dark grey or white or black, relying on the amounts of carbon and iron [Aïtcin, 2008; Thomas, 2013].

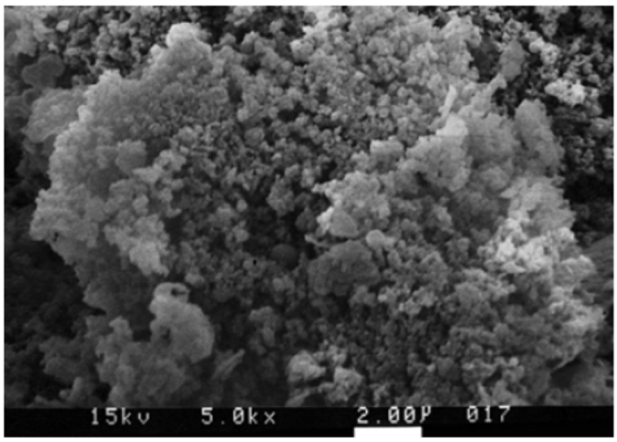


***Figure 3 : Scanning electron microscope micrograph of silica fume particles at 20,000X [Kosmatka et al., 2003]***

Due to a high level of purity and specific area of the silica fume, its type can control and alter the UHPC properties on account of its rapid pozzolanic reaction that could more actively enhance the strength development of UHPC in comparison with other pozzolanics [Spiesz and Brouwers, 2014]. The roles of silica fume can be summarized as follows:

(i) Increase the packing density: Silica fume is considered as a microfiller due to its physical influence that relevant to its particles size. These particles are inserted into the space between cement particles on one hand, and also fill the spaces between the larger particles of cement and aggregate on the other hand. So the packing closed around the cement particles and available water is decreased. As a result, a dense structure of the hydration products is formed with least voids between the particles and the packing density of the matrix is progressed [Richard et Cheyrezy, 1995; Lee et Chisholm, 2005; Zdeb, 2013; Fehling et al., 2014; Korpa et al., 2014]. Usually the silica fume-to-cement ratio used for

UHPC is about 0.25-0.3, which is compatible with the ideal filling effective, and it approachs to the sufficient dosage that ensures full consumption of the liberated lime from the cement hydration [Richard et Cheyrezy, 1995; Ahmad et al., 2015].

(ii) Improvement of rheology: thanks to the active role of silica fume with its spherical particles extremely fine and chemical composition characterised by lower carbon and impurities contents. By these properties, high interparticle forces have lubrication effect. The pores are filled by the lower content of superplasticizer which increases the conglomeration of silica fume particles during the mixing and in accordance with the framework of the packing density optimization the mix becomes viscous [Zdeb, 2013; Fehling et al., 2014; Korpa et al., 2014].

(iii) Production of secondary hydrates due to a decrease of the calcium hydroxide content in the interfacial transition zone between the aggregate particles and the cement paste matrix. This weakest portion is quite interestingly modified by obstruction of precipitation of large and oriented portlandite crystals on the aggregate surface. This has useful impact on mechanical and durability properties of the material [Lee et Chisholm, 2005; Müller et Haist, 2012; Zdeb, 2013].

### 3.3. Crushed quartz

Crushed crystalline quartz powder with its particle size around (10–15) µm is utilized as filler in UHPC. Because of quartz powder is considered as a reactive component, it performs as superior paste-aggregate interface filler. At thermal curing, when the UHPC mixtures subjected to temperatures overriding 90°C, extra silica is needful to adjust the $CaO/SiO_2$ ratio of the binder. Therefore, a crushed quartz for a mean particle size of (10-15) µm was applied due to its higher reactivity [Lee et Chisholm, 2005; Spiesz and Brouwers, 2014].

Quartz powder employed in UHPC as a rule is unlike quartz sand in terms of particle size, mineral composition, water requirement and workability. The water requirement of powders and the soft particles consisted of a layer of adsorbed water around the particles and a further prerequisite quantity for stuffing the intergranular voids of the powder matrix. Thereby, the suitable estimation of the water content is significant to cover all particles with a water layer of a particular thickness [Jankovič et al., 2011].

### 3.4. Quartz sand

From a historical point of view, many researchers proved that the maximum particle packing and the elimination of interparticle pores could induce higher strength of concrete. Based on that, the coarse aggregate in UHPC is substituted by fine quartz sand (< 600 µm) with a nearly optimum grain size distribution, by integrating a homogeneous gradation of fine and

coarse particles in the mixture. Generally, the following features of substitution the coarse aggregate by quartz sand are [Menefy, 2007; Spiesz and Brouwers, 2014]:

(i) Higher granular packing, resulting in a high density of UHPC;

(ii) Higher pozzolanic reaction at heat curing leading to higher early strength;

(iii) Lower micro cracking in the paste-aggregate interface.

The size and shape of the fine particles should be taking into account to select the adapted sand. Concerning the mineral composition, quartz displays the following usefulness [Richard and Cheyrezy, 1995]:

(i) High rigidity;

(ii) Compacted interfacial transition zone (ITZ);

(ii) Easily obtainable and economic.

Indeed, the most permeable part of a concrete is the paste-aggregate interface, and therefore, the removal of coarse aggregates helps in enhancing the durability of UHPC. Decrease of the ITZ zone leads to increase the tensile strength and decrease the porosity of the composite matrix [Ahlborn et al., 2008].

### 3.5. Water and superplasticizer

In order to idealise performance of UHPC, water content should be stayed low to be safe that there is no excess. The w/c used in UHPC ranges between 0.15 and 0.25 [Sadrekarimi, 2004], and majorly relies upon the water requirements which are significant because of the high surface area of the ingredients used in the mixture, and also bases on the superplasticizer dosage utilized [Menefy, 2007]. This range of w/c not only produces the highest strength, but also encloses that all the water in the mixture will be joint in forming C-S-H and will generate voids. This volume is less than that required for hydrating all the cement to make sure that all water is used in the hydration/pozzolanic reaction. Nevertheless, this small water amount already does not supply enough water to the mixture [Sadrekarimi, 2004]. The specific surface area of the components is not the only governing factor on water demand, packing is critical too. Improving packing saves water lost in the porosity of the particles skeleton at fresh state. This water is better used as a water film lubricating grains, to improve workability.

Superplasticizers or high range water reducers are chemical admixtures applied to maintain a good dispersibility and high workability of fresh mixture. These admixtures should restrict to the materials that own both hydrophilic and hydrophobic sets in their molecular chains, and have a relatively plane adsorption shape. This limitation is important for the dispersibility and affects the cement hydration [Courtial et al., 2013].

Polycarboxylate-based dispersing agents are most effective superplasticizers in spite of them retarding effect, which can cause problems, and hence their compatibility with the cement

should be checked [Kang, 2010]. They are adsorbed on the surface of both clinker phases and hydration products. As a consequence, the cement particles are dispersed, which results in plastic mixture [Müller and Haist, 2012].

Superplasticizers have substantial functions for developing the UHPC to be very intensive with high strength and high workability. During the mixing, the electric charges on the solid particles resort to collect and hinder a perfect distribution of the water between these particles, then prohibiting eventually an ideal re-division of the hydrates produced between these solid particles. In this way, the paste has a lower primary flowability. Indeed, the superplasticizer reduces the water surface tension. Its addition to the water, superplasticizer is necessary in order to facilitate the fluid percolation between the solid particles, to grant an appropriate water permeability to these dense mixtures and to obtain high flowability [Morin et al., 2001]. For the low w/b in UHPC, the dosage of superplasticizer is about 3 times more than that in ordinary concrete. To ensure a high workability and compatibility between cement and superplasticizer, it is advised to utilize a cement having lower quantities of both $C_3A$ and alkalis because of the ability of superplasticizer, with high content, to deagglomerate the particles of both cement and silica fume [Richard and Cheyrezy, 1995; Yazıcı et al., 2010].

### 3.6. Steel fibres

Although the superior compressive strength of UHPC in the absence of fibres, it is considered as very brittle and has a limited tensile strength besides the behaviour of the material that is completely linear and elastic, corresponding to a fracture energy less than 50-90 J/m$^2$ [Müller and Haist, 2012; Ahmad et al., 2015].

Steel fibres are tightly incorporated into the very dense and compacted UHPC matrix. Thus, the high bond stresses can be delayed [Fehling et al., 2014]. Steel fibres can hinder the propagation of micro and macro-cracks and thereby width of crack is reduced and consequently the permeability too [Ahmad et al., 2015]. Moreover, during the failure of matrix the static friction between matrix and fibres does not cause breakage of fibres themselves, hence improves ductility [Fehling et al., 2014]. Short and slender fibres in accordance with DIN EN 14889-1, having maximum diameter of 0.2 mm, a length of 9-17 mm and made from high strength steel with a tensile strength ≥ 2000 N/mm$^2$ are considered to be an optimal choice. A length/diameter ratio of at least 65 is suitable [Fehling et al., 2014]. An ideal amount of 6.2% (by weight of UHPC) of steel fibres is endorsed by Ductal [Ahmad et al., 2015].

## 4. Optimization of UHPC mixtures

One manner of fulfilling optimum packing of the fine particles is through experimentation. Other manner is to utilize numerical modelling to optimize the packing density on the grounds of the characteristics of the raw ingredients measured beforehand. The numerical grading optimization of particle combinations for concrete and their fundamentals have been explained mainly by De Larrard [De Larrard, 1999]. Most models considered spherical particles. A sphere-depending model was utilized to find a grading curve which enables optimum usage of the space with aggregate particles as shown in Fig. 4 [Fehling et al., 2014].

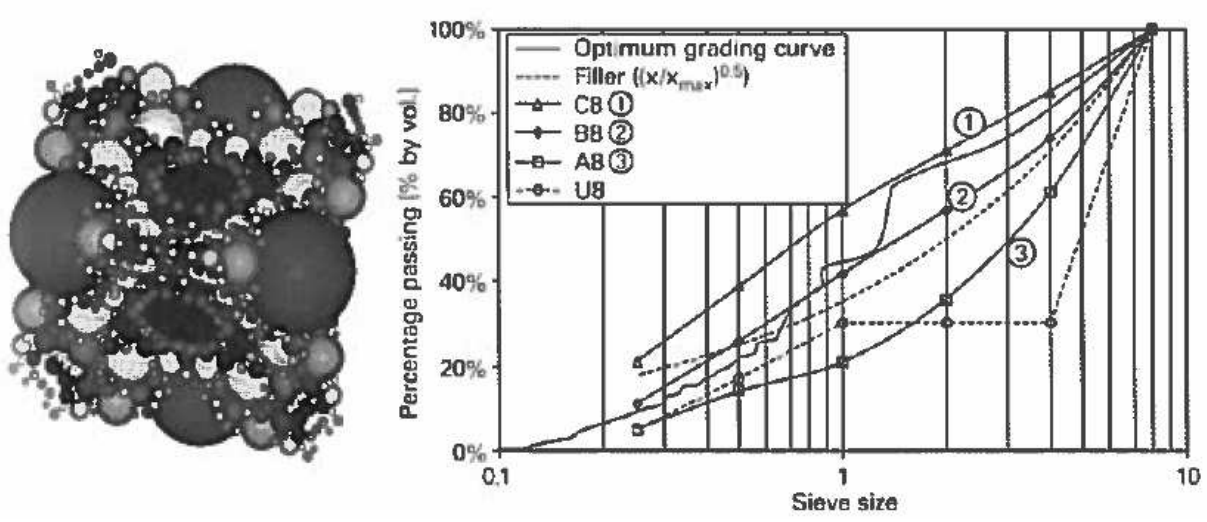


***Figure 4 : Optimum positioning and sizes for a rhombohedral packing [Fehling et al., 2014]***

The grading curve reveals, as a significant condition for usage in actual UHPC mixtures, that many individual particle size ranges are lost. This conduct the “filler particles” to reach the spaces allocated to them within the “scaffold” of larger particles. Where high proportions of fine particles are necessitated, the form of the particles is further significant. Meaning that it is might to make far better predictions of, for example, the water requirements of a mixture of fine particles and thus how this impacts the UHPC workability [Fehling et al., 2014].

However, these numerical models for grading optimization are not employed in this study on the basis that these models have some limits, particularly in presence of fine compounds.

Considering most recent developments on the use of SCM in replacement of clinker in UHPC mixtures, some research works were carried out on the synergies between used SCMs, for instance, silica fume versus slag dosages. It is interesting to note that Formagini [Formagini, 2005] and HOLCIM explored UHPFRC mixtures with massive use of slag and a low dosage

of silica fume by optimization of packing (8 to 10% mass only compared to typically 20 to 26% mass in CEM I bases mixtures) because of:

(i) High specific surface area of the components utilized;

(ii) Improved workability due to improved (optimized) packing, leading to keep the water lost in the porosity of the particles, and thus this water is considered as lubricated tool.

## 5. References

[Abbas et al., 2015] S. Abbas, A.M. Soliman, M.L. Nehdi, Exploring mechanical and durability properties of ultra-high performance concrete incorporating various steel fibre lengths and dosages. Constr. Build. Mater. 75 (2015) 429-441.

[Ahlborn et al., 2008] T.M. Ahlborn, E.J. Peuse, D.L. Misson, Ultra-High-Performance-Concrete for Michigan Bridges Material Performance – Phase I. Research report RC-1525, Center for Structural Durability Michigan Technological University, 2008, pp.1-181.

[Ahmad et al., 2015] S. Ahmad, A. Zubair, M. Maslehuddin, Effect of key mixture parameters on flow and mechanical properties of reactive powder concrete. Constr. Build. Mater. 99 (2015) 73-81.

[Aïtcin, 2008] P.C. Aïtcin, Binders for durable and sustainable concrete, series of modern concrete technology 16, 1st Edition, Taylor and Francis Group, 2008.

[Courtial et al., 2013] M. Courtial, M.-N.D. Noirfontaine, F. Dunstetter, M.S-. Frehel, P. Mounanga, K. Cherkaoui, A. Khelidj, Effect of polycarboxylate and crushed quartz in UHPC: Microstructural investigation. Constr. Build. Mater. 44 (2013) 699-705.

[De Larrard, 1999] F. De Larrard, Concrete Mixture-Proportioning – A scientific approach. Modern Concrete Technology series, N°9, E& FN SPON, Londres, 1999.

[Fehling et al., 2014] E. Fehling, M. Schmidt, J. Walraven, T. Leutbecher, S. Fröhlich, Ultra-high performance concrete UHPC: Fundamentals-Design-Examples, Wilhelm Ernst & Sohn, 10245 Berlin, Germany, 2014.

[Formagini, 2005] S. Formagini, Dosagem científica e caracterização mecânica de concretos de altíssimo desempenho, Rio de Janeiro, Doctoral thesis, 2005.

[Habashi, 2011] M.S. Habashi, Ultra high performance and high early strength concrete. Proceeding in the 36th Conference on Our World in Concrete & Structures Singapore, 2011.

[Jankovič et al., 2011] K. Jankovič, G. Čirovič., K. Nikolič, B. Bojovič, Mechanical properties of Ultra-High Performance Concrete (UHPC) self compacting concrete with different mineral admixtures. Roman. Jour. Mater. 41 (3) (2011) 211-218.

[Kang, 2010] S-T. Kang, Flow-dependent fibre orientation distribution and its effect on the tensile behavior of ultra high performance cementitioius composites, Department of Civil and Environmental Engineering, Korea, Doctoral Thesis, 2010.

[Korpa et al., 2014] A. Korpa, T. Kowald, R. Trettin, Principles of development, phase composition and nanostructural features of multiscale Ultra High Performance Concrete modified with pyrogenic nanoparticles – A review article. Ame. Jour. Mater. Sci. App. 2 (2) (2014) 17-30.

[Kosmatka et al., 2003] S.H. Kosmatka, B. Kerkhoff, W.C. Panarese, Design and Control of Concrete Mixtures, Portland Cement Association, 14th Edition, 2003.

[Lee et Chisholm, 2005] N. P. Lee, D. H. Chisholm, Reactive powder concrete, Study Report, BRANZ Ltd, No.146, Judgeford, Newzealand, 2005.

[Menefy, 2007] L. Menefy, Investigation of reactive powder concrete and its damping characteristics when utilized in beam elements, Griffith School of Engineering, Australia, Doctoral Thesis, 2007.

[Morin et al., 2001] V. Morin, F. C. Tenoudji, A. Feylessoufi, P. Richard, Superplasticizer effects on setting and structuration mechanisms of ultrahigh-performance concrete. Cem. Concr. Res. 31 (2001) 63-71.

[Mounanga et al., 2012] P. Mounanga, K. Cherkaoui, A. Khelidj, M. Courtial, M.-N.D. Noirfontaine, F. Dunstetter, Extrudable reactive powder concretes hydration, shrinkage and transfer properties. Europ. Jour. Env. Civ. Eng. 16 (2012) 99-114.

[Müller, M. Haist, 2012] H. S. Müller, M. Haist, New types of high performance concretes-potentials for innovations in concrete construction. Inn. Mater. Tech. Conc. Cons. ACES Workshop, Springer Science + Buisness Media B. V., 2012, pp.43-58.

[Price, 2009] R.A. Price, Mechanics of fibre reinforced reactive powder concrete (RPC)", Initial Thesis Report, 2009.

[Richard and Cheyrezy, 1995] P. Richard, M. Cheyrezy, Composition of reactive powder concretes. Cem. Concr. Res. 25 (1995) 1501-1511.

[Sadrekarimi, 2004] A. Sadrekarimi, Development of a light weight reactive powder concrete. Jour. Adv. Concr. Tech. 2 (2004) 409-417.

[Spiesz and Brouwers, 2014] R. Yu, P. Spiesz, H.J.H. Brouwers, Effect of nano-silica on the hydration and microstructure development of Ultra-High Performance Concrete (UHPC) with a low binder amount. Constr. Build. Mater. 65 (2014) 140-150.

[Thomas, 2013] M. Thomas, Supplementary Cementing Materials in Concrete, Taylor & Francis Group, LLC, 2013.

[Yazıcı et al., 2010] H. Yazıcı, M.Y. Yardımcı, H. Yiğiter, S. Aydın, S. Türkel, Mechanical properties of reactive powder concrete containing high volumes of ground granulated blast furnace slag. Cem. Concr. Compos. 32 (2010) 639-648.

[Zdeb, 2013] T. Zdeb, Ultra-high performance concrete – properties and technology. Techn. Sci. 61 (2013) 183-193.

[Zdeb, 2015] T. Zdeb, Influence of the physicochemical properties of Portland cement on the strength of reactive powder concrete. Proc. Eng. 108 (2015) 419-427.

# Part 1. Literatures review

# Chapter 2. Ground granulated blast furnace slag

## Table of Contents



## List of figures



## List of tables

## 1. Introduction

The reaction of the granulated blast furnace slags in a complex mixture of binder is a very complicated process, which deserves special attention. Unlike ordinary concrete, the behaviour of concrete based on blast furnace slag is not sufficiently controlled. In this chapter, the origin and the mineralogical composition of the slag will be presented. Then, the chemical behaviour of the slag in a cementitious matrix will be described as a function of the composition of the matrix. At the end of this chapter, the well-known activation methods will be presented: chemical and thermal activations.

## 2. Definition

Ground granulated blast furnace slag (Fig. 1), also named slag cement, is made from iron blast furnace slag; it is a metallic hydraulic glassy granulated cementing material, which is an industrial by-product from the manufacture of iron utilized in steelmaking [Kosmatka et al., 2003; Thomas, 2013].

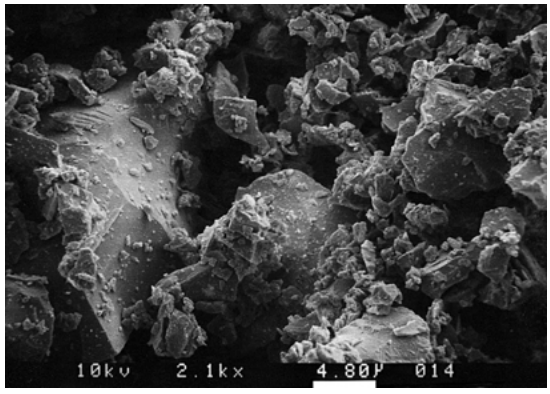


***Figure 1 : Scanning electron microscope of slag particles [Kosmatka et al., 2003]***

## 3. History

The slag cement usage in building applications has attracted a lot of interest since several centuries on account of its economic, engineering, and environmental benefits that make it as an environmentally friendly material, and also favourite to the traditional binders in application [Chen, 2007].

In 1774, Loriot utilized the slag as a mortar after merging with hydrated lime. Since then the slag is being used as a cementitious substance. Thereafter, slag cement usage has been widespread in the world like the slag-lime cement which was applied in the underground metro construction in Paris starting in 1889 while in the United States the blended Portland blast furnace slag cement was initially generated in 1896. Till the 1950's, slag was

fundamentally employed in the production of Portland cement as raw material to manufacture cement clinker, and since that time slag cement became obtainable as an independent product-added to the concrete mixing. It was first evolved in South Africa, subsequently acquired the fame in many other countries, like the United States and Canada whereas in Europe, cement containing slag has been used for more than 100 years. The renown of the slag increased rapidly, synchronizing with the publication of standard specifications for utilization of ground granulated blast furnace slag in concrete and mortars [Lamond and Pielert, 2006; Chen, 2007]. Yearly, around 250 million tons of slag created, from which only 90 million tons are utilized in the concrete manufacture [Ahmed et al., 2016]. According to standards in the United States (ASTM C595-05) and Europe (EN 197-1), the slag content in the cement can be up to 70-95% of slag (by mass) respectively [Chen, 2007]. In France, some composite cements like (CEM II/B-S, CEM III/A 42.5 and CEM III/C 32.5) are produced by mixing clinker with limited content of GGBFS.

## 4. Origin and production

The creation of blast furnace slag (i.e., Fe slag) is around 10% of the total steel production [Aydın et Baradan, 2014]. It was manufactured in a blast furnace jointly with Fe [Piatak et al., 2015]. Fig. 2 shows a schematic of an iron blast furnace.

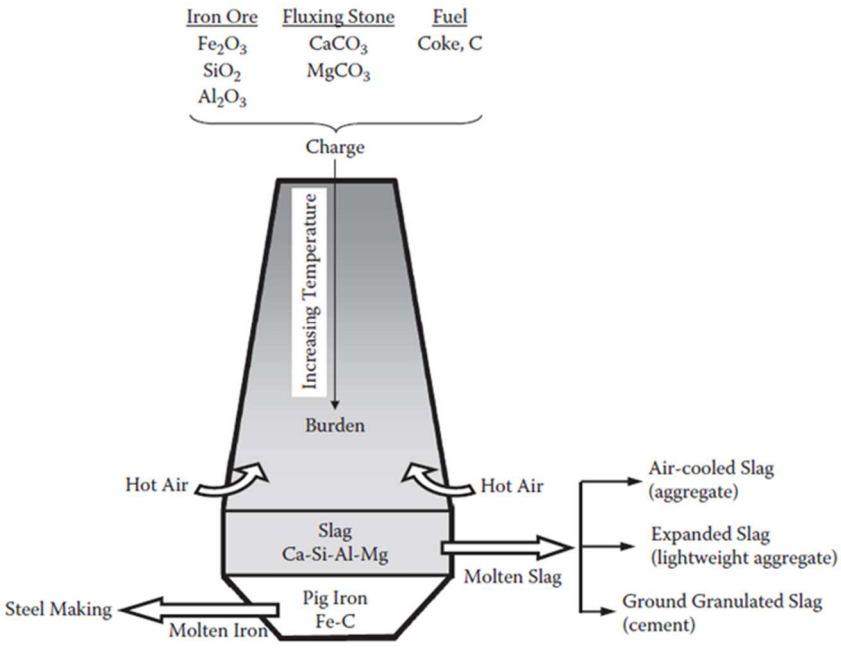


***Figure 2 : Schematic layout of an iron blast furnace [Thomas, 2013]***

The charge, comprising of three parts: iron ore, a fluxing stone (as a rule an integration of limestone and dolomite), and coke as fuel, is constantly fed into the top of the furnace whilst hot air is blasted in farther down. When the burden goes to the bottom of the furnace it lits, so the temperatures exceed 2000°C [Thomas, 2013]. The final outputs, tapped cyclically from the bottom of the blast furnace, are molten iron and molten slag [Lamond and Pielert, 2006]. The molten iron which resulted from a decrease of iron oxide from the ore, drowned to the bottom of the furnace because of its high density [Thomas, 2013], and sent to the steel production facility [Lamond and Pielert, 2006]. Concerning molten slag it is formed from the remaining constituents, which combine the calcium and magnesium from the fluxing stone, the alumina and silica gangues from the iron ore, and a little quantity of ash from the coke. All these constituents form a fused melt that floats above the intensive molten iron [Thomas, 2013].

The cooling rate and manner impact the slag properties, which influence its commercial applications. Thereby, the treatment of molten slag can be made by three methods, two of which can result in the material that becomes slag cement. Granulated slag is produced when the molten metal is quickly quenched in a "granulator" with high contents of water to fabricate a sand-like, glassy "granule" that can be finely ground into slag cement. Slag granules are same to clinker through their requirements of grinding before they can be divided as hydraulic cement. Thus, the glass morphology (noncrystalline) of these granules permit the material to be cementitious, once finely ground. Stockpiled granules are transferred to a grinding mill and ground to a fine powder. As a consequence, the slag cement powder is forming [Lamond and Pielert, 2006; Piatak et al., 2015].

## 5. Composition

The basic oxides in the GGBFS are lime (CaO), silica ($SiO_2$), alumina ($Al_2O_3$), magnesia (MgO) and some secondary contents ($SO_3$, FeO or $Fe_2O_3$, $TiO_2$, $K_2O$, $Na_2O$, etc.). All these compounds can alter from one blast furnace to another within narrow limits as shown in Table 1, leading to consistent output comparatively from one blast furnace. This alteration does not have a dramatic effect on the slag reactivity as a cementitious material [Chen, 2007; Aïtcin, 2008].

The oxides shown in Table 1, represent each of main chemical concentrations and composition of crystalline oxides and silicates. Therefore, slag compositions can be plotted on ternary phase diagrams ($CaO\text{-}SiO_2\text{-}Al_2O_3$) [Piatak et al., 2015]. In comparative with the typical oxide composition of clinker, BFS commonly includes less lime, more silica, alumina and magnesia than clinker. Alkalines ($Na^+$, $K^+$) are included in ordinary blast furnace slag moderately. Respecting manufacture of cement, the appropriate slag is nearly quite glassy, whereas Portland cement clinker is usually crystalline. Nevertheless, a specific content of

crystalline mineral is still as a result encountered when the phase composition of slag is investigated. Those phases majorly encompass melilite, merwinite, bredigite and spinelle, all of which are frequently less reactive than the origin glass that they substitute through crystallization [Chen, 2007].

***Table 1 : Chemical composition of some slags [Chen, 2007]***

| *Compounds(%)* | *French slags* | *North American slags* |
|---|---|---|
| $SiO_2$ | 29-36 | 33-42 |
| $Al_2O_3$ | 13-19 | 10-16 |
| CaO | 40-43 | 36-45 |
| $Fe_2O_3$ | < 4 | 0.3-20 |
| MgO | < 6 | 3-12 |
| $S^-$ | < 1.5 | - |

## 6. Hydraulic reactivity

Because of higher C/S ratio than the other pozzolans, slag may be regarded as a latently hydraulic instead of pozzolanic, i.e. it reacts with water [Canut, 2012], chemically hardens, and does so under water. Ingredients of the Portland cement and slag produce C-S-H during amalgamating with water. Even so, hydrated Portland cement as well produces about 15 to 25% calcium hydroxide (by mass) which is a very soluble mineral [Lamond and Pielert, 2006]. Fig. 3 compares the hydraulic and pozzolanic effects of the slag with other supplementary cementing materials, accompanied with calcium hydroxide content [Canut, 2012].

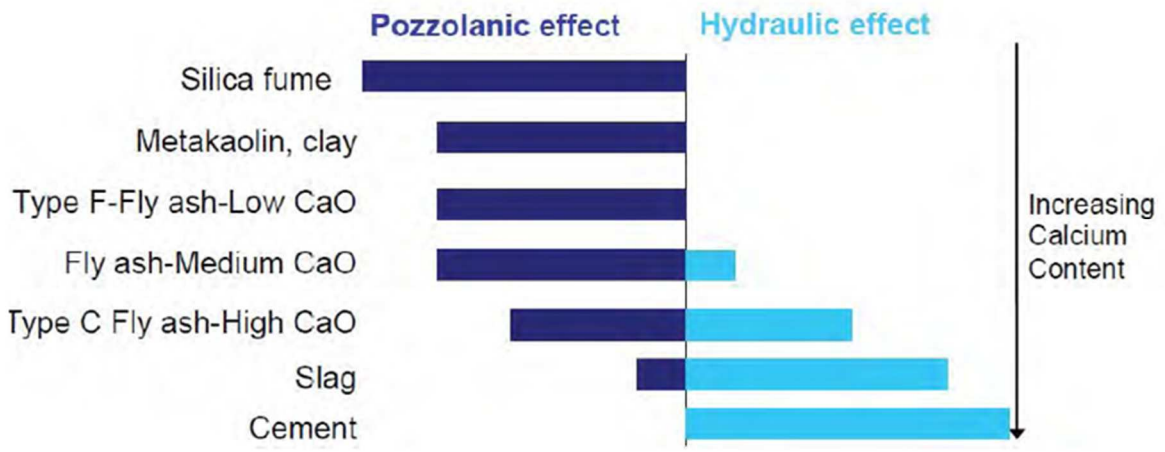


***Figure 3: Hydraulic and pozzolanic effects of slag and supplementary cementing materials with calcium hydroxide content [Canut, 2012]***

The reasons of a lime dilution in the Portland cement and also the reaction between the calcium hydroxide Portland cement product with the glass phase of the slag (to make more C-S-H), achieve the highly content of C-S-H and lower calcium hydroxide (CH) in the combination of slag/Portland cement. As a result, more robust aggregate/paste bond, better strength, and superior durability are acquired for the slag/Portland cement combination [Lamond and Pielert, 2006].

The reactivity of slag/Portland cement binders is dissimilar to the slag reactivity that is extremely slow. The Portland cement/slag interaction in the mortar and concrete controls the reactivity of them in mortar and concrete, and counts on some parameters like: alkali concentration, chemical composition and glass amount of slag, fineness of both Portland and slag cements, slag cement proportions and curing temperature [Lamond and Pielert, 2006].

Mutual relations amongst the following factors impact the reactivity and effectiveness of slag. These factors are glass content, particle size, and slag chemistry. In addition, several factors may influence slag output quality [Lamond and Pielert, 2006; Chen, 2007; Kim et al., 2011; Beushausen et al., 2012; Thomas, 2013; Piatak et al., 2015]:

- Particle size and/or Blaine fineness;
- Glass content;
- Chemical composition;
- Basicity;
- Colour;
- Loss on ignition;
- Chloride content;
- Titanium content.

Some of these factors are sharing for their effect on the slag reactivity and also quality assurance, thus it will be discussed as the following:

### 6.1. Fineness

The particle size of the GGBFS is less than 45 µm whereas its particle shape is angular as shown in Fig.1, despite the surface texture is slightly finer than cement, and the specific surface area is in the range of 400 to 600 $m^2/kg$ (Blaine fineness method). The relative density (specific gravity) for GGBFS is around of 2.85 to 2.95 while the bulk density varies from 1050 to 1375 $kg/m^3$ [Kosmatka et al., 2003; Newman and Choo, 2003].

Although the slag reactivity relies more precisely on the particle size distribution, specific surface area, and surface morphology [Al-Otaibi, 2002; Kim et al., 2011], the influence of it (i.e. slag) is corresponding to its fineness especially as it was finer than the Portland cement.

Meaning that higher fineness of slag, the higher reactivity, and accordingly the lower setting time, and better strength of the blended mixtures [Al-Otaibi, 2002; Chen, 2007; Aïtcin, 2008]. Indeed, grinding slag independently instead of inter-grinding with cement at the mill has a main advantage to increase the fineness. Because of the high hardness of slag for grinding in comparative with the Portland cement, an inter-ground blend will be caused in the cement being finer than the slag, which is against of what is coveted. Thereby, ideal fineness can be obtained through grinding of slag and cement independently [Lamond and Pielert, 2006].

### 6.2. Glass content

Broadly, the content of glass in the BFS is a significant parameter in identifying its role in the concrete mixture or its hydraulicity (i.e. slag), as crystalline slag has less important reactivity [Lamond and Pielert, 2006; Thomas, 2013]. The granulation process in the slag processing method is essential. Quick chilling or quenching of the molten slag prevents the configuration of a crystalline skeleton. As a result, this fast cooling is needful, and for this reason, the slag will consist of mostly glass or amorphous material [Lamond and Pielert, 2006].

In reality, the linear relationship between the slag glass content and the mortars strength is proved [Thomas, 2013]. Little quantities of crystalline minerals in the slag do not impact the achievement of its importantly. Nevertheless, it is useful for strength and durability of blended slag mixtures [Chen, 2007]. For instance, the crystalline material (up to 5%) can increase strength while the effect on strength is less remarkable when the crystalline merwinite is up to 30% [Thomas, 2013]. However, the existence of high content of crystalline minerals decreases the slag reactivity perceptibly, so the performance of the slag is weak [Chen, 2007].

### 6.3. Chemical composition

The chemical composition of the slag changes with the kind of iron being fabricated and the type of ore being utilized [Sajedi and Abdul Razak, 2010]. It has a fundamental function in its hydraulic activity and hence the microstructure and properties of the blended concrete. Neutral or alkaline slag is better than acidic slag [Al-Otaibi, 2002].

Slag activity is beneficial through the large extents of CaO, $Al_2O_3$ and MgO whereas a high amount of $SiO_2$ raises the viscosity. It is simply to produce $CaSiO_3$ and the high silicate glass that reduces the slag activity, and which is specified by each of content, properties, and chemical composition of amorphous glass [Desouky et al., 2013].

The Basicity Index ($BI=CaO/SiO_2$) is one of the most significant factors that describes technical properties and stability of the slag. When the slag has less BI, the hydration and decaying hazard are less too [Kasina and Michalik, 2012]. Therefore, the more basic the slag, the higher reactivity of it. Various researchers suggested some basicity indices or

hydraulic moduli to appreciate the hydraulic reactivity of GGBFS as shown in Table 2 [Tokaya, 2016].

***Table 2 : Suggested basicity indices of GGBFS [Tokaya, 2016]***

| *No.* | *Index or modulus* | *Limits of good performance* |
|---|---|---|
| 1 | $\frac{CaO}{SiO2}$ | 0.3-1.4 |
| 2 | $\frac{CaO + MgO}{SiO2}$ | >1.4 |
| 3 | $\frac{CaO + MgO + \frac{2}{3}Al2O3}{SiO2 + \frac{1}{3}Al2O3}$ | >1 |
| 4 | $\frac{CaO + MgO + Al2O3}{SiO2}$ | >1 |
| 5 | $\frac{CaO + MgO}{SiO2 + Al2O3}$ | 1-1.3 |
| 6 | $\frac{CaO + 1.4MgO + 0.56Al2O3}{SiO2}$ | >1.65 |

However, there are numerous equations for predicting the slag reactivity as observed in Table 2. Index 4 is considered as the most widely used modulus [Thomas, 2013]. Generally, the lower slag basicity index, the lower strength of mortar or concrete. Also the small contents of CaO and $Al_2O_3$ affect the strength gain, particularly in the earlyages that means the strength at these ages get larger with the augmentation of $Al_2O_3$ which is caused by the augmentation of the formed ettringite at the earlyages. [Mudersbach et al., 2011; Thomas, 2013].

Minor elements in slag, like P, F, S, Mn and Ti, usually have noteworthy effect on type of slag. High amount of $Fe_2O_3$ reduces the slag reactivity [Al-Otaibi, 2002]. It is worth mentioning that the fineness and glass content of the BFS are evenly or more important than the chemical composition for their action on the slag reactivity [Tokaya, 2016].

## 7. Hydration

Slag is neither a hydraulic binder, nor a pozzolanic material. During the mixing of slag with water, the slag does not harden nor integrate directly with the liberated lime from the $C_3S$ and $C_2S$ to produce secondary C-S-H [Aïtcin, 2008]. Therefore, the longterm performance of blended mixtures with slag is extra complicated and significant than conventional mixtures. The hydration reaction of the slag may need some years to be fulfilled, compared to the

cement alone, that indicates the dissimilarity of the hydration mechanism between the Portland cement and slag. After one year, around 90-100% of the clinker is hydrated in the binder while only around 50-70% of the slag is hydrated at the same time [Chen, 2007; Sajedi and Abdul Razak, 2010; Merzouki et al., 2013].

In fact, there are two main reactions of the hydration of BFS; initially, and through the early hydration, the dominant reaction is with alkali hydroxide whereas the next reactions are dominant with calcium hydroxide. The perfect motivity of Portland cement returns to presence of three major activators of slag thatare: lime, calcium sulphate, and alkalis [Aïtcin, 2008]. When a finely ground slag is mixed with water, initial hydration is very lazier and delayed than the Portland cement with water. The hydration of slag relied on the alkali amount in cement [Sajedi and Abdul Razak, 2010]. Thus, the slag reacts with alkali metal hydroxides that are liberated from merging of the Portland cement with water [Merzouki et al., 2013], leading to collapse and disband of the glassy structure of slag because of high pH value in the pore solution (>13.0) [Sajedi and Abdul Razak, 2010], and an immune acidic layer of gel is formed around the slag particles as an alternative about little dissolved $Ca^{2+}$ ions. Generally, the higher the dissolution, the quicker the reaction of the material to hydrated phases [Bellmann and Stark, 2009]. This acidic layer tentatively prevents the slag decay. Nonetheless, the released lime as a result of $C_3S$ and $C_2S$ hydration reacts with this layer of gel to form both of C-S-H and $C_4AH_{13}$ [Aïtcin, 2008]. Slag hydration consumes calcium hydroxide and utilizes it for further production of C-S-H [Sajedi and Abdul Razak, 2010].

Also when the slag particles will osculate the water, the sulphate ions go into solution to the prime layer of hydrate formed around these particles, producing a rough and less impenetrable layer of hydrate, compared to acidic layer of gel. The hydration of slag can be fast due to existence of its particles in the saturated solution of $Ca^{2+}$ ions, besides the good crystallines that are formed within the particle of slag. Finally, the hydrated structure is produced as shown in Fig. 4 [Aïtcin, 2008; Chen, 2007].

Compared to Portland cement, BFS contains less lime and then less calcium hydroxide $Ca(OH)_2$, that is not formed through slag particles reaction [Sajedi and Abdul Razak, 2010].

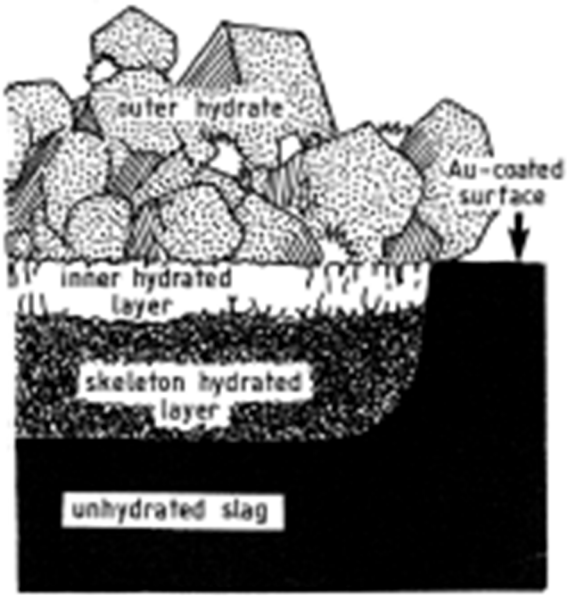


***Figure 4 : Schematic representation of the hydration of slag [Chen, 2007]***

Slag hydration counts on some major factors including: the slag reactivity, the pore solution composition, the activators for example sulfates and portlandite (CH), temperature and the w/b of the mixture. Some of these factors are affected by the hydration of cement. Thereby, hydration reactions of the blended mixtures with slag are affected in return. For instance, the hydration of $C_3S$, $C_3A$ and $C_4AF$ can quicken at various degrees that's why slag incorporation [Merzouki et al., 2013].

Slag can alter the hydration kinetics, and decrease the heat evolution which is linked to strength and also as an indicator of the slag reactivity [Sajedi and Abdul Razak, 2010; Altan et Erdoğan, 2012]. When the portlandite content (CH) amounts to a particular value, the reaction with calcium hydroxide is predominant which is in charge of the appearance of more peak in the hydration heat curves [Merzouki et al., 2013]. The Slag hydration rate in the blended mixtures is similar to that of $C_2S$ in Portland cement paste. The activation energy of slag reaction in cement is around 50–59 kJ/mol, which is larger than that of Portland cement itself (about 40 kJ/mol). Thus, the criticality of slag reaction to the curing temperature exceeds that of Portland cement [Chen, 2007].

The important phases existing in the blended mixtures with slag comprise C-S-H, $Ca(OH)_2$, sulfoaluminate phases AFt, AFm and hydroltacite like phase. Fig. 5 displays the brief of the hydration products that can form with taking into account the presented oxides in slag [Kocaba, 2009].

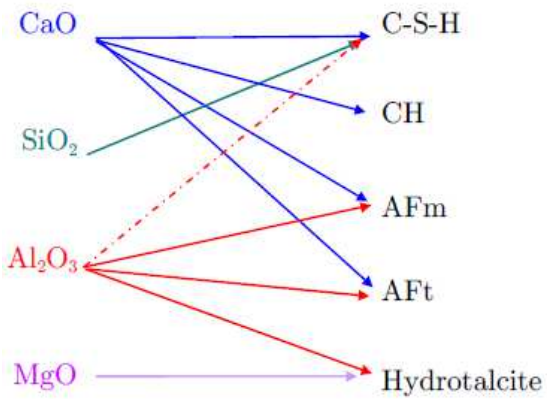


***Figure 5 : Summarized schematic for assessing the phases from the slag oxides [Kocaba, 2009]***

The hydrated composition of the slag is changed: C-S-H has usually a C/S amount of about 1.2 and Al/Ca amount about 0.19. As well the slag preferred the ferrite phase hydration. In Fig. 6, gathering of phases explained comparable results for blended mixture with slag: decrease of portlandite, production of C-S-H with a lower C/S ratio and consumption of monocarbonate [Canut, 2012].

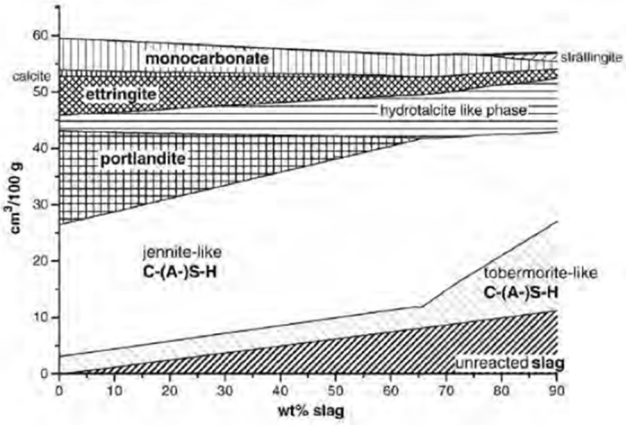


***Figure 6 : Gathering of phases in hydrated slag paste [Canut, 2012]***

C-S-H is the more plentiful product in blended mixture with slag. Commonly, its C/S ratio (in moles) is less than that in the Portland cement paste. Nevertheless, the C/S ratio in C-S-H stays larger than the C/S ratio in the slag alone (about 1.0–1.1), pointing to extreme calcium request by the slag hydration. This request is created either by the CH produced from Portland cement hydration, or by the lower C/S ratio in the C-S-H. The CH formed by the Portland cement hydration represents not only as an activator or incentive to the slag hydration but as an interactive too [Chen, 2007].

## 8. Activation

The disadvantages of BFS which including: Retarding the setting time of concrete that protracts construction, reducing the early strength gain remarkably in particular of substitution with high contents of slag, and slowing the hydration reaction [Kim et al., 2011; Mounanga et al., 2011]. All these disadvantages could be adjusted by specific patterns named as activation.

Activated slag cement (ASC) is a blast furnace slag that subjected to techniques of activators either are chemical or thermal means or combination of them, which have the efficiency to boost the slag reactivity through the hydration.

Since the slag has a changed composition contingent the raw materials and the industrial operation, the activation process influences and differs with both of the chemical and phase compositions of slag; thus, each slag response in an uneven way to the activation manner [Aydın and Baradan, 2014]. The comprehending of this response links with the assimilation of the hydration and microstructure growth. But overall, the better slag is the readily activated in a cementitious medium, because this readiness of activation is based on the mineralogical composition and fineness of the slag [Ben Haha et al., 2011].

### 8.1. Chemical activation

Chemical activation can be defined as the utilization of several chemical materials (powders or solutions), (sulfates and/or alkalis) in order to activate the possibility of cementitious constituents' reactivity. Generally, the activator can be added through the cement/slag grinding or can be disbanded in the mixing water and added through cement/slag mixtures mixing. The addition technical is straightforward and does not require further instruments [Sajedi and Abdul Razak, 2011].

When the activator reacts chemically with the slag, the pH of the combination rises, and when it reaches a critical value, the glassy slag skeleton is troubled, the reactivity is liberated and the slag will react with the water to form its special cementitious gels [Newman and Choo, 2003]. The Portland cement pore solution is an appropriate environment, which consists of one of alkali hydroxides. Slag can be enabled by Portland cement, which is most typical, and as well by chemical alkalis presenting the concept of alkali-activated slag (AAS). AAS cement is a combination of calcium-rich GGBFS and an alkali component [Al-Otaibi, 2002]. The chemical reactions that happen between the Portland cement, the water and the slag are very complicate and are summarized below [Newman and Choo, 2003]:

- Primary reaction:

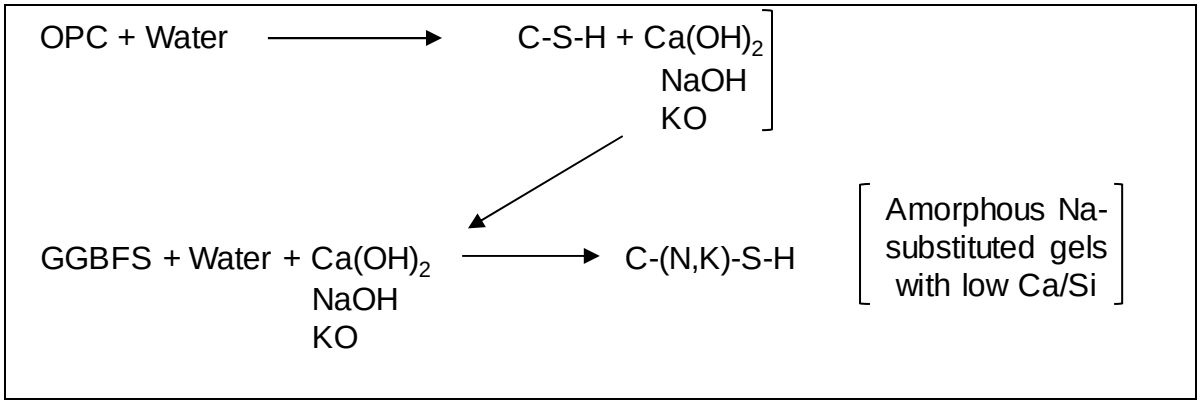


- Secondary reaction:

(i) Portland cement primary reaction products + GGBFS;

(ii) Portland cement primary reaction products + GGBFS primary reaction products.

The typical concentration of $Na_2O$ or $K_2O$ is in the range of 3-5.5 % by weight of slag whereas others successfully used quantity between 7-8 %. –The higher $Na_2O$ concentration, the higher mechanical strength but in Portland cement the content of $Na_2O$ is ordinarily less than 0.8%, so the risk of alkali-aggregate reaction is probably in the AAS [Al-Otaibi, 2002; Bellmann et Stark, 2009; Mithun et Narasimhan, 2014].

The rate and the products of these reactions are impacted by chemical composition, fineness, content, and relative proportions of the Portland cement and slag together. Also the temperature can affect the Portland cement reaction [Newman and Choo, 2003; Sajedi et Abdul Razak, 2010]. The principal product of hydration in AAS is C-S-H with a low C/S and depends on the slag composition and the type of activators utilized; hydrotalcite intimately intermixed with the C-S-H in the MgO in the slag and in some cases an AFm phase too, most likely strätlingite. This produced C-S-H may contain a higher amount of $Al_2O_3$, depending upon the initial composition of the slag [Ben Haha et al., 2011]. The minor hydrated products will alter the nature of both of slag and activator [Sajedi and Abdul Razak, 2010].

Hydration products are in charge of gained strength whereas pores have an unfavorable impact on strength. For alkali-activated slag cement, the following are the main factors determining the strength of cement pastes and mortars [Sajedi and Abdul Razak, 2010]:

(i) Slag nature, fineness, water/slag ratio;

(ii) Activator nature, amount, time of its addition, and modulus ratio;

(iii) Admixtures in the mixture, and curing temperature.

Since more than 70 years, the endeavors to activate the BFS using alkalis were begun [Altan and Erdoğan, 2012]. Many investigations on AAS have been done in the Ukraine at the 1950s [Wang and Scrivener, 1995]. AAS have been manufactured and used in limited

construction projects in the former Soviet Union, China and others. For example, the construction of high story residential buildings, special concrete pavements for heavy loaded trucks, prestressed reinforced concrete, and stabilization and solidification of hazardous and radioactive wastes [Aydın and Baradan, 2014]. During the 1970s, the interest in alkaline activation of slag has increased noticeably in other countries [Wang and Scrivener, 1995]. AAS have been employed in some applications in South Africa and Canada but the industrial experience of precast products using these types of cement is widespread in Eastern Europe, Finland and France [Al-Otaibi, 2002]. An adjusted kind of AAS has been applied in little contents in the USA since 1987 [Wang and Scrivener, 1995]. Compared to the Portland cement concrete, the AAS cement concrete behaviour was excellent during its usage in the same field through 1999–2000 years. Inversely in Turkey, AAS has a quite limited investigation and importance hence, it is considered as a not common substance [Aydın and Baradan, 2014].

Alkalis activated slag was awarded the interesting and observation as an alternative and substitutional to Portland cement due to its environmental and economic features plus several significant features. These features include: enhancement of earlyage strength, aggregate-matrix interface, and durability, and reducing each of hydration heat, porosity, and hydrates solubility [Aydın and Baradan, 2014]. For the heat of hydration, the released heat of AAS is around one third to half that of Portland cement and also is lower than that of low-heat Portland cement. Thanks to smaller C/S in the total hydration products, leading to little hydration energy than those in –Portland cement [Al-Otaibi, 2002]. As a consequence, the utilization of AAS technical allows the potential usage of waste materials [Heikal et al., 2014].

Regardless of the efficiency of the activator kind which is quite important for impacting the intensity and rate of the process of activation, and likewise the material performance, the most popular alkaline activators that are mainly available and economical can be divided into four groups as the following [Sajedi and Abdul Razak, 2010; Heikal et al., 2014]:

- Caustic alkalis, MOH;
- Non-silicate weak acid salts: $M_2CO_3$, $M_2SO_3$, $M_3PO_4$, MF, etc;
- Silicates, $M_2O.nSiO_2$;
- Non-silicate strong acid salts, $M_2SO_4$.

Where M represents an alkali metal, for example, Na, K, Li [Al-Otaibi, 2002]. The most appropriate choice of the activator quality and quantity is very significant for each type of slag [Aydın and Baradan, 2014].

Sodium and potassium hydroxides are utilized abundantly for their great competency of activation with slag. None the less, these activators have some negatives such as rapid setting time, the toxicity due to high pH and subsequently high cost [Jeong et al., 2016]. Sodium and potassium compounds have extra similar properties, and there is a secondary

divergence between them [Sajedi and Abdul Razak, 2010]. However, the concentration of $Na_2O$ and silica modulus ($SiO_2/Na_2O$) of these solutions are most critical properties for characterizing these alkalis [Gebregziabiher et al., 2015].

In addition to C-S-H as a main hydrated product when the activation is achieved by NaOH, the phases of $C_2ASH_8$ and $C_4AH_{13}$ are revealed $C_2ASH_8$ or gehlenite hydrate that is an AFm phase that has a common layer of aluminosilicate anion. A significant amount of MgO in the slag leads to form $M_4AH_{13}$ instead of $C_4AH_{13}$ [Sajedi and Abdul Razak, 2010].

Aside from the influence of both of fineness and chemical composition of slag as well as activator kind on the slag reactivity and activation process, other factors can influence as the following [Al-Otaibi, 2002]:

(i) Addition methods of activator: Three manners for adding the alkali activator to the slag that including: in solution, in the solid form ground together with slag, and in the solid form where the alkali activator is added independently to the mixture. Solid form addition does not only achieve hugely lower strength than the solution form but it generates a high fluctuation too due to lower solubility of this alkali in the mixture and supply of it for reaction. During storage, the solid alkali might absorb moisture which will block its activating action. Because of the high solubility of NaOH, it can be used as a solution or solid but the solution form is better from the strength standpoint.

(ii) Dosage: In spite of the presence of many investigations about the assessment of ideal content of alkali, the results are considered as conflicting. However, these studies indicated that the higher dosage, the preferable strength. $Na_2O$ content in slag can represent a second method to express about the alkali dosage. Higher $Na_2O$, higher strength but there is a particular limit of $Na_2O$ that the increment of strength gain will discontinue although this relies on each of slag, activator and curing condition.

(iii) Modulus of water glass solution: It can be defined by the molecular ratio ($SiO_2/Na_2O$) which is named as the silica modulus (MS) because these significant constituents are accountable for the hydration degree and the strength development. The alkali activates the slag while the silica $SiO_2$ produces the silica gel. Hence, for a specific $Na_2O$ content, the more silica, the higher modulus, the rapid setting, the higher strength. Many attempts were made to detect the ideal water glass modulus value that has a preferable effect for AAS concrete mixtures, and some of these efforts proposed that this modulus is around 1 to 2 whereas others suggested this modulus within the range of 1 to 1.5.

### 8.2. Thermal activation

As a consequence of released hydration heat of Portland cement in the concrete, contrast of temperatures occurs that has an enormous impact on its earlyage mechanical performance [Sajedi and Abdul Razak, 2010]. That's why a higher reaction activation energy in this process, resulting from the growth of temperature [Sajedi and Abdul Razak, 2011]. Thereby, BFS is avoided in applications when high earlyage strength is desired [Barnett et al., 2006].
Further investigations have proved that the activation energy of the hydration for the blended Portland cement with slag is more than Portland cement alone. Also the higher the substitution level of slag, the higher activation energy. Slag exhibits a higher reactivity with lime than other glassy pozzolans under ordinary circumstances. Other investigations have found that the high apparent activation energy of slag than Portland cement, making it quite sensitive to elevated temperatures [Sajedi and Abdul Razak, 2011]. Likewise, the slag hydration in AAS cement system is susceptible to elevated temperatures [Al-Otaibi, 2002]. During early hydration the common influence of both of alkalis and heat may be harmonic [Sajedi and Abdul Razak, 2011]. While high temperatures produce some crystalline products, the hydration products of AAS appear to rule amorphous at average temperatures. This depends on nature of the slag and the water glass solution [Al-Otaibi, 2002].
The strength gains of blended mixtures with slag that subjected to high temperatures are importantly improved at early ages. Usually, the heat release from sizable structural members is leisurely during the construction, because after casting, particularly through the initial few days the binder exothermic reaction increases the temperature remarkably. Then the earlyage strength will be raised [Barnett et al., 2006] unlike the advanced ages where the blended mixture strength is reduced. Probably, this different behaviour is attributed to the dense hydrated phases development about the unreacted cement particles, hindering more hydration. The hydration products are distributed irregularly, forming larger pores in the microstructure [Mounanga et al., 2011].

## 9. References

[Ahmed et al., 2016] S.A. Ahmed, M.H. Seleem, A.A. Badawy, A.A. Elakhras, Role of granulated blast furnace slag and ground clay bricks powders in self-compacting concrete Part 1: Fresh and hardened properties. Proceeding of the International Conference of Engineering Sciences and Applications, Aswan, Egypt, 2016.

[Aïtcin, 2008] P.C. Aïtcin, Binders for durable and sustainable concrete, series of modern concrete technology 16, 1st Edition, Taylor and Francis Group, 2008.

[Al-Otaibi, 2002] S. Al-Otaibi, Performance of alkali-activated slag concrete, Department of Civil and Structural Engineering University of Sheffield, UK, Doctoral Thesis, 2002.

[Altan et Erdoğan, 2012] E. Altan, S.T. Erdoğan, Alkali activation of a slag at ambient and elevated temperatures, Cem. Concr. Comp. 34 (2012) 131–139.

[Aydın et Baradan, 2014] S. Aydın, B. Baradan, Effect of activator type and content on properties of alkali-activatedslag mortars. Compo. Par. 57 (2014) 166-172.

[Barnett et al., 2006] S.J. Barnett, M.N. Soutsos, S.G. Millard, J.H. Bungey, Strength development of mortars containing ground granulated blast-furnace slag: Effect of curing temperature and determination of apparent activation energies, Cem. Concr. Res. 36 (2006) 434–440.

[Bellmann et Stark, 2009] F.Bellmann, J. Stark, Activation of blast furnace slag by a new method.Constr. Build. Mater.39 (2009) 644–650.

[Ben Haha et al., 2011] M. Ben Haha, B. Lothenbach, G. Le Saout, F. Winnefeld, Influence of slag chemistry on the hydration of alkali-activated blast-furnace slag-Part I: Effect of MgO. Cem. Conr. Res. 41 (2011) 955-963.

[Ben Haha et al., 2011] M. Ben Haha, G. Le Saout, F. Winnefeld, B. Lothenbach, Influence of activator type on hydration kinetics, hydrate assemblage and microstructural development of alkali activated blast-furnace slags. Cem. Conr. Res. 41 (2011) 301-310.

[Beushausen et al., 2012] H. Beushausen, M. Alexander, Y. Ballim, Early-age properties, strength development and heat of hydration of concrete containing various South African slags at different replacement ratios. Constr. Build. Mater. 29 (2012) 533-540.

[Canut, 2012] M.M.C. Canut, Pore structure in blended cement pastes, Department of Civil Engineering Technical University of Denmark, Denmark, Doctoral Thesis, 2012.

[Chen, 2007] W. Chen, Hydration of slag cement: Theory, modeling, and application, University of Twente, The Netherlands, Doctoral Thesis, 2007.

[Desouky et al., 2013] O.A. Desouky, S.E. Mansour, E.M. Negim, A.M. Najar, A. Saltanat, U. Nakan, Thermal behaviour and microstructure of blended Portland cement with libyan steelmaking slag. Euro. Jour. App. Sci. 5 (4) (2013) 118-126.

[Gebregziabiher et al., 2015] B.S. Gebregziabiher, R. Thomas, S. Peethamparan, Very early-age reaction kinetics and microstructural development in alkali-activated slag. Cem. Conr. Comp. 55 (2015) 91-102.

[Heikal et al., 2014] M. Heikal, M.Y. Nassar, G. El-Sayed, S.M. Ibrahim, Physico-chemical, mechanical, microstructure and durability characteristics of alkali activated Egyptian slag. Constr. Build. Mater. 69 (2014) 60-72.

[Jeong et al., 2016] Y. Jeong, J.E. Oh, Y. Jun, J. Park, J.-h. Ha, S.G. Sohn, Influence of four additional activators on hydrated-lime [$Ca(OH)_2$] activated ground granulated blast-furnace slag. Cem. Conr. Comp. 65 (2016) 1-10.

[Kasina et Michalik, 2012] M. Kasina, M. Michalik, Characterization of convertor slag in terms of slag instability. Euro. Mine. Conf. 1(2012).

[Kim et al., 2011] H.S. Kim, J.W. Park, Y.J. An, J.S. Bae, C. Han, Activation of ground granulated blast furnace slag cement by calcined alunite", Mater. Trans. 52(2) (2011) 210-218.

[Kocaba, 2009] V. Kocaba, Development and evaluation of methods to follow microstructural development of cementitious systems including slags, ÉcolePolytechniqueFédérale of Lausanne, Switzerland, Doctoral Thesis, 2009.

[Kosmatka et al., 20013] S.H. Kosmatka, B. Kerkhoff, W.C. Panarese, Design and Control of Concrete Mixtures, Portland Cement Association, 14th Edition, 2003.

[Lamond et Pielert, 2006] Lamond J. F., Pielert J. H., "Significance of Tests and Properties of Concrete and Concrete-Making Materials", ASTM International, ASTM Stock No.: STP169D, 2006.

[Merzouki et al., 2013] T. Merzouki, M. Bouasker, N. Khalifa, P. Mounanga, Contribution to the modeling of hydration and chemical shrinkage of slag-blended cement at early age. Constr. Build. Mater. 44 (2013) 368-380.

[Mithun et Narasimhan, 2014] B.M. Mithun, M.C. Narasimhan, Self-cured alkali activated slag concrete mixes-an experimental study. Int. Jour. Civ. Env. Str. Cons. Arch. Eng. 8(4) (2014) 477-482.

[Mudersbach et al., 2011] D. Mudersbach, P. Drissen, H. Motz, Improved slag qualities by liquid slag treatment. Proceeding of the 2nd International Slag Valorisation Symposium, Leuven, Belgium, 2011.

[Mounanga et al., 2011] P. Mounanga, M.I. Ahmad Khokhar, R. El Hachem, A. Loukili, Improvement of the early-age reactivity of fly ash and blast furnace slag cementitious systems using limestone filler. Mater. Struct. 44 (2011) 437-453.

[Newman et Choo, 2003] J. Newman, B.S. Choo, Advanced concrete technology-constituent material, Series of modern concrete technology 16, 1st Edition, Elsevier Ltd, 2003.

[Piatak et al., 2015] N.M. Piatak, M.B. Parsons, R.R. Seal II, Characteristics and environmental aspects of slag: A review. App. Geo. 57 (2015) 236-266.

[Sajedi et Abdul Razak, 2010] F. Sajedi, H. Abdul Razak, The effect of chemical activators on early strength of ordinary Portland cement-slag mortars. Constr. Build. Mater. 24 (2010) 1944-1951.

[Sajedi, H. Abdul Razak, 2010] F. Sajedi, H. Abdul Razak, Thermal activation of ordinary Portland cement–slag mortars. Mater. and Des. 31 (2010) 4522-4527.

[Sajedi et Abdul Razak, 2011] F. Sajedi, H. Abdul Razak, Effects of thermal and mechanical activation methods on compressive strength of ordinary Portland cement–slag mortar. Mater. and Des. 32 (2011) 984-995.

[Thomas, 2013] M. Thomas, Supplementary Cementing Materials in Concrete, Taylor & Francis Group, LLC , 2013.

[Tokaya, 2016] M. Tokaya, Cement and concrete mineral admixtures, Taylor and Francis Group, 2016.

[Wang et Scrivener, 1995] S.-D. Wang, K.L. Scrivener, Hydration products of alkali activated slag cement. Cem. Conr. Res. 25(3) (1995) 561-571.

# Part 1. Literatures review

# Chapter 3. UHPC properties: BFS content and activation methods

## Table of Contents



## List of figures

# 1. Introduction

In this chapter, UHPC properties will be presented. Firstly, the microstructure will be described through several tests used in the literature such as analysis of mineral phases by X-ray diffraction (XRD) as well as thermogravimetric analysis (TGA). The porosimetry applied to this type of material will be also described. The mechanical properties will then be presented by linking them to the microscopic behaviour, which may explain the obtained extraordinary resistance of the UHPCs. This chapter will be closed by a synthesis on the durability of these concretes that are very resistant to frost, carbonation as well as penetration of the gases and chloride ions.

# 2. Microstructural characterizations

## 2.1. X-Ray diffraction (XRD)

Cheyrezy et al. [Cheyrezy et al., 1995] studied XRD analysis of different UHPC formulations as a function of heat treatment temperature and pressure applied before and during the setting. The basic formulation consists of: Ordinary Portland Cement (OPC): 1, silica fume: 0.25, sand: 1.1, w/b: 0.12. Some formulations contain crushed quartz (40% by weight of cement) or steel fibres (approximately 2% in volume). The UHPC formulations are: B20°C/SC-basic formulation heated at 20°C, soft cast (setting pressure 1 atm); BQ200°C/SC-basic formulation with crushed quartz heated at 200°C, pressed (setting pressure 625 atm); BF250°C/SC-basic formulation with steel fibres heated at 250°C, soft cast; and BQF400°C/P-basic formulation with crushed quartz and steel fibres heated at 400°C, pressed (setting pressure 625 atm). They observed the appearance of peaks of $C_3S$ and $C_2S$ for un-hydrated cement, even for cured specimens at elevated temperatures while the portlandite peak can not be distinguished for the UHPC specimens cured at temperatures of 200ºC or greater. This emphasizes the activation of pozzolanic reaction with temperature. Also, the ettringite was not demonstrated in XRD as shown in Fig. 1. The lower content of $C_3A$ in the cement utilized and minimal w/c in this concrete can clarify this phenomenon. The xonotlite existed in XRD as exhibited in Fig. 1 for the UHPC mixtures heated at 250ºC and 400ºC whereas it was not revealed for temperatures of 200ºC or lower.

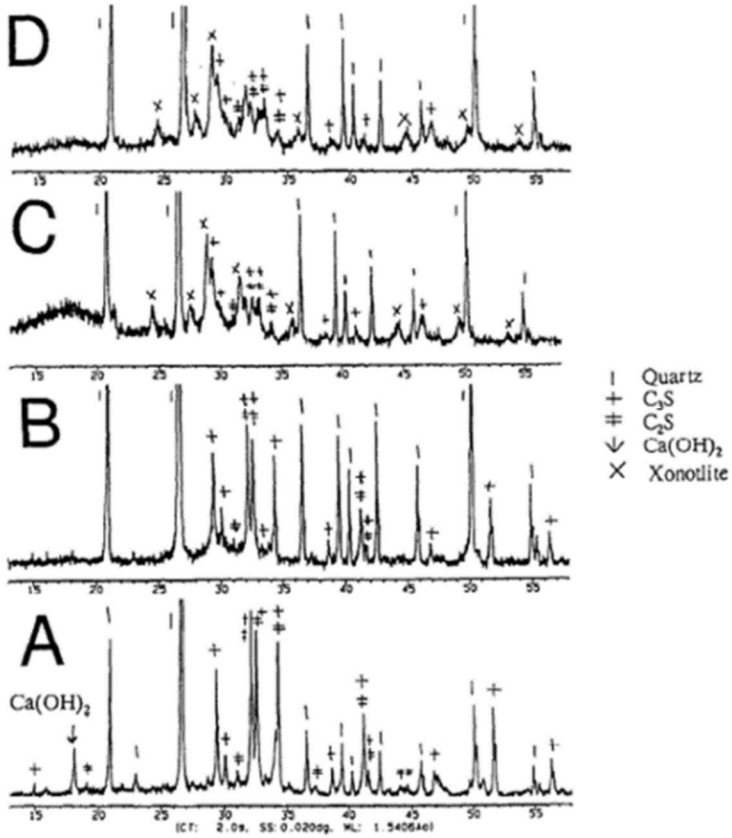


***Figure 1: XRD spectra of UHPC specimens: A (B20ºC/SC); (B) BQ200ºC/SC; (C) BF250ºC/SC; (D) BQF400ºC/P [Cheyrezy et al., 1995]***

Helmi et al. [Helmi et al., 2016] emphasized what was revealed by Cheyrezy et al. [Cheyrezy et al., 1995] through XRD diffractograms as demonstrated in Fig. 2 The main powders in the composition of UHPC mixture used, consist of CEM I 52.5 (498 kg/m$^3$), condensed micro silica (208 kg/m$^3$) and GGBFS (332 kg/m$^3$). Four combinations of treatments were applied in this study: (A) without pressure and cured in water; (B) without pressure and heat cured in a drying oven; (C) with pressure and cured in water; (D) with pressure and heat cured in a drying oven. A static pressure of 8 MPa was applied 5 h after casting, and all samples were demoulded after 2 days. After that a staged heat curing cycle was applied as following: preheated at 40°C for 2 h before increasing to 240°C at a rate of 50°C/h; cured at 240°C for 48 h; decreased at 50°C/h down to 40°C. After this step, heat-cured samples were stored in water at 20°C until testing. Fig. 2 explains the loss of the portlandite peaks ($2\Theta$ = 18.1° and 28.7°) following heat treatment (B and D) after the thermal treatment accompanied by a decrease in $C_2S/C_3S$ peak intensity and appearance of remarkable intensity for the shouldered xonotlite peaks ($2\Theta$ = 28.9° and 31.7°) neighbouring to the major calcite peak ($2\Theta$ = 29.5°). For this reason, filling would be expected to take place within the capillary pores [Shi et al., 2015].

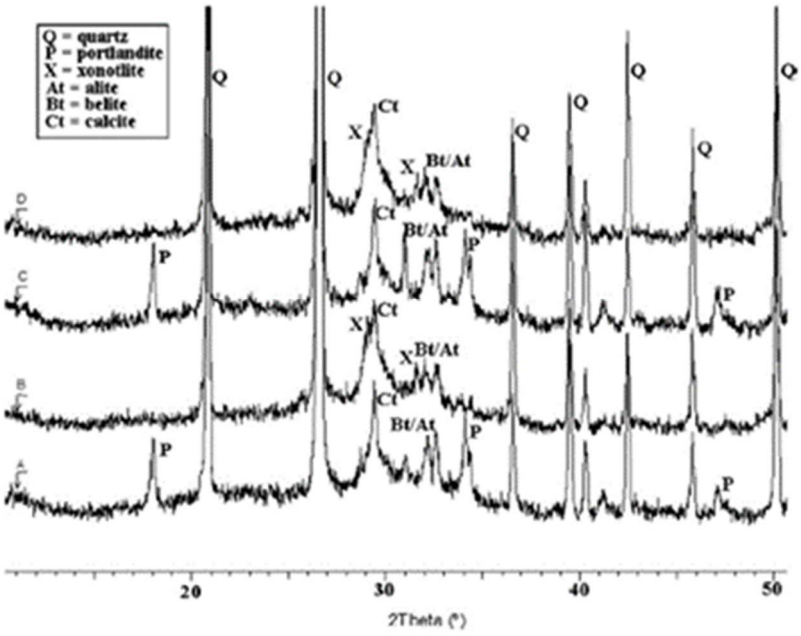


***Figure 2: XRD spectra for UHPC mixtures [Helmi et al., 2016]***

Al-Otaibi [Al-Otaibi, 2002] noted that the main phases of blended OPC with 60% slag (w/c=0.48) at 28 and 90 days as exhibited in Fig. 3 through XRD patterns were: Gehlenite (G), calcium carbonate (CC), calcium hydroxide (CH) and ettringite (E). Gehlenite is linked with anhydrous slag. Several peaks perhaps denote the existence of tetracalcium aluminate 13 hydrate ($C_4AH_{13}$) with the potential of carbonated phases. Also, no obvious difference can be detected in the intensities with time.

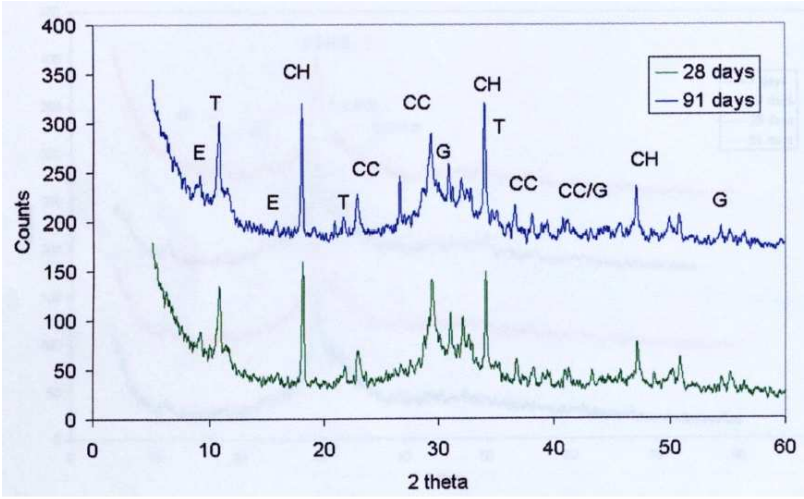


***Figure 3: XRD patterns of blended cement with 60% slag underwater curing [Al-Otaibi, 2002]***

Al-Otaibi observed that XRD patterns were quite comparable for whole AAS mixtures (OPC, 60%BFS, w/c=0.48, 4 and 6% of sodium silicate (water-glass)), and no obvious distinguish could be shown with diverging the concentration of $Na_2O$ or the MS of the activators. Thus, typical XRD patterns for the AAS are demonstrated in Fig. 4. Peaks exhibiting weakly crystalline C-S-H were revealed about 3.03 Å, 2.85 Å, and 2.70 Å. Several broad peaks found about 7.70 Å and 1.90 Å possibly specify the hydrotalcite existence, that is a magnesium aluminum carbonate hydroxide hydrate. This is because of the high magnesium amount of the slag utilized about 12%. It is as well established that the hydration products in the alkali-slag matrix are recognized to be a C-S-H gel with lower C/S ratio, zeolite-type minerals and silica gel [Al-Otaibi, 2002].

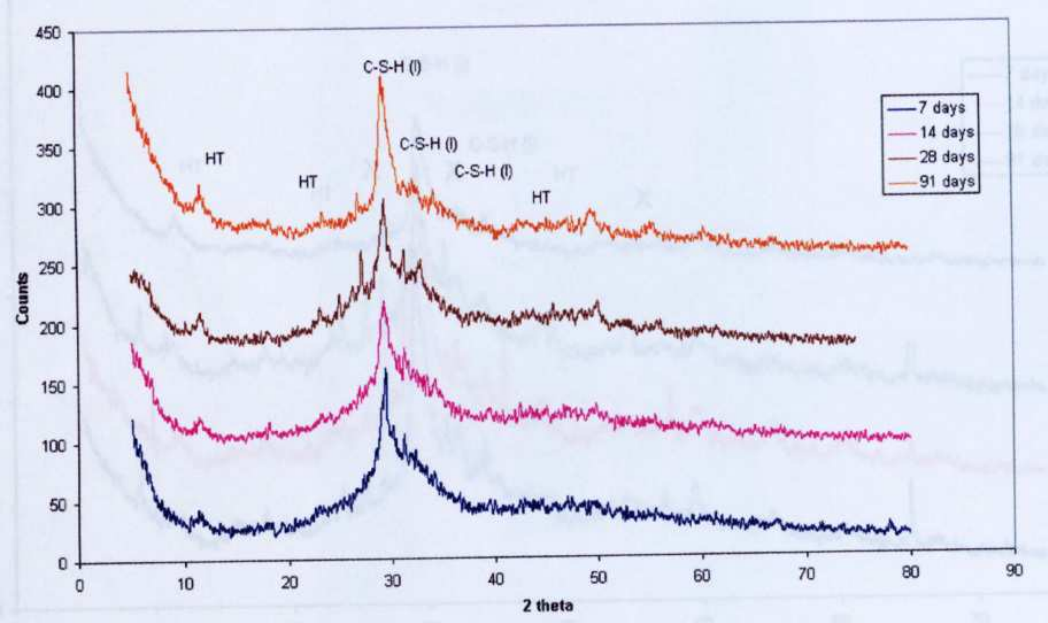


***Figure 4: XRD patterns of AAS underwater curing [Al-Otaibi, 2002]***

Abd-El.Aziz et al. [Abd-El.Aziz et al., 2012] studied the influence of high temperatures on blended slag mixtures having two types of BFS(water cooled slag and air cooled slag) from iron industry. After 24 hours of manufacture the specimens were demoulded and put in water tank for various high temperatures (25-100°C). As exhibited in Fig. 5, the increase of curing temperature increases the slag reactivity, leading to rise the consumption rate of portlandite through the pozzolanic reaction to generate further hydration products. Thereby, the free lime diminishes. The advancement of hydration from where the generation of additional hydrates by the slag and thermal activation which quickens the rate of pozzolanic reaction with the released portlandite, results in enhancing the chemically combined water amount, and the total pore size lowers with curing temperature for all blended mixtures. However, this water diminishes when the curing temperature rises from 75 up to 100ºC because of conversion of

the initially produced C-S-H with greater combined water amount to C-S-H owning little-combined water amount.

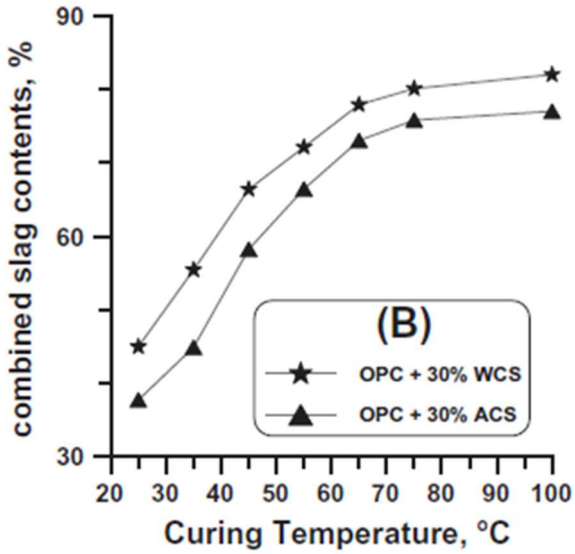


***Figure 5: Combined slag contents of plain OPC and pozzolanic cement pasted containing 30% of water cooled slag (WCS) or air cooled slag (ACS) and cured for 28 days as a function of curing temperature [Abd-El.Aziz et al., 2012]***

## 2.2. Thermogravimetric analysis (TGA)

Cheyrezy et al. [Cheyrezy et al., 1995] studied the thermal analysis (TGA/DTG) of several mixtures of UHPCs subjected to different treatment conditions (temperatures around 20-400ºC and setting pressure). The basic formulation (B20°C/SC) consists of: Ordinary Portland Cement (OPC): 1, silica fume: 0.25, sand: 1.1, w/b: 0.12. It heated at 20°C, soft cast (setting pressure 1 atm). Some formulations contain crushed quartz (40% by weight of cement) or steel fibres (approximately 2% in volume). Fig. 6 explains the TGA/DTG curves of reference mixture (B20ºC/SC) and shows that the mass loss between 20ºC and the temperature of the first DTG peak was ascribed to loss of non-chemically bound water in hydrates. For temperatures exceeding that of the prime DTG peak, the water losses on account of structural water (C-S-H dehydration, portlandite dehydroxylation). The DTG peak between 420°C and 500°C was specified as portlandite dehydroxylation while the DTG peak between 750°C and 850°C was ascribed to calcite decarbonation.

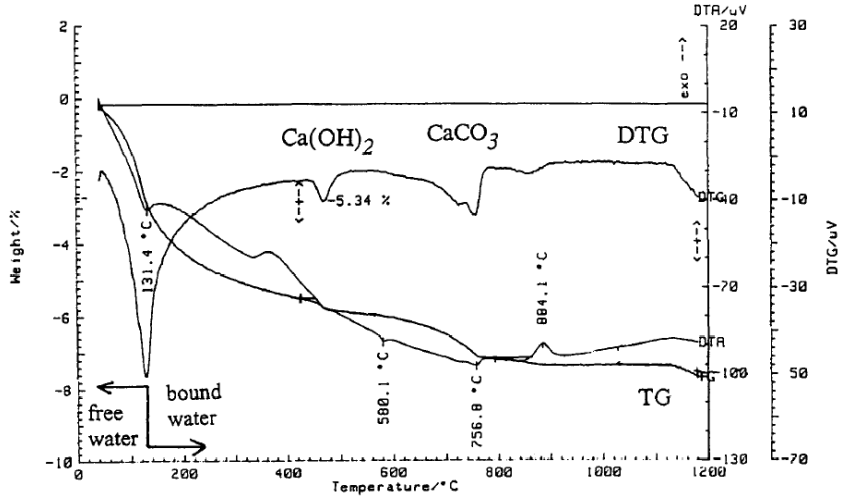


***Figure 6: Thermogravimetric curve of reference mixture of UHPC (B20ºC/SC) [Cheyrezy et al., 1995]***

Yu et al. [Yu et al., 2015] investigated TGA of UHPCs (reference and blended mixtures with 30% of slag, fly ash, and limestone powder by weight of cement). The mixtures were prepared and tested at room temperature of 21°C. It was revealed that there is further portlandite in the reference mixture accompanied with higher cement content compared to the blended mixtures with mineral admixtures like the slag. As shown in Fig. 7, the mass loss of portlandite of the UHPC containing slag is the least at 28 days, that indicates that the pozzolanic activity of slag is relatively more significant. Hence, additional portlandite has formerly been consumed. The mass loss of portlandite keeps less in the blended mixture with slag than the reference UHPC after 91 days as exhibited in Fig. 8. Therefore, the partial substitution of cement by generated dense C-S-H, which filled the pore structure in a blended mixture of UHPC. As a result, the UHPC with perfect performance can be formed with comparatively little cement quantity.

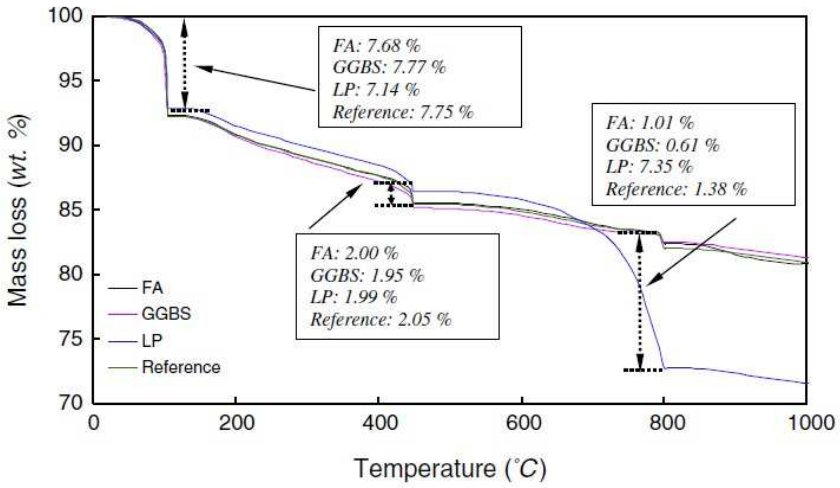


***Figure 7: Thermal analysis results (TGA) of UHPC pastes with different mineral admixtures (after hydrating for 28 days) [Yu et al., 2015]***

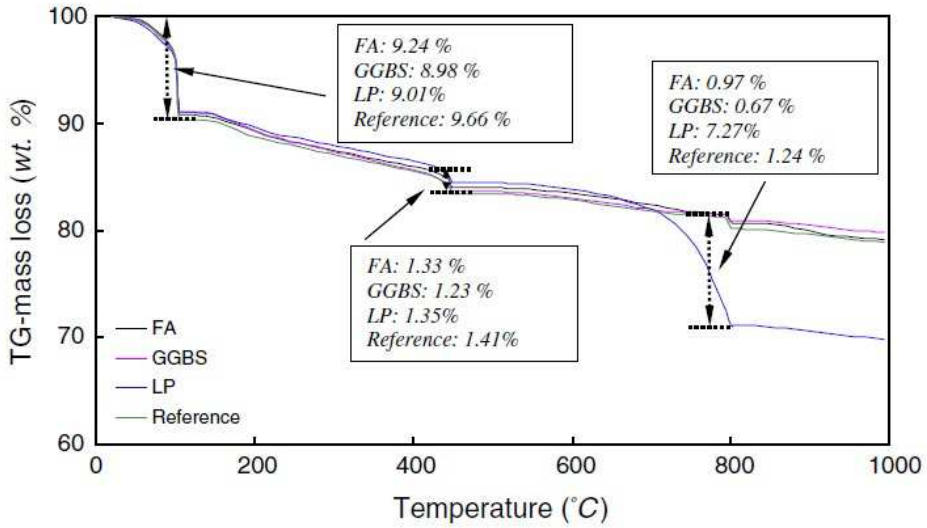


***Figure 8: Thermal analysis results (TGA) of UHPC pastes with different mineral admixtures (after hydrating for 91 days) [Yu et al., 2015]***

Holthuizen [Holthuizen, 2016] reported the thermograms for carbonated and uncarbonated cement paste containing CEM I 42.5N replaced by 40% of slag (w/c=0.5, cured in fog room). As demonstrated in Fig. 9, both TGA curves severely interfere till 460ºC for uncarbonated specimens. These specimens comprise the portlandite that dehydrates at 460ºC. The mass loss is lower than that of cement specimens, pointing to a little existence of portlandite in these specimens having 40% slag. In addition, the mass loss at 760ºC for uncarbonated cement paste specimens, pointing to that the calcite is less than that of cement.

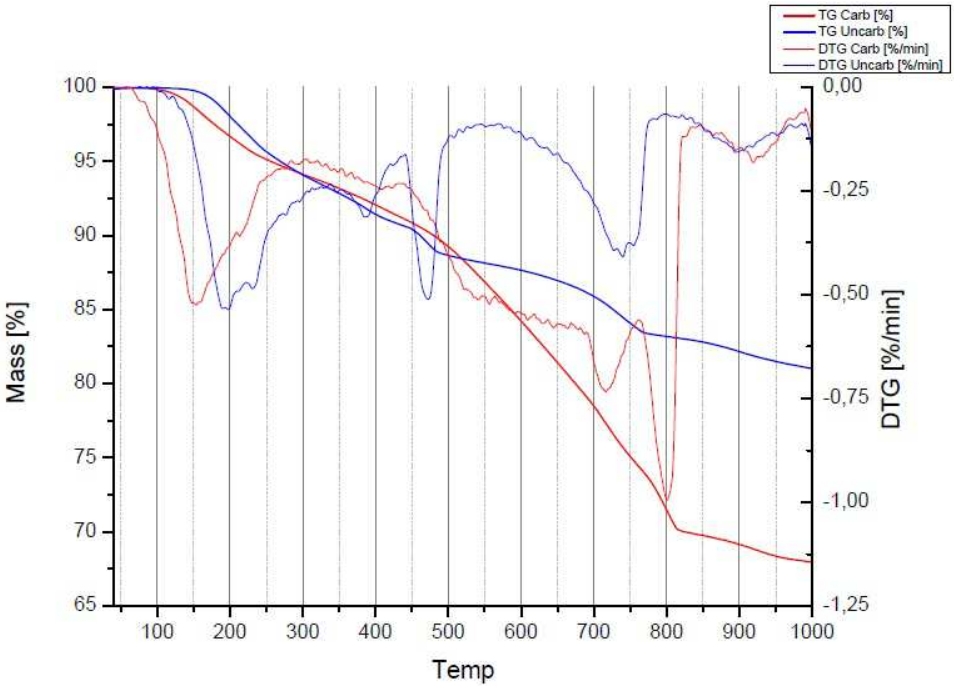


***Figure 9: TGA and DTG curves of carbonated and uncarbonated cement paste with 40% slag at 90 days [Holthuizen, 2016]***

As exhibited -in Fig. 10, the mass loss for carbonated cement specimens at a temperature of 160ºC is lower than that for uncarbonated specimens, which were likewise remarked for cement and other slag rates. In comparison with all cement blends, blended paste of CEM III/B 42.5N with 70% slag has the lowest portlandite quantity after hydration on account of the lowest mass loss at 480ºCas shown in the TGA curves. If we regard the standard hydration processes for either cement or slag, it cannot be explicated why or how this calcite was produced. One of the causes might be that natural carbonation of powders happens faster than in solid state [Holthuizen, 2016].

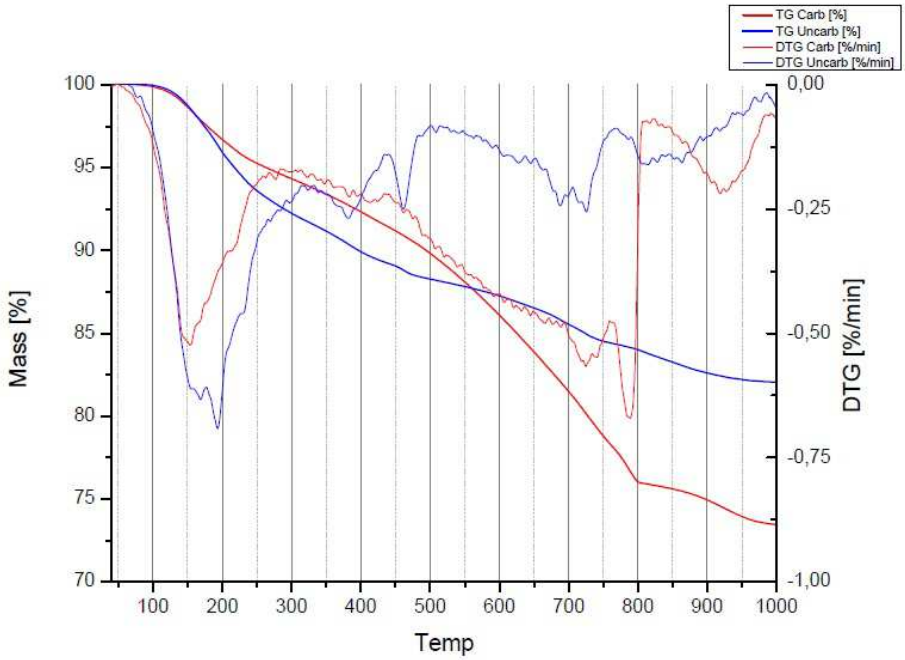


***Figure 10: TGA and DTG curves-carbonated and uncarbonated cement paste with 70% slag at 90 days [Holthuizen, 2016]***

## 2.3. Scanning electron micrograph (SEM)

Fig. 11 [Wang et al., 2012] shows a SEM image of UHPC with (20% GGBFS, 10% silica fume, w/b=0.16). According to this image, a quite compact skeleton in the hardened paste of the UHPC with a small number of air pores can be observed. This is due to cement hydration and the pozzolanic impact of silica fume and slag that consumes most of the portlandite crystals and transforms them to C-S-H.

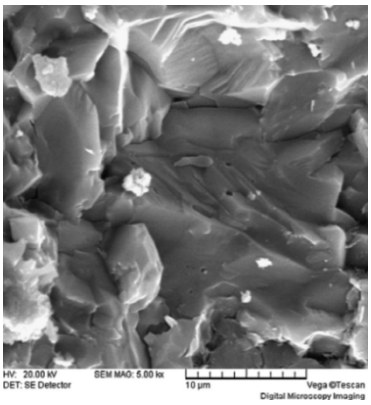

***Figure 11: SEM image of hardened paste of UHPC at 180 days [Wang et al., 2012]***

Tam et al. investigated the microstructure of UHPC (Cement=761 kg/m$^3$, silica fume=247 kg/m$^3$, w/b=0.2). At the ambient temperature, the skeleton of the new C–S–H generated is mainly amorphous or weakly crystalline skeleton that owns same characteristics of a rigid gel. According to SEM analysis in Fig. 12, C–S–H appears four various shapes: (a) Needle-shaped crystals with size of 0.5–2 µm long and 0.2 µm wide; (b) Plate-like crystals; (c) Irregular hexagonal panel crystals; and (d) Dense C–S–H paste oriented from the edge of hydrated cement [Tam et al., 2010].

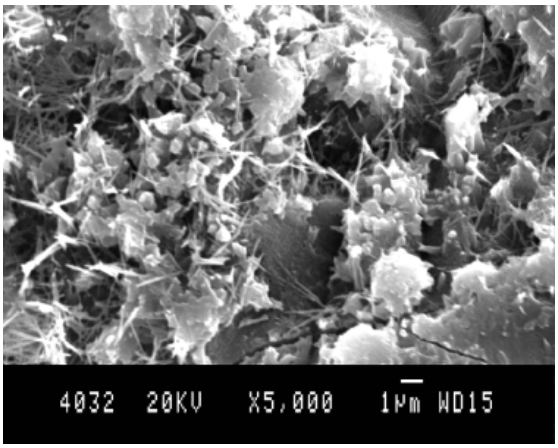


***Figure 12: SEM images of UHPC showing various shapes of hydration crystals in the forms of pike and flower [Tam et al., 2010]***

Courtial et al. [Courtial et al., 2013] revealed that the perfect homogeneous matrix of the UHPC (CEM I 52.5N, amorphous white silica fume, crystalline crushed quartz, w/c=0.16) through existence of much anhydrous cement (appeared as a light grey), hydrate compounds (appeared as medium grey) and perfect dispersion of silica fume due to the polycarboxylate superplasticizer impact. The ITZ is filled by hydrates emerging from the pozzolanic reaction of silica fume. Moreover, the crushed quartz distribution is homogeneous everywhere the UHPC paste as demonstrated -in Fig. 13(left) on the grounds that its favorite position at a closed link with the aggregate particles in the ITZ. As exhibited n Fig. 13(right)

the crushed quartz particles appeared as a rod-like shape as well as there is high quantity of belite in the residual clinker for the UHPC mixture [Courtial et al., 2013].

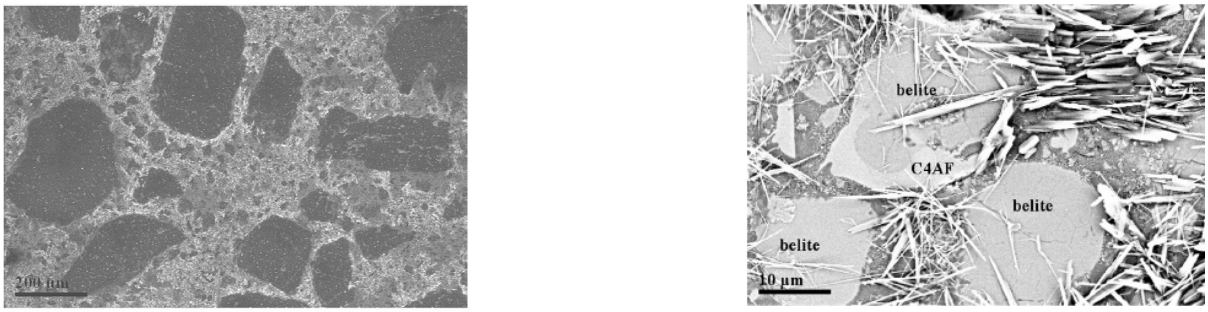


***Figure 13: Micrographs of UHPC: left) Secondary electron image, right) Back-scattered electron image [Courtial et al., 2013]***

The increase of slag content in the blended concrete leads to that the microstructure is unorganized and becomes into the block one for binders with the slag and cement (CEM I) proportion 70:30 and existed by alternated sections corresponding to the crystallized and amorphous components (Fig. 14(left)). For the blended mixture with ultimate slag amount of 90%, it was demonstrated in Fig. 14(right) that the structure displayed by the slag particles, which are feebly binding between each other on the surface by some amount of hydration products, is distinctive. The positions of the gels are apparent in the disconnected spaces in the blended specimens [Schuldyakova et al., 2016].

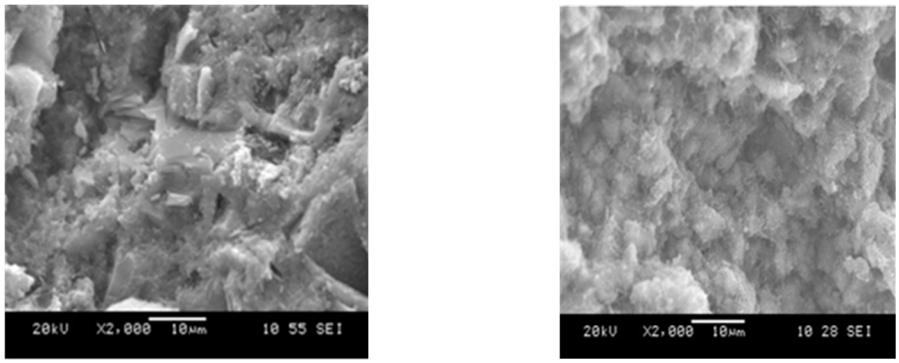


***Figure 14: The hardened cement paste structure under normal maturing at 28 days on the basis of binding medium with left) 50/50 slag and cement proportion, right) 90/10 slag and cement proportion [Schuldyakova et al., 2016]***

Slag incorporation alters the morphology of hydration products due to the modification of C-S-H composition, and it also changes the pore structure in a hardened composite matrix through existence of interweaving thick needles ettringite and capillary pores lower than 10–50 µm which could be filled up with pozzolanic reaction product like C–S–H gel having little density [Siddique, 2008]. The compacted pore structure with smaller porosity is caused by a more considerable amount of C–S–H due to larger slag amounts. Calcium opulent C-S-H is fibrillar in its origin that gradually modifies to a foil-like morphology when the quantity of slag

raises, frequently such the C-S-H shown in alkali-activated matrices. The slag hydration in blended concrete is obvious in Fig. 15 through generation of a darkened hydration rim increasing circularly, opulent in hydration products [Whittaker, 2014].

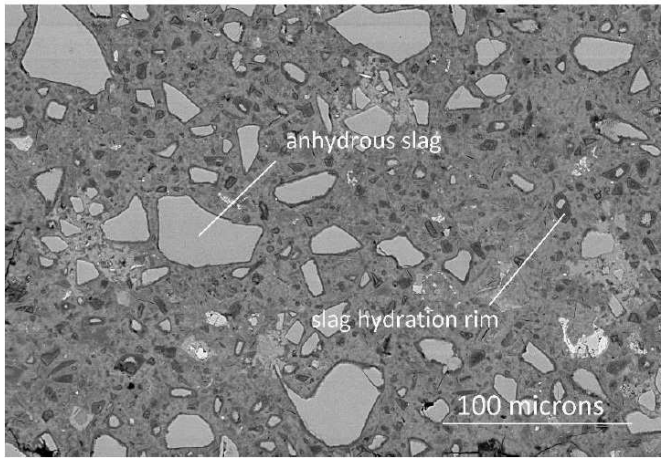


***Figure 15: SEM-BSE micrograph of a slag cement paste, with 70% slag, cured for 180 days [Whittaker, 2014]***

Indeed, the pore structure of AAS system is controlled by the comparatively quick precipitation mechanism of a gel-such C–S–H in the pore space. The internal area between the slag particles is easily quite filled with C–S–H gel after 24 -hours in the case of utilization of high efficient activators like NaOH [Kovtun et al., 2015]. NaOH-activated slag cement comprises a diffuse reaction ring around the hydrating slag particles (most obviously shown in Fig. 16(left)) as well denoting a diffusion-controlled reaction. Compared to the major reaction products in hydrated Portland cement is C-S-H with lower amounts of C-A-S-H and portlandite, the major reaction product of activated slag cement is calcium aluminosilicate-hydrate (C-A-S-H) [Thomas et al., 2016].

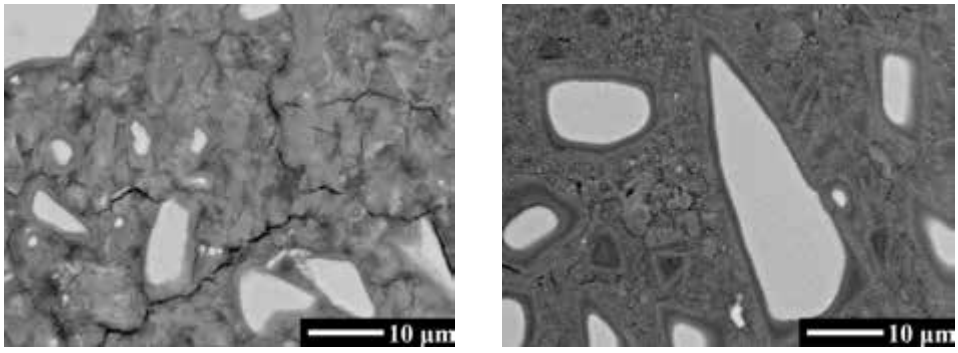


***Figure 16: Microstructure of NaOH-activated slag cement after: (left) 12 hours; and (right) 28 days of hydration [Thomas et al., 2016]***

## 2.4. Porosity

From the porosity standpoint the collateral effect of hydration on UHPC porosity is as the following: With a reason of quite little w/c, the capillary porosity fades and the ITZ is filled up with C–S–H hydrates generated by the pozzolanic reaction of silica fume [Shi et al., 2015]. For instance, the capillary pores turn into discontinuous for UHPC owning w/c=0.2 and only 26% of cement has hydrated in place of 54% for HPC that holding w/c=0.33 [Wang et al., 2015]. Cheyrezy et al. [Cheyrezy et al., 1995] found that cumulative porosity ranged from 3.75 nm to 100 µm and not more than 9% for different formulations of UHPC subjected to various curing methods. The basic formulation consists of: Ordinary Portland Cement (OPC): 1, silica fume: 0.25, sand: 1.1, w/b: 0.12. Some formulations contain crushed quartz (40% by weight of cement) or steel fibres (approximately 2% in volume). The UHPC formulations are: B20°C/SC-basic formulation heated at 20°C, soft cast (setting pressure 1 atm); BQ200°C/SC-basic formulation with crushed quartz heated at 200°C, pressed (setting pressure 625 atm); BF250°C/SC-basic formulation with steel fibres heated at 250°C, soft cast; and BQF400°C/P-basic formulation with crushed quartz and steel fibres heated at 400°C, pressed (setting pressure 625 atm). As shown in Fig. 17, the obtained diminution in cumulative porosity in B20°/SC and B90°C/SC agrees with a lessening in the threshold value while for other mixtures (BQ200°C/SC), the threshold value is quite little and cannot be revealed from mercury intrusion. Hence, the cumulative porosity is ignored (Fig.17).

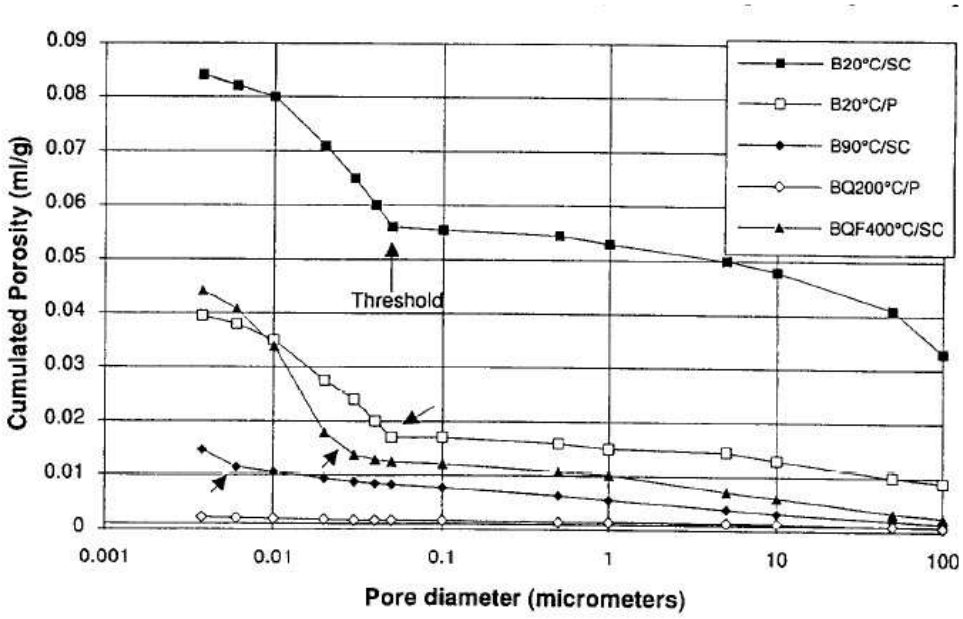


***Figure 17: UHPC cumulative porosity versus pore diameter [Cheyrezy et al., 1995]***

Duan et al. [Duan et al., 2013] found that the incorporation of mineral admixtures like slag achieves a highly compacted ITZ, optimized pore skeleton and plausible pore size

distribution in particular at later ages. Similar observations were indicated by Hadj-Sadok et al. [Hadj-sadok et al., 2011] who reported that the porosity and pore size distribution of blended slag mixtures tend to develop in order to be smaller and finer, compared to the pores of the conventional mixture at 90 days. Zhou et al. [Zhou et al., 2006] observed that when the curing age elongates, the content and size of capillary pores reduce. Furthermore, the gel pores content grows in the first seven days, and after that their sizes make smaller. Likewise, when the replacement level of slag is not more than 70%, the more considerable slag amount attains a finer pore structure and a small C-S-H at a later age. As for slag replacement level exceeding 70%, the microstructure turns into highly porous accompanied with the slag amount augmentation.

The AAS concrete is distinguished through its fine pore skeleton compared to that of conventional concrete. At the same w/b the hydration products have further gel pores, and the mixtures have less capillary pores, leading to small porosity. At later ages the microstructure evolution of hydrating AAS mixtures is controlled through the slow growth. This correlates entirely with the slow strength development at later ages [Chen, 2007]. Rengguang et al. [Rengguang et al., 2015] found that the porosity of blended slag specimens subjected to high temperatures at early age does not efficiently decrease at later ages. At early age the high temperature quickens the reaction of composite binders and generates a compact hydration product shell on the non-hydrated particles. This shell prevents the water migration into the shell and limits the more hydration of non-hydrated binder particles at later age.

## 3. Mechanical performance

On account of the extraordinary compressive strength of UHPC, it has sensitivity to some parameters like quality of cementitious composites, quality of curing (standard or heat treatment), particle size of aggregate, production techniques selected, etc. Richard and Cheyrezy stated for UHPC that if the soft cast and cured at ambient conditions, its compressive strength may reach 200 MPa, and its value might get larger to 800 MPa when the pressure molding is adopted. Hence, the weight of structure that constructed by only UHPC can be diminished by one-third to one-half the weight of traditional reinforced concrete structure under the same load [Corinaldesi and Moriconi, 2012; Yoo and Banthia, 2016]. Mounanga et al. [Mounanga et al., 2012] stated that this advancement in mechanical behaviour could be ascribed by a superior cement hydration and a close granular packing of the UHPC with crushed quartz integration, that introduce a particle size distribution intermediates between the cement and silica fume utilized.

UHPC mixtures with massive use of BFS were studied first in the laboratory since 1993. Among others, Formagini [Formagini, 2005] developed UHPFRC with clinker replacement by

slag. Packing was optimized by means of the Compressible Packing Model of De Larrard [De Larrard, 1999], applied to multiple components with particle size distributions. The mixture had 1011 kg/m$^3$ CP III 40 (30 to 54% slag), silica fume/cement=5.8%, w/b=0.17, 2% fibres 12/0.18 mm, 2.6% wollastonite. HOLCIM developed with EPFL UHPFRC based on slag cement with 20 to 34% clinker. It contained 1277 kg/m$^3$ cement type CEM III B 32.5 N thus maximum 434 kg/m$^3$ clinker, and 95.8 kg/m$^3$ Grey silica fume from Elkem (7,8% mass cement). This strain hardening mix has been applied successfully at the industrial scale in Switzerland since 2006. It is interesting to note that both cited references show UHPFRC mixtures with massive use of slag and a low dosage of silica fume (8 to 10% mass only compared to typically 20 to 26% mass in CEM I bases mixtures from literature), without activation of slag by additional chemicals or thermal treatments, and without detrimental effect on mechanical properties. This effect could be linked to the need of alkalinity to activate slag and the competing pozzolanic reactions between silica fume and slag.

Yazıcı et al. [Yazıcı et al., 2009] observed that there is a higher drop of compressive strength of UHPC mixture G40 (cement=498 kg/m$^3$, silica fume=173 kg/m$^3$, blast furnace slag=332kg/m$^3$, w/b=0.15) at two days when the slag replacement rate reached 40% while at 28 days the compressive strength is so closed to that of reference UHPC (CTRL) as exhibited in (Fig. 18). Moreover, the compressive strength of G40 is close to that of reference UHPC after autoclave curing under 2.0 MPa pressure for 8 hours (210°C). Larger values of compressive strength appear after steam curing (100°C for 3 days) due to the pozzolanic reaction at high temperatures in which lower reactive form of silica in silica fume and BFS shows pozzolanic reaction that normally remains unreacted inert filler under standard curing.

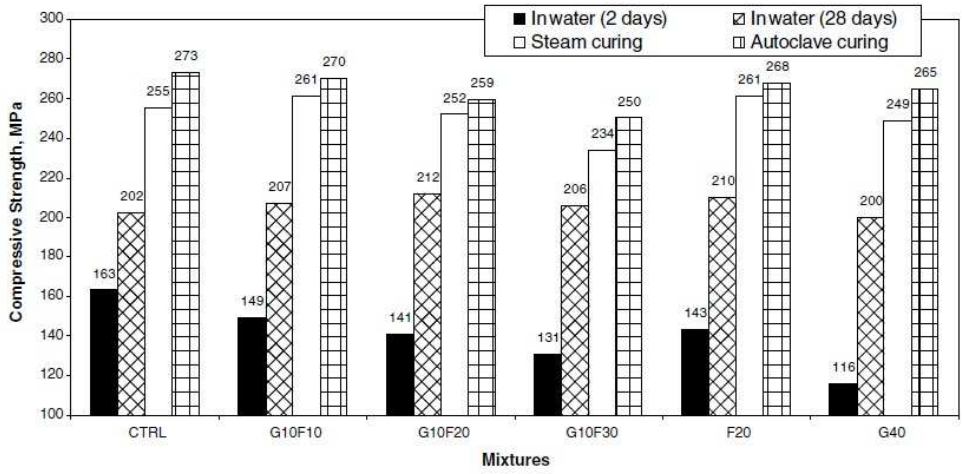


***Figure 18: The influence of GGBFS and/or FA content and curing regime on compressive strength [Yazıcı et al., 2009]***

As for Gupta [Gupta, 2014], a decrease in early compressive and flexural strengths occurred at slag amounts of 40 and 60% in UHPC mixtures ($G_1$, $G_2$) whereas growth in later strength at slag amount of 80% in $G_3$ mixture compared to reference UHPC mixture (CEM I 52.5N, silica fume (10, 15 and 20% by cement, w/b= 0.2) as shown in Fig. 19.

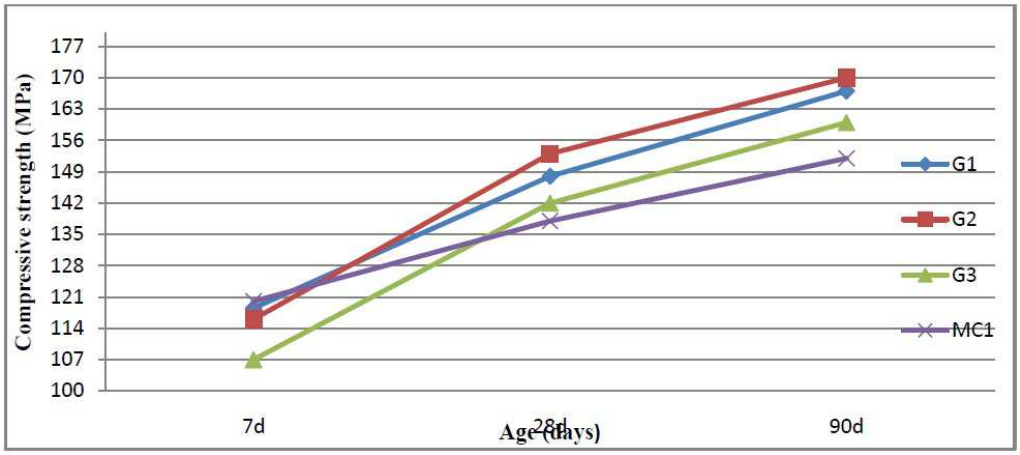


***Figure 19: Strength development of three GGBS mixtures cured by water [Gupta, 2014]***

Also Shi et al. [Shi et al., 2015] found that at three days slag lowered the UHPC compressive strength in particular when the slag content was more than 25%. This early strength reduced from 84 MPa to 78 MPa while at 56 days the compressive strength reached 125 MPa when the slag content raised from 10% to 20% by cement. According to Sajedi and Abdul Razak [Sajedi and Abdul Razak, 2010], it is evident that when the slag substitution level is 40% by weight of OPC mortar (OSM/40) the early strength at three days will be markedly decreased while at later ages higher compressive strength was obtained with 60% slag (OSM/60) compared to the reference mortars (OM-wc and OM-ac) having w/b=0.33, and with both curing types including water and air as appeared in Fig. 20.

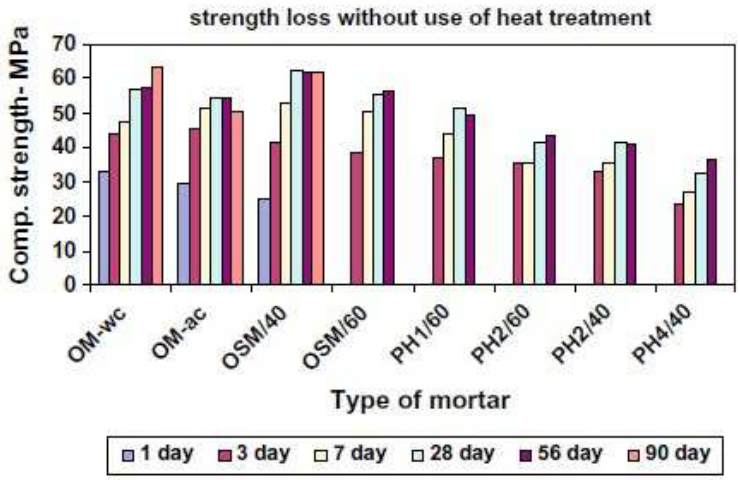


***Figure 20: The relationship between compressive strength versus type of mortar for study of strength loss [Sajedi and Abdul Razak, 2010]***

Activator dosage is considered as one of the factors that influence on the strength of alkali activated slag concrete among other factors [Sajedi and Abdul Razak, 2010]. Bougara et al. [Bougara et al., 2009] show through Fig. 21 that the strength gain of alkali-activated slag mixtures (w/b=0.5, cured at 20°C) is notably lower than that for OPC mortar and does not fulfil the same level of strength even at later age. At early age the strength of slag mortar is lower than 50% of that OPC mortar. Among the two activators used in this investigation, i.e. NaOH and KOH, slag mortar activated by KOH yielded the highest compressive strength at all ages. Enhancing KOH quantity from 2 M to 3 M led to an enhancement in strength but no improvement was noted after this level as observed in Fig. 22. Therefore, the optimum concentration of alkaline agent was found to be 3 M. Sajedi and Abdul Razak [Sajedi and Abdul Razak, 2010] got best compressive strengths at the slag content up to 60% which activated by 1% of KOH. The compressive strength rises with rising of slag glass amount too, mostly as for the later ages. Nonetheless, slag with fully transparent glass does not permanently attain the largest strength.

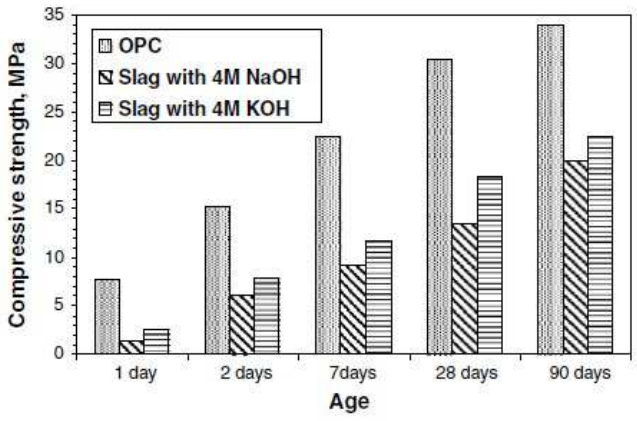


***Figure 21: Effect of the type of activator on the compressive strength [Bougara et al., 2009]***

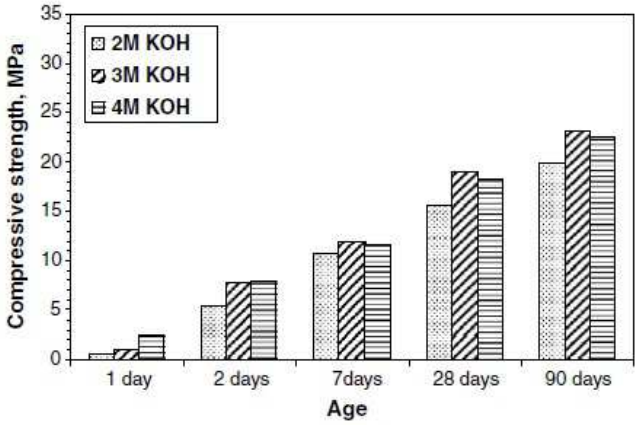


***Figure 22: Effect of alkali dosage of KOH on compressive strength [Bougara et al., 2009]***

Thermal activation is usually used to increase the hydration rate and speed strength development of the blended slag mixtures at early ages [Sajedi and Abdul Razak, 2010]. The main influences are the improved crystallization of the hydrates and activation of pozzolanic reaction. The typical range of temperatures around 80-90ºC is applied for 1-2 days. Several types of researches reported that the heating at 90ºC for 48 hours increases the strength. Throughout this duration, the pozzolanic reactions are quickened to great extent and the microstructure of the hydrated products is mutated to become further denser, even so these products still amorphous. As a result, the compressive and flexure tensile strengths will be higher [Altan et Erdoğan, 2012; Fehling et al., 2014]. Castellano et al. [Castellano et al., 2016] showed that the increase in temperature from 20ºC to 40-60ºC markedly raises early strength. After seven days the crossover effect for compressive strength exhibits in cement, resulting in a less later strength while the temperature increases. This harmful impact is revealed at 28 days for 40% of slag, and it is not noticed for 80% of slag until 365 days. Sajedi et Abdul Razak [Sajedi and Abdul Razak, 2011] noted that at 90days sample with 50% of slag (OSM/50-T-ac) has higher strength compared to the reference (OM-T-ac) by around 12.3% after treatment at 60ºC for 20 hours. Also even seven days the strengths of both mixtures were almost the same. However, the strength of OSM/50-T-ac at 28 days was exceeding than that of (OM-T-ac) by around 6% as shown in Fig. 23. It should note that both mixtures had w/b=0.33, and cured at 28±4°C and relative humidity of 65±20%.

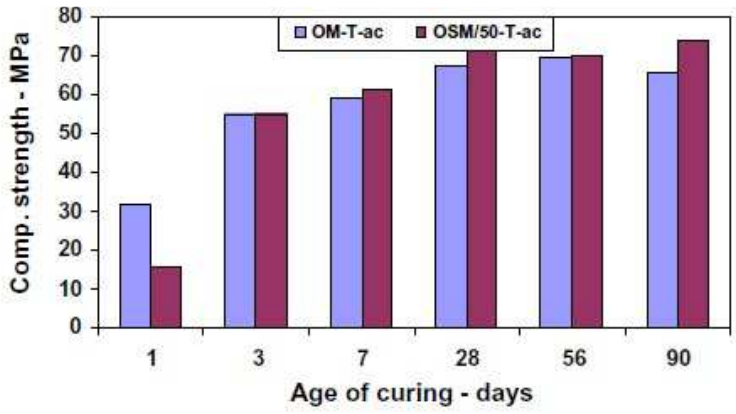


***Figure 23: Variations of compressive strength versus age of curing for OSM/50-T-ac [Sajedi and Abdul Razak, 2011]***

The same thing with Bougara et al. [Bougara et al., 2009] who demonstrated that the temperature increment from 20ºC to 40ºC and 60ºC grew the early strength of mixtures with 30 and 50% of slag whereas the later strength lowered.

# 4. Durability properties

## 4.1. Gas permeability

In the presence of various types of pores in the UHPC from where their size, distribution, shape and continuity, many of these pores give a share in permeability while others do not. During the hydration, the size and continuity of the pores would dominate the coefficient of permeability in the hydrated cementitious matrix. Thereby, UHPC has the least permeability through the small and discontinuous pores existing in the highly homogenous, compacted and dense matrix. As for hydration revenues, the capillary network turned into winding more and more as interconnected pores were closed due to the C-S-H generation which could cause a persistent reduction in coefficient of permeability [Wang et al., 2015]. Mounanga et al. [Mounanga et al., 2012] explained the great difference between the coefficients of gas permeability of ordinary, high, and ultrahigh performance concretes for more than 90 days as shown in Fig. 24. The gas permeability of the UHPCs was quite minimal than the other concrete kinds.

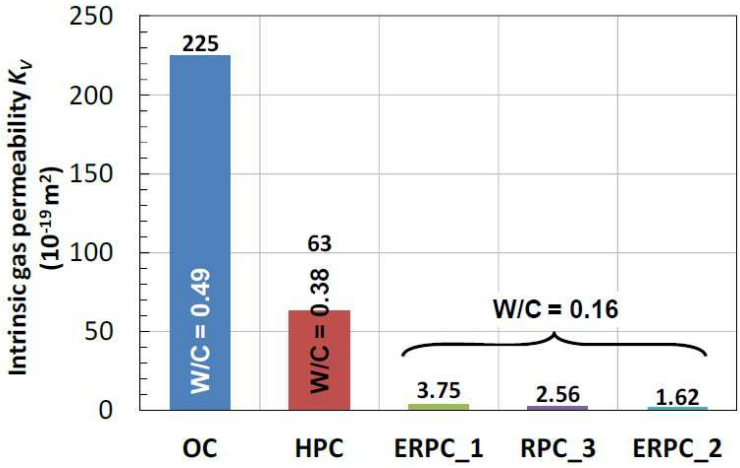


***Figure 24: Comparison of intrinsic gas permeabilities between ordinary (OC), high (HPC), and ultra-high performance concrete (Reactive powder concrete (RPC) & Extrudable RPC) [Mounanga et al., 2012]***

Blended mixtures with slag exhibit a finer pore matrix system than Portland cement mixture [Alamri, 1988]. The microstructure is thus altered as pores are partially filled with C-S-H instead of portlandite. Comprehensive pore size is made smaller and the pores interconnectivity extra tortuous. As a result, the permeability remarkably lowers, aggregate/paste binding strengthens, and hence higher durability [Lamond and Pielert, 2006].

Cheng et al. (cited by [Hossain et al., 2016]) examined the impact of slag contents of 0%, 40% and 60% on the permeability of the concrete specimens. They observed that the

permeability coefficients are $2.56x10^{-13}$, $1.52x10^{-13}$, and $1.32x10^{-13}$ m/s sequentially. Also, they deduced that the more extensive slag content generates highly compacted skeleton and decreases the permeation coefficients of the blended concretes.

The universal finer pore structure connected with slag rate as shown -in Fig. 25, and the increment of the number of smaller pores is accompanied with the slag content raise as well as the total pore size distribution becomes finer [Newman and Choo, 2003].

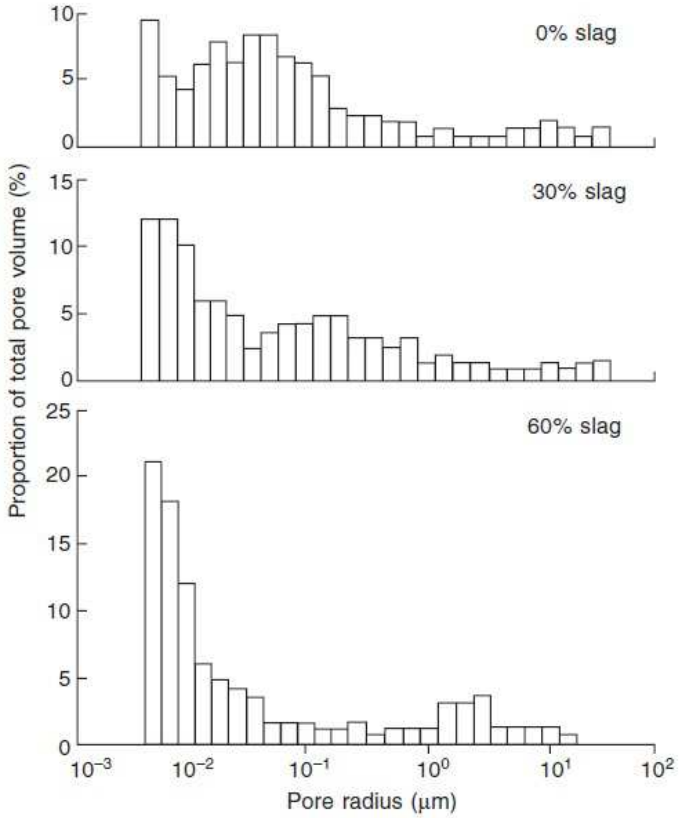


***Figure 25: Influence of slag content on pore size distribution of pastes [Newman and Choo, 2003]***

Al-Otaibi [Al-Otaibi, 2002] noted that the blended mixture with 60% slag had oxygen permeability more than Portland cement mixture (w/b=0.48, moist curing) with a value of $2x10^{-16}$ $m^2$ at 7 days, lowering with age to $1x10^{-16}$ $m^2$ at 90 days. This was ascribed to the latent slag hydration when it keeps during the advanced ages.

Generally, AAS concrete can achieve favorable properties like less permeability and better resistance to brutal attacks if it correctly developed and cured. Nonetheless, these benefits may be differed noticeably from research to another depending on the chemistry between constituents from diverse origins and the alkaline activator concentration. The curing methods (temperature, humidity and duration) among several elements can also importantly affect the reactivity and the phase aggregation of the hardened cement [Provis and van Deventer, 2014; Bernal et al., 2015]. Reddy et Titak [Reddy and Tilak, 2015] deduced that

the activated slag concrete with NaOH (w/c=0.48, 8% $Na_2O$, 4% hydrated lime) exhibits lower permeability among AAS mixtures followed by other chemical activators (sodium silicate-SS8, sodium silicate with hydrated lime-SS8L4, sodium hydroxide-SH8L4, sodium carbonate-SC8) mixtures, that all have more permeability until 28 days (Fig. 26).

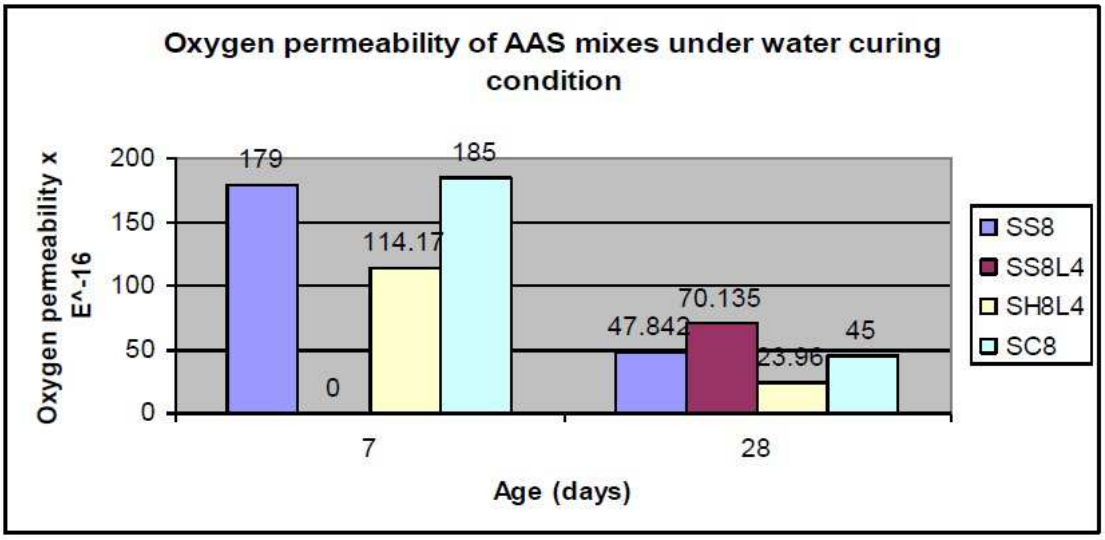


***Figure 26: Oxygen permeability of control mixes at different ages investigated [Reddy and Tilak, 2015]***

The study on the impact of thermal activation of slag on the permeability of concrete has to be related to the pore structure. Bakker established that the blended slag specimens were less permeable than Portland cement specimens for 7 days with heat curing at 80ºC, that were tested at the end of the curing time. The thermally activated slag produces further precipitations between adjacent slag and cement particles. Slag conducts in an opposite way to this, thermal activation what causes smallest permeabilities measured [Alamri, 1988].

## 4.2. Chloride diffusion

Mineral admixtures like slag could ameliorate the chloride penetration resistance of UHPC, and the binder composition is a well-recognized effective element on chloride ingress in the concrete [Wang et al. 2015; Van Noort et al., 2016]. The smaller chloride diffusion coefficient of blended slag concrete is linked with its permeability, i.e. the pore structure (tortuosity and constrictivity) and the fraction of capillary pores. Blending of Portland cement with slag forms a binder which possesses denser microstructure through generating secondary C-S-H, compared to Portland cement matrix [Holthuizen, 2016; Van Noort et al., 2016]. Furthermore, slag significantly enhanced the susceptibility of chloride binding in particular the susceptibility of chemical chloride-binding [Siddique, 2008]. This high susceptibility of the chloride binding is tightly linked to the remarkably lower porosity of the blended slag cement matrix than Portland cement paste [Müller, 2007].

Hussain et al. (cited by [Wang et al., 2015]) observed that the average pore size of Portland cement concrete was 1.57–2 times greater than that of slag concrete due to the potential hydraulicity reaction of slag which in turn boosts the dense cement matrix, and reduces the pore size. Consequently, the diffusion coefficient decreases in conjunction with the blending of higher slag amounts.

Accompanied with augmentation of slag quantity, both of the transmission and elapsed times, where ions of chloride permeate the specimens, were elongated and the inclinations of the steady state periods were reduced. This indicates that when higher slag amounts are blended, the transmission times are quite prolonged and the chlorides ingress is entirely made smaller, Fig. 27 [Yeau and Kim, 2005].

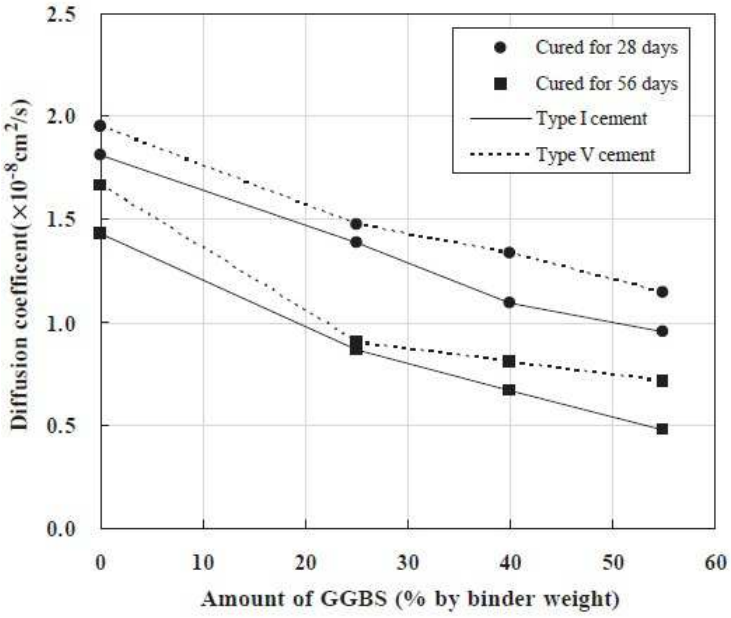


***Figure 27: The diffusion coefficients of chloride-ions in concrete containing slag (w/c=41.8%, water cured) [Yeau and Kim, 2005]***

Yeau et al. (cited by [Zhutovsky and Hooton, 2016]) blended the concrete mixtures with slag amounts of 25, 40 and 55% at constant w/b of 0.42. Regardless of the curing times before exposure, they established that the chloride diffusion reduced with the rise of slag amount in the concrete mixtures, and with the 55% slag having the lowest chloride diffusion coefficient.

A sophisticated pore structure considers as a hindrance to stop the chloride ions diffusion into AAS concrete through existence of quite lower calcium content in AAS composition as compared to Portland cement, and thus it has insufficient chloride penetration [Chi, 2012; Roa-Rodriguez et al., 2014]. Both of performance and reaction of AAS from where the kind and quantity of reaction products which impact the chloride transport behaviour of the material, were affected by several factors including type and dosage of activator, chemical and mineral composition of the slag, temperature and pH. Indeed, the further evolution of

AAS microstructure escorts by higher $Na_2O$% quantity in the activator because of decrease of free cations in the pore solution of the AAS concrete that leads to augment the hydrates amount in the AAS concrete [Chi, 2012].

Numerous studies explored the chloride diffusion of AAS mixtures with various slag rates at room temperature. Roy et al. deduced that the blended mixtures with NaOH-activated slag and KOH-activated slag have steady state chloride diffusion on account of zeolites (aluminosilicate minerals) generation which maintains excellent durability in spite of zeolites presence in the hydration products of AAS is in disagreement as yet [Siddique, 2008]. Bernal et al. [Bernal et al., 2011] have used various slag contents (300, 400, and 500 kg/m$^3$) in the alkali-activated binders and showed that the pore solutions with high concentrations of $Na^+$ and $OH^-$, resulting in enhanced charge transfer (which was indicator of chloride diffusion). Blending cement with high replacement levels of slag achieves a decrease in charge passed more than the amelioration in chloride mobility. A more substantial dosage of each of $Na^+$ and $OH^-$ is ready in the pore solution of AAS binders. The active $Na^+$ ions that filled the pores of the substance should be existing to resist the diffusion of $Cl^-$ ions, therefore, the charge transfer rises as seen in Fig. 28. Likewise, the perfect curing of AAS concrete refines the pore structure of the activated binding system that gives rise to lower the chlorides penetration compared with Portland cement concrete [Hossain et al., 2015].

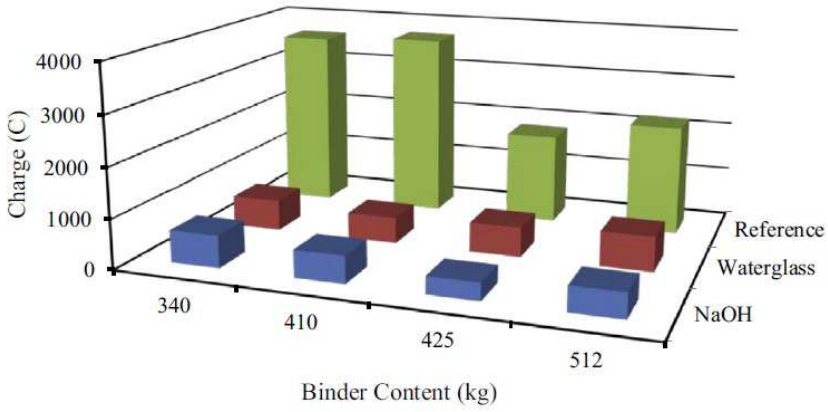


***Figure 28: Charge passed (as an indicator of chloride diffusion) activated slag concretes [Hossain et al., 2015]***

Several researchers highlighted the effect of thermal activation of slag on the chloride diffusion of the blended slag concrete. Chini et al. (cited by [Zhutovsky and Hooton, 2016]) reported that the high temperatures made the durability better of blends containing 50% slag through deficiency of ingress of chlorides and extension of corrosion time when these blended specimens subjected to temperatures of 23, 71 and 93°C for 28 and 91 days. Besides, Acquaye et al. [Acquaye, 2006] remarked that Portland cement mixture (0%BFS) as shown in Fig. 29 exhibited higher chloride penetration values at higher temperatures of 71

and 82°C for 28 and 91 days compared to the quite lower penetration values for the blended mixtures with 50% slag.

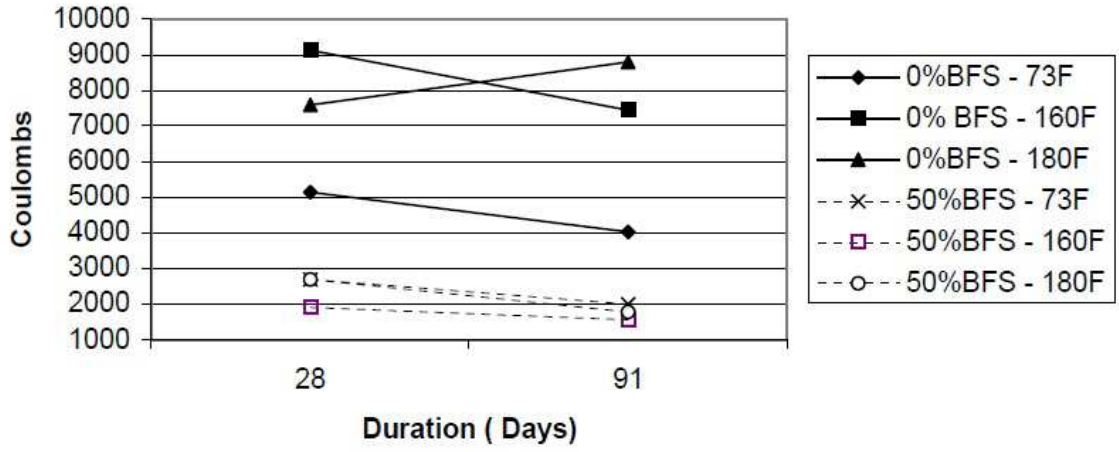


***Figure 29: Chloride ion penetration results for 0% BFS and 50% BFS mixtures (w/c=0.4) [Acquaye, 2006]***

## 4.3. Carbonation

The highly dense interior structure in the UHPC through minimal w/b, fine efficacious particles, and hydrates filling in cement gel pores and tiny cracks diminishes the pore size, alters pore formation, and impedes the carbon dioxide to penetrate into concrete and react with portlandite [Juanhong et al., 2009].

After happening the slag reactions, the pore structure is superfine due to impacts of reaction and filling property of slag, that is helpful in keeping the pore size to a minimum, and making the pore volume porous, then moisture transfer slacks and carbonation depth lessens [Chi et al., 2002; Bertin et al., 2016]. Holthuizen [Holthuizen, 2016] deduced the fact of proportionality of slag content and depth of carbonation after subjection the blended specimens with various slag contents to 3% of $CO_2$ for 23 weeks. Mixtures with slag amounts of 55 and 70% exhibit that the carbonation depth is in connection with the exposure time. For lower slag contents, carbonation depth and time appear to have a linear relationship. Also Holthuizen [Holthuizen, 2016] indicated that blended slag mortar specimens with high slag content carbonate quicker about twice than for Portland cement mortar specimens (w/c=0.5, cured in fog room) (Fig. 30).

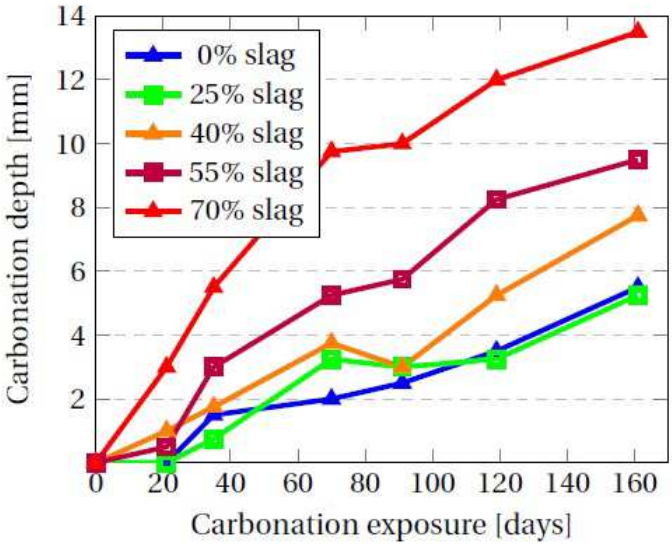


***Figure 30: Carbonation advancement of mortar specimens exposed to 3% $CO_2$ for 23 weeks [Holthuizen, 2016]***

Researchers accomplished on alkali-activated slag concretes, have detected that these substances exhibit likely severe sensitivity to carbonation compared with traditional concrete on account of the divergences in the deterioration mechanism and their pore matrices. Moreover, this conduct which is reliant on the alkali activator quality utilized, becomes further significant when silicates are being used to activate the binder, compared to those activated with another products, like hydroxides, carbonates, and sulfates [Bernal et al., 2011]. According to Puertas et al., (cited by [Hossain et al., 2015]) there is small carbonation in Portland cement concrete while extra profound and intensive carbonation are in AAS concrete after four months. Also NaOH activator attained less depth of carbonation in the activated mixture around 3 mm than that with $Na_2SiO_3$ where the extent reached 10 mm.

Additionally, carbonation could just be blocked by exposing the paste to high humidity during the curing. Therefore, the thermal activation of slag was beneficial for the carbonation resistance of the blended mixtures of the UHPCs despite that impact of the temperature on the blended slag concrete counts on the slag nature. Concrete carbonation ingress of thermally-activating slag specimens is permanently found lower than that of specimens without activation, which reflects that the slag thermal activation is susceptive to enhance the concrete capability of anti-carbonation. Behim et al. remarked that the heat treated mixture with 50% slag at 60ºC, has higher resistance to the action of $CO_2$ than traditional mixture as well as this resistance depends on both duration and conditions of heating. Regourd (cited by [Hu et al., 2015]) showed high densification and compactness in the pore structure of HPC containing slag after exposure to thermal treatment.

### 4.4. Freezing and thawing cycles

According to Voort (cited by [Fládr et al., 2016]), UHPC by its minimal porosity has a resistance to freeze-thaw cycles up to six times in comparison to conventional concrete. Wang et al. [Wang et al., 2015] stated that after 1000 cycles of freezing and thawing, the compressive strengths of regular concrete (RC), high strength mortar (HSM) and reactive powder concrete (RPC) decreased by 57%, 16% and 6% respectively. Thus, the freezing-thawing resistance of RPC was preferable compared to RC and HSM as observed in Fig. 31.

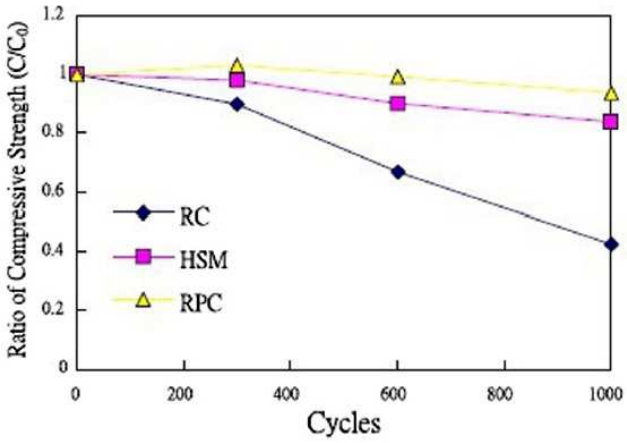


***Figure 31: Ratio of compressive strength of RPC in comparison with RC and HSM [Wang et al., 2015]***

Juanhong et al. [Juanghong et al., 2009] applied curing methods of UHPC specimens (reactive powder concrete-RPC and high-volume fly ash reactive powder concrete-FRPC) that including steam curing at 90°C for 24 hours then the specimens were placed in 90°C hot water till to room temperature for four days, thereafter they were exposed to the freezing and thawing cycles and were taken out after every 100 cycles for measuring mass variation. When the number of cycles of RPC specimens reaches 1600, no obvious cracks on the specimen surface and the mass loss is zero (Fig. 32).

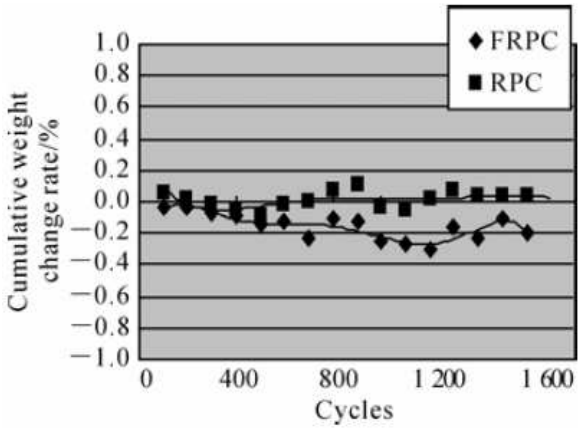


***Figure 32: Mass change of UHPC specimens [Juanghong et al., 2009]***

Graybeal et al. (cited by [Hájek and Fiala, 2008]) showed that both UHPC specimens exposed to steam curing before testing and untreated UHPC specimens, have so limited damage after 690 cycles of freezing and thawing. The UHPC specimens that were untreated, persistent to hydrate and acquired strength through the testing. -In Fig. 33, the results of mass change support that UHPC is quite resistant to damage reasoned by freezing and thawing. The whole systems appeared mass growth throughout the test around 0.2% growth after 125 cycles, compared with the untreated specimens. In the typical experiment of freezing and thawing, specimen will lose mass as it damages. These specimens exhibited extremely low harmful throughout the test. Nevertheless, it pretends that in place of damaging through the cycling, these specimens were taking on water and probably even hydrating [Graybeal, 2006].

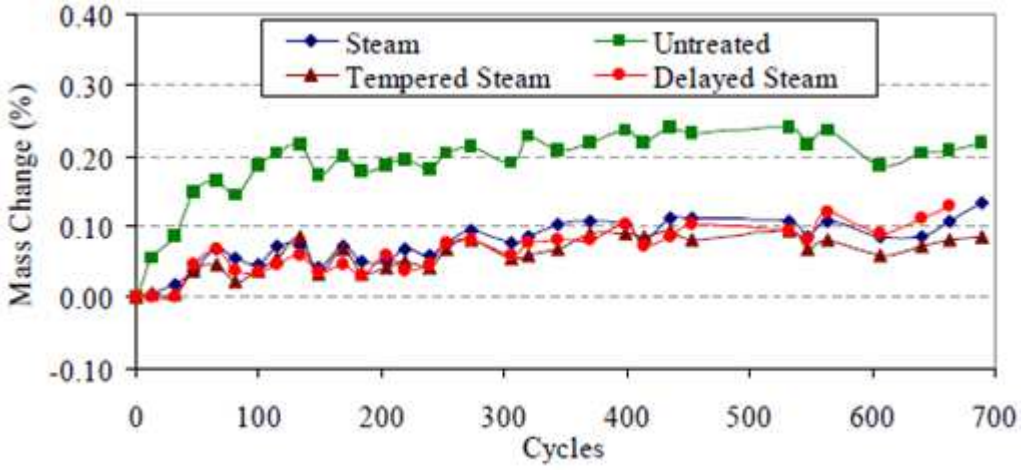


***Figure 33: Mass change of prisms during freeze-thaw testing [Graybeal, 2006]***

Slag has a comparatively proportionate particle size. Hence, air entrainment is commonly no further changing compared to Portland cement concrete. Moreover, the sufficient strength should be evolved in any concrete before the prime freezing cycle and the frequent cycles of freezing and thawing on the basis that the strength development of blended slag concrete is entirely latent at early ages and highly sensitive to the temperature [Lamond and Pielert, 2006]. In the case of substitution of slag, the resistance of freezing and thawing lowers with a growth of slag quantity [Fares, 2008]. The scaling strength of concrete was enhanced when the slag substitution rate ranges from 25 to 35% by cement but it was dropped fastly when the substitution rate exceeds 40%. Even so, slag amount is not the sole parameter governing scaling resistance on the grounds that there are other relevant parameters like curing manners [Seo et al., 2017].

More recently many researchers studied alkali-activated slag concrete establishing significant resistance of freezing and thawing which makes AAS mostly appropriate for application in cold weather with extensive spread of deicing salts [Al-Otaibi, 2002; Thomas et

al., 2016]. Furthermore, the frost resistance of alkali-activated slag concrete is reliant on several parameters including activator kind, pore solution chemistry, porous skeleton, freezing rate, and curing circumstances. Fu et al. (cited by [Najimi, 2016]) utilized an integrated compound of both sodium hydroxide and sodium silicate to improve alkali-activated slag concrete. Also they detected that lower than 1% mass loss after 300 cycles of freezing and thawing; both appearing favorable frost resistance of alkali-activated slag concrete due to the dense matrix of activated concrete made it impenetrable to water breakthrough, and also the large compressive strength that made it durable in negative temperatures. Likewise, Talling et al. (cited by [Provis and Van Deventer, 2014]) found that the usage of Na silicate to activate the slag, achieves granted excellent resistance to freezing and thawing cycles (1000 cycles at +20/-15ºC) compared to NaOH-activated specimens that failed in the range of 200-700 cycles.

## 5. Environmental impacts

For UHPC mix design, the incorporation of higher cement amount reaching 1000 kg/m$^3$ has a negative environmental footprint. The use of high content of superplasticizer to ensure the workability of UHPC increases the environmental impact.

In comparative with ordinary concrete, the environmental impacts of UHPC have to be assessed considering its usage. The latter will govern the structure design and performance and then the concrete's volume. Müller et al. [Müller et al., 2014] compared the environmental impact indicators for Normal Performance Concrete (C30) and UHPC (C190) and highlighted their dependence on the functional unit (Fig. 34). Indeed, considering a volume-based analysis, UHPC has more impacts than NPC particularly in terms of photochemical ozone creation and nitrification potentials. Authors explained this difference by the more abundant cement and superplasticizer amounts and mainly by the steel fibres incorporation in UHPC, compared to NPC. Conversely, when these environmental impacts are studied considering durability properties (Fig. 34 (right)), the use of UHPC seems more interesting than NPC [Müller et al., 2014; Ghafari et al., 2015].

The UHPC technique could contribute to reduce its cost and decrease both embodied energy and $CO_2$ releases [Nematollahi et al., 2012]. According to Voo and Foster [Voo and Foster, 2010], the UHPC retaining wall requests lower embodied energy and emits about 49% less $CO_2$. Furthermore, the UHPC solution decreases by circa 43% the 100-years global warming potential (GWP). This observation contradicts with that of Russel and Graybeal [Russell and Graybeal, 2013] in a study of life cycle assessment (LCA) of bridges that were made according to German standards. In this study, it was indicated that the environmental footprint of UHPC-bridge reached up to 2.5 times that of traditional concrete one. Therefore,

the environmental impacts of UHPC should be lowered through limiting the quantities of Portland cement, steel fibres, and superplasticizer.

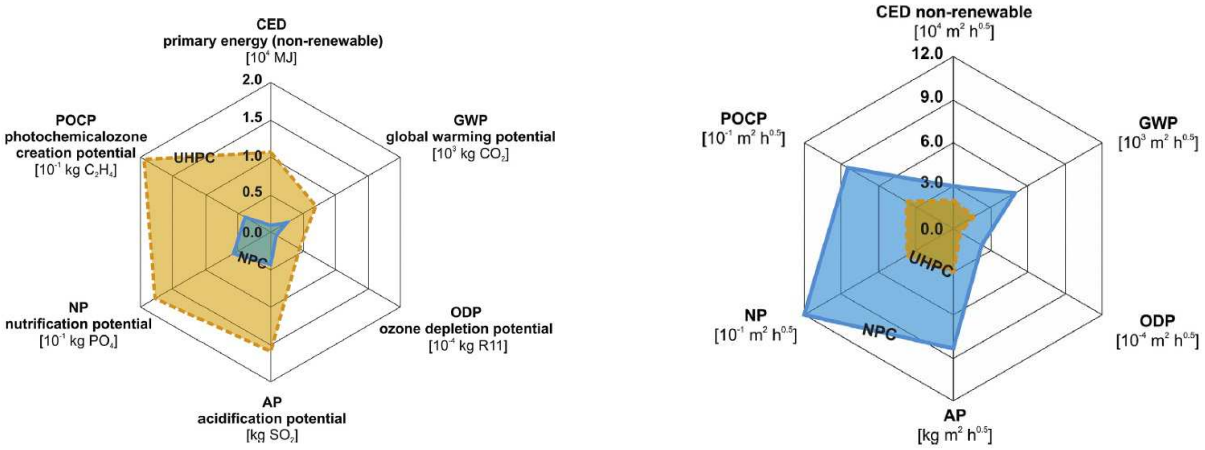


***Figure 34: Comparison of environmental impact assessmentresults in representative UHPC mixtures, (left): Referring to the strengthlevel, (right): Referring to the individual coefficients of water absorption $w_{24}$, NPC = 0.5 kg/(m² $h^{0.5}$) and $w_{24}$, UHPC = 0.05 kg/(m² $h^{0.5}$) [Müller et al., 2014]***

The use of supplementary cementing materials could be considered as exciting alternative for decreasing cement content, making UHPC more sustainable. Yu et al. [Yu et al., 2015] reported that the emission of $CO_2$ increases with the compressive strength (Fig. 35). The latter is proportional to cement content. Authors also showed that for the same compressive strength, the partial substitution of cement with slag, fly ash, and limestone powder decreases embedded $CO_2$ emission compared to other UHPCs.

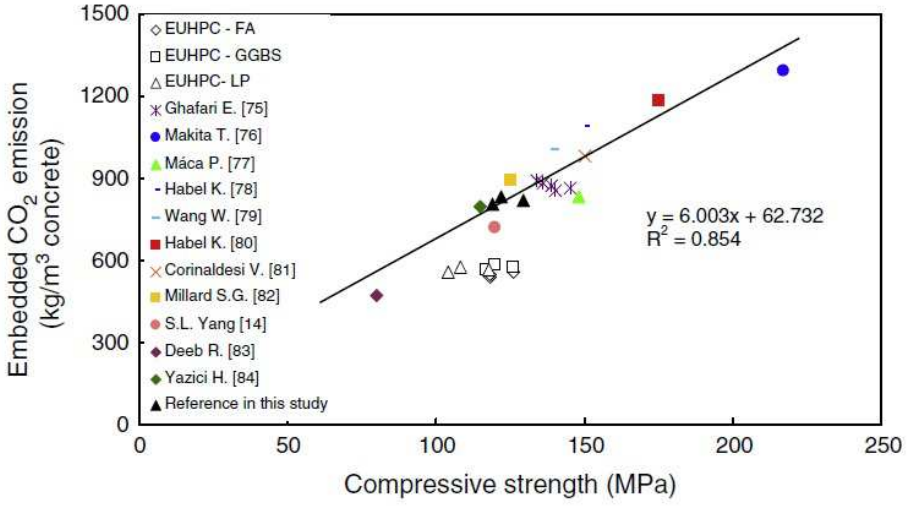


***Figure 35: Comparison of embedded $CO_2$ emission for developed eco-friendly UHPC (EUHPC) and other UHPCs or UHPFRCs [Yu et al., 2015]***

Recently, Kim et al. [Kim et al., 2016] carried out LCA analysis on 1 $m^3$ of UHPCs integrating lower energy intensive ingredients, in comparative with reference one (UHPC-1). Their results were presented in Fig. 36, displayed a noticeable lowering in all environmental impacts when cement is partially substituted. For example, for UHPC-4, where 50% of cement is substituted with slag, renewable primary energy input (PEI), non-renewable PEI, global warming potential (GWP), eutrophication potential (EP) and acidification potential (AP) decrease by circa 31%, 35%, 46%, 7% and 22% respectively.

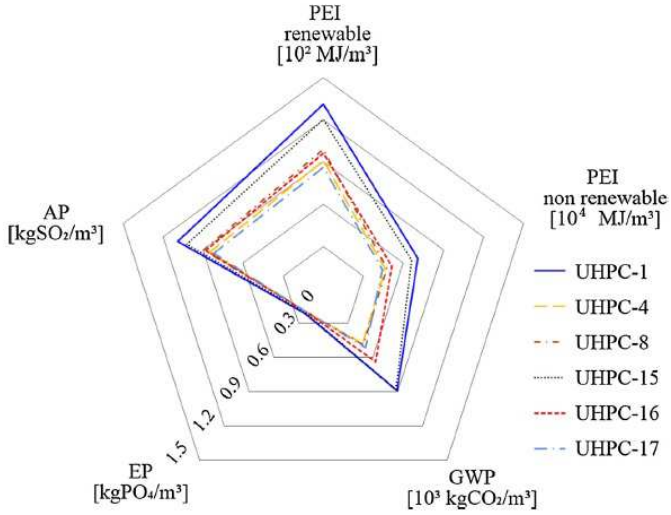


***Figure 36 : Comparison of environmental impacts for different UHPC mixtures [Kim et al., 2016]***

These results agreed with those of Randl et al. [Randl et al., 2014]. The latter observed a considerable decrease of environmental impacts when slag is incorporated as partial substitution of cement in UHPC; 32% of PEI non-renewable, 24% of PEI renewable, 42% of GWP and 20% of AP.

## 6. References

[Abd-El.Aziz et al., 2012] M.A. Abd-El.Aziz, S. Abd.El.Aleem, M. Heikal, Physico-chemical and mechanical characteristics of pozzolanic cement pastes and mortars hydrated at different curing temperatures. Const. Build. Mater. 26 (2012) 310-316.

[Acquaye, 2006] S. Acquaye, Effect of high curing temperatures on the strength, durability and potential of delayed ettringite formation in mass concrete structures, The Graduate School of the University of Florida, Florida USA, Doctoral Thesis, 2006.

[Alamri, 1988] A.M. Alamri, Influence on curing on the properties of concretes and mortars in hot climates, Department of Civil Engineering, The University of Leeds, UK, Doctoral Thesis, 1988.

[Al-Otaibi, 2002] S. Al-Otaibi, Performance of alkali-activated slag concrete, Department of Civil and Structural Engineering, University of Sheffield, Sheffield, United Kingdom, Doctoral Thesis, 2002.

[Altan and Erdoğan, 2012] E. Altan, S. T. Erdoğan, Alkali activation of a slag at ambient and elevated temperatures. Cem. Concr. Compos. 34 (2012) 131-139.

[Bernal et al., 2011] S. A. Bernal, R. Mejía de Gutiérrez, A.L. Pedraza, J.L. Provis, E.D. Rodriguez, S. Delvasto, Effect of binder content on the performance of alkali-activated slag concretes. CemConcr Res. 41 (2011) 1-8.

[Bernal et al., 2011] S. A. Bernal, M. Nedeljković, Y. Zuo, G. Ye, Effect of binder content on the performance of alkali-activated slag concretes. Cem. Concr. Res. 41 (2011) 1-8.

[Bernal et al., 2015] S. A. Bernal, R. San Nicolas, J. S. J. van Deventer, J. L. Provis, Water content modifies the structural development of sodium metasilicate-activated slag binders. Jour Latin-American Ass Qua Con Path Rec Con (ALCONPAT Journal). 5 (1) (2015) 28-39.

[Bertin et al., 2016] M. Bertin, O. O. Metalssi, V. B. Bouny, M. Saillio, Changes in microstructure and pore structure of low-clinker cementitious materials during early stages of carbonation. Proceedings of 2nd International Conference on Concrete Sustainability ICCS16, Madrid, Spain, 2016, pp.1-12.

[Bougara et al., 2009] A. Bougara, C. Lynsdale, K. Ezziane, Activation of Algerian slag in mortars. Constr. Build. Mater. 23 (2009) 542-547.

[Castellano et al., 2016] C.C. Castellano, V.L. Bonavetti, H.A. Donza, E.F. Irassar, The effect of w/b and temperature on the hydration and strength of blastfurnace slag cements. Constr. Build. Mater. 111 (2016) 679-688.

[Chen, 2007] W. Chen, Hydration of slag cement: Theory, modeling, and application, University of Twente, The Netherlands, Doctoral Thesis, 2007.

[Cheyrezy et al., 1995] M. Cheyrezy, V. Maret, L. Frouin, Microstructural analysis of RPC (Reactive Powder Concrete). Cem. Concr. Res. 25 (7) (1995) 1491-1500.

[Chi et al., 2002] J. M. Chi, R. Huang, C. C. Yang, Effects of carbonation on mechanical properties and durability of concrete using accelerated method. Jour Mar Sci Tech. 10 (1) (2002) 14-20.

[Chi, 2012] M. Chi, Effects of dosage of alkali-activated solution and curing conditions on the properties and durability of alkali-activated slag concrete. Constr. Build. Mater. 35 (2012) 240-245.

[Corinaldesi et Moriconi, 2012] V. Corinaldesi, G. Moriconi, Mechanical and thermal evaluation of Ultra High Performance Fibre Reinforced Concretes for engineering applications. Constr. Build. Mater. 26 (2012) 289-294.

[Courtial et al., 2013] M. Courtial, M.-N. de Noirfontaine, F. Dunstetter, M. Signes-Frehel, P. Mounanga, K. Cherkaoui, A. Khelidj, Effect of polycarboxylate and crushed quartz in UHPC: Microstructural investigation. Cem. Concr. Res. 44 (2013) 699-705.

[De Larrard, 1999] F. De Larrard, Concrete Mixture-Proportioning – A scientific approach. Modern Concrete Technology series, N°9, E& FN SPON, Londres, 1999.

[Duan et al., 2013] P. Duan, Z. Shui, W. Chena, C. Shen, Efficiency of mineral admixtures in concrete: Microstructure, compressive strength and stability of hydrate phases. App. Clay. Sci. 83-84 (2013) 115-121.

[Fares, 2008] G. Fares, New cementitious system: the case of glass frit, Department of Civil Engineering, University of Sherbrooke, Canada, Doctoral Thesis, 2008.

[Fehling et al., 2014] E. Fehling, M. Schmidt, J. Walraven, T. Leutbecher, S. Fröhlich, Ultra-high performance concrete UHPC: Fundamentals-Design-Examples, Wilhelm Ernst &Sohn, 10245 Berlin, Germany, 2014.

[Fládr et al., 2016] J. Fládr, P. Bílý, J. Vodička, Experimental testing of resistance of ultra-high performance concrete to environmental loads. Proc. Eng. 151 (2016) 170-176.

[Formagini, 2005] S. Formagini, Dosagem científica e caracterização mecânica de concretos de altíssimo desempenho, Rio de Janeiro, Doctoral thesis, 2005.

[Ghafari et al., 2015] E. Ghafari, H. Costa, E. Júlio, Critical review of eco-efficient ultra high performance concrete enhanced withnano materials. Constr. Build. Mat. 101 (2015) 201-208.

[Graybeal, 2006] B.A. Graybeal, Material Property Characterization of Ultra-High Performance Concrete. FHWA-HRT-06-103, Office of Infrastructure Research & Development, Federal Highway Administration, 2006, pp.1-186.

[Gupta, 2014] S. Gupta, Development of ultra-high performance concrete incorporating blend of slag and silica fume as cement replacement. International Journal of Civil and Structural Engineering Research. 2 (1) (2014) 35-51.

[Hadj-sadok et al., 2011] A. Hadj-sadok, S. Kenai, L. Courard, A. Darimont, Microstructure and durability of mortars modified with medium active blast furnace slag. Constr. Build. Mat. 25 (2011) 1018-1025.

[Hájek and Fiala, 2008] P. Hájek, C. Fiala, Environmentally optimized floor slabs using UHPC-contribution to sustainable construction. Proceedings of the 2nd International Symposium on Ultra High Performance Concrete, Kassel, Germany, 2008, pp.879-886.

[Helmi et al., 2016] M.Helmi, M.R. Hall, L.A. Stevens, S.P. Rigby, Effects of high-pressure/temperature curing on reactive powder concrete microstructure formation. Const. Build. Mater. 105 (2016) 554-562.

[Holthuizen, 2016] P. E. Holthuizen, Chloride ingress of carbonated blast furnace slag cement mortars, Section of Materials and Environment, Delft University of Technology, Netherlands, Master Thesis, 2016.

[Hossain et al., 2015] M.M. Hossain, M.R. Karim, M.K. Hossain, M.N. Islam, M.F.M. Zain, Durability of mortar and concrete containing alkali-activated binder with pozzolans: A review. Constr. Build. Mater. 93 (2015) 95-109.

[Hossain et al., 2016] M.M. Hossain, M.R. Karim, M. Hasan, M.K. Hossain, M.F.M. Zain, Durability of mortar and concrete made up of pozzolans as a partial replacement of cement: A review. Const Build Mat. 116 (2016) 128-140.

[Hu et al., 2015] J. Hu, L.-A. Hou, K. Li, Influence of steel slag on the properties of steam-cured concrete. Proceedings of 2nd International conference on machinery, materials engineering, chemical engineering and biotechnology (MMECEB), Chongqing, China, 2015, pp.141-145.

[Juanhong et al., 2009] L. Juanhong, S. Shaomin, W. Lin, Durability and microstructure of reactive powder concrete. Jour Wuhan Uni Tech-Mater. Sci. Ed. 24 (3) (2009) 506-509.

[Kim et al., 2016] H. Kim, T. Koh, S. Pyo, Enhancing flowability and sustainability of ultra high performance concrete incorporating high replacement levels of industrial slags. Const. Build. Mat. 123 (2016) 153-160.

[Kovtun et al., 2015] M. Kovtun, E. P. Kearsley, J. Shekhovtsova, Chemical acceleration of a neutral granulated blast-furnace slag activated by sodium carbonate. Cem. Concr. Res. 72 (2015) 1-9.

[Lamond and Pielert, 2006] J.F. Lamond, J.H. Pielert, Significance of tests and properties of concrete and concrete-making materials, ASTM International, West Conshohocken, PA, ASTM Stock No.: STP169D, 2006.

[Mounanga et al., 2012] P. Mounanga, K. Cherkaoui, A. Khelidj, M. Courtial, M.-N. de Noirfontaine, F. Dunstetter, Extrudable reactive powder concretes hydration, shrinkage and transfer properties. Eur Jour EnvCiv Eng. 16 (1) (2012) 1-20.

[Müller, 2007] C. Müller, Ground granulated blast furnace slag (GGBS) as a concrete additive-current situation and scenarios for its use in Germany, Technical Report, The Federal Association of the German Ready-Mixed Concrete Industry (BTB), Institute for Building Materials- Research (FEhS), Association of German Cement Works (VDZ), 2007.

[Müller et al., 2014] H. S. Müller, M. Haist, M. Vogel, Assessment of the sustainability potential of concrete and concrete structures considering their environmental impact, performance and life time. Const Build Mat. 67 (2014) 321-337.

[Najimi, 2016] M. Najimi, Alkali-activated natural pozzolan/slag binder for sustainable concrete, Department of Civil and Environmental Engineering and Construction, The Graduate College, University of Nevada, Las Vegas, Doctoral Thesis, 2016.

[Newman and Seng Choo, 2003] J. Newman, B. Seng Choo, Advanced Concrete Technology: Constituent Materials, Linacre House, Jordan Hill, Oxford OX2 8DP, Elsevier Ltd. UK, 2003.

[Provis and van Deventer, 2014] J.L. Provis, J.S.J. van Deventer, Alkali Activated Materials: State of the Art Report, RILEM TC 224-AAM, Springer, 2014.

[Randl et al., 2014] N. Randl, T. Steiner, S. Ofner, E. Baumgartner, T. Mészöly, Development of UHPC mixtures from an ecological point of view. Constr. Build. Mater. 67 (2014) 373-378.

[Reddy et Tilak, 2015] A.N. Reddy, U.V. Tilak, Drying shrinkage and durability studies on alkali activated slag concrete using different activators. Ijirset. 4 (11) (2015) 11483-11492.

[Rengguang et al., 2015] L. Rengguang, D. Shidong, Y. Peiyu, Microstructure of hardened complex binder pastes blended with slag. Jour. Chin. Cera. Soc. 43 (5) (2015) 610-618.

[Roa-Rodriguez et al., 2014] G. Roa-Rodriguez, W. Aperador, A. Delgado, Resistance to chlorides of the alkali-activated slag concrete. Int. J. Electrochem. Sci. 9 (2014) 282-291.

[Russell and Graybeal, 2013] H. G. Russell, B.A. Graybeal, Ultra-High Performance Concrete: A state of the art report for the bridge community. FHWA-HRT-13-060, Office of Infrastructure Research & Development, Federal Highway Administration, 2013, pp.1-171.

[Sajedi and Abdul Razak, 2010] F. Sajedi, H. Abdul Razak, The effect of chemical activators on early strength of ordinary Portland cement-slag mortars. Constr. Build. Mater. 24 (2010) 1944-1951.

[Sajedi et Abdul Razak, 2011] F. Sajedi, H. Abdul Razak, Effects of thermal and mechanical activation methods on compressive strength of ordinary Portland cement–slag mortar. Mater. and. Des. 32 (2011) 984-995.

[Schuldyakova et al., 2016] K.V. Schuldyakova, L.Ya. Kramara, B.Ya. Trofimov, The properties of slag cement and its influence on the structure of the hardened cement paste. Proc. Eng. 150 (2016) 1433-1439.

[Seo et al., 2017] T. Seo, Y. Jung, J. Kim, O. Na, Durability of steam-cured concrete with slag under the combined deterioration of freeze-thaw cycles and de-icing chemicals. Proceedings of the fib. International Federation for Structural Concrete, Structural Concrete. 18 (2017) 75-83.

[Shi et al., 2015] C. Shi, D. Wang, L. Wu, Z. Wu, The hydration and microstructure of ultra-high-strength concrete with cement–silica fume–slag binder. Cem. Concr. Compos. 61 (2015) 44-52.

[Shi et al., 2015] C. Shi, Z. Wu, J. Xiao, D. Wang, Z. Huang, Z. Fang, A review on ultra high performance concrete: Part I. Raw materials and mixture design. Const. Build. Mater. 101 (2015) 741-751.

[Siddique, 2008] R. Siddique, Waste Materials and By-Products in Concrete, Springer-Verlag Berlin Heidelberg, 2008.

[Tam et al., 2010] C. M. Tam, V. W. Y. Tam, K. M. Ng, Optimal conditions for producing reactivepowder concrete. Maga. Conc. Res. 62 (10) (2010) 701-716.

[Thomas et al., 2016] R. J. Thomas, H. Ye, A. Radlińska, S. Peethamparan, Alkali-activated slag cement concrete: A closer look at a sustainable alternative to portland cement. Concr. Intern. 38 (1) (2016) 33-38.

[Van Noort et al., 2016] R. van Noort, M. Hunger, P. Spiesz, Long-term chloride migration coefficient in slag cement-based concrete and resistivity as an alternative test method. Constr. Build. Mater. 115 (2016) 746-759.

[Voo and Foster, 2010] Y.L. Voo, S.J. Foster, Characteristics of ultra-high performance “ductile“ concrete and its impact on its sustainable construction. IES. Jour. Civ. Struc. Eng. 3 (3) (2010) 168-187.

[Wang et al., 2012] C. Wang, C. Yang, F. Liu, C. Wan, X. Pu, Preparation of ultra-high performance concrete with common technology and materials. Cem. Concr. Comp. 34 (2012) 538-544.

[Wang et al., 2015] D. Wang, C. Shi, Z. Wu, J. Xiao, Z. Huang, Z. Fang, A review on ultra high performance concrete: Part II. Hydration, microstructure and properties. Constr. Build. Mat. 96 (2015) 368-377.

[Whittaker, 2014] M. J. Whittaker, The impact of slag composition on the microstructure of composite slag cements exposed to sulfate attack, The University of Leeds, School of Civil Engineering, Doctoral Thesis, 2014.

[Yazıcı et al., 2009] H. Yazıcı, M.Y. Yardımcı, S. Aydın, A.S. Karabulut, Mechanical properties of reactive powder concrete containing mineral admixtures under different curing regimes. Constr. Build. Mater. 23 (2009) 1223-1231.

[Yeau and Kim, 2005] K. Y. Yeau, E. K. Kim, An experimental study on corrosion resistance of concrete with ground granulate blast-furnace slag. Cem. Concr. Res. 35 (2005) 1391-1399.

[Yoo and Banthia, 2016] D.-Y. Yoo, N. Banthia, Mechanical properties of ultra-high-performance fibre-reinforced concrete: A review. Cem. Concr. Compos. 73 (2016) 267-280.

[Yu et al., 2015] R. Yu, P. Spiesz, H.J.H. Brouwers, Development of an eco-friendly Ultra-High Performance Concrete (UHPC) with efficient cement and mineral admixtures uses. Cem. Concr. Res. 55 (2015) 383-394.

[Zhou et al., 2006] J. Zhou, G. Ye, K. van Breugel, Hydration process and pore structure of portland cement paste blended with blast furnace slag. Proceedings of the 6th International Symposium on Cement & Concrete and Canmet, 2006, pp.1-7.

[Zhutovsky et Hooton, 2016] S. Zhutovsky, R. D. Hooton, Effect of supplementary cementitious materials on the resistance of mortar to physical sulphate salt attack. Resilient Infrastructure. (MAT)-742. (2016) 1-11.

# Part 2. Experimental program

# Chapter 4. Testing methods

## Table of Contents



## List of figures

## Résumé

Dans ce chapitre nous présentons les différentes méthodes d'activation et de caractérisation, utilisées dans le cadre de notre thèse. Il s'agit de présenter dans l'ordre :

Les méthodes d'activation : (i) l'activation chimique avec la solution KOH, utilisée pour les bétons à fort dosage en laitiers des hauts fourneaux (LHF) et (ii) l'activation thermique, avec une température de 90°C et une durée de 48 heures, appliquée aux bétons contenant 50% et 80% de LHF ;

- Les méthodes de caractérisation au jeune âge : (i) la maniabilité en mesurant l'affaissement au mini cône, (ii) le temps de prise avec l'essai Vicat, (iii) le dégagement de chaleur en conditions semi-adiabatiques et (iiii) le retrait de séchage avec le rétractomètre à potence ;
- Les méthodes de caractérisation microstructurale : (i) l'analyse DRX sur des échantillons réduits à <63µm, dans le but de quantifier les différents phases (ii) l'analyse thermogravimétrique dans le but de suivre l'évolution des phases en corrélation avec l'avancement de l'hydratation, (iii) la microscopie électronique à transmission, permettant de visualiser la microstructure des échantillons et son évolution dans le temps et (iiii) la porosimétrie au mercure dans le but de quantifier la porosité totale et la distribution porale des bétons étudiés ;
- Les méthodes de caractérisation mécanique : la flexion, la compression et la traction par fendage ;
- Les méthodes de caractérisation de la durabilité : (i) la perméabilité au gaz, grâce à un dispositif spécifique pour les bétons à faible perméabilité, (ii) la diffusion des ions chlore en régime permanant, avec une adaptation de l'essai pour les bétons ultra-haute performance (BUHP), (iii) la carbonatation accélérée avec une concentration en $CO_2$ de 50% et (iii) des essais de gel/dégel pour une durée d'un an.

# 1. Introduction

In this chapter, we present details on the different activation and characterization methods, applied in our research work. Two activation methods are used; chemical and thermal. The first one is applied by adding potassium hydroxide (KOH) in order to compensate for the lack of alkalis when cement is substituted while the second aims at producing blended mixtures of UHPCs with the same performance of reference UHPC at 90 days. The characterization methods include: fresh and early age characterization (min slump flow, setting time, hydration and total shrinkage), microstructural characterization (XRD, TGA, TEM and MIP), mechanical characterization (flexure, compressive and splitting tensile strengths), and durability one (gas permeability, chloride diffusion, carbonation and freezing/thawing). For the latter, existent methods are adapted to assess these properties precisely.

# 2. Activation methods

## 2.1. Chemical activation

The use of mineral additions in particular BFS, decelerates the hydration kinetic of concrete and induces a decrease of its early age properties. Indeed, the substitution of cement decreases the alkalis content of concrete. These alkalis promote the reaction of BFS by destroying its chemical bounds and accelerate its reaction with water and then the development of concrete strength. To compensate for this lack of alkalis, KOH could be added but its addition could affect negatively the environment and concrete rheology, and thus it should be greatly controlled.

Considering the quantity of equivalent sodium oxide $[Na_2O_{eq}]$ brought by cement (0.24%), the quantity of lost alkalis is calculated when cement is substituted with BFS, and then the concentration of potassium hydroxide (KOH) necessary to compensate for these lost alkalis is quantified. Potassium hydroxide is chosen in this study for its compatibility with the thermal treatment. Alkalis coming from KOH are also easily differentiated from those of cement, if necessary, particularly for microscopic observations. The first concentration of chemical activator is called $[KOH]_1$. The calculation method of the latter is presented below, for $UHPC_4$, where 80% of cement is substituted with BFS.

The total quantity of alkalis arising from cement is:

$$[Na_2O_{eq}]_{Total} = Q_c \times [Na_2O_{eq}] \quad \text{Eq.1}$$

Where $Q_c$ and $[Na_2O_{eq}]$ are the cement content and that of alkalis per gram of cement respectively. The latter is given by cement producer, around 0.24% for CEM I 52.5 used.

Thereby, for reference UHPC, the cement dosage $Q_c$ is 977 kg/m$^3$, bringing 2.35 kg/m$^3$ of $[Na_2O_{eq}]_{Total}$.

When 80% of cement is volume-substituted with BFS, the cement content becomes 195.4 kg/m$^3$ bringing only 0.47 kg/m$^3$ of $[Na_2O_{eq}]$. Hence, the loss of alkalis that should be compensated for is 1.88 kg/m$^3$ of $[Na_2O_{eq}]$. The equivalent of this alkalis' dosage can be expressed by number of moles and calculated as the following:

$$n\ (Na_2O_{eq}) = 1.88/([Na]x2+[O]) \quad \text{Eq. 2}$$

Where $[Na]$ and $[O]$ are the molar mass of sodium and oxygen, and are 23 and 16 respectively. Therefore, $n\ (Na_2O_{eq})$ is 30.255 moles and $n\ (Na)$ is 60.51 moles.

Finally, the equivalent quantity of KOH bringing the needed alkalis can be calculated as the following:

$$[KOH]_1 = n\ (Na)\ x\ ([K]+[O]+[H]) \quad \text{Eq. 3}$$

Where $[K]$, $[O]$ and $[H]$ are 39 g/mol, 16 g/mol and 1 g/mol respectively. Therefore, $[KOH]_1$ = 3.39 kg/m$^3$.

This concentration is then increased to two $[KOH]_2$ and three $[KOH]_3$ times to improve the early age compressive strength of UHPC without affecting its workability by maintaining a slump flow of 30 cm. The optimization of this concentration is detailed in chapter5.

## 2.2. Thermal activation

The thermal activation is employed to accelerate the concrete maturity for an equivalent age. The latter corresponds to $t_T = t_x - t_0$, where $t_0$ and $t_x$ are the time of water/binder contact and the theoretical time for obtaining the same level of concrete maturity in the case of conservation at 20°C.

Generally, the level of maturity depends on hydration reactions and their progress degree ($\xi$). The evolution of $\xi$ versus temperature could be approximated by Arrhenius' law applied on all hydration reactions of cement [Regourd and Gautier, 1980]:

$$\dot{\xi} = \frac{d\xi}{dt} = \tilde{A}(\xi)\exp\left(-\frac{E_a}{RT}\right) \quad \text{Eq. 4}$$

Where $A$ is the chemical affinity; $\xi$is the progress degree of hydration reactions; $E_a$ is the activation energy (J.mol$^{-1}$); $R$ is the constant of perfect gas (8.314 J.mol$^{-1}$.K$^{-1}$); and T is the concrete temperature along the test.

To estimate the equivalent age $t_T$ for applied moderate thermal treatments, equation 4 could be integrated between initial ($t_{initial}$) and final ($t_{final}$) times as the following:

$$t_T = \int_{t_{initial}}^{t_{final}} \exp\left[\frac{E_a}{R}\left(\frac{1}{293} - \frac{1}{T(t)}\right)\right].dt \quad \text{Eq. 5}$$

$t_T$ could be approximated as the following:

$$t_T = \sum_{i=1}^{n} \Delta t_i . \exp\left[\frac{E_a}{R}\left(\frac{1}{293} - \frac{1}{T(t)}\right)\right] \quad \text{Eq. 6}$$

Where $t_T$ is the equivalent age for chosen temperature; $\Delta ti$ is the duration of concrete exposure to $T_i$; $T_i$ is the temperature of concrete during $\Delta ti$ (in Kelvin); $E_a$ is the activation energy; and $R$ is the constant of perfect gas.

For simplification, $E_a$ is considered as constant and resulting from all hydration reactions of binder; and the values of $E_a/R$ are 4000 K and 6000 K for CEM I and CEM III respectively [Kazemi-Kamyab, 2013; Francisco, 2014]. For this study, a high BFS content is explored (up to 62% of whole binder). Thus, the binder could be assimilated to composed cement; CEM III. The thermal activation is particularly applied on concretes with high BFS contents ($UHPC_3$ containing 50% BFS and $UHPC_4$ containing 80% BFS) in order to ensure the same long term properties of reference $UHPC_1$ (0% BFS). Therefore, the equivalent age should exceed 90 days.

As shown -in Fig. 1, after 24 hours of casting, the specimens were demoulded and aluminium-wrapped in order to avoid water evaporation along the thermal treatment. The temperature of 90°C was applied for 48 hours before testing UHPC specimens. This results in thermally activated UHPC with equivalent age of 103 days.

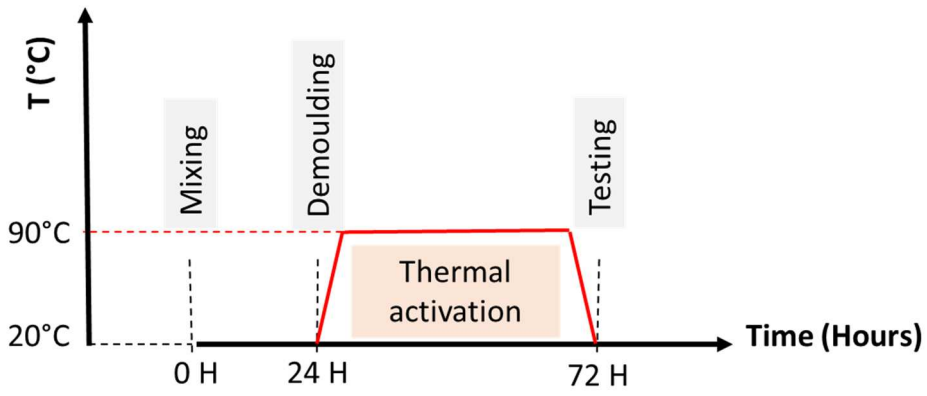


***Figure 1: Thermal activation mechanism applied in the study***

# 3. Fresh and early age characterization

## 3.1. Workability

A mini slump flow test is carried out on different UHPC mixtures according to EN 12350-8 [EN 12350-8, 2008] with small cone ($Ø_1$=5 cm, $Ø_2$=10 cm, l=15 cm) as shown in Fig. 2. The test was conducted at a temperature of 20±2ºC.

***Figure 2: Steps of mini slump flow test***

## 3.2. Setting time

Setting time of the UHPC mixtures is determined according to the standard specification NF P15-431 [NF P15-431, 1994] using Vicat apparatus (Fig. 3). The test was conducted at a temperature of 20±2ºC.

***Figure 3: Vicat apparatus***

## 3.3. Hydration

The hydration test consists of measuring the temperature and heat of hydration of concretes by means of semi-adiabatic calorimetry that known as Langavant method. This method is described in European Standard EN 196-9 [EN 196-9, 2010] as the following: the fresh concrete (approximately 1900 g) is introduced in an insulated flask which is placed

into calorimeter (Fig. 4) in order to quantify the emitted heat in accordance with the development of the temperature. This latter is measured with platinum resistance thermometer and the test is conducted in a regulated room at 20±2ºC.

***Figure 4: Semi-adiabatic calorimeters***

### 3.4. Total shrinkage

The total shrinkage of UHPC is measured on prisms (40x40x160) $mm^3$ according to the standard specification NF P15-433 [NF P15-433, 1994]. The measurements are carried out using a retractometer equipped with digital comparator (Fig. 5). The latter has an accuracy of 0.001 mm.

After demoulding, specimens are stored at temperature of 20±2ºC and relative humidity of 50±5%. The length change amount is measured every day for the first 60 days, once a week from 60 to 90 days, and once a month from 90 to 365 days. The relative deformation ε is calculated by the following:

$$\varepsilon = \frac{\Delta l(t)}{L} = \frac{dl(t) - dl(t0)}{L} \qquad \text{Eq.7}$$

where *dl(t) and dl($t_0$)* are the read measurements on comparator at *t* and $t_0$ respectively. *L* is the length of invar rod.

***Figure 5: Retractometer***

# 4. Microstructural characterization

## 4.1. X-ray diffraction (XRD)

A Bruker D8 X-ray diffractometer in θ–2θ configuration with incident beam monochromator with CuKα radiation (λ=1.54Å) operating at generator voltage of 40 kV and current of 30 mA, -is used for theanalysis. XRD analysis is done at 3 and 90 days. The UHPC specimen is crushed in a percussion crusher and thereafter put in an agate mixture. A surplus of ethanol is appended (to prevent more hydration of the cement and to support grinding) and the mixture is ground by hand to a fine powder (< 63 µm).

## 4.2. Thermogravimetric analysis (TGA)

This test is gathered by a thermal analyzer NETZSCH STA 449 F3 as shown -in Fig. 6 under dynamic nitrogen atmosphere, and is carried out on 250 mg powderedspecimens undergoing a heating from 30°C to 1250°C, applied with a rate of 10°C/min. At testing ages of 3 and 90 days, the specimens were crushed and powdered (< 315 µm) and methanol -is employed for discontinuing hydration.

***Figure 6:Thermogravimetric analyser***

The outputs of the test are the loss in mass per degree Celsius and the differential thermogravimetric (DTG) curves. The mass loss because of the liberation of bound water (H), decomposition of portlandite (CH), and liberation of $CO_2$, is measured in respective temperature intervals and the accurate limits for the temperature intervals are specified counting on the derivative thermogravimetric curves (DTG). The mass loss of bound water through dehydration of some hydrates (C-S-H, ettringite, etc.) occurrs between 180 and 300ºC, corresponding to the dehydration of portlandite occurring between 450 and 530ºC. The decarbonation of calcium carbonate takes place between 700 and 900ºC.

## 4.3. Transmission electron microscopy (TEM)

Both observation and analysis of the specimen are carried out using Transmission Electron Microscope FEI Tecnai G2-20 instrument operating at 200 kV accelerating potential. It is equipped with a filament of lanthanum hexaboride LaB6, a double tilt holder and Gatan digital camera as seen -in Fig. 7. Analysis -is performed by EDAX/EDX spectrometer.

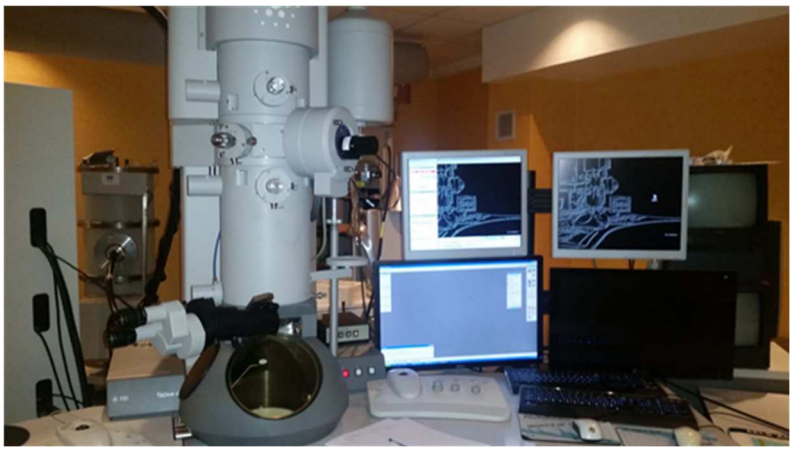

**Figure 7: Transmission electron microscope**

## 4.4. Porosity and pore size distribution

The Mercury Intrusion Porosity (MIP) test is carried out on 1 $cm^3$ specimen at 3 and 90 days, using an Autopore IV porosimeter (Fig. 8). At 3 days specimens are immersed in methanol to stop hydration reaction progress before drying at 105°C and testing.

***Figure 8: Mercury intrusion porosimeter***

## 5. Mechanical characterization

For mechanical properties, fresh concrete is introduced in steel moulds without vibration. The moulds are stored for 24 hours before demoulding. Then the prisms of (40 ×40 ×160) $mm^3$are plastic-wrapped, avoiding any drying and stored in fog room at 20ºC. At 3 and 7 days, compressive strength is measured by means of 300 kN load-machine. Every result is the average of three tests. The splitting tensile strength is carried out on cylindrical specimens of 110 mm diameter by 220 mm height for 3 and 28 days. The specimens are tested using 2000 kN-press machine. For each mixture, two cylinders are tested and the mean value is reported.

## 6. Durability

### 6.1. Gas permeability

Gas permeability is carried out in the GeM laboratory on 5 cm-thick specimens according to XP P18-463 [XP P18-463, 2011] with some modifications in order to assess the extremely low permeability of UHPC at high accuracy. To measure the quite low gas flow through tested specimens, a high precision flowmeter -is used. Fig. 9 shows the permeability device used.

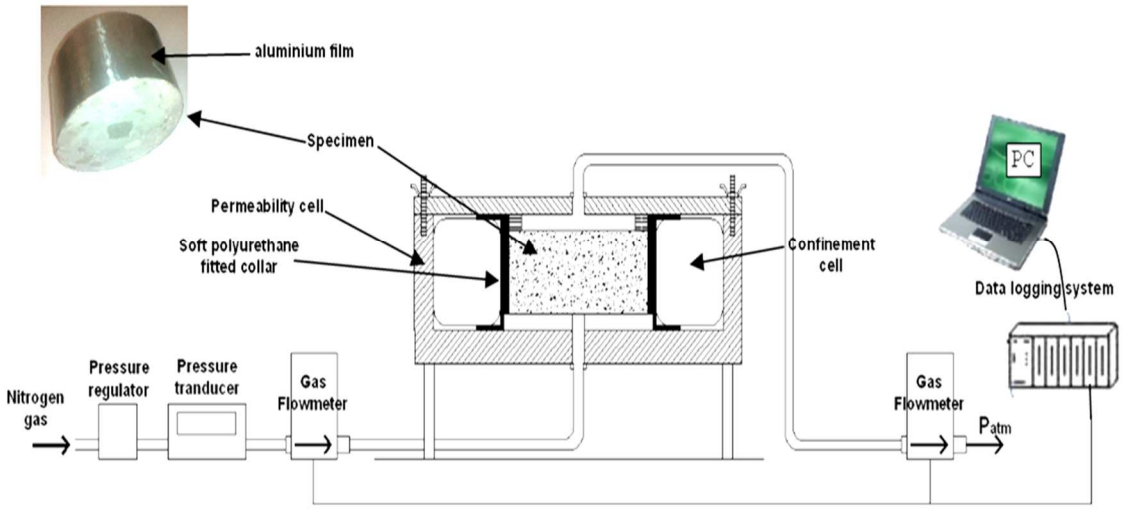


***Figure 9: Schematic layout of the permeability device***

The gas permeability is measured on UHPC discs of 11 cm diameter and 5 cm thickness, aged of more than 90 days, oven-dried at 105°C for several weeks until constant mass (± 0.01 g), and cooled for 48 hours in a desiccator at 20 ± 1°C. The intrinsic gas permeability is determined by a particular set up developed in GeM laboratory with nitrogen as the neutral percolated gas. The testing method consists of applying various differential

pressures on the concrete disc and measuring the steady flow of gas passing through the specimen. The intrinsic coefficient of permeability, as defined by Klinkenberg [Klinkenberg, 1941], -is then calculated assuming a laminar flow, compressible fluid and steady state of flow in the specimen.

## 6.2. Chloride diffusion

A migration test under an electric field has been carried out in non-steady state conditions according to the French standard XP P18-462 [XP P18-462, 2012]. This method allows the determination of apparent chloride diffusion coefficient ($D_{app}$) from the measurement of chloride penetration depth ($X_d$) in the material by the colorimetric method. After cutting the cylinder specimen in three parts the middle one is cut in two specimens with 2.5 cm-thick specimen as exhibited in Fig. 10.

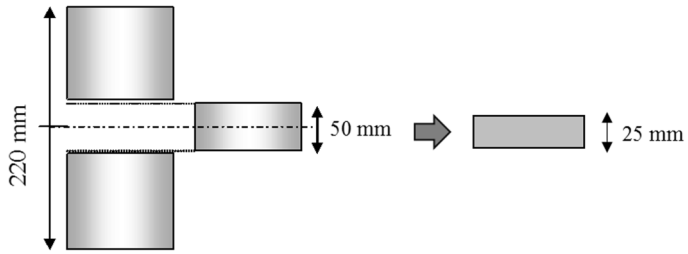


***Figure 10: Disc extraction for chloride diffusion test***

Everyone is saturated with basic solution (NaOH+KOH) for one week using desiccator and vacuum pump (Fig. 11). Fig. 12 explains the different steps ofspecimen's saturation and exhibits the great difference between ordinary/high performance concrete and -ultra-high performance one. Indeed, for the formers, the -specimen's thickness is 5 cm and its saturation lasts through 3 days. In order to ensure its saturation, the UHPC thickness is decreased by two times and its exposure duration to basic solution is extended to one week.

***Figure 11: Vacuum saturation set up***

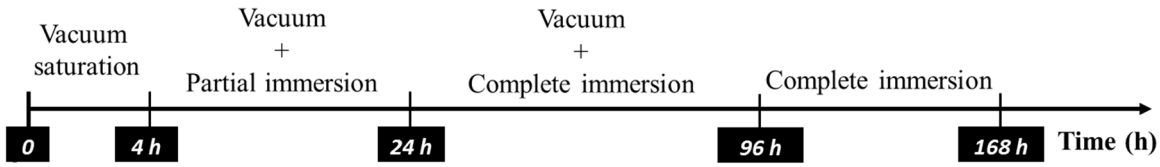


***Figure 12: Saturation procedure of UHPC specimen***

After its saturation, disc is placed between two chambers (Fig. 13) containing solutions of NaOH (0.025 mol/L) and KOH (0.083 mol/L). NaCl (0.513 mol/L) -is added in the upstream solution, and a 30-V potential difference is applied between the two parallel sides of the concrete specimen for at least one month. Then, UHPC disc is cut in two parts which are sprayed by 0.05 M of $AgNO_3$ solution. As a result, white silver chloride precipitation is observed, indicating the chloride depth (Fig. 14). The latter allows the calculation of the apparent chloride diffusion coefficient [Arliguie and Hornain, 2007].

***Figure 13: Chloride migration cells***

***Figure 14: Chloride diffusion depth after spraying by $AgNO_3$***

## 6.3. Carbonation

Accelerated carbonation test is conducted according to the French standard procedure XP P18-458 [XP P18-458, 2008]. For each UHPC mixture, three cube specimens (40x40x40) $mm^3$ are put in the oven at 45ºC for two weeks, then in the climatic chamber for 1 month at 20ºC and 65±5% RH. Thereafter the specimens are put inside the carbonation box as shown in Fig. 15, and subjected to an atmosphere with 1 and 50% of $CO_2$ for six months and 1 year respectively, at 20±2°C and 65±5% RH. Subsequently each specimen -is split to two portions, and the ingress depth -is measured from all sides by the indicator solution (Phenolphthalein $C_{20}H_{14}O_4$) spraying on sections of the split portions. When the solution is applied on the freshly broken surface of UHPC specimen, the edges of the specimen that

remain colourless are considered as carbonated-, and -the depth of carbonation is measured from the edge surface to where that the indicator solution coloured the specimen by purple. The carbonation depth for each specimen can be determined by estimating the average of the depths at 10 different points along the edge of broken surface.

***Figure 15: Carbonation box for accelerated carbonation test***

## 6.4. Freezing-thawing cycles

After their demoulding, UHPC specimens are plastic-wrapped, and stored in fog room at 20±2°C for 90 days. Then, they are subjected to 1000 cycles for one year. As exhibited -in Fig. 16, each cycle is 6 -hours with a temperature variation between 9°C and −18ºC. The resistance of UHPC to freezing and thawing is measured through their mass and length variations. These measurements are carried out on prisms of (40x40x160) $mm^3$ specimens weekly along the first three months, then monthly up to 1000 cycles (one year). Each result of mass and length change represents the average of three readings.

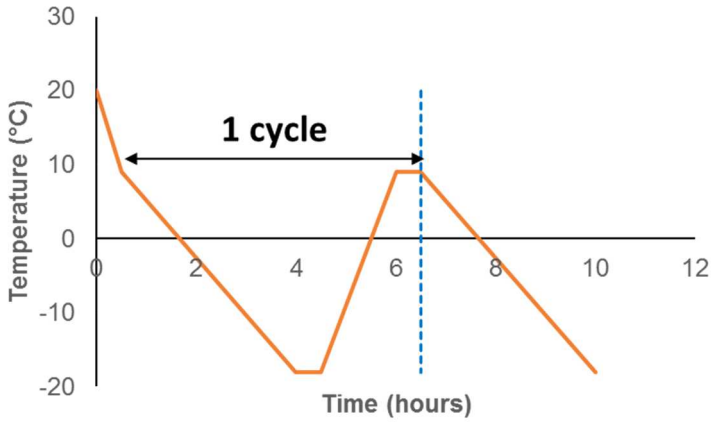


***Figure 16: Scenario of freezing/thawing cycle***

# 7. References

[Arliguie and Hornain, 2007] G. Arliguie, H. Hornain, Grandeurs associées á la durabilité des bétons: GranDuBé, Association Française de Génie Civil, L´école Nationale des Ponts et Chaussées, 2007.

[EN 196-9, 2010] EN 196-9: Methods of testing cement – Part9: Heat of hydration – Semi-adiabatic method, 2010. European Standard.

[EN 12350-8, 2008] EN 12350-8: Testing fresh concrete – Part 8: self-compacting concrete – Slump-flow test, 2008, European Standard.

[Francisco, 2014] P. Francisco, Déformations différées des bétons fibrés à ultra hautes performances soumis à un traitement thermique (in French). Thesis, ENS Cachan, 2014, 134 pages.

[Kazemi-Kamyab, 2013] M. H. Kazemi-Kamyab, Autogenous shrinkage and hydration kinetics of Sh-UHPFRC under moderate to low temperature curing conditions. Thesis, EPFL, 2013, 333 pages.

[Klinkenberg, 1941] J. Klinkenberg, The permeability of porous media to liquids and gases, in drilling and production practice. American Petroleum Institute, New York (1941) 200-213.

[NF P15-431, 1994] NF P 15-431: Hydraulic binders – Methods for testing cement – Setting time, 1994, French Standard.

[NF P15-433, 1994] NF P15-433: Methods of testing cement – Determination of shrinkage and swlling, 1994. French Standard.

[Regourd and Gautier, 1980] M. Regourd, F. Gautier, Behaviour of concretes subjected to accelerated hardening (in French). Journ. of Constr. Mater. 725 (1980) 240-248.

[XP P18-463, 2011] XP P18-463: Concrete-Testing gas permeability on hardened concrete, November, 2011.

[XP P18-462, 2012] XP P18-462: Testing hardened concrete – Chloride ions migration accelerated test in non-steady-state conditions – Determining the apparent chloride ions diffusion coefficient, 2012. European Standard.

[XP P18-458, 2008] XP P18-458: Tests for hardened concrete – Accelerated carbonation test – Measurement of the thickness of carbonated concrete, 2008.

# Part 2. Experimental program

# Chapter 5. Mixture design and early age investigations

## Table of Contents



## List of figures



## List of tables

## Résumé

Dans ce chapitre, nous nous intéressons à la possibilité de réduire l'empreinte écologique du béton à ultra haute performance (BUHP), en diminuant son dosage en ciment, tout en considérant son prix et ses propriétés au jeune âge. De ce fait, une étude préliminaire a été menée dans le but de formuler un BUHP à partir des matériaux locaux. Danc ce béton, la fumée de silice (FS) a été partiellement remplacée par du quartz broyé (QB).

Les résultats de l'étude préliminaire ont montré que :

- l'utilisation d'un malaxeur à haute énergie est nécessaire pour avoir un mélange homogène et maniable. La forme en étoile de la pale et l'inclinaison de la cuve, qui tournent à vitesse très rapide et en sens opposés, permettent un meilleur cisaillement du mélange, malgré son faible rapport Eau/Liant ;
- De par sa composition chimique d'un copolymère acrylique, le polycarboxylate ACP1 permet d'assurer une meilleure maniabilité, parmi les six superplastifiants testés. Grâce à ses longues chaînes, ce superplastifiant est adsorbé sur les particules solides, ce qui permet une diminution de la quantité d'eau et assure une meilleure rhéologie ;
- Grâce à sa forte teneur en carbone, sa forte absorption et sa réactivité élevée, la fumée de silice grise (silicon) améliore la résistance à la compression au jeune âge du BUHP plus que la fumée de silice blanche (zirconium). Cette dernière permet une meilleure maniabilité.

Une fois la formule de référence optimisée, nous avons procédé à la substitution du ciment par des laitiers des hauts fourneaux (LHF), à hauteur de 30, 50 et 80%. La caractérisation au jeune âge des mélanges à base de LHF a montré que :

- Pour un taux de substitution de ciment de 30%, les particules de LHF augmentent la densité, améliorent la maniabilité du béton, favorisent la réaction du ciment et accélèrent la prise. Cela améliore la résistance à la compression du BUHP au jeune âge de 3%. En effet, la nucléation hétérogène dû à la forte surface spécifique des LHF prévaut sur la dilution liée à la réduction du dosage en ciment ;
- Pour des forts dosages en LHF (50% et 80%), l'effet de dilution domine et les particules solides sont très dispersées. De ce fait, plus de temps est nécessaire pour l'hydratation du ciment et le début de prise. Par conséquent, la production de portlandite est ralentie, ce qui retarde la réaction des LHF et diminue la résistance à la compression au jeune âge par 26% et 66% pour BUHP3 et BUHP4 ;
- L'ajout du KOH, à forte concentration, permet de compenser le manque des alcalins et augmente le pH, ce qui favorise la dissolution du laitier et sa réaction. Cela accélère la

réaction d'hydratation, réduit le temps de prise et améliore la résistance à la compression à 3 et 7 jours par 42% et 11%, respectivement ;

En conclusion, un BUHP a été optimisé avec des matériaux locaux. Avec un dosage en LHF à 30%, le dosage en superplastifiant est divisé par deux et la résistance à la compression du béton est légèrement améliorée au jeune âge, sans avoir besoin de l'activer. Cela diminue l'empreinte écologique et le coût de BUHP formulé, en comparaison avec le béton de référence.

Pour un fort dosage en LHF, la résistance à la compression au jeune âge chute et une activation chimique semble atténuer cette chute. Toutefois, une forte concentration de KOH est indispensable, afin de compenser la diminution de résistance, ce qui affecte la maniabilité de BUHP. D'où la nécessité d'explorer d'autres modes d'activation.

# 1. Introduction

This section aims at decreasing the environmental footprints of UHPC by decreasing its cement content and considering its early age properties. The first part of this section is dedicated to the optimization of reference mixture, considering the used materials and mixing method. The second part deals with the effect of BFS content (30%, 50% and 80%) on fresh and early age properties of blended UHPCs, in comparison with reference one. The objective is to design a blended UHPC with the same workability of $UHPC_1$ (0% of BFS), measure its initial and final setting times, assess its reaction heat in semi-adiabatic conditions, and measure its total deformations (shrinkage). Furthermore, the effect of chemical activation is taken into account through these investigations by adding KOH in order to compensate for the lack of alkalis when 80% of cement is substituted with BFS.

# 2. Materials and mix design

## 2.1. Materials used

The materials used in this study are of local origin (France). The cement used is CEM I 52.5 N PM ES (Le Teil´s plant). Its chemical composition is -shown in Table 1. It contains 97% of clinker and 2.8% of gypsum. The mass percentages of principal constituents of main clinker phases, given by Bogue's formula are: 67.8% of $C_3S$, 16.6% of $C_2S$, 4.0% of $C_3A$ and 7.2% of $C_4AF$. This type of cement is chosen because of its highly compressive strength as well as its resistance in aggressive environments containing chlorides, sulfates...etc.

In the current study, four types of mineral admixtures have been considered: Blast furnace slag (BFS) provided by ECOCEM, and two types of silica fumes(SF) including grey type (S95 B DM) and white type (S95 DM). Both types are commercialized by CONDENSIL. The fourth mineral admixture is the limestone filler (Betocarb HP-OG) provided by ORGON. The main physical properties and chemical composition of the cement and all the mineral admixtures are given in Table 1.

Fig. 1 depicts the X-ray diffractograms of cement, Blast Furnace Slag, Grey (silicon) and White (zirconium) Silica Fumes. The figure shows the major phases of cement; $C_2S$ and $C_3S$. The highest peaks of rays are observed at $2\Theta = 34.32°$ for $C_2S$ and $2\Theta = 32.16°$ for $C_3S$. Besides, the XRD patterns of BFS and SF show that they have mainly an amorphous character too. The small peaks on XRD pattern of white SF represent $ZrO_2$. The vitreous aspect of BFS is clearly illustrated by a large halo on XRD pattern at $2\Theta = 29.60°$.

***Table 1: Chemical compounds (mass percentages), fineness and density of materials used***

| | Portland cement (%) | Blast furnace slag (%) | Grey silica fume (%) | White silica fume (%) | Limestone filler (%) |
|---|---|---|---|---|---|
| CaO | 65 | 43.9 | 0.3 | - | - |
| $SiO_2$ | 22 | 37.4 | 95 | 86 | - |
| $Al_2O_3$ | 2.78 | 10.9 | - | > 6% | - |
| $Fe_2O_3$ | 2.42 | 0.7 | - | | - |
| $K_2O$ | 0.17 | 0.24 | - | | - |
| MgO | 0.76 | 6.5 | - | | - |
| $Na_2O$ eq. | 0.24 | 0.46 | 0.08 | 0.15 | 0.005 |
| $SO_3$ | 2.2 | 0.1 | 0.06 | - | 0.001 |
| MnO | 0.01 | - | - | - | - |
| $TiO_2$ | 0.17 | 0.5 | - | - | - |
| Cl- | <0.1 | 0.01 | 0.02 | - | 0.001 |
| $S^{2-}$ | <0.1 | 0.8 | - | - | - |
| Specific area ($cm^2/g$) | 3555* | 4450* | 250000** | 140000** | 4620 |
| Density (-) | 3.17 | 2.9 | 2.24 | 2.20 | 2.7 |

**Blaine method, ** BET method*

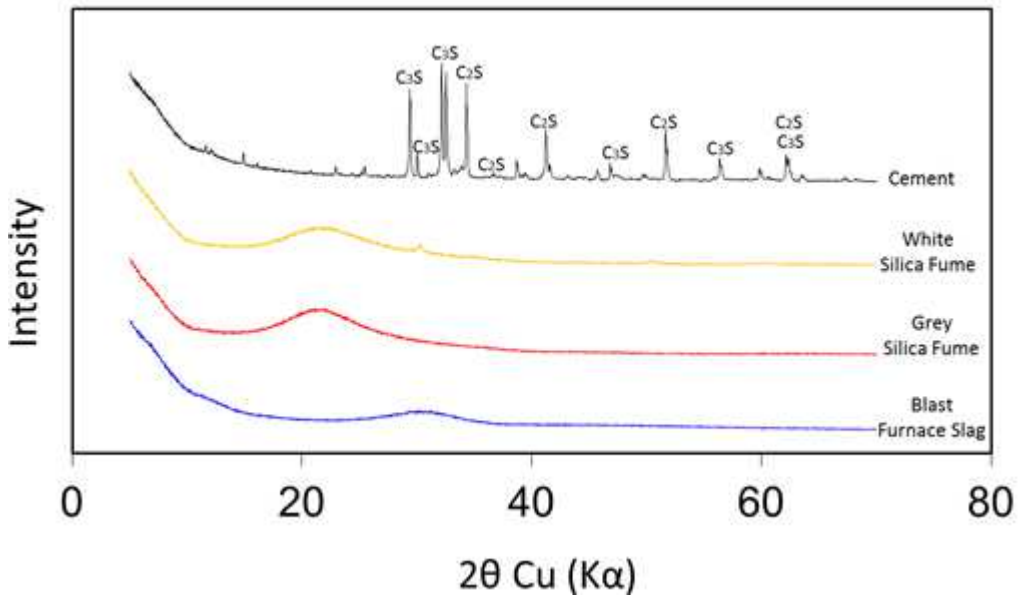


***Figure 1: X-ray diffraction (XRD) patterns of materials used***

Fig. 2 shows a slag particle containing metallic fibres which could be attributed to the iron manufacture (origin of slag in a blast furnace). The EDX analysis (Fig. 3) of this particle confirms the presence of metallic components. According to Fig. 3, the slag particle contains aluminium, silicon, iron, and carbon ions in disordered combination with oxygen, which agrees with the provided chemical composition of slag used [Abdulkareem et al., 2018]. The copper comes from specimen carrier. Generally, the chemical composition of slag influences on its reactivity which enhances with enhancing alkalinity and as well with enhancing calcium, alumina and magnesium amounts, and lowering silica and magnesia amounts [Mounanga et al., 2011].

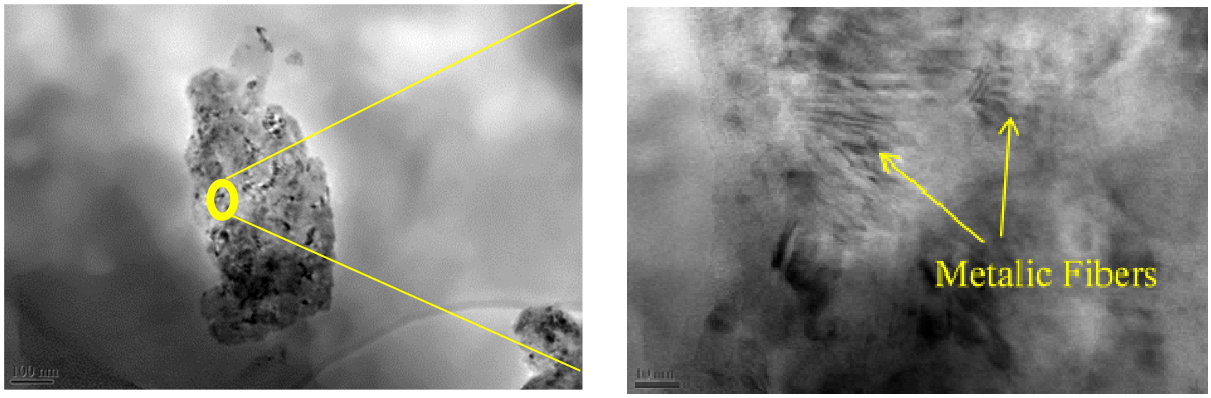


***Figure 2: TEM image of slag particle at 100 nm (left) and 10 nm (right)***

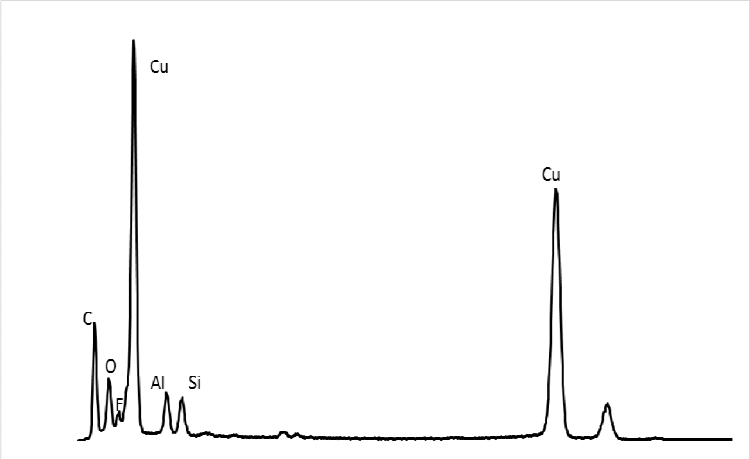


***Figure 3: EDS analysis of slag particle***

Crushed quartz (CQ) is used as a partial substitution of SF, manufactured by Sibelco and marketed as C500 (0–20 µm). It contains more than 99.1% of $SiO_2$ and its specific area and density are 10435 cm²/g and 2.65 respectively. Quartz sand (QS)
containing more than 99% of $SiO_2$, is manufactured by Sibelco and marketed as CV32 (0 – 500 µm). Its specific area and density are 124 cm²/g and 2.65 respectively. Tap water is used for all produced mixtures along this study.

Seven superplasticizers are examined in this research workincluding: Ether Polycarboxylate (EPL), Polycarboxylate (PL), two patterns of Polycarboxylate and Phosphonate (PLPH1 and PLPH2), two patterns of Acrylic Copolymer (ACP1 and ACP2), and Acrylic (AC). All cited superplasticizers are manufactured in France from various companies, and considered as very high water reducers. However, they have different molecular structures which govern their mechanism of action and performance, when they are incorporated in UHPC mixtures. The characteristics of the whole superplasticizers are shown in Table 2.

***Table 2: Basic characteristics of tested superplasticizers***

| Properties | EPL | PL | PLPH1 | PLPH2 | ACP1 | ACP2 | AC |
|---|---|---|---|---|---|---|---|
| Colour | brown | brown | yellow | brown-orange | yellow | light brown | amber yellow |
| Density (-) | 1.05 | 1.08 | 1.055 | 1.08 | 1.085 | 1.06 | 1.09 |
| Solid content | 19.9 | 31 | 30.5 | 29.9 | 41 | 30 | 30.5 |

## 2.2. Manufacture of UHPC mixtures

The basic mixture of UHPC was designed by Cheyrezy et al. [Richard and Cheyrezy, 1995] who eliminated the coarse aggregates to enhance the homogeneity and microstructure of concrete. Mounanga et al. [Mounanga et al., 2012] improved this homogeneity by incorporating crushed quartz as partial substitution of silica fume in the extrudable reactive powder concrete as an UHPC. This optimized mixture of UHPC is shown in Table 3.

In this research work, slag is incorporated as partial substitution of cement to improve concrete packing by providing grains with fineness lying between those of cement and SF. Three levels of volume percentages of slag have been explored (20%, 50% and 80%). The contents of SF, QS, CQ and water are kept constant. Superplasticizer content is adjusted to obtain the same workability of the reference mixture of $UHPC_1$ (0% BFS). This workability is measured through mini slump flow test and fixed at 30 cm for a high flowable UHPC. As mentioned before, the third concentration of $[KOH]_3$ is used to improve the early age performance of UHPC, considering that it should be optimized in order not to affect its workability by maintaining a mini slump flow of 30 cm.

***Table 3: Basic UHPC mix design [Mounanga et al., 2012]***

| Content | CEM I 52.5 PM ES | QS | SF | CQ | SP | Water |
|---|---|---|---|---|---|---|
| Mass ratio | 1 | 1.1 | 0.25 x 3/4 | 0.25 x 1/4 | 1.8% | 0.16 |

Inasmuch of variety of nature, chemical and physical characteristics of the constituents in the basic UHPC mixture showed in Table 3, compared to those used in the current study, preliminary investigations are carried out in order to design UHPC mixture with optimum and harmonic ingredients. These investigations deal with different parameters of mixture design including: (1) Suitable mixer; (2) More compatible superplasticizer; (3) Saturation dosage of superplasticizer; (4) Optimal w/b; (4) Optimal type of silica fume and (5) Optimal mixing time. To justify the sequencing of these investigations, it should be noticed that the choice of Portland cement type is accurate due to its highly mechanical performance besides its highly resistance to aggressive attacks. Thus, the first step consists of checking the compatibility of the used superplasticizer with the combined binder (cement + silica fume + crushed quartz).

Both type and dosage are chosen to reach a required workability of UHPC. This latter is the key parameter for researching the minimum w/b without compromising concrete implementation. The last step of this investigation is optimizing the mixing duration using the more suitable mixer.

Regarding to the mixing procedure of these constituents of UHPC, all the solid compounds are mixed for 30 seconds at slow speed. The superplasticizer is dissolved in net mixing water and added as a liquid solution. The net mixing water depends on the solid content of the used superplasticizer type. Then the solution of water and dissolved superplasticizer is added and mixed with the powders at high speed. The mixing time depends greatly on mixer type, i.e. conventional or high energy one.

When the alkaline activator (potassium hydroxide) is used, the basic solution should be prepared by some hours before, for the purpose of avoiding the increase of temperature resulting from its exothermic reaction. After that the adjusted dosage of superplasticizer is dissolved in this solution (water + dissolved KOH) before its addition to the dry components during the process of mixing. The preparation of all specimens and testing procedures were achieved in a regulated laboratory at a temperature of 20±2ºC.

## 3. Results and discussions

### 3.1. Preliminary investigations and mixture design

The objective of this section is to design UHPC with required workability. The latter depends on used mixer, materials and superplasticizer type and dosage. These parameters have to be checked, in relation with used binder. Then the mixing duration should be optimized.

#### 3.1.1. Suitable mixer

The first step of this work is to test a conventional mixer. The tested mixture is that designed by Mounanga et al. [Mounanga et al., 2012] as shown in Table 3 where the used cement and white silica fume are replaced with cement and grey silica fume. After 30 min of mixing, there is no cohesion between the grains and the mixture is not homogeneous for two reasons: i) Low speed of mixer and ii) Geometry of its blade. Therefore, the mixer does not produce enough energy to promote the particles dispersion, and its blade does not provide high shear stress to disperse the dry powders and homogenize concrete mixture. These observations agree with those of Parant [Parant, 2003] and Cherkaoui [Cherkaoui, 2010]. The former concluded that the conventional mixer is not suitable with fibred UHPC because of its blades which agglomerate the fibres, and the mixing time is increased. For the latter, more than 20 min are necessary to reach the required workability of UHPC containing white silica fume. Therefore, to avoid this problem, despite the low water-to-binder ratio, a mixer with high energy (Eirich intensive mixer) is used as shown in Fig. 4. It has a star-blade, tilted drum, and

high mixt speed of up to 40 m/s (opposed currents). This results in optimum dispersion of particles, and high mixt homogenization with low mixing time [Parant, 2003; Schachinger et al., 2004].


***Figure 4: Eirich intensive mixer used***

### 3.1.2. Superplasticizer/ binder compatibility

UHPCs are designed, not only to have high mechanical performance (loww/b) but also to be highly densified and workable. Their workability should be managed to ensure their properties in the site. Indeed, the rheological properties of concrete are responsible on its mechanical and durability ones. In recent study, Choi et al. [Choi et al., 2016] reported that one of the interesting methods for estimating the rheological properties of UHPC is mini slump test. This simple method is applied in this section to compare between different superplasticizers examined as stated before. For all superplasticizers, the same dosage of 3% (solid content, per gram of cement) is applied. This content is chosen to exceed the saturation dosage significantly [Parant, 2003]. Beyond this content, the concrete workability will not be improved surely.

Fig. 5 shows the mini slump flow of reference $UHPC_1$ with w/b of 0.14 for the examined superplasticizers. Two groups can be distinguished; the first group including (PL, PLPH2 and AC) with a mini slump flow around 15 cm, and the second group including (PLPH1, EPL, ACP1 and ACP2) with a mini slump flow exceeding 25 cm. In this group, ACP1 and ACP2 achieve the required workability of 30 cm.

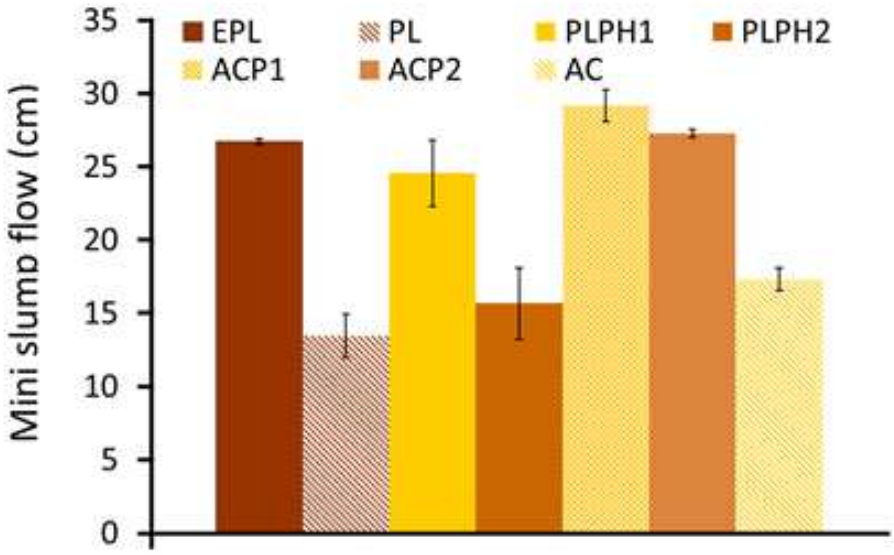


***Figure 5: Mini slump flow measurements of examined superplasticizers***

Generally, the chemical and physical behaviour of superplasticizer is dominated by length, degree of polymerization and the density of graft chains [Boukendakdji et al., 2012]. Thanks to their polymer structure and polyoxyalkylene side chains, ACP1 and ACP2 induce better cement dispersion, which makes a steric repulsion through sets of anionic carboxylic [Ferrari et al., 2007]. The graft chains of the polymer molecules on the surface of the cement grains would prevent by themselves through flocculating these grains into large and irregular agglomerates. Once the side chain density reduces, the adsorption of molecules enhances. Aside from that the molecular weight of these superplasticizers has a fundamental impact on their functions due to that when the molecular weight in polymers becomes larger, both the adsorption and workability are relatively increased [Palacios et al., 2009]. Consequently, the shorter the major chain and the longer and further plentiful the side chains, the larger and extra enduring workability [Puertas et al., 2005; Zingg et al. 2009].

To choose one of the superplasticizers (ACP1 and ACP2), they are examined at a same dosage of 3% in terms of the mini slump flow at w/b ratios of 0.12 and 0.14, and the 7-days compressive strength at w/b of 0.14 as shown in Table 4.

***Table 4: Comparison between ACP1 and ACP2***

| SP | Mini slump flow (cm) at w/b=0.12 | Mini slump flow (cm) at w/b=0.14 | 7-Days compressive strength (MPa) |
|---|---|---|---|
| ACP1 | 20 | 30 | 120 |
| ACP2 | 0 | 27 | 113 |

For a w/b of 0.14, ACP1 gives the higher slump flow which results in best dispersion of binder particles, and thus better homogeneity and packing. This explains the improvement of UHPC compressive strength (at 7 days), compared to UHPC based on ACP2. This difference is more important for lowerw/b. For w/b of 0.12, ACP2 does not allow any cohesion between particles, and therefore the measured slump flow is zero. Despite the decrease of workability of UHPC containing ACP1 at w/b of 0.12, the manufacture of UHPC is possible. This superplasticizer is marketed as Sika Viscocrete Krono 20 HE.

### 3.1.3. Saturation dosage of superplasticizer

The assessment of saturation dosage of the superplasticizer ACP1 must be carried out by examining wide range of dosages (0.5 to 5%), as demonstrated in Fig. 6. At each dosage the workability should be checked by measuring mini slump flow, and the test is carried out on mixtures with w/b of 0.14.

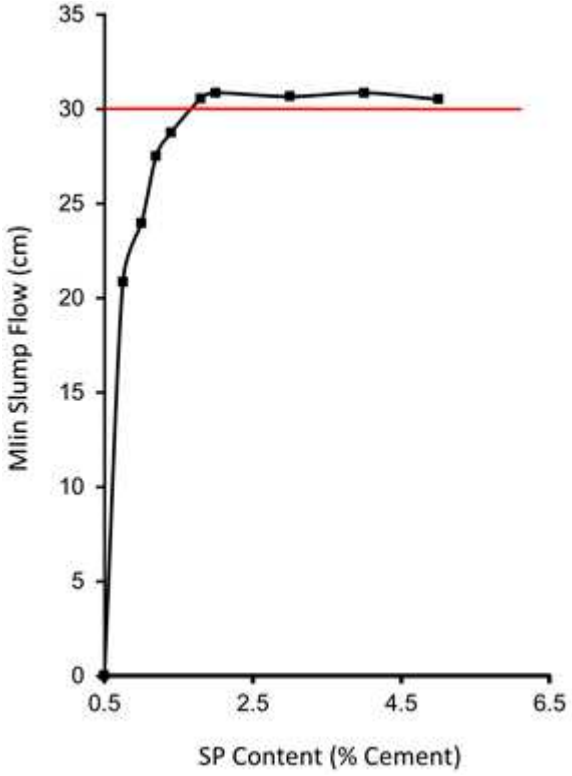


***Figure 6: Assessment of saturation dosage for superplasticizer ACP1***

From the figure shown, it was shown that beyond a content of 3% of superplasticizer, no remarkable improvement in UHPC workability could be noticed, confirming the suitable choice of this dosage that used to compare between all superplasticizers. Secondly, it was found that the saturation point of the superplasticizer ACP1 is 1.8%. This content relies on the active substances (i.e. solid content) in the superplasticizer that maintain the required mini slump

flow of 30±1 cm. The solid content of ACP1 is about 41% which is located within the empirical range of 30-45% for the effectual superplasticizers in the UHPC [Fehling et al., 2014].

### 3.1.4. Water-to-binder ratio

In order to obtain UHPC mixture with accepted properties, it is substantial to explore the optimal w/b. Water/binder and workability of UHPC have so far closed linkage due to that the flowability of the binder paste is quite impacted by the mixing water quantity, therefore the w/b is tested within the range of 0.10-0.18 so as to choose the optimum value as shown in Fig. 7.

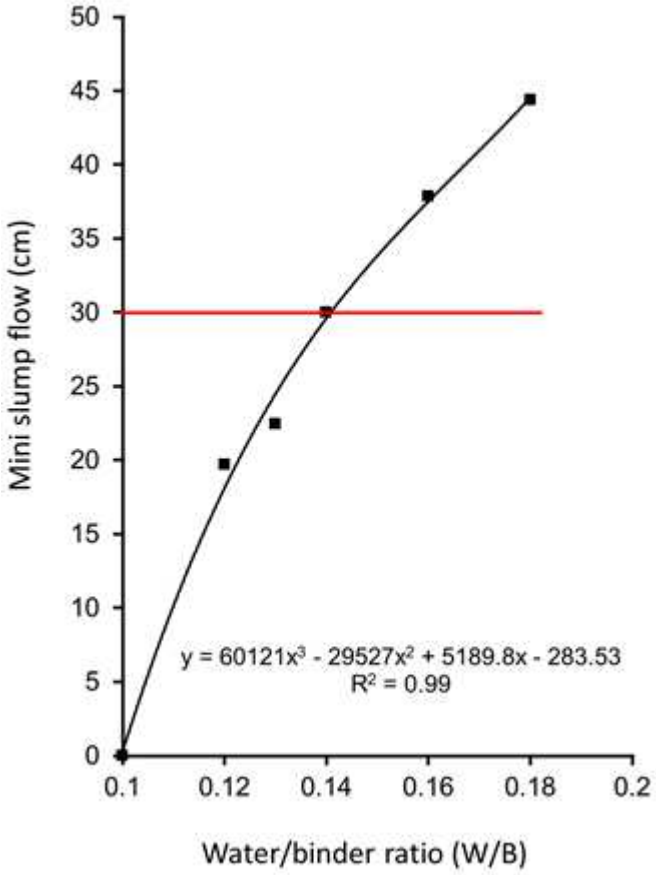


***Figure 7: Assessment of the optimum w/b for reference UHPC***

For high w/b (0.16 and 0.18), the slump flow of UHPC exceeds 37 cm. As packing density and workability are intimately attached, the high workability of concrete could increase the volume of capillary pores which results in compressive strength decrease [Kim et al., 2015]. Thereby, w/b is decreased to 0.14 (w/c = 0.175) to obtain a slump flow of 30 cm. At this value of w/b the matrix packing density is optimum and the mixture does not exhibit any bleeding or segregation. For lower w/b, the slump drops greatly and the matrix packing is not ensured. This might affect negatively the properties of UHPC [Fehling et al., 2014; Šerelis et al., 2015].

### 3.1.5. Type of Silica Fume

Two silica fumes were tested for comparison. The first one is silicon SF with 95% ±3 of $SiO_2$ whereas the second is zirconium SF with 86% of $SiO_2$. The physical and chemical characteristics of both SF are shown in Table 1. They are compared through workability and 7-days compressive for SF-to-cement mass ratio of 25% × 3/4 (the other quarter is crushed quartz), w/b of 0.14 and with 1.8% of ACP1. Results are presented in Table 5.

***Table 5: Comparison between grey and white silica fumes***

| Silica fume | Mini slump flow (cm) | 7-Days compressive strength (MPa) |
|---|---|---|
| Grey silica fume | 29 | 119 ± 1.80 |
| White silica fume | 33 | 113 ± 2.1 |

The chemical composition of silica fume, its specific area and its degree of agglomeration have a remarkable effect on the workability of UHPC mixtures and their mechanical properties [Mounanga et al., 2011]. In particular, the amount of carbon and alkali impurities has a great effect on superplasticizer adsorption and then on concrete fluidity [Sadrekarimi, 2004; Sakai et al., 2009].

As indicated by its colour, the grey silicon SF contains more carbon than the white zirconium one. Carbon adsorbs the superplasticizers and hinders adsorption of grey SF particles, which results in workability decrease by 12%. This result agrees with that of Coppola et al. [Coppola et al., 1996]; an increase by 29% of w/b in UHPC containing grey silica fume was necessary to reach the same flow table of UHPC containing the white one. They explained this difference by the high dispersibility of white silica fume even in absence of superplasticizer, compared to grey one. Although the grey SF has a negative effect on UHPC workability, it improves its 7-dayscompressive strength by 5%, compared with white SF. The high reactivity of grey SF and its high specific area justify this outcome. Indeed, grey SF consumes more portlandite, which promotes the development of more strong C-S-H, and improves the bond between cement and quartz sand. Aside from that the physical filler effect prevails at early age while the pozzolanic one dominates in long term. This results in microstructure refinement and compressive strength increase [Rougeau and Borys, 2004; Shihada and Arafa, 2010]. In contrast, the white type has lower pozzolanic reaction which decelerates the compressive strength development at early age. The hydration products are not sufficient to bridge various particles together. Therefore, several particles were still disconnected and could move readily.

These obtained results agree with those of Serelis et al. [Šerelis et al., 2015] and Coppola et al. [Coppola et al., 1996]. The former showed the high amount of portlandite consumed by SF

particles with high specific area, reflecting their reactivity and occurrence of the delay in compressive strength development when white silica fume is used.

Despite negative effect of grey SF on UHPC workability, compared with white SF, the former is more reactive and has better effect on early age compressive strength. As mentioned earlier, the objective of this research is to develop eco-friendly UHPC with high content of BFS, so the risk is the drop of early age mechanical properties of UHPC. In addition, the production of white SF is no longer available in France and its usage increases the environmental foot prints of concrete due to its important delivery distance. For these reasons, grey SF is utilized in this study.

### 3.1.6. Optimum mixing time

The mixing time is a basic parameter for obtaining a steady and workable UHPC, and inasmuch of its extreme prominence, it should be assessed accurately to avoid the high consumption of mixer energy as possible without changing the flowability of the produced UHPC mixture. The wide range of mixing times depends on several variables such as mixer quality, mixing procedure, batch size, level of mixer filling, temperature, etc [Russell and Graybeal, 2013; Fehling et al., 2014].

In this section, the reference UHPC mixture is tested at three mixing times, for a required workability of 30 cm. For all tests, the mixing of dry powders lasts 0.5 min with low speed. The obtained results of total mixing time are presented in Table 6, and indicated that: i) A 3.5 min are sufficient to produce UHPC with mini slump flow of 30 cm, and ii) Beyond this mixing time, no improvement of concrete workability was taken place.

***Table 6: Examined mixing times of UHPC mixture***

| Mixing time (min) | Mini slump flow (cm) |
|---|---|
| 3.5 | 30±1 |
| 4.5 | 31 |
| 5.0 | 31 |

## 3.2. Workability

The workability of UHPC is measured through mini slump flow test. This simple method, that could be used in laboratory and in the site, is applied in this section to estimate the required content of superplasticizer for the UHPC mixtures containing slag in order to achieve the same workability of reference one ($UHPC_1$). Table 8 reports the obtained dosage of SP for every studied UHPC. Even if for all blendedmixtures of UHPC, the required SP dosage to reach 30 cm-slump flow does not exceed that of reference concrete (SP=1.8%), concretes behave differently. Their properties depend greatly on BFS content. For $UHPC_2$, the substitution of 30% of cement induces a drop of SP content (-58%) to achieve the mini slump flow of $UHPC_1$.

Two phenomena, occurring simultaneously, can explain this drop: i) the decrease in the amount of $C_3A$ available to adsorb and consume admixture, and ii) the improvement of packing and then the particles' cohesion and viscosity. Indeed, decreasing of cement content decreases $C_3A$ amount, and thus the admixture is absorbed onto the silicate phases of the clinker and onto the slag particles [Palacios et al., 2009]. In addition, the presence of slag particles makes the mixture more cohesive and decreases bleeding water and segregation. Kim et al. [Kim et al., 2015] and Palacios et al. [Palacios et al., 2009] observed an increase in fluidity of slag-blended cement mixture, compared with ordinary one. They showed that for the same SP dosage, the slump flow was enhanced by 9% and 16%for the slag contents of 15% and 30% respectively. Also Yu et al. [Yu et al., 2015] showed that cement needs more superplasticizer (+40%) to reach a certain slump flow, compared to binder with BFS.

Despite the increase of BFS content in both $UHPC_3$ and $UHPC_4$, the required SP dosage to achieve the same mini slump flow of reference concrete is 2.13 and 2.4 times respectively that of $UHPC_2$; the lubrication effect of BFS and the fluidizing one of superplasticizer seem to be mitigated by water demand of BFS particles. Indeed, slag particles enhance matrix packing and promote cohesion, which improves the rheological behaviour of concrete in fresh state. In addition, the decrease of cement content decreases the amount of $C_3A$, which induces an increase of slump flow. This explanation was supported by Alonso and Puertas [Alonso and Puertas, 2015] and Palacios et al. [Palacios et al., 2009]. The former emphasized on the affinity and reactivity of $C_3A$ with superplasticizer admixture, and the second explained that SP admixture is absorbed onto BFS particles when the amount of cement and then $C_3A$ amount decrease.

On the other hand, BFS particles have high specific area and absorb more water, which allows free movement of the particles, and results in a decrease of workability [Gharfi et al., 2014]. This phenomenon counterbalances that of lubrication.

When KOH is added, the SP content is kept constant but the mixing period of $UHPC_4$-$[KOH]_3$ is extended by 30 sec, compared to that of $UHPC_4$. This observation is in accordance with that of Puertas et al. [Puertas et al., 2014] who concluded that the increase of mixing time is possible to avoid fast setting and improve the workability of chemically activated slag-concrete. In fact, even in the first minutes the chemical activator could affect the smooth sliding planes and reduces the lubrication effect of BFS particles. Moreover, the dissolution of KOH increases the liquid/solid of basic solution, grows its density, and thus diminishes the mini slump flow of concrete [Alonso et al., 2017].

Afterword the preliminary investigation and the optimization of superplasticizer content in order to obtain the required workability, the outcome UHPC mixtures are presented in Table 7.

***Table 7: UHPCs mix proportions***

| Components (kg/m³) | $UHPC_1$ (0%BFS) | $UHPC_2$ (30%BFS) | $UHPC_3$ (50% BFS) | $UHPC_4$ (80% BFS) | $UHPC_4$-$[KOH]_3$ (80% BFS) |
|---|---|---|---|---|---|
| Cement | 977.00 | 683.90 | 488.50 | 195.40 | 195.40 |
| Silica fume | 183.00 | 183.00 | 183.00 | 183.00 | 183.00 |
| Crushed quartz | 61.00 | 61.00 | 61.00 | 61.00 | 61.00 |
| Blast furnace slag | 0 | 268.10 | 446.90 | 715.00 | 715.00 |
| Quartz sand | 1075.00 | 1075.00 | 1075.00 | 1075.00 | 1075.00 |
| Superplasticizer | 25.31 | 10.54 | 22.49 | 25.31 | 25.31 |
| Superplasticizer (%) | 1.80 | 0.75 | 1.60 | 1.80 | 1.80 |
| Water | 145.63 | 160.39 | 148.44 | 145.63 | 140.65 |
| Potassium hydroxide | - | - | - | - | 10.17 |
| Slump flow (cm) | 30 | | | | |

## 3.3. Setting time

The rate of setting of cementitious materials results from chemical and physical behaviours in relation with the initial porosity of mixture and the binder reactivity. An important quantity of hydrates is necessary when the matrix is initially porous to reach the percolation threshold [Torrenti and Benboudjema, 2005]. These formed hydrates depend greatly on binder reactivity. In our case, the initial porosity is kept constant for all concretes, as w/b and water-to-solid volume ratios are unchanged. There are just two variables in the studied mixtures: dosage of SP and content of BFS, which is incorporated as volume substitution of cement. Thereby, the measured setting time period is mostly governed by early age reactivity of binder. Table 8 summarizes the obtained results of setting time for all studied mixtures. As shown, the effect of BFS on setting time depend on its content, and the dosage of superplasticizer.

***Table 8: Vicat setting times of studied UHPCs***

| Mix designation | Initial setting time (min) | Final setting time (min) | Setting time period (min) |
|---|---|---|---|
| $UHPC_1$ | 330 | 420 | 90 |
| $UHPC_2$ | 150 | 180 | 30 |
| $UHPC_3$ | 450 | 510 | 60 |
| $UHPC_4$ | 750 | 930 | 180 |
| $UHPC_4$-$[KOH]_3$ | 660 | 690 | 30 |

For $UHPC_2$ (BFS content of 30% and SP dosage of 0.75%), the initial and final setting times are accelerated by 2.2 and 2.3 times respectively, compared to that of reference concrete. The setting time period is also decreased by 3 times when 30% of BFS is incorporated. Two parameters could explain this difference:

The superplasticizer dosage: $UHPC_1$ contains two times more SP than $UHPC_2$, which participates significantly in decelerating of both initial and final setting times of the$UHPC_1$. Furthermore, the presence of slag accelerates the hydration of CEM I and shortens the setting time period by 3 times ofmixture, compared to that in $UHPC_1$. This result is compatible with

that of Mounanga et al. [Mounanga et al., 2011]. Indeed, these authors did not observe any modification of initial setting time of mortars containing 25% and 50% of BFS. However, the setting time period of the blended mixture with 50% BFS was shortened by 30%, compared to that of reference mortar.

In presence of BFS, there is more water available to the reaction of CEM I. This phenomenon, explained by dilution effect, is counterbalanced by the acceleration of cement hydration [Ballim and Graham, 2009; Mounanga et al., 2011]. Indeed, slag particles act as nucleation sites for the formation of calcium hydroxide. This behaviour is attributed to their high specific area, compared to that of cement (+25%) and has a physical origin, as reported by Cyr et al. [Cyr et al., 2005]. In fact, their results on mineral admixtures, particularly inert ones, highlighted that the presence of fine particles with very high specific area could activate the cement hydration by heterogeneous nucleation [Lawrance et al., 2003; Cyr et al., 2005]. As well the physical effect of the fine particles is dominating at early age, causing an acceleration of hydration and setting of cement matrix.

For $UHPC_3$, SP content is 1.6% which is lower than that of $UHPC_1$ by 11%. Thus, the delay of initial setting is attributed to BFS content in this mixture (50% BFS). With high BFS content, the dilution effect governs the hydration acceleration, which results in deceleration of initial setting of $UHPC_3$ by 36%, compared to $UHPC_1$. Once setting initiated, the physical effect of BFS particles through the heterogeneous nucleation of formed hydrates occurs, leading to an acceleration in setting and reduction in its period. The latter is 1.5 times lower than that of $UHPC_1$.

With very high BFS content (80%), the early age concrete behaviour is different. Its initial and final setting times are increased by 2.27 and 2 times respectively, compared to that of $UHPC_1$ (Table 8). The dilution phenomenon governs the hydration and setting processes, and the cement particles are suspended materials. Moreover, the w/c is 5 times more in $UHPC_4$ than in $UHPC_1$. Consequently, around 15.5 hours were necessary to reach the final setting beside that the setting time period was 3 hours for $UHPC_4$. To remedy this delay, KOH was added, in order to provide necessary alkalis for BFS reaction. The effect of BFS particles would be of physical and chemical origins. The comparison between setting time results of $UHPC_4$ and $UHPC_4$-$[KOH]_3$ exhibited clearly the great effect of KOH in accelerating setting, so the initial and final setting times decreased by 12% and 25.8% respectively as demonstrated in Table 8. The addition of chemical activator causes the dissolution of glass structure of BFS and promotes its reaction, which results in decreasing the effect of dilution by decreasing liquid-to-solid ratio. This phenomenon is more pronounced, once setting is initiated. Thus, setting period of $UHPC_4$-$[KOH]_3$ is reduced by 6 and 3 times, compared to that of $UHPC_4$ and $UHPC_1$ respectively.

### 3.4. Hydration

Fig. 8 gives the variation of the reaction heat for the UHPC mixtures while the reaction heat flow measured for these mixtures was presented in Fig. 9. Also, Table 9 summarizes the main measured and normalized characteristics values of the semi-adiabatic hydration curves, where $t_{max}$ is the time of maximum heat flow and Imax is the maximum intensity of heat flow.

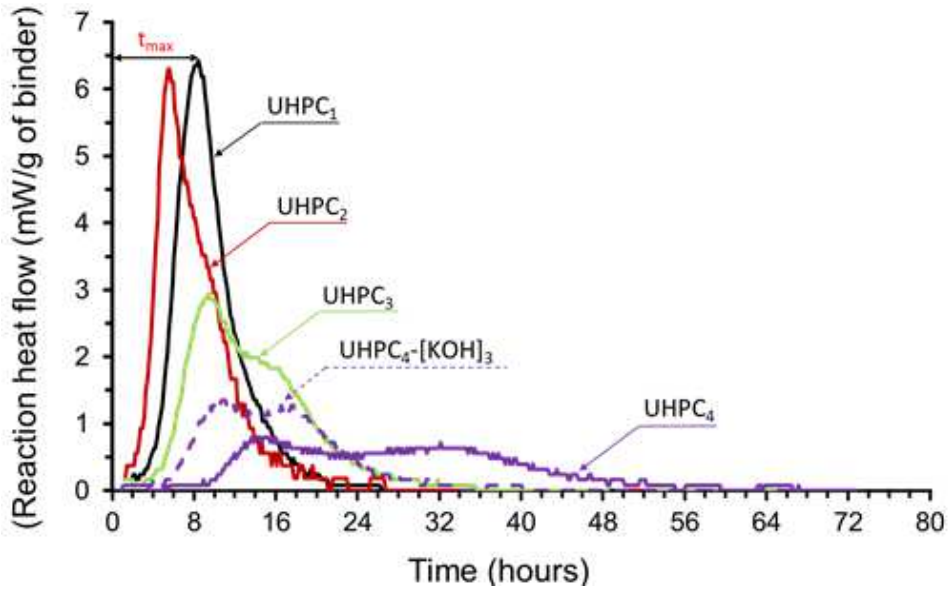


***Figure 8: Reaction heat of studied UHPC mixtures***

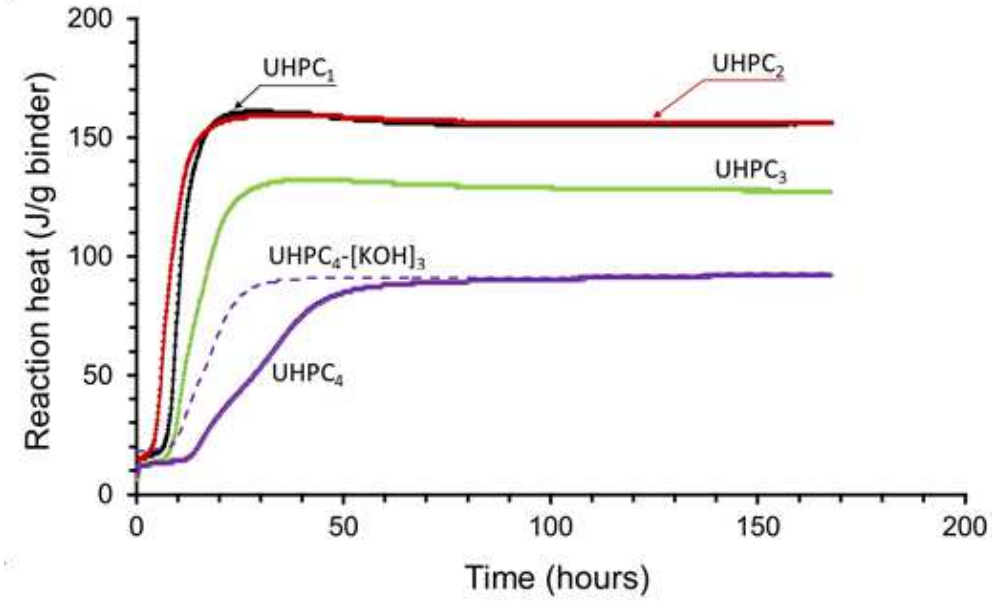


***Figure 9: Reaction heat flow of studied UHPC mixtures***

As observed, the maximal heat reaction and heat flow peak of $UHPC_1$ are respectively 161 J/g of the binder and 6.43 mW/g of the binder, and the time to reach the maximum reaction heat is 1572 min. This result highlights the great difference between a semi-adiabatic and an isothermal test. For the latter, the heat flow is low, in comparison with the former. Mounanga et al. [Mounanga et al., 2012] tested an UHPC with similar composition ($ERPC_4$) in isothermal conditions and measured a heat flow of 0.52 mW/g. This peak appears after 3324 min.

***Table 9: Hydration characteristics of UHPC mixtures***

| Mixtures | Reaction heat | | Time of maximum heat flow- $t_{max}$ | | Maximum intensity of heat flow- $I_{max}$ | |
|---|---|---|---|---|---|---|
| | Measured value $Q_{max}$ (J/g binder) | Time of maximum reaction heat (min) | Measured value $t_{max}$ (min) | Normalized value $\frac{t_{max}}{t_{max}(UHPC1)}(-)$ | Measured value $I_{max}$ (mW/g of binder) | Normalized value $\frac{I_{max}}{I_{max}(UHPC1)}(-)$ |
| $UHPC_1$ | 161 | 1572 | 502 | 1 | 6.43 | 1 |
| $UHPC_2$ | 159 | 1595 | 335 | 0.67 | 6.30 | 0.98 |
| $UHPC_3$ | 132 | 2109 | 569 | 1.13 | 2.94 | 0.46 |
| $UHPC_4$ | 91 | 3241 | 900 | 1.79 | 0.79 | 0.12 |
| $UHPC_4$-$[KOH]_3$ | 91 | 2401 | 651 | 1.30 | 1.35 | 0.21 |

The replacement of cement with slag results in a reduction of produced reaction heat and in the magnitude of the peak of heat flow. A great decrease of temperature is also measured, when BFS content increased; the maximal temperature is 67.4°C, 66.5°C, 54.1°C, 37.2°C and 41.4°C, respectively for $UHPC_1$, $UHPC_2$, $UHPC_3$, $UHPC_4$ and $UHPC_4$-$[KOH]_3$. This is related to the dilution effect of slag and its slow reaction. The latter releases less heat than that of Portland cement [Ballim and Graham, 2009; Bougara et al., 2009; Mounanga et al., 2011; Beushausen et al., 2012; Merzouki et al., 2013; Jang et al., 2014; Tran, 2015]. The influence of low BFS content on hydration seems rather low and profile of hydration characteristics of the $UHPC_2$ (30% slag) shows a closed behaviour to that of $UHPC_1$ as exhibited in Figs. 8 and 9. The maximal heat reaction and heat flow peak of $UHPC_2$ are respectively 159 J/g of binder and 6.3 mW/g of the binder and the time of maximum reaction heat is 1595 min. The kinetic of early hydration is different, when 30% of cement is replaced with BFS. In the presence of BFS particles, the peak of heat flow appears 167 min before that of Portland cement, even if the time to reach the maximum reaction heat is quite the same.

To better explain this phenomenon, the following reasons should be considered: i) The superplasticizer inhibits the dissolution of anhydrous cement particles, which decelerates the hydration reaction. This phenomenon results from the complexation of $Ca^{2+}$ ions by the

superplasticizer and the adsorption of the polymer on the anhydrous grain surfaces [Jansen et al., 2012]; ii) The lower water content of UHPC and its high solid one decrease the free water in cementitious system [Yu et al., 2015], which results in restriction of $Ca^{2+}$ and $OH^-$ diffusion. Hence, pozzolanic reaction of SF is postponed, and the early hydration is decelerated. Both reasons explain the delay in initial and final setting and in the apparition of the peak of heat flow for $UHPC_1$, in comparison with $UHPC_2$. Otherwise, even if the superplasticizer participates largely in the hydration kinetic of UHPCs, prevailing on other parameters, the presence of low content of BFS in $UHPC_2$ contributes in the acceleration of binder hydration. This behaviour is attributed to the physical effect of BFS particles. They promote the reaction of cement by heterogeneous nucleation, thanks to their fineness [Cyr et al., 2005]. This results in acceleration of cement reaction. Thereby, the alkalis, provided by cement, and subsequently, portlandite increases the pozzolanic reaction of SF and BFS [Meinhard and Lanckner, 2008; Merzouki et al., 2013]. The higher portlandite amount, the more enhanced hydraulic/pozzolanic reaction of BFS, which jointly provides further emitted heat.

For 50% and 80% of cement substitution, the reaction heat decreased by 18% and 43%, and the maximal magnitudes are reached after 2109 min and 3241 min for $UHPC_3$ and $UHPC_4$ sequentially. The lesser pozzolanic and hydraulic activity of BFS is basically linked with its potential to dissolve and to react with portlandite so as to produce further hydrated products through the pozzolanic reaction. This phenomenon depends on BFS content; more the BFS content, higher the dilution effect. Hence, the heat reaction decreases and postpones the hydration acceleration. Indeed, two peaks appear: the first peak (2.94 mW/g for $UHPC_3$ and 0.79 mW/g for $UHPC_4$) is related to cement reaction and the second one is related to BFS phases hydration. The peaks appear at 600 and 960 min for $UHPC_3$ and at 900 and 1920 min for $UHPC_4$ respectively. The first peak is created on account of hydration of $C_3A$ from the cement that melts and reacts with both of the $Ca^{2+}$ and $SO_4^{-}$ ions existing in the liquid phase to produce ettringite. As well it is attached with the decay of calcium silicate phases. The height of the second peak was less, so it exhibits as a shoulder. It is named as ‘‘silicate peak” which is characterized by fast growth and a slow reduction of the heat-flow rate, relying on the slag proportion. The fast hydration of $C_3S$ is related to the development of second-phase C–S–H (i.e., C–S–A–H) and the precipitation of portlandite [Bougara et al., 2009; Meinhard and Lanckner, 2008]. As both concretes contain the same or less superplasticizer content than $UHPC_1$, the slow behavior is attributed to the low cement content, which limits the rate of portlandite.

As shown in Table 9, the maximal reaction heat measured on $UHPC_4$ and $UHPC_4$-$[KOH]_3$ is 91 J/g. The chemical activator accelerates hydration reaction and decreases by 26% the time to reach the maximal heat reaction. The heat released at once upon touch between the slag and the activator is backed to wetting and dissolution of slag grains and production of melted

silicate classes [Kashani et al., 2014]. The hydration operation was affected by the sodium amount and, the larger $Na_2O$ was connected to advanced hydration levels. A significant number of Si-O and Al-O bonds in the slag glass structure was destroyed, resulting in acceleration of dissolution of Si and Al ions that is followed by precipitation of less-solubility calcium silicate, calcium aluminate and magnesium aluminate hydrates because of excessed ionic amounts in the liquid state. So the slag hydration is highly hurried as a result of an increase of pH to 12 for the liquid phase plus the ettringite production [Wu et al., 1990]. The same effect is noticed in Fig. 9, showing the earlier apparition of both peaks, in comparison to $UHPC_4$. The first peak, related to the cement reaction appears 240 min earlier. It results in the destruction of slag bonds Ca-O, Mg-O, Si-O-Si, Al-O-Al, and Al-O-Si. The second peak, related to BFS reaction is more pronounced and is accelerated by 960 min. It occurs on account of the production of a Si–Al layer all over the surface of slag particles and, eventually, the generation of the hydration products promptly after the ionic amounts in the pore solution amounts to the critical rate impeding more reaction [Pacheco-Torgal et al., 2008]. .

The obtained results confirm those of needle test and show the role of BFS particles and chemical activator on the early age hydration of binder.

### 3.5. Total shrinkage

Fig. 10 shows the results of total shrinkage test, as a length change of whole UHPC specimens for one year whereas Fig. 11 shows the variation of the mass of whole specimens for the same period.

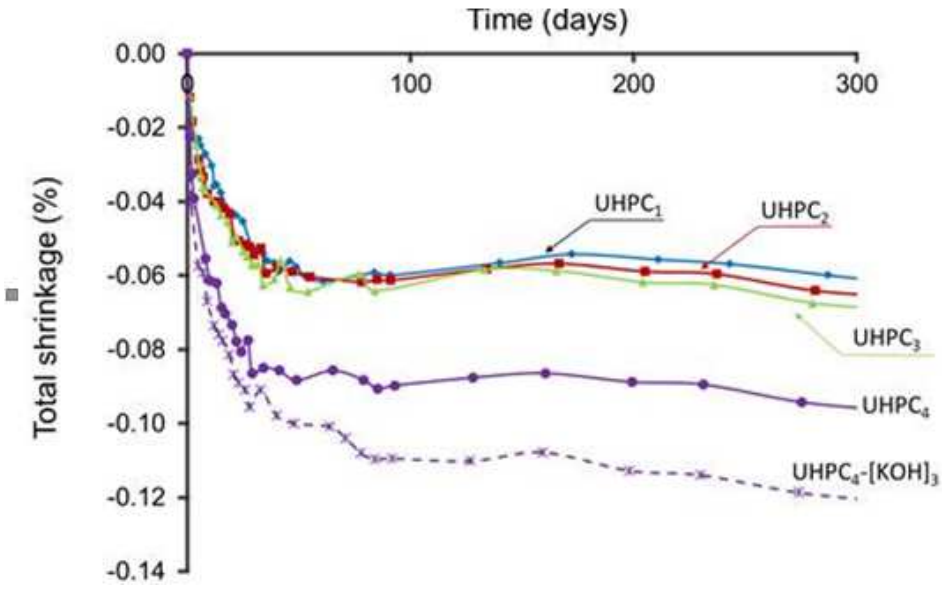


***Figure 10: Variation of length of UHPCs specimens for one year***

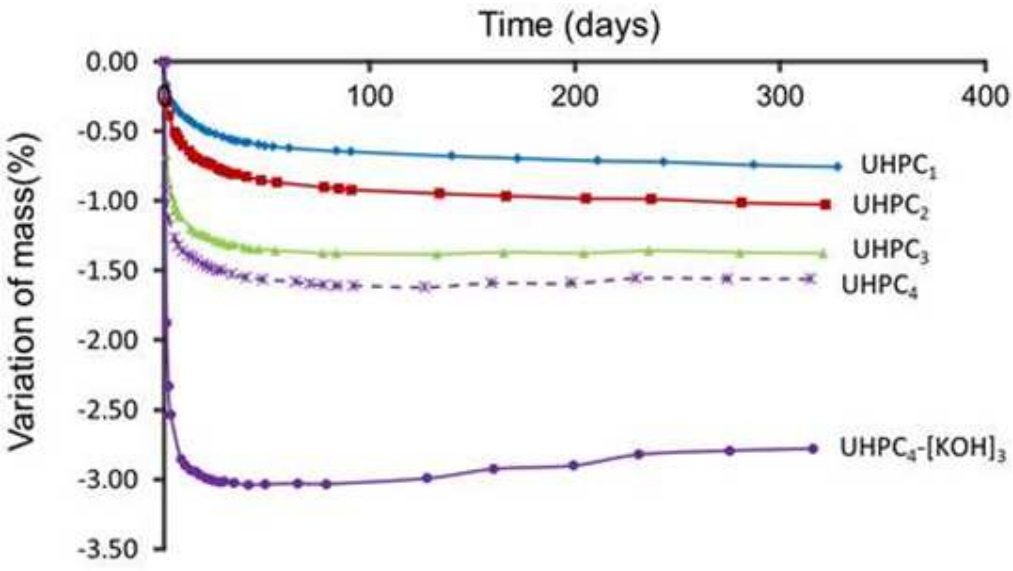


***Figure 11: Variation of mass of UHPCs specimens for one year***

According to Figs 10 and 11, the total shrinkage increases with the increase of cement replacement by slag. This increase is more remarkable for $UHPC_4$ with the higher BFS content. It reaches more than 67% that of $UHPC_1$. However, all amounts of total shrinkage are quite lower. This is due to the that the slag has a lower elastic modulus than the cement as well as the significant refinement of the pore structure of blended mixtures. The generation of slag reaction products fills large capillary voids and reduces the capillary porosity. In addition to filler role of BFS, the pores are filled with C-S-H instead of portlandite [Liu et al., 2015]. This results in increasing resistance against total shrinkage strains by reducing the capillary voids volume in the blended mixtures. The volume of gel pores in C-S-H system was as well affected by Ca/Si ratio of cementitious binder that is modified on account of total shrinkage. Wang [Wang, 2011] stated that the ternary mixture of cement-silica fume-slag promotes the hydration and reacts with portlandite, and the hydration products can increase the density of hardened cement paste through filling smaller pores and voids that majorly participate to keep the total shrinkage of blended concrete specimens at a minimum and, thence restrict it [Wang, 2011; Hossain et al., 2016]. Slag reactivity can be realized by particle size distribution in addition to chemical composition. The removal of adsorbed water accompanied with the incorporation of slag refined the pore size distribution of the blended matrix. The pore refinement could be considered as a reason of diminished water loss and, consequently lessened shrinkage deformations [Wang, 2011].

The chemical activation with $[KOH]_3$ increased the total shrinkage of the $UHPC_4$-$[KOH]_3$ around 33%, compared to that in $UHPC_4$ as shown in Fig. 10. Nevertheless, the amount of it is so limited. Indeed, Collinsa and Sanjayan established that the pore structure was further significant in limiting the shrinkage in AAS concrete than the water loss on the grounds that the

pore size distribution and the C-S-H gel characteristics have a critical effect on the total shrinkage. [Collinsa and Sanjayan, 2000; Thomas et al., 2017]. In the case of the $UHPC_4$-$[KOH]_3$ mixture, the proportion of pores in the micropore size range tends to be higher than $UHPC_4$, and the number of pores within the capillary range is lower than $UHPC_4$ (i.e. lower mesopores) amount fulfilled a lower capillary stresses and lower the cracking tendency and shrinkage. [Neto et al., 2008]. Besides, the total shrinkage of mortars augments with an augmentation of liquid/slag ratio. This ratio specifies the quantity of evaporable water in the mortar and the rate at which water can move towards the specimen surface. Thereby, the quantity of activator dosage highly affects mechanical properties, porosity, and the hydration degree, that are determining parameters for the evolution of shrinkage. [Chi et al., 2015].

## 4. Conclusions

This chapter dealt with the mixture design and early age investigations of eco-friendly UHPC. The following conclusions can be drawn:

- The use of high energy mixer has a great interest for UHPC. Its blade's form and high mixt speed result in homogeneous and workable concrete despite the low (0.14) and short mixing duration (3.5 min);
- The polycarboxylate superplasticizer (ACP1), by its chemical skeleton of acrylic copolymer ensures the best workability of UHPC. Thanks to its short backbone with carboxyl groups and its long side chains, so ACP1 is adsorbed on binder particles, leading to ensure the water reduction and improve concrete workability by steric hindrance;
- Thanks to its high absorption and reactivity, grey silica fume (silicon) improves early age compressive strength of UHPC, compared to white one (zirconium). The latter ensures better workability;
- In UHPC, the substitution of 30% of cement by BFS improves its density packing, increases its workability, accelerates its setting duration, promotes the cement hydration, and grows the total shrinkage. Indeed, the dilution effect related to the reduction of cement content occurs with the heterogeneous nucleation one related to the fineness of BFS particles; the first makes more water available for cement reaction (more slump flow or less superplasticizer dosage for the same workability) and the second increases the cement hydration.
- For cement replacement with 50 and 80% of BFS, dilution effect is dominating and the binder particles are very dispersed and there is more sufficient time for occurrence of hydration reaction and setting initiation. The production of portlandite is restricted and BFS reaction is postponed. Thus, the capillary pores are filled with C-S-H in place of portlandite. - The presence of KOH solution with high concentration supplies sufficient alkalis, which increases pH, promotes the dissolution of slag glass structure and its reaction. This results in hydration reaction acceleration, setting duration reduction, and total shrinkage increment.

# 5. References

[Abdulkareem et al., 2018] O. M. Abdulkareem, A. Ben Fraj, M. Bouasker, A. Khelidj, Mixture design and early age investigations of an environmentally friendly UHPC. Const. Build. Mater. 163 (2018) 235-246.

[Alonso and Puertas, 2015] M.M. Alonso, F. Puertas, Adsorption of PCE and PNS superplasticisers on cubic and orthorhombic C3A. Effect of sulfate. Constr. Build. Mater. 78 (2015) 324-332.

[Alonso et al., 2017] M.M. Alonso, S. Gismera, M.T. Blanco, M. Lanzon, F. Puertas, Alkali-activated mortars: Workability and rheological bahaviour. Constr. Build. Mater. 145 (2017) 576-587.

[Ballim and Graham, 2009] Y. Ballim, P.C. Graham, The effects of supplementary cementing materials in modifying the heat of hydration of concrete. Mater. Struct. 42 (2009) 803-811.

[Beushausen et al., 2012] H. Beushausen, M. Alexander, Y. Ballim, Early-age properties, strength development and heat of hydration of concrete containing various South African slags at different replacement ratios. Constr. Build. Mater. 29 (2012) 533-540.

[Bougara et al., 2009] A. Bougara, C. Lynsdale, K. Ezziane, Activation of Algerian slag in mortars. Constr. Build. Mater. 23 (2009) 542-547.

[Boukendakdji et al., 2012] O. Boukendakdji, E. Kadri, S. Kenai, Effects of granulated blast furnace slag and superplasticizer type on the fresh properties and compressive strength of self-compacting concrete. Cem. Concr. Compos. 34 (2012) 583-590.

[Cherkaoui, 2010] K. Cherkaoui, Caractérisation de la microstructure et comportement à court et long terme d'un Béton de Poudre réactive, Université d'Evry, France, Doctoral Thesis, 2010.

[Chi et al., 2015] M.-C. Chi, J.-J. Chang, R. Huang, Strength and drying shrinkage of alkali-activated slag paste and mortar. Adv. Civ. Eng. (2015) 1-7.

[Choi et al., 2016] M.S. Choi, J.S. Lee, K.S. Ryu, K-T. Koh, S.H. Kwon, Estimation of rhelogical properties of UHPC using mini slump test. Constr. Build. Mater. 106 (2016) 632-639.

[Collinsa and Sanjayan, 2000] F. Collinsa, J.G. Sanjayan, Effect of pore size distribution on drying shrinkage of alkali-activated slag concrete. Cem. Concr. Res. 30 (2000) 1401-1406.

[Coppola et al., 1996] L. Coppola, R. Troli, T. Cerulli, The influence of materials on the performance of reactive powder concrete", International Conference on High-Performance Concrete and Performance and Quality of Concrete Strutures, Florianopolis, Brasil, (47) (1996) 502-513.

[Cyr et al., 2005] M. Cyr, P. Lawrence, E. Ringot, Mineral admixtures in mortars. Quantification of the physical effects of inert materials on short-term hydration. Cem. Concr. Res. 35 (2005) 719-730.

[Fehling et al., 2014] E. Fehling, M. Schmidt, J. Walraven, T. Leutbecher, S. Fröhlich, Ultra-high performance concrete UHPC: Fundamentals-Design-Examples, Wilhelm Ernst & Sohn, 10245 Berlin, Germany, 2014.

[Ferrari et al., 2007] G. Ferrari, F. Surico, P. Clemente, M. Gamba, L. Badesso, Chemically reactive superplasticizers with improved workability retention. Proceedings of the 3rd Central European Congress on Concrete Engineering, Visegrád, Hungary, 2007, pp.135-142.

[Gharfi et al., 2014] E. Gharfi, H. Costa, E. Julio, A. Portugal, L. Duraes, The effect of nanosilica addition on flowability, strength and transport properties of ultra high performance concrete. Mater. Des. 59 (2014) 1-9.

[Hossain et al., 2016] M.M. Hossain, M.R. Karim, M. Hasan, M.K. Hossain, M.F.M. Zain, Durability of mortar and concrete made up of pozzolans as a partial replacement of cement: A review. Constr. Build. Mater. 116 (2016) 128-140.

[Jang et al., 2014] J.G. Jang, N.K. Lee, H.K. Lee, Fresh and hardened properties of alkali-activated fly ash/slag pastes with superplasticizers. Constr. Build. Mater. 50 (2014) 169-176.

[Jansen et al., 2012] D. Jansen, J. Neubauer, F. Goetz-Neunhoeffer, R. Haerzschel, W.-D. Hergeth, Change in reaction kinetics of Portland cement caused by a superplasticizer – Calculation of heat flow from XRD data. Cem. Conr. Res. 42 (2012) 327-332.

[Kashani et al., 2014] A. Kashani, J.L. Provis, G.G. Qiao, J.S.J. Van Deventer, The interrelationship between surface chemistry and rheology in alkali activated slag paste. Constr. Build. Mater. 65 (2014) 583-591.

[Kim et al., 2015] H. Kim, T. koh, S. Pyo, Enhancing flowability and sustainability of ultra high performance concrete incorporating high rplacement levels of industrial slags. Constr. Build. Mater. 123 (2015) 153-160.

[Lawrence et al., 2003] P. Lawrence, M. Cyr, E. Ringot, Mineral admixtures in mortars. Effect of inert materials on short-term hydration. Cem. Concr. Res. 33 (2003) 1939-1947.

[Liu et al., 2015] R. Liu, S. Ding, P. Yan, Microstructure of hardened complex binder pastes blended with slag. Jour. Chin. Ceram. Soc. 43 (5) (2015) 610-618.

[Meinhard and Lackner, 2008] K. Meinhard, R. Lackner, Multi-phase hydration model for prediction of hydration-heat release of blended cements. Cem. Concr. Res. 38 (2008) 794-802.

[Merzouki et al., 2013] T. Merzouki, M. Bouasker, N. Khalifa, P. Mounanga, Contribution to the modeling of hydration and chemical shrinkage of slag-blended cement at early age. Constr. Build. Mater. 44 (2013) 368-380.

[Mounanga et al., 2011] P. Mounanga, M.I. Ahmad Khokhar, R. El Hachem, A. Loukili, Improvement of the early-age reactivity of fly ash and blast furnace slag cementitious systems using limestone filler. Mater. Struct. 44 (2011) 437-453.

[Mounanga et al., 2012] P. Mounanga, K. Cherkaoui, A. Khelidj, M. Courtial, M.-N.D. Noirfontaine, F. Dunstetter, Extrudable reactive powder concretes hydration, shrinkage and transfer properties. Europ. Jour. Env. Civ. Eng. 16 (2012) 99-114.

[Neto et al., 2008] A.A.M. Neto, M.A. Cincotto, W. Repette, Drying and autogenous shrinkage of pastes and mortars with activated slag cement. Cem. Concr. Res. 38 (2008) 565-574.

[Pacheco-Torgal et al., 2008] F. Pacheco-Torgal, J. Castro-Gomes, S. Jalali, Alkali-activated binders: A review Part 1. Historical background, terminology, reaction mechanisms and hydration products. Constr. Build. Mater. 22 (2008) 1305-1314.

[Palacios et al., 2009] M. Palacios, Y.F. Houst, P. Bown, F. Puertas, Adsoprtion of superplasticizer admixtures on alkali-activated slag pastes. Cem. Concr. Res. 39 (2009) 670-677.

[Parant, 2003] E. Parant, Mécanismes d'endommagement et comportements mécaniques d'un composite cimentaire fibré multi-échelles sous sollicitations sévères : fatigue, choc, corrosion, ENPC, France, Doctoral Thesis, 2003.

[Puertas et al., 2005] F. Puertas, H. Santos, M. Palacios, and S. Martínez-Ramírez, Polycarboxylate superplasticiser admixtures: effect on hydration, microstructure and rheological behaviour in cement pastes. Adv. Cem. Res. 17 (2005) 77-89.

[Puertas et al., 2014] F. Puertas, C. Varga, M.M. Alonso, Rheology of alkali-activated slag pastes. Effect of nature and concentration of the activating solution. Cem. Concr. Compos. 53 (2014) 279-288.

[Reddy et Tilak, 2015] A.N. Reddy, U.V. Tilak, Drying shrinkage and durability studies on alkali activated slag concrete using different activators. Int. Jour. Inn. Res. Sci. Eng. Tech. 4 (11) (2015) 11483-11492.

[Richard and Cheyrezy, 1995] P. Richard, M. Cheyrezy, Composition of reactive powder concretes. Cem. Concr. Res. 25 (1995) 1501-1511.

[Rougeau and Borys, 2004] P. Rougeau, B. Borys, Ultra high performance concrete with ultrafine particles other than silica fume. Proceedings of the International Symposium on Ultra High Performance Concrete, Kassel, Germany, 2004, pp.213-225.

[Russell and Graybeal, 2013] H.G. Russell, B.A. Graybeal, Ultra-high performance concrete: A state-of-the-art report for the bridge community, Office of Infrastructure Research & Development Federal Highway Administration, FHWA-HRT-13-060, 2013.

[Sadrekarimi, 2004] A. Sadrekarimi, Development of a light weight reactive powder concrete. Jour. Adv. Concr. Tech. 2 (2004) 409-417.

[Sakai et al., 2009] E. Sakai, Y. Kakinuma, K. Yamanmoto, M. Daimon, Relation between the shape os silica fume and the fluidity of cement paste at low water to powder ratio. Jour. Adv. Concr. Tech. 7 (2009) 13-20.

[Schachinger et al., 2004] I. Schachinger, J. Schubert, O. Mazanec, Effect of mixing and placement methods on fresh and hardened Ultra High Performance Concrete (UHPC). Intern. Sympos. On high Performance Concrete: Ultra High performance concrete 2004 (2004) 575-586.

[Šerelis et al., 2015] E. Šerelis, V. Vaitkevičius, V. Kerševičius, M. Deligia, Influence of water to cement ratio with different amount of binder on properties of ultra-high performance concrete. Jour. Sust.e Arch. and Civ. Eng. 1 (2015) 78-86.

[Shihada and Arafa, 2010] S. Shihada, M. Arafa, Effects of silica fume, ultrafine and mixing sequences on properties of ultra high performance concrete. Asi. Jour. Mater. 2 (2010) 137-146.

[Thomas et al., 2017] R.J. Thomas, D. Lezama, S. Peethamparan, On drying shrinkage in alkali-activated concrete: Improving dimensional stability by aging or heat-curing. Cem. Concr. Res. 91 (2017) 13-23.

[Torrenti and Benboudjema, 2005] J.M. Torrenti, F. Benboudjema, Mechanical threshold of cementitious materials at early age. Mater. Struct. 38 (2005) 299-304.

[Tran, 2015] V. Tran, Effect of mineral and chemical admixtures on durability of cementitious systems, University of South Florida, USA, Master Thesis, 2015.

[Wang, 2011] X. Wang, Drying Shrinkage of Ternary Blends in Mortar and Concrete, Iowa State University, Master Thesis, 2011.

[Wu et al., 1990] X. Wu, W. Jiang, D.M. Roy, Early activation and properties of slag cement. Cem. Concr. Res. 20 (1990) 961-974.

[Yu et al., 2015] R. Yu, P. Spiesz, H.J.H. Brouwers, Development of an eco-friendly Ultra-High Performance Concrete (UHPC) with efficient cement and mineral admixtures uses. Cem. Concre. Compos. 55 (2015) 383-394.

[Zingg et al. 2009] A. Zingg, F. Winnefeld, L. Holzer, J. Pakusch, S. Becker, R. Figi, L. Gauckler, Interaction of polycarboxylate-based superplasticizers with cements containing different $C_3A$ amounts. Cem. Concr. Compos. 31 (2009) 153-162.

# Part 2. Experimental program

# Chapter 6. Microstructural properties of UHPCs

## Table of Contents



## List of figures

## List of tables

## Résumé

Ce chapitre traite de l'effet du dosage en laitiers des hauts fourneaux (LHF) sur les propriétés microstructurales des BUHP avec et sans activation. Ce travail de recherche est réalisé à deux échelles; micro, par (i) la quantification des différentes phases resultant de la réaction d'hydratation (ii) l'évaluation de la porosité et macro en étudiant les propriétés mécaniques des BUHP formulés. Pour mettre en lumière la reaction latente du LHF et l'intérêt de l'activation chimique et thermique dans l'amélioration des propriétés des BUHP, les propriétés mécaniques sont mesurées à 3 et 90 jours et les résultats sont correlés à l'état de la microstructure aux mêmes âges.

Les résultats du travail mené ont montré que:

- Avec 30% de LHF, la nucléation hétérogène l'emporte sur la dilution, ce qui accélère l'hydratation du ciment et par consequent celles des additions minerals (LHF et FS). Cela augmente le taux d'hydrates qui viendront améliorer la densité du béton et ainsi diminuer sa porosité;
- Pour un fort dosage en LHF (BUHP3 avec 50% et BUHP4 avec 80%), l'effet de dilution l'emporte sur la nucleation hétérogène. Par conséquent, des faibles taux de portlandite et d'hydrates sont produits. Cela augmente la porosité, notamment au jeune âge. A 90 jours, la reaction pouzzolanique génère plus d'hydrates et la microstructure devient plus dense, avec beaucoup de nanopores et une faible porosité totale;
- L'activation alcaline avec [KOH]3 provoque la réaction du laitier, ce qui favorise la consommation de la portlandite produite par la réaction du ciment. Les hydrates formées viennent combler la porosité et rendent le mélange plus dense, malgré son jeune âge. L'activation chimique améliore également la qualité de l'interface, comme le montrent les images MET;
- L'activation thermique accélère la réaction des particules solides, ce qui augmente la consommation de portlandite. Par conséquent, le taux d'hydrates formées augmente. Ces dernières, comblent les pores, améliorent la densité du béton et rendent la porosité plus fine. Comme l'activation chimique, l'activation thermique améliore considérablement la qualité de l'interface pâte/quartz.

# 1. Introduction

The microstructure of UHPC is known to be homogeneous and dense, thanks to its high packing density and finer pores. This important parameter depends on the materials composition, the mixture manufacture, activation methods, etc. This section deals with the effect of BFS content on hydration reaction, and then on the amount of formed phases which affects the state of the microstructure. This research work is carried out on blended UHPCs with different BFS contents in comparative with reference one. The state of the microstructure is studied at 3 and 90 days through XRD and TGA analysis in order to assess the different phases in relation with hydration progress. These measurements are correlated with TEM observations and porosity assessing which show clearly the modification in pore distribution versus time and BFS content. In addition, the effect of chemical and thermal activation on the microstructural properties is taken into consideration.

# 2. Results and discussion

## 2.1. X-ray diffraction (XRD)

XRD analysis was carried out to examine the hydration progress and the formed phases in UHPCs at early and later ages in relation with BFS content variation The latter is sensitive to chemical and thermal activation, which should be evidenced by obtained XRD patterns for activated UHPCs.

Fig. 1 shows the XRD patterns of different UHPCs at 3 days. As observed, there are similar intensities of quartz (Q) peaks for all tested UHPCs which have the same contents of both crushed quartz and quartz sand. After 3 days of hydration there is low content of portlandite (P), and no trace of belite ($C_2S$).

The portlandite intensities are quite the same for both $UHPC_1$ and $UHPC_2$. These intensities are decreased and the peaks become weaker with the increment of cement replacement with BFS in both $UHPC_3$ and $UHPC_4$. Indeed, the hydration acceleration of $UHPC_2$ in presence of 30% of BFS [Abdulkareem et al., 2016; Abdulkareem et al., 2018] induces an acceleration of portlandite production which is counterbalanced by its rapid consumption by silica fume and blast furnace slag. For high BFS content, the quantity of produced portlandite decreases and its consumption by pozzolanic reaction of silica fume and slag increases [Ashraf et al., 2009; Kocaba, 2009]. This results in very small quantities of portlandite even after 3 days of hydration [Abdulkareem et al., 2018]. This portlandite reacts with BFS and SF to produce C-S-H [Ben Haha et al., 2011]. Its amorphous nature led to emerge evident peaks at 32.65°2θ, 34.1°2θ, and 60.2°2θ in all diffractographs. As shown in Fig. 1, the C–S–H intensities are higher in $UHPC_1$ at 3 days, and start to lower little by little with BFS content increase. C-S-H peaks are particularly low for $UHPC_4$. As well there are some un-hydrated calcium silicates

($C_3S$). Unreacted alite is more prominent in the $UHPC_1$ than the other blended mixtures of UHPCs, and decreased with the growth of slag content.

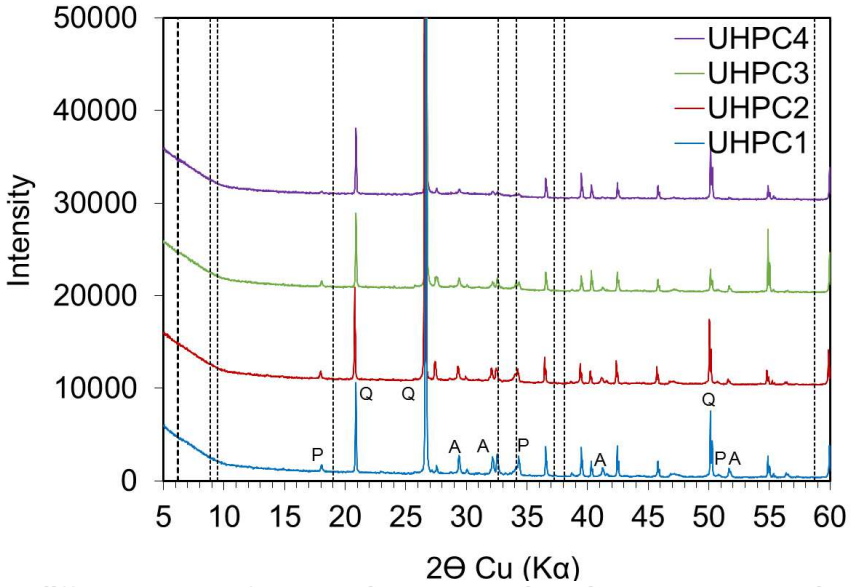


***Figure 1: X-ray diffractograms of UHPC mixtures at 3 days (Q=Quartz, P=Portlandite, A=Alite, Hidden line=C-S-H)***

Fig. 2 exhibits a reduction of portlandite and alite amounts at 90 days through a weak reflection peaks compared to that at 3 days. The former is consumed by the pozzolanic reaction of SF and BFS which continues to later ages. The second reflects the continuity of hydration reaction of cement, and then the decrease of unreacted particles amount. The low cement content in $UHPC_4$ explains the absence of alite peak at 90 days and also the lack of portlandite content, which results in decreasing of produced C-S-H. Also it was observed that the peaks of C-S-H in all UHPC mixtures at 90 days exceed slightly those at 3 days, indicating the progress of hydration phenomenon in long term and the growth in C-S-H at the cost of portlandite because of the pozzolanic reaction [Ashraf et al., 2009] and the hydraulic latent one of BFS.

Fig. 3 shows the influence of chemical activation by $[KOH]_3$ on $UHPC_4$ at 3 and 90 days through XRD patterns. It was evident that the addition of $[KOH]_3$ solution to the 80% of slag in the $UHPC_4$ leads to absence of the portlandite at 3 and 90 days. As for $UHPC_4$, the speed of free portlandite liberation from the cement hydration did not override its consumption by silica fume and slag through pozzolanic reaction. Besides, the addition of chemical activator promotes BFS reactivity which results in increasing its consumption of portlandite. The extra lower contents of portlandite and C-S-H imply that evolution of $UHPC_4$-$[KOH]_3$ hydration at 90 days might be restricted. The lower reflection peaks of the $UHPC_4$-$[KOH]_3$ at 90 days are related to the stopped liberation of portlandite from the hydration of alite and belite phases which become quite small too at this age.

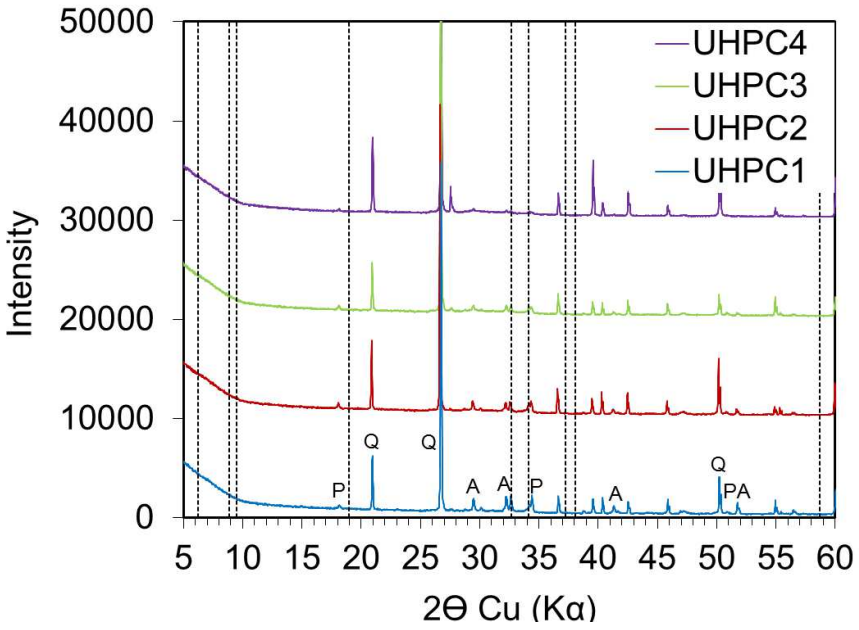


***Figure 2: X-ray diffractograms of UHPC mixtures at 90 days (Q=Quartz, P=Portlandite, A=Alite, Hidden line=C-S-H)***

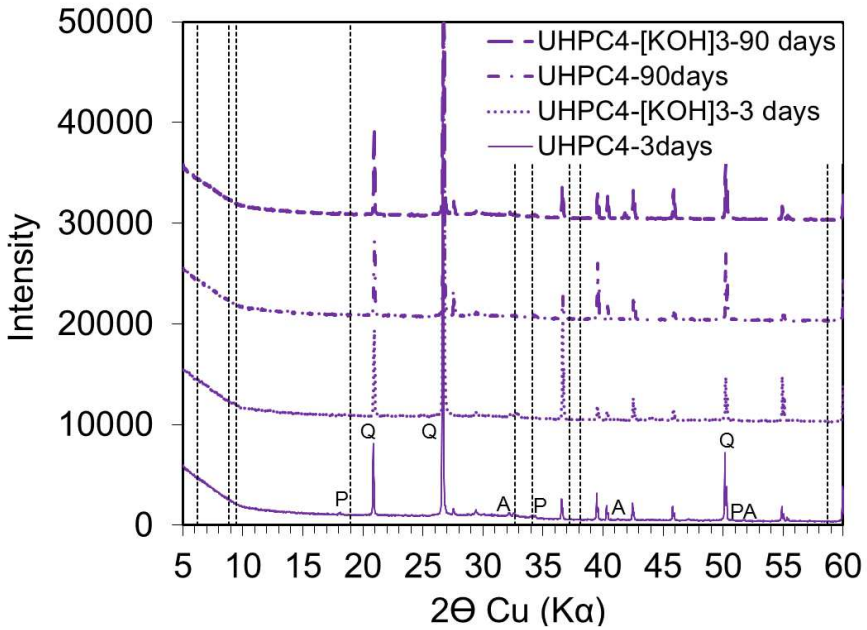


***Figure 3: X-ray diffractograms of UHPC$_4$ mixtures with and without chemical activation (Q=Quartz, P=Portlandite, A=Alite, Hidden line=C-S-H)***

From Fig. 4, it was observed that the effect of thermal activation through XRD traces is quite obvious for both UHPC$_3$ and UHPC$_4$. The major phases specified for hydrated cement are C–S–H gel, unhydrated $C_3S$ and portlandite. It was noticed that intensities of the diffraction lines of quartz and $C_3S$ raised with thermal treatment of UHPC$_3$ and UHPC$_4$. On the contrary, the intensities of the diffraction lines corresponding to portlandite of both thermal activated mixtures are located at 18°2θ (4.921 Å), 34.1°2θ (2.627 Å) and 50.8°2θ (1.796 Å) which are lowered than those of non-activated mixtures. The similar XRD patterns of activated and

non-activated mixtures at 90 days highlight the efficiency of chosen temperature and duration for boosting the hydration of UHPCs with high BFS contents. As known, the elevated temperature is applied to quicken the cement hydration and boost the secondary hydration between cementitious materials and portlandite.

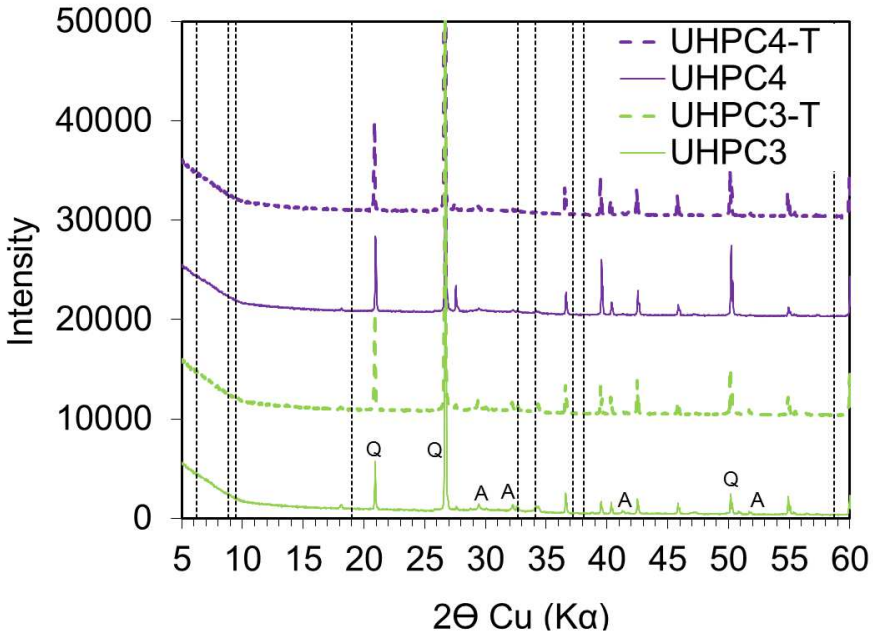


***Figure 4: X-ray diffractograms of UHPC$_3$ and UHPC$_4$ mixtures with and without thermal activation (Q=Quartz, P=Portlandite, A=Alite, Hidden line=C-S-H)***

The prime reaction of BFS is enhanced by temperature with a view of augmentation of the solubility of alkali hydroxides and the great providing of portlandite liberated through the cement hydration. In contrast, the quantity of portlandite generating from the cement hydration and the slag consumption appears an opposite equilibrium in the blended slag at advanced ages. For UHPC$_4$-T, the decrease of portlandite peaks is the more remarkable alteration which takes place during the thermal activation as shown in Fig. 4.

## 2.2. Thermogravimetric analysis (TGA)

The TGA and DTG curves of whole UHPC mixtures after hydration at 3 and 90 days are presented in Figs. 5-6 and 7-8 respectively. Likewise, Table 1 demonstrates the amounts of mass loss of each of portlandite, calcite, and the amounts of chemically bound water from TGA for whole UHPC mixtures.

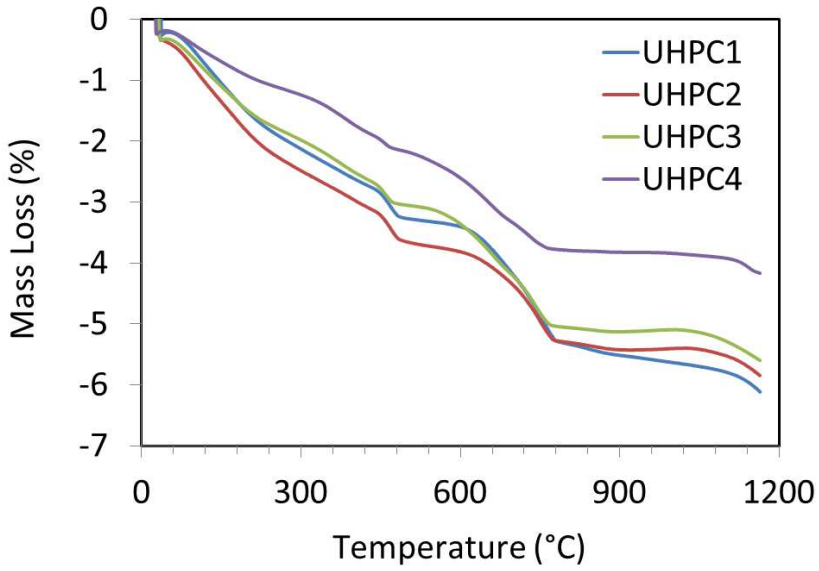


***Figure 5: TGA curves of UHPC mixtures at 3 days***

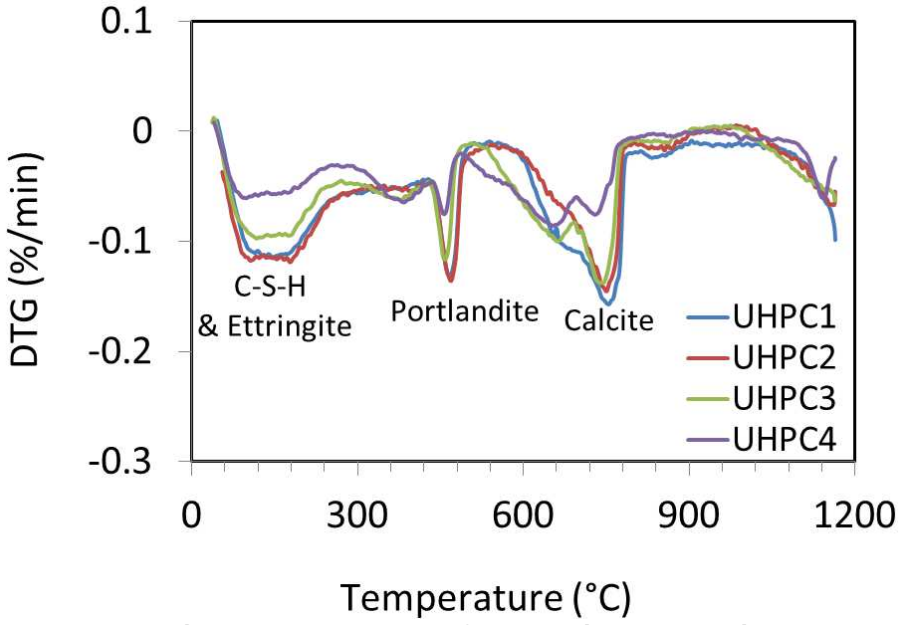


***Figure 6: DTG curves of UHPC mixtures at 3 days***

The TGA curves in Fig. 5 exhibit the mass loss for the hydrated UHPCs at 3 days, showing the dehydration, dehydroxylation or calcination of remained ettringite, portlandite decomposition and calcite decarbonation sequentially. It can be noted that all the tested specimens demonstrate a comparable trend of mass loss. Nonetheless, the rates of their mass loss in each temperature range are dissimilar, denoting that the quantities of the materials reacting at each treatment stage are diversified and reliant on the cement replacement level with slag, in particular when this level reached 80% in the $UHPC_4$.

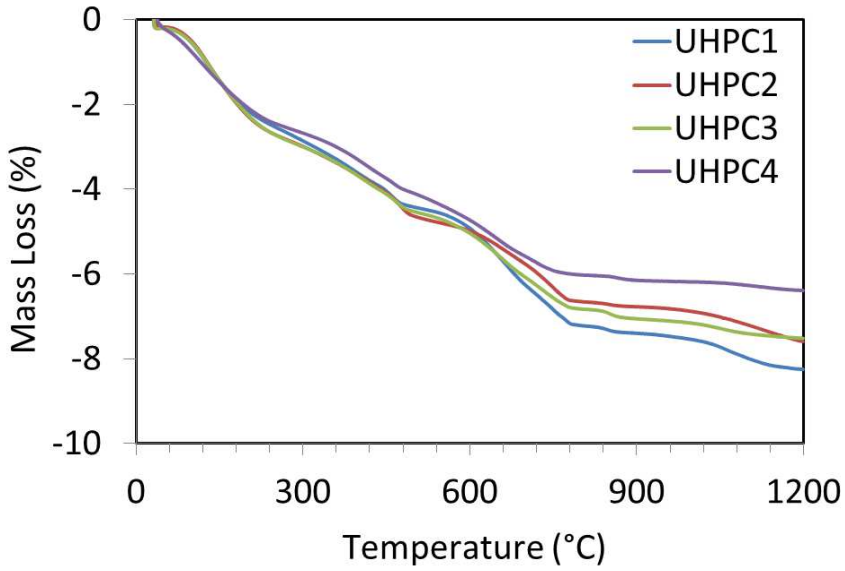


***Figure 7: TGA curves of UHPC mixtures at 90 days***

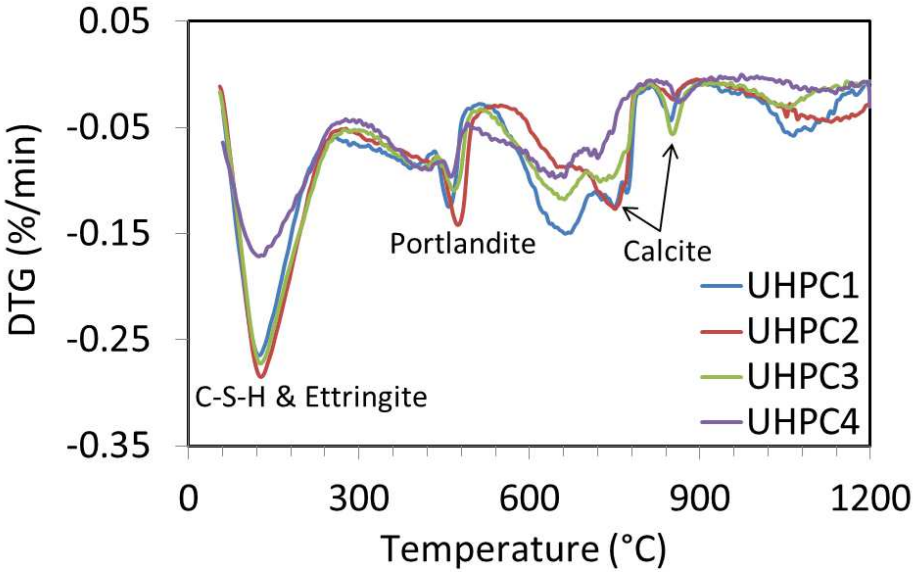


***Figure 8: DTG curves of UHPC mixtures at 90 days***

***Table 1: Mass loss percentages (%) of reaction products from TGA of UHPC mixtures***

| Mix designation | Bound water (%) | Portlandite (%) | Calcite (%) |
|---|---|---|---|
| $UHPC_1$-3 days | 3.9 | 1.42 | 3.3 |
| $UHPC_2$-3 days | 3 | 1.35 | 3.1 |
| $UHPC_3$-3 days | 4.1 | 0.93 | 2.6 |
| $UHPC_4$-3 days | 2.8 | 0.35 | 2.1 |
| $UHPC_4$-$[KOH]_3$-3 days | 4.4 | 0 | 4.2 |
| $UHPC_3$-T | 4.8 | 0 | 1.2 |
| $UHPC_4$-T | 3.7 | 0 | 0.2 |
| $UHPC_1$-90 days | 4.8 | 0.86 | 5.3 |
| $UHPC_2$-90 days | 4.9 | 0.8 | 3.3 |
| $UHPC_3$-90 days | 4.8 | 0.73 | 4 |
| $UHPC_4$-90 days | 4.1 | 0.22 | 2.5 |
| $UHPC_4$-$[KOH]_3$-90 days | 3.8 | 0.3 | 1.8 |

The results establish that the higher slag content, the lower measured mass loss. This was clearly shown in Table 1 through the shortage of mass loss percentages from $UHPC_1$ to $UHPC_4$ at 3 days in terms of the chemically bound water that lowered from 3.3 % to 2.1%, portlandite lowering from 1.42% to 0.35%, and calcite lowering from 3.9% to 2.8% respectively. Generally, the slag incorporation in cement generates a reduced portlandite quantity in the hydration product with a reason of the dilution impact in addition to the portlandite consumption through the pozzolanic reaction [Ashraf et al., 2009]. When the portlandite is formed during the cement hydration, some of this generated compound is consumed by silica fume and slag reaction and this consumption is increased with the increase of slag amount. Besides, the reduction in portlandite quantity with slag content growth induced a lateness in concrete hydration. This smaller amount of portlandite is ascribed to its consumption by the pozzolanic reaction of silica fume and slag to form supplemental C-S-H [Khalifa et al., 2013]. Thus, the mass loss of portlandite of the blended mixtures of UHPC is the least at early ages when compared to $UHPC_1$. Likewise, the results exhibit that the substitution of the Portland cement with slag diminishes the quantity of C-S-H and C-A-H formed at 3 days compared to that in the $UHPC_1$. The phases quantification related to mass change for the UHPC mixtures was accompanied with an occurrence of major peaks in DTG curves as shown in Fig. 6. The prominence of these peaks can be attributed to the evaporation of free water, portlandite and calcite decompositions sequentially. The depth of the endothermic peak of both C-S-H and ettringite lessens with growth of slag content. The decrease of the portlandite content in the UHPCs containing slag restrict the promotion of slag pozzolanic reaction, and the already-produced pore structure in these blended mixtures cannot be filled by the recently produced C-S-H.

As expected, the content of chemically bound water in the UHPC mixtures remarkably increases at 90 days, as shown in Table 1. As well there is a growth in the measured mass loss in the UHPC mixtures with growing age to 90 days, proposing a continuous hydration with time as demonstrated -in Fig. 7. The mass loss of portlandite stills lower in the UHPC mixtures containing slag compared to $UHPC_1$ on the basis that the particular cementitious matrix of UHPC limits the slag pozzolanic reaction to a great extent, leading to that a quite small slag amount can react with portlandite beyond 90 days. Besides, the data exhibit that the portlandite consumption in all UHPC mixtures increased with the progress of the hydration age. Compared to the portlandite quantities at 3 days, the mass loss amounts at 90 days are reduced by 39%, 41%, 21% and 37% for $UHPC_1$, $UHPC_2$, $UHPC_3$ and $UHPC_4$ respectively. The increment of slag substitution rate attains a decrease in non-evaporable water on account of the feeble hydraulic activity of the slag blended matrix [Kourounis et al., 2007]. From Fig. 8, it was observed that the peaks of both C-S-H and ettringite in all UHPC mixtures at 90 days are deeper than that at 3 days, indicating growth in C-S-H at the cost of

portlandite because of the pozzolanic reaction [Ashraf et al., 2009]. The peaks of portlandite of all blended mixtures of UHPC have reduced depths due to the dilution impact and the portlandite consumption by pozzolanic reaction. In addition, there are different peaks of calcite as observed in Fig. 8. Indeed, some phases such $MgCO_3$, $MnCO_3$ and $FeCO_3$ can decompose at lowered temperatures compared to that of calcite. However, all observed curves show clearly the decrease of calcite amount when cement content decreases.

Fig. 9 shows the mass loss for alkali-activated and non-activated $UHPC_4$. This figure highlights the rapid decrease of mass for activated UHPC at 3 and 90 days, compared to those of non-activated ones. The difference is clearly shown -in Fig. 10 where the peak corresponding to C-S-H decomposition is particularly high for activated UHPC. At 3 days a plateau is observed for non-activated $UHPC_4$, denoting the delay of hydrates formation for high BFS content and in absence of any activator. Using KOH seems promoting BFS reaction and accelerating hydrates development at early age, as shown in Table 1, for $UHPC_4$-$[KOH]_3$. At 90 days, measured peaks of C-S-H are quite the same for both activated and non-activated UHPCs. The activation of $UHPC_4$ increases the chemically bound water at 3 days by two times, denoting an acceleration of slag reaction which consumes all produced portlandite. Thus, the hydration reaction is rapidly stopped, which explains the low content of the chemically bound water in $UHPC_4$-$[KOH]_3$ at 90 days, compared to non-activated one. The obtained results agree with those of hydration [Abdulkareem et al., 2018] where the use of KOH accelerated the apparition of second peak of heat flow corresponding to the BFS reaction by 16 hours.

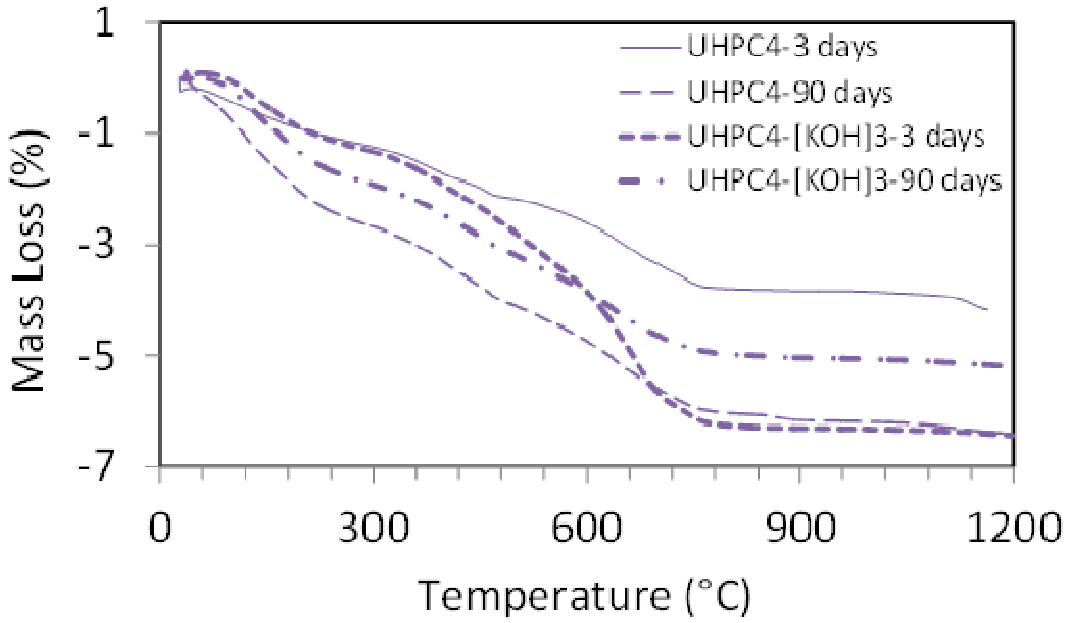


***Figure 9: TGA curves of $UHPC_4$ mixtures with and without chemical activation***

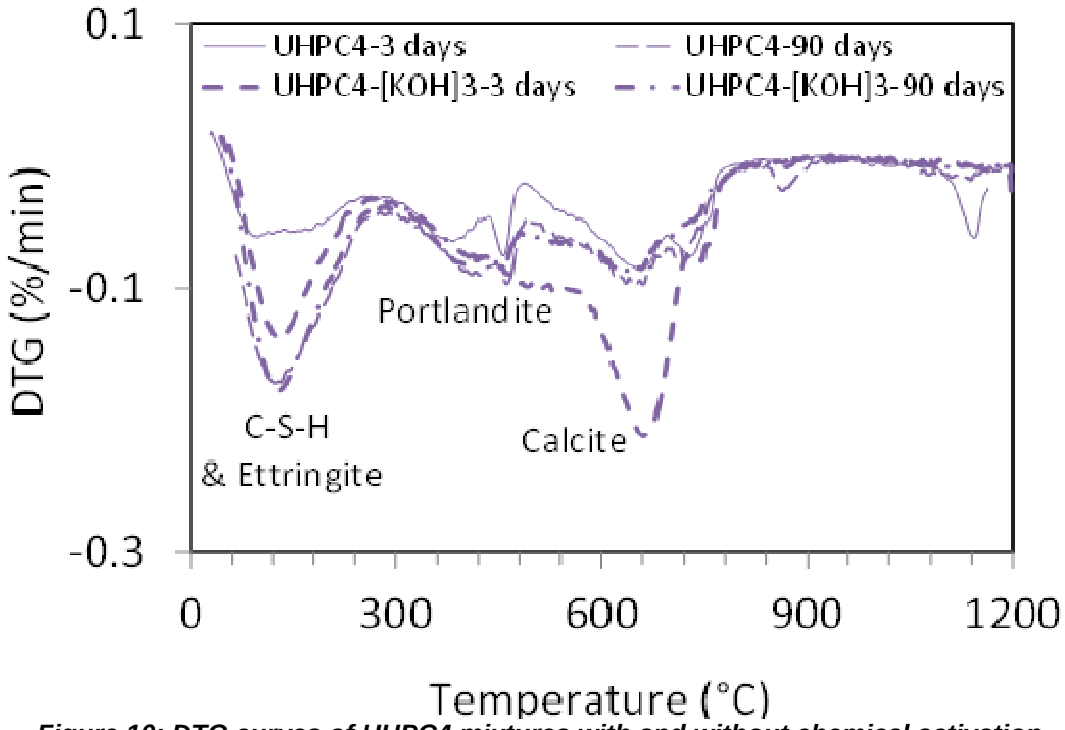


***Figure 10: DTG curves of UHPC4 mixtures with and without chemical activation***

In order to obtain the same performance of $UHPC_1$ at 90 days, concretes with high slag contents were thermally-activated. As expected, Fig. 11 illustrates the great mass loss at early age for thermally activated UHPCs, in comparative with non-activated $UHPC_1$. Thereafter, the mass loss curves have similar trend. Fig. 12 shows that this increase corresponds particularly to dehydration of C-S-H. Indeed, thermal activation promotes cement hydration and pozzolanic reaction [Heikal et al., 2015]. This results in increasing C-S-H content of $UHPC_3$ and $UHPC_4$ by circa 6 and 4 times respectively. $UHPC_3$-T and $UHPC_4$-T contain higher quantity of C-S-H by 4 and 4.6 times that in $UHPC_1$. From Table 1, it was noted that even if the measured chemically bound water is quite the same for $UHPC_3$-T and $UHPC_1$ (4.8%), it was lower for $UHPC_4$ (3.7%). The high content of slag of the $UHPC_4$ affects the hydration progress despite the application of thermal activation which could result in compressive strength decrease.

As for chemical activation, thermal one promotes cement and mineral additions reactions, which increase the portlandite consumption. Table 1 shows the total consumption of portlandite in $UHPC_3$-T and $UHPC_4$-T and the presence of small quantity of calcite proportional to their cement contents.

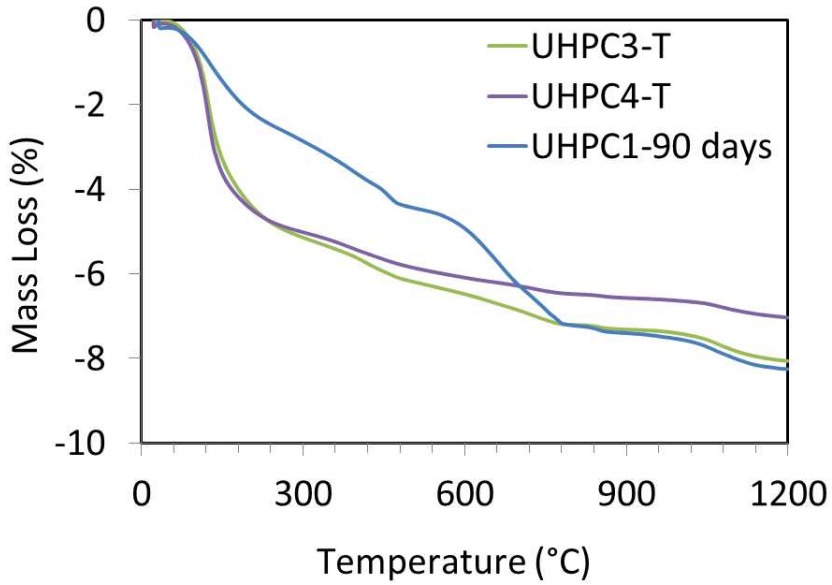


***Figure 11: Comparison of TGA curves for thermally activated UHPC$_3$ and UHPC$_4$ mixtures with the reference one at 90 days***

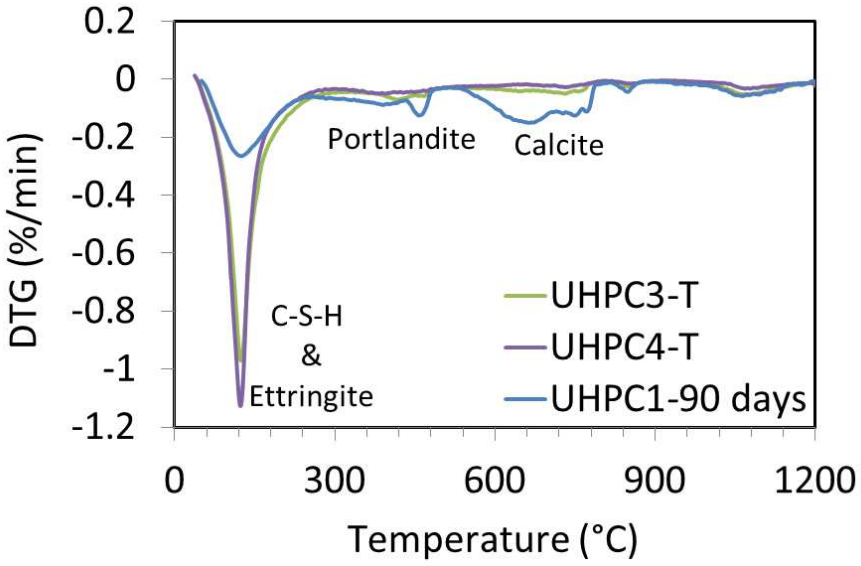


***Figure 12: Comparison of DTG curves for thermally activated UHPC$_3$ and UHPC$_4$ mixtures with the reference one at 90 days***

## 2.3. Transmission electron microscopy observations (TEM)

Transmission electron microscope test is carried out on different UHPCs to investigate their microstructure, and follow their hydration progress at nanometric scale. The high resolution of this technique could give precious informations on formed phases and their interactions, depending on: i) The BFS content; ii) The hydration age; and iii) The applied activation.

Fig. 13 displays the quite dense internal structure of UHPC$_1$ with perfect quartz particles/hydrated paste interfaces. The quartz particles have an angular shape with a sharp border while silica fume particles have different morphological features that exhibit as light grey spheres with different volumes. The interface between the silica fume particles and the

matrix is not easy to distinguish and appear as cloudy, denoting that some hydration reactions occur on silica fume particles surface. Due to its high specific area, silica fume can play filler role by filling spaces and ensuring a compact microstructure. It is porous and water-consuming material and needs portlandite in solution to dissolve which is not easy to be fulfilled with a minimal w/b. Thus, silica fume particles stay unhydrated, and act as nucleation centers to attract the water with a purpose of reacting with cement rapidly, leading to quicken the hydration. The hydrated products display as light grey assemblages developed on the surface of silica fume particles as shown in Fig. 13. This phenomenon is known as heterogeneous nucleation [Abdulkareem et al., 2018b]. Fig. 14 shows that after 90 days the formed hydrates are accumulated on the surface of silica fume particles due to their ultra-fineness [Gatty et al., 2001; Tam et al., 2010]. These particles reacted partially with portlandite, which explains the disappearance of the spherical silica fume particles partly.

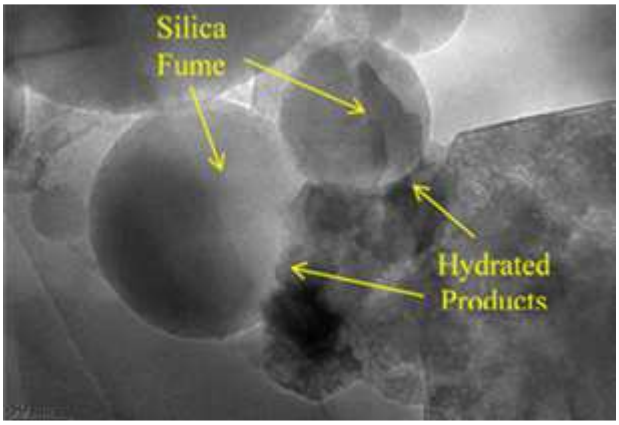


***Figure 13: TEM image of UHPC$_1$, showing the heterogeneous nucleation***

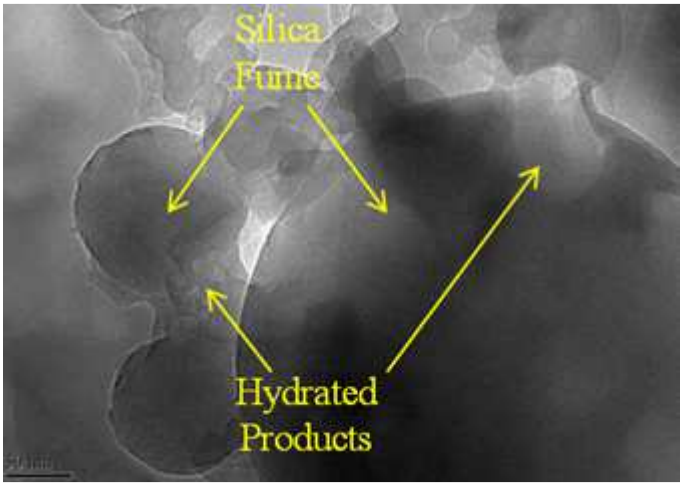


***Figure 14: TEM image of UHPC$_1$, showing the partially reaction of silica fume***

-In Fig. 15, the pore structure of $UHPC_1$ appears very dense, with good binding between aggregates and cement matrix. Moreover, the porosity is extremely lessened with a view of silica fume existence. The perfect dispersion of dark grey particles of the crushed quartz and quartz sand in the paste can be observed as well as the significant homogeneity of the paste between those particles. In this paste, it can be noticed the good dispersion of silica fume, confirming the beneficial effect of superplasticizer on UHPC homogeneity [Courtial et al., 2013]. The piecemeal dissolution of silica fume and its reaction with the portlandite generate new hydrates of C–S–H. The additional C–S–H gel produced in the paste occupies large spaces, reinforces the interconnection of the blended mixture, and consequently the $UHPC_1$ becomes highly densified and impenetrable [Tam et al., 2010].

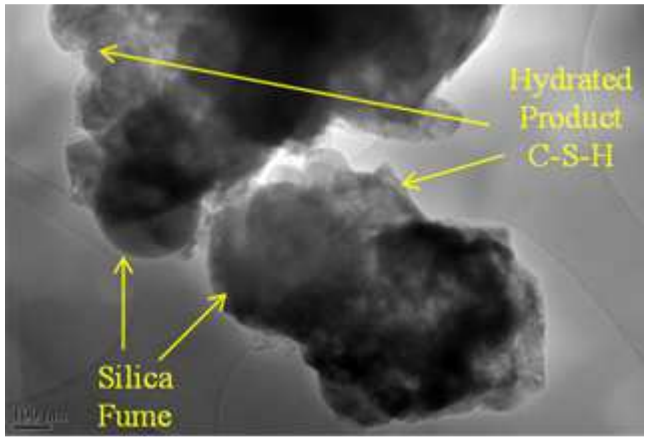


***Figure 15: TEM image of $UHPC_1$, showing the hydrated products (C-S-H)***

The hydration products such as C-S-H gels formed on the surface of silica fume particles have irregular shapes and their presence showing silicium and calcium as major components. Generally, in the UHPC the gels of C-S-H vary in their micro skeleton (through their pores size) from low density to high density C-S-H. Usually, the size of these pores is lower than 10 nm. At advanced ages of hydration, the content of C-S-H with high density increases and the pores size of UHPC decreases greatly, resulting in further compact skeleton [Ashraf et al., 2009]. The incorporation of 30% of slag in $UHPC_2$ achieves high compactness in its microstructure and remarkable decrease in capillary porosity. As shown in Fig. 16, the densified microstructure of $UHPC_2$ with little porosity at 90 days can be represented by the extra fine pores as white points, indicating that there is a refined pore structure. The particles of the composite binder were close to each other because of minimal w/b that made porosity smaller [Kocaba, 2009]. As well the entry diameter of capillary pores significantly decreased from early age to later age. The slag reaction proceeds to generate hydration products filling the large pores continuously at a prolonged hydration age. As a matter of fact, the substitution of 30% of cement with slag in $UHPC_2$ reduced the inter-particles space, leading to boost the compactness of granular matrix and grow the packing

density in conjunction with little water needed for filling the voids between the solid particles. Thus, the bulk density was improved and porosity was decreased.

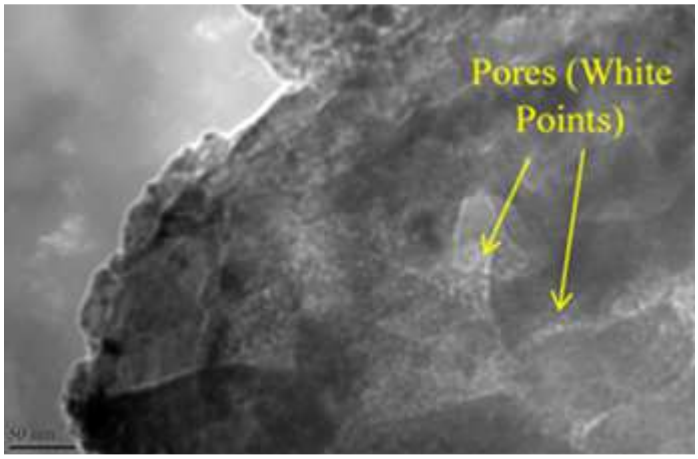


***Figure 16: TEM image of UHPC$_2$, showing its pore structure***

Beside unreacted silica fume particles, there are unreacted BFS particles, which improve the packing density of UHPC and refine its pore structure by their filler effect. To investigate the effect of high BFS content, TEM analysis is carried out on UHPC$_4$ (with 80% of BFS) at 3 and 90 days to highlight the latent reaction of slag. Fig. 17 exhibits the microstructure of UHPC$_4$ cured for 3 days (left) and 90 days (right). As shown, there are many non-reacted particles of silica fume and large pores at 3 days. This indicates that for lower w/b, the larger slag substitution rate, the larger volume of capillary pores. Because of the latent slag reaction at early age in the composed binder cured at ambient conditions, the voids and capillary pores are not efficiently filled with the limited quantity of hydration products (i.e. C-S-H with low density) which are already generated at early age. Consequently, the content of coarse pores is high.

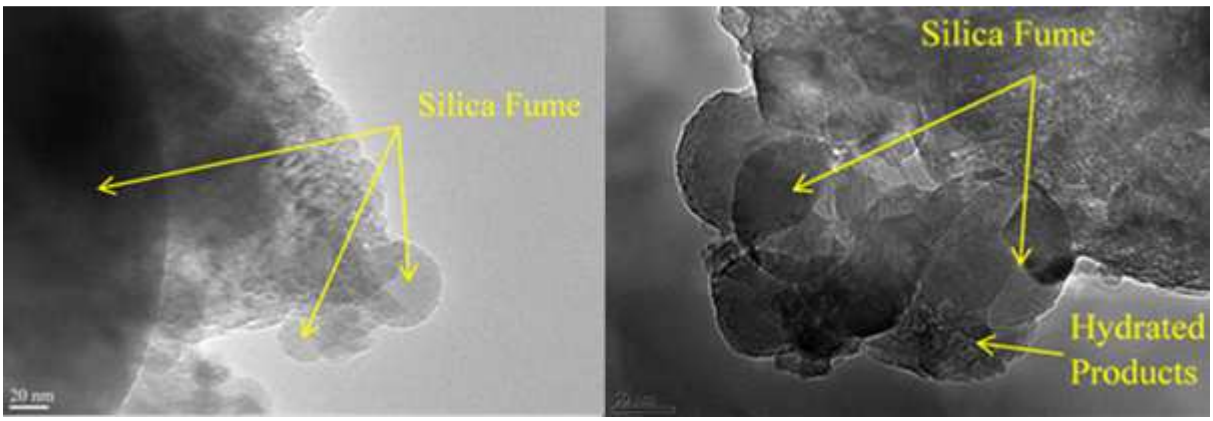


***Figure 17: TEM image of UHPC$_4$ cured at 3 days (left) and 90 days (right)***

At 90 days, $UHPC_4$ appears with high packing density. This result agrees with that of Mehdipour and Khayat [Mehdipour and Khayat, 2017] who concluded that the inter-particle forces become comparatively great with the reduction of the particle size, and in consequence the packing density increased. As observed in XRD analysis, the high content of BFS induces a decrease in portlandite production, and makes the slag reaction restricted. Thereby, beside the formed hydrates slag and silica fume particles play filler role through filling inter-particles spaces, and improve the packing density of mixture. It should be remarked that due to higher specific surface of silica fume, it is more susceptible to react with water than slag. This can be confirmed through the existence of much hydrates around silica fume particles as shown. Thereby, many anhydrous or partially hydrated particles of slag and silica fume act as fillers. From chemical viewpoint, silica fume particles act as nucleation sites where the hydrates, emerging from pozzolanic reaction are formed and fill the ITZ perfectly. This results in strong binding silica fume/hydrates, compared with binding silica fume/quartz particles as shown in Fig. 18.

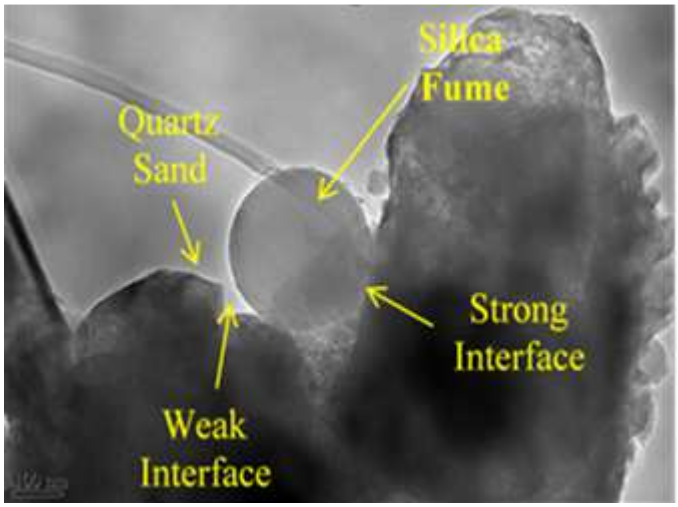


***Figure 18: TEM image of $UHPC_4$ at 90 days, showing different ITZs***

As mentioned earlier, $UHPC_4$ was thermally-activated to achieve the same properties of reference concrete at 90 days. Fig. 19 shows the low porosity of $UHPC_4$-T since the cement hydration and pozzolanic reaction were greatly activated. This was obvious through the reduction of pores as a result of activation so the density enhances and the hydration products increase on the basis that the heat treatment accelerates the reaction of both slag and silica fume particles. Fig. 19 shows clearly the high density and the high quality of ITZ that is filled perfectly with hydrates.

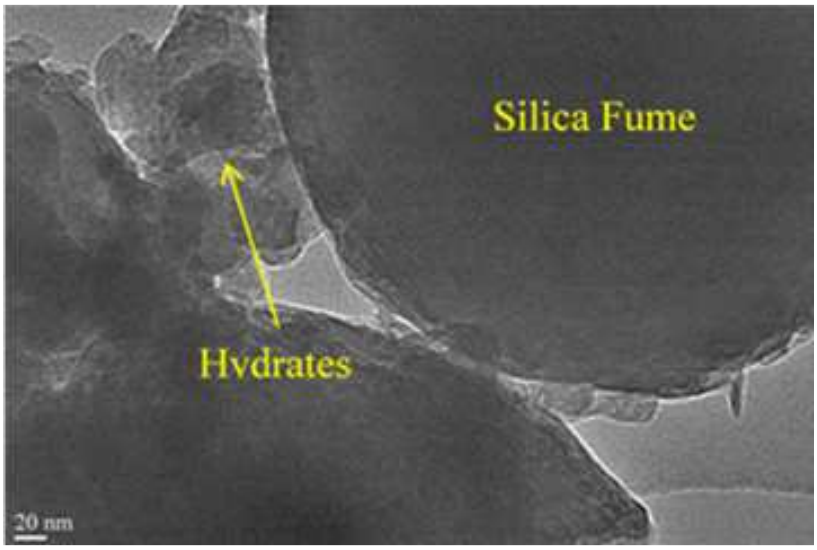


*Figure 19: TEM image of UHPC$_4$-T*

## 2.4. Porosity and pore size distribution

Figs. 20 and 21 show the cumulative intrusion curves and pore size distribution curves respectively, for different studied UHPCs at 3 days. The measured total porosities are summarized in Table 2.

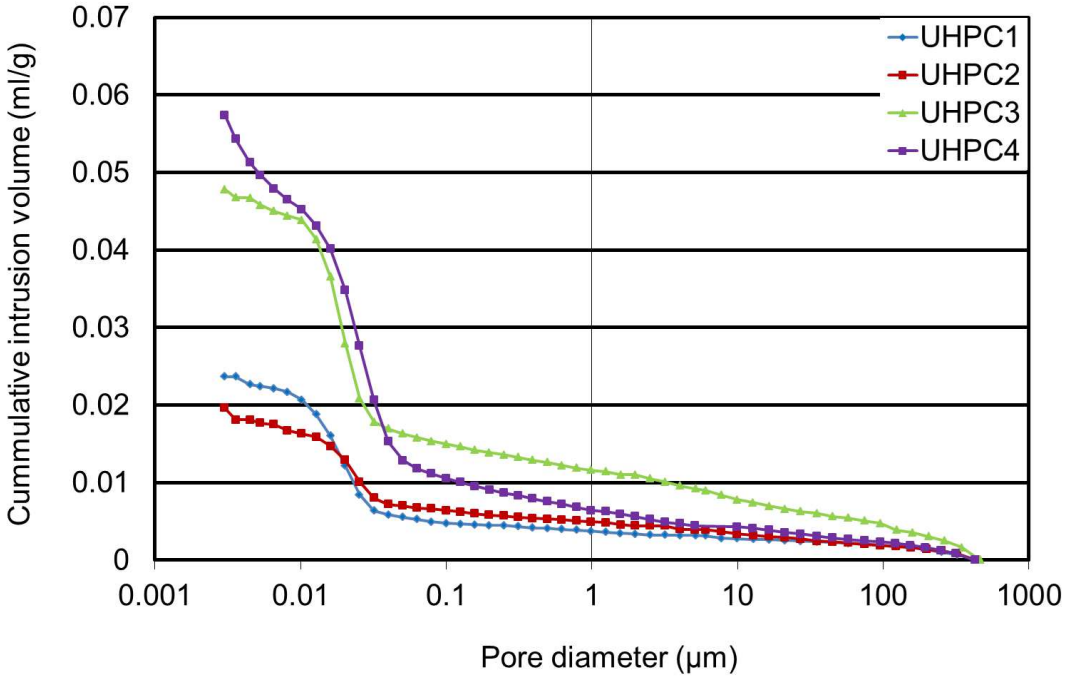


*Figure 20: Cumulative intrusion volume of UHPC mixtures at 3 days*

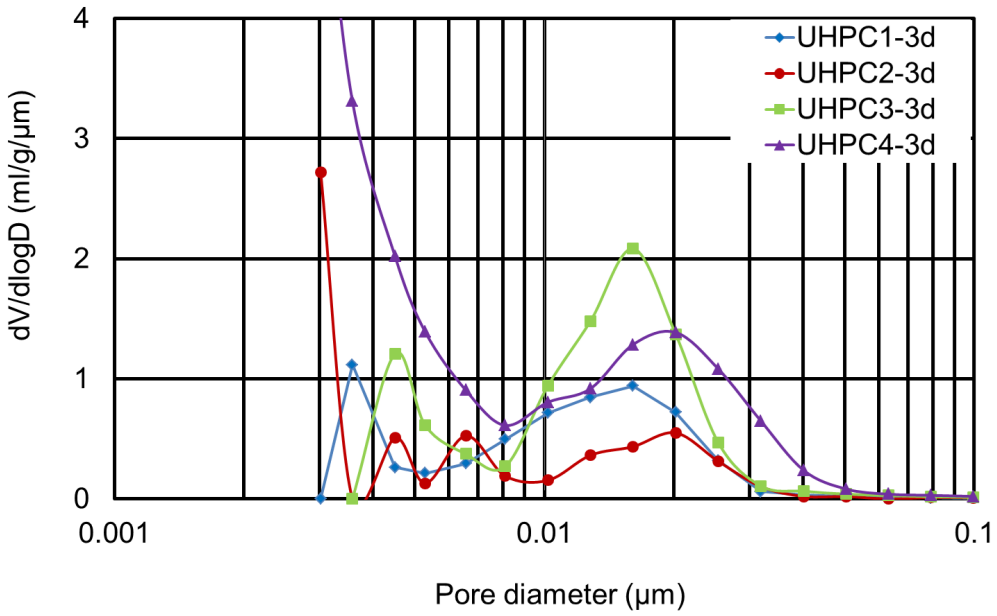


***Figure 21 : Pore size distribution of UHPC mixtures at 3 days***

***Table 2: Total porosity of UHPC specimens***

| Mix designation | Total porosity (%) | |
|---|---|---|
| | 3 days | 90 days |
| $UHPC_1$ | 5.45 | 4.81 |
| $UHPC_2$ | 4.47 | 3.85 |
| $UHPC_3$ | 10.51 | 2.51 |
| $UHPC_4$ | 12.57 | 4.04 |
| $UHPC_4$-$[KOH]_3$ | 7.72 | 4.14 |
| $UHPC_3$-T | 2.64 | |
| $UHPC_4$-T | 4.09 | |

As shown in Fig. 21, the most probable pore diameters of $UHPC_1$ at 3 days are of 0.0036 and 0.016 µm, indicating the fineness of porous network despite the early age. This result can be explained by the major role of silica fume, which decreases the matrix porosity by two manners:

- Filler impact: silica fume particles fill the voids between cement particles themselves and the spaces between cement and aggregate particles as shown by TEM image in Fig. 14;
- Pozzolanic reaction: silica fume reacts with portlandite to form further C–S–H gel as remarked in Fig. 1 through XRD analysis and in Fig. 15 through TEM image respectively, resulting in an extra decrease in both of pore diameter and capillary porosity during hydration progress [Shi et al., 2015].

For $UHPC_2$, three peaks of pore diameters are observed in Fig. 21; 0.0045 µm, 0.0065 µm and 0.0202 µm, indicating the physical role of BFS in refining the microstructure of UHPC. This results in decreasing slightly its porosity, compared to $UHPC_1$, despite the latent

reaction of BFS. This observation agrees with TGA/DTG results, showing an increase of hydrates content in presence of low BFS content and low dosage of superplasticizer. At 3 days, the pores diameters become large particularly in presence of high BFS content. For $UHPC_3$, 0.0045 µm and 0.01608 µm have been measured and for $UHPC_4$, one mean pore diameter of 0.0202 µm is observed. The larger slag substitution rate, the larger volume of capillary pores that exceeds 10 nm. Because of the latent slag reaction at early age, the voids and capillary pores are not efficiently filled with the limited quantity of hydration products, as observed through XRD analysis for $UHPC_3$ and $UHPC_4$ in Fig. 1. Consequently, the content of capillary pores is high as clearly seen in Fig. 17 (left) through TEM image for $UHPC_4$. When pH of pore solution reaches up to 12.6, the slag begins to react with portlandite in order to generate the hydration products, and accordingly the slag reaction positively impacts on the pore system evolution by lessening the critical pore size to be miniature, i.e. refine the porosity. In another meaning, the critical pore diameter augments side by side with the slag substitution rate augmentation at early age [Zhou et al., 2006; Berodier et Scrivener, 2015; Rengguang et al., 2015].

At 90 days the total intrusion volume decreases (Fig. 22), particularly for $UHPC_3$ and $UHPC_4$, proportionally to the decrease of total porosity. Indeed, like porosity, the total volume intrusion decreased by 3 times between 3 and 90 days for 50% and 80% BFS content. This result indicates the progress of hydration reaction and the production of hydrates, filling the pores (Fig. 23) and decreasing the porosity of UHPC.

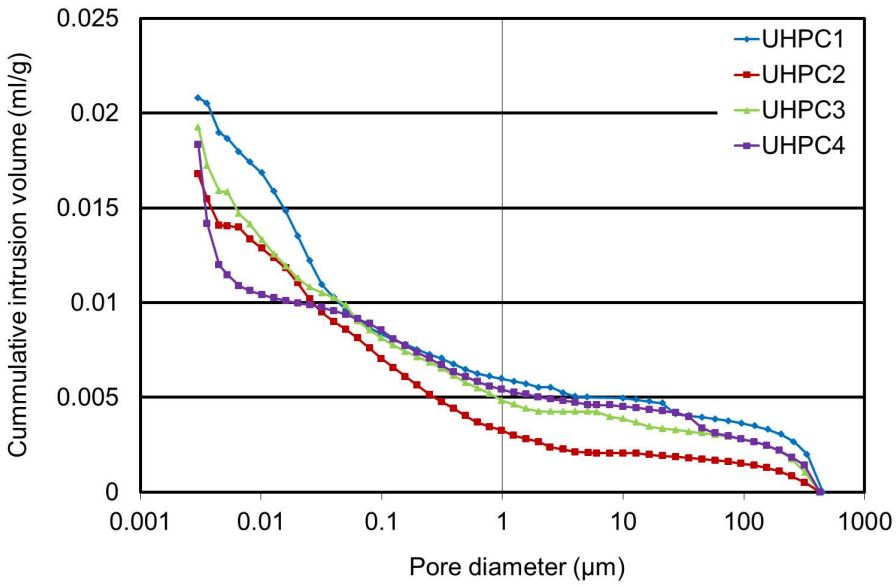


***Figure 22: Cumulative intrusion volume of UHPC mixtures at 90 days***

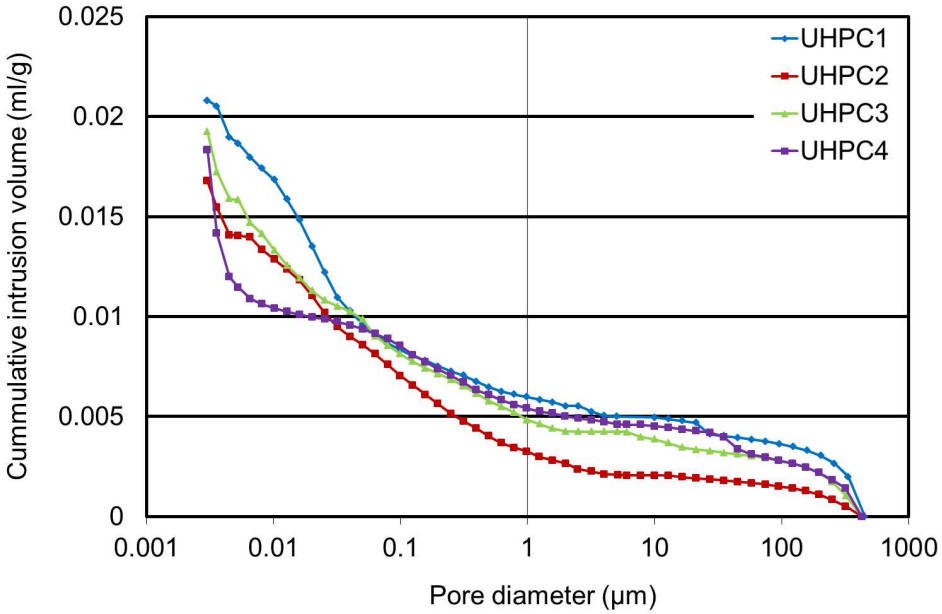


***Figure 23: Pore size distribution of UHPC mixtures at 90 days***

From Fig. 23, it was noted that the volume of pores exceeding 10 nm decreases greatly and the total porosity diminished for all UHPC at 90 days. $UHPC_1$ has more capillary pores (10 nm) than other UHPCs and two peaks of nanopores of3.6 and 5.3 nm. The substitution of cement with 30% of BFS refines the microstructure at 90 days by filling the capillary pores, so only a peak of 6.6 nm is observed. When 50% BFS is used in $UHPC_3$, this peak is 5.3 nm. For $UHPC_4$ (80% BFS), the capillary pores disappeared, denoting the filling role of BFS particles. At 90 days, BFS particles react partially, as shown in TEM observations, denoting their physical role of filling spaces between cement particles. Furthermore, pores are partially filled with C-S-H produced through the hydration of slag. This results in refining microstructure and decreasing the total porosity [Ramezannianpour, 2014; Rengguang et al., 2015]. Obtained results agreed with those of bibliography, even if the measured total porosities are lesser. Indeed, Cheyrezy et al. [Cheyrezy et al., 1995] tested an UHPC with w/b of 0.12. The measured total porosity is 7% and the peak diameter of 70 nm was observed. Loukili et al. [Loukili et al., 1999] demonstrated that observed peak moves from 30 nm to 20 nm when the hydration of UHPC (w/b = 0.2) progresses from 1 to 7 days. They explained this observation by the pozzolanic reaction of silica fume.

Fig. 24 exhibits the volume-diameter curves of the $UHPC_4$ without and with chemical activation to detect the change in porosity and pore size distribution of this mixture under activation effect, and to show the development of pores of this mixture at 3 and 90 days. Also Fig. 25 shows the critical pore diameters for these mixtures.

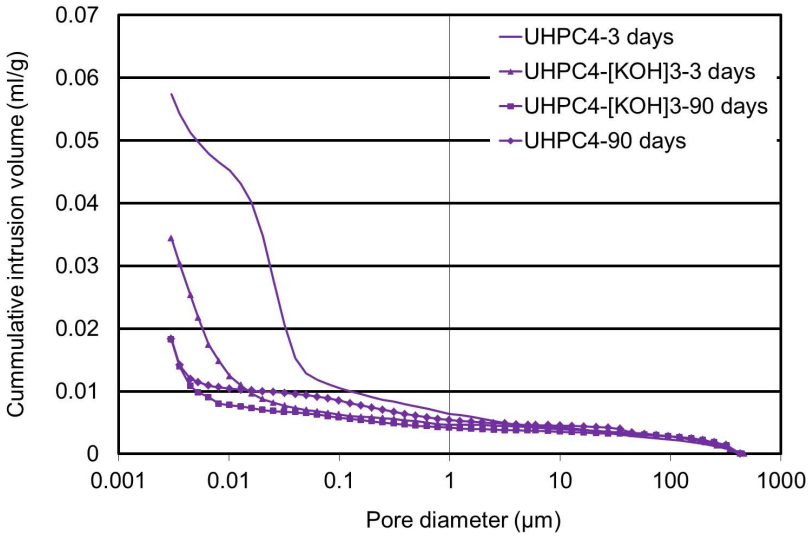


***Figure 24: Cumulative intrusion volume of UHPC$_4$ mixtures without and with chemical activation***

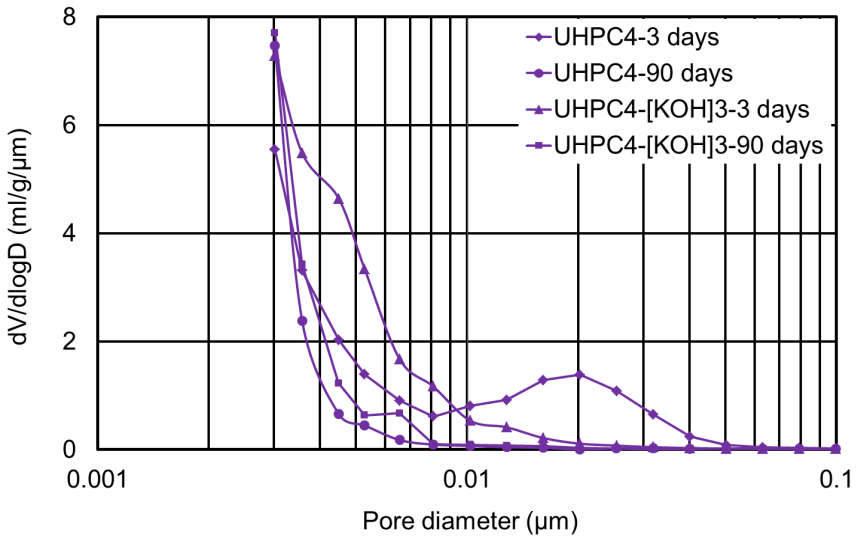


***Figure 25: Pore size distribution of UHPC$_4$ mixtures without and with chemical activation***

As exhibited in Fig. 25, the addition of chemical activator causes a great reduction in capillary pores particularly at early age, and an increase in the volume of nano-pores. As known, the AAS paste is distinguished by its finer matrix system compared to that of cement paste on the basis that for the same w/b, the hydration products have further gel pores and the pastes have lesser capillary pores [Chen, 2007]. Several researches have established that when a suitable chemical activator is utilized, the alkali-activated slag paste has less porosity, smaller pores, and the proportion of micro pores seems to be larger while the proportion of capillary pores is less than Portland cement paste [Collinsa and Sanjayan, 2000; Shi et al., 2006]. The microstructure evolution of hydrating AAS paste is governed by the quick alterations at early ages, and the latent evolution later [Chen, 2007]. This was discussed before through XRD analysis in Fig. 3.

Figs. 26 and 27 show the pores volume and the pore size distribution of thermally-activated mixtures ($UHPC_3$ and $UHPC_4$) respectively, compared to $UHPC_1$ at 90 days. As shown in Table 2, the measured porosities of non-activated $UHPC_3$ and $UHPC_4$ at 90 days and those thermally-activated are quite the same. Compared to $UHPC_1$, both $UHPC_3$-T and $UHPC_4$-T have less capillary pores and contain more nano-pores, denoting the beneficial effect of thermal activation in refining microstructure and decreasing porosity. This result agrees with those of Feylessoufi [Feylessoufi et al., 1996] and Matte [Matte, 1999]. The former observed a peak of 2.5 nm for thermally-treated UHPC with w/b of 0.12, and the second measured a porosity of 6% for treated UHPC (w/c = 0.18) at 90°C.

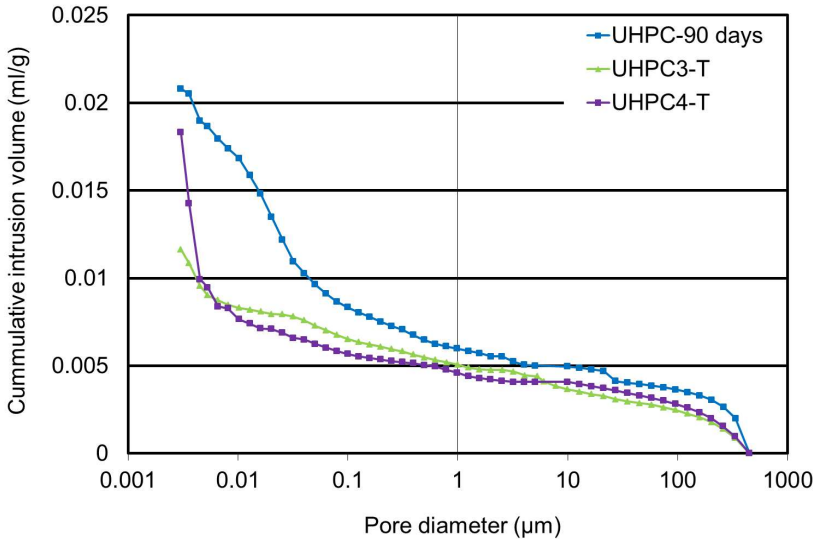


***Figure 26: Cumulative intrusion volume of $UHPC_1$ compared to the thermally activated mixtures of $UHPC_3$ and $UHPC_4$***

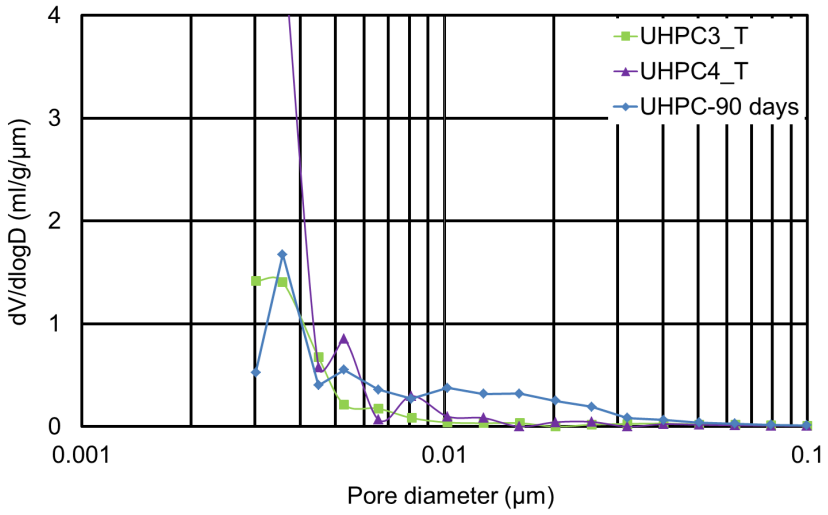


***Figure 27: Pore size distribution of $UHPC_1$ compared to the thermally activated mixtures of $UHPC_3$ and $UHPC_4$***

## 3. Conclusions

The following conclusions can be drawn:

- For cement replacement with 30% of BFS, the hydration reaction is accelerated, promoting the portlandite formation and increasing the content of C-S-H at 3 and 90 days according to XRD analysis. This results in refining the UHPC porosity, leading to a compact microstructure as shown in TEM images.

- For cement replacement with 50 and 80% of BFS, the portlandite and C-S-H intensities are lowered particularly at 3 days. Therefore, the capillary pores are enlarged and the total porosity increased. At 90 days the hydrates content increased, filling capillary pores and reducing the total porosity of UHPC.

- The chemical activation by $[KOH]_3$ solution for the 80% of BFS in the $UHPC_4$ boosted BFS reactivity by providing adequate alkalis that heightened its consumption of portlandite. The alkaline solution promotes the dissolution of slag glass structure, and BFS reaction is quickened. As a result, the developed hydrates fill capillary pores and refine the microstructure.

- The thermal activation lowered the portlandite intensities in $UHPC_3$ (50% BFS) and $UHPC_4$ (80% BFS) according to XRD analysis. So, the pozzolanic reaction was highly activated due to the solubility intention of the alkali hydroxides and the large supplying of portlandite released during the cement hydration, leading to decrease the pore size distribution, get bigger the density, grow the hydration products, and develop the quality of ITZ through good filling with hydrates as observed by TEM image. Consequently, the thermal activation is highly efficient for developing the microstructure of UHPC with high BFS contents.

## 4. References

[Abdulkareem et al., 2016] O.M. Abdulkareem, A. Ben Fraj, M. Bouasker, A. Khelidj, Early age and mechanical properties of environmentally friendly ultra high performance concrete. Proceedings of the 9th International Concrete Conference: Environment, Efficiency, and Economic Challenges for Concrete, Dundee, Scotland, 2016, pp.827-838.

[Abdulkareem et al., 2018] O. M. Abdulkareem, A. Ben Fraj, M. Bouasker, A. Khelidj, Mixture design and early age investigations of an environmentally friendly UHPC. Const. Build. Mater. 163 (2018) 235-246.

[Abdulkareem et al., 2018b] O. M. Abdulkareem, A. Ben Fraj, M. Bouasker, A. Khelidj, Effect of chemical and thermal activation on the mechanical performance of an environmentally friendly UHPC. Const. Build. Mater. (2018) Accepted.

[Ashraf et al., 2009] M. Ashraf, A.N. Khan, Q. Ali, J. Mirza, A. Goyal, A.M. Anwar, Physico-chemical, morphological and thermal analysis for the combined pozzolanic activities of minerals additives. Const. Build. Mater. 23 (2009) 2207-2213.

[Ben Haha et al., 2011] M. Ben Haha, G. Le Saout, F. Winnefeld, B. Lothenbach, Influence of activator type on hydration kinetics, hydrate assemblage and microstructural development of alkali activated blast-furnace slags. Cem. Concr. Res. 41 (2011) 301-310.

[Berodier et Scrivener, 2015] E. Berodier, K. Scrivener, Evolution of pore structure in blended systems. Cem. Concr. Res. 73 (2015) 25-35.

[Chen, 2007] W. Chen, Hydration of slag cement: Theory, modeling, and application, University of Twente, The Netherlands, Doctoral Thesis, 2007.

[Cheyrezy et al., 1995] M. Cheyrezy, V. Maret, L. Frouin, Microstructural analysis of RPC (Reactive Powder Concrete). Cem. Concr. Res. 25 (7) (1995) 1491-1500.

[Collinsa and Sanjayan, 2000] F. Collinsa, J.G. Sanjayan, Effect of pore size distribution on drying shrinkage of alkali-activated slag concrete. Cem. Concr. Res. 30 (2000) 1401-1406.

[Courtial et al., 2013] M. Courtial, M.-N.D. Noirfontaine, F. Dunstetter, M.S-. Frehel, P. Mounanga, K. Cherkaoui, A. Khelidj, Effect of polycarboxylate and crushed quartz in UHPC: Microstructural investigation. Constr. Build. Mater. 44 (2013) 699-705.

[Feylessoufi et al., 1996] A. Feylessoufi, F. Villiéras, L.J. Michot, P. De Donato, J.M. Cases, P. Richard, Water, environmental, and nano-structural network in a reactive powder concrete. Cem. Concr. Compo. 18 (1) (1996) 23-29.

[Gatty et al., 2001] L. Gatty, S. Bonnamy, A. Feylessoufi, C. Clinard, P. Richard, H. Van Damme, A transmission electron microscopy study of interfaces and matrix homogeneity in ultra-high-performance cement-based materials. Jour. Mater. Sci. 36 (2001) 4013-4026.

[Heikal et al., 2015] M. Heikal, O.K. Al-Duaij, N.S. Ibrahim, Microstructure of composite cements containing blast-furnace slag and silica nano-particles subjected to elevated thermally treatment temperature. Const. Build. Mater. 93 (2015) 1067-1077.

[Khalifa et al., 2013] N.E. Khalifa, M. Bouasker, P. Mounanga, N. Benkahla, Physico-chemical study of cementitious materials based on binary and ternary binders. Chem. Mat. Res. 4 (2013) 19-24.

[Kocaba, 2009] V. Kocaba, Development and evaluation of methods to follow microstructural development of cementitious systems including slags, École Polytechnique Fédérale of Lausanne, Switzerland, Doctoral Thesis, 2009.

[Kourounis et al., 2007] S. Kourounis, S. Tsivilis, P.E. Tsakiridis, G.D. Papadimitriou, Z. Tsibouki, Properties and hydration of blended cements with steelmaking slag. Cem. Concr. Res. 37 (2007) 815-822.

[Loukili et al., 1999] A. Loukili, A. Khelidj, P. Richard, Hydration kinetics, change of relative humidity, and autogenous shrinkage of ultra-high-strength concrete. Cem. Concr. Res. 29 (4) (1999) 577-584,

[Matte, 1999] V. Matte, Durability of ultra high performance concrete: Role of cementitious matrix, ENS Cachan University of Sherbrooke, Canada, Doctoral Thesis, 1999.

[Mehdipour and Khayat, 2017] I. Mehdipour, K. H. Khayat, Effect of particle-size distribution and specific surface area of different binder systems on packing density and flow characteristics of cement paste. Cem. Concr. Compo. 78 (2017) 120-131.

[Ramezannianpour, 2014] A. A. Ramezannianpour, Cement Replacement Materials: Properties, Durability, Sustainability, Springer-Verlag Berlin Heidelberg, Germany, 2014.

[Rengguang et al., 2015] L. Rengguang, D. Shidong, Y. Peiyu, Microstructure of hardened complex binder pastes blended with slag. Jour. Chin. Cera. Soc. 43 (5) (2015) 610-618.

[Shi et al., 2006] C. Shi, P.V. Krivenko, D. Roy, Alkali-activated cements and concretes, 1st Edition, Taylor & Francis group, 2006.

[Shi et al., 2015] C. Shi, D. Wang, L. Wu, Z. Wu, The hydration and microstructure of ultra-high-strength concrete with cement-silica fume-slag binder. Cem. Concr. Comp. 61 (2015) 44-52.

[Tam et al., 2010] C. M. Tam, V. W. Y. Tam, K. M. Ng, Optimal conditions for producing reactive powder concrete. Maga. Conc. Res. 62 (10) (2010) 701-716.

[Zhou et al., 2006] J. Zhou, G. Ye, K. van Breugel, Hydration process and pore structure of portland cement paste blended with blast furnace slag. Proceedings of the 6th International Symposium on Cement & Concrete and Canmet, 2006, pp.1-7.

# Part 2. Experimental program

# Chapter 7. Mechanical properties of UHPCs

## Table of Contents



## List of figures

## Résumé

Ce chapitre traite de l'effet du dosage en laitiers des hauts fourneaux (LHF) sur les propriétés mécaniques des BUHP avec et sans activation. Nous nous intéressons à la résistance à la flexion, la résistance à la compression, et la résistance à la traction par fendage. Les essais de flexion/compression ont été réalisés sur des éprouvettes prismatiques 4 x 4 x 16 à 3, 7, 28 et 90 jours, alors que l'essai de traction a été réalisé sur des éprouvettes cylindriques 11 x 22 cm, à 3 et 28 jours.

De nos résultats, nous pouvons tirer les conclusions suivantes :

- Avec 30% de LHF, les propriétés mécaniques du béton sont améliorées, indépendamment de l'âge. En effet, et comme expliqué dans les chapitres précédents, avec un faible taux de LHF, la réaction d'hydratation du ciment est accélérée, favorisant ainsi celle du laitier et de la fumée de silice. Cela accélère la formation des hydrates, densifie la microstructure et diminue la porosité du béton. Par conséquent, les propriétés mécaniques sont améliorées, aussi bien au jeune âge qu'à long terme. Pour 30% de LHF, aucune activation n'était nécessaire et les performances du béton de référence sont atteintes, avec un dosage en ciment et un dosage en superplastifiant moindre ;
- Pour un fort dosage en LHF ($BUHP_3$ avec 50% et $BUHP_4$ avec 80%), l'effet de dilution l'emporte sur la nucléation hétérogène. Par conséquent, des faibles taux de portlandite et d'hydrates sont produits. De ce fait, le mélange a une faible porosité et sa résistance chute remarquablement, notamment au jeune âge. A long terme, la réaction de la fumée de silice et celle du laitier viennent améliorer la densité du béton et remplir la porosité, ce qui réduit la difference entre le béton de référence et $BUHP_3$ et $BUHP_4$.Toutefois, une activation s'impose afin de combler cette difference ;
- L'activation alcaline du $BUHP_4$ avec $[KOH]_3$ provoque la réaction du laitier, ce qui améliore les propriétés microstructurales du mélange. Cela augmente de 42% la résistance du $BUHP_4$ à 3 jours, sans pour autant atteindre celle du béton de référence ;
- L'activation thermique accélère la réaction des particules solides, ce qui augmente le taux d'hydrates formées. Par conséquent, la microstructure est plus dense et les propriétés mécaniques sont améliorées. Le cycle thermique adopté semble être efficace pour un taux de LHF de 50%. En effet, la résistance à la compression du $BUHP_3$-T dépasse de 7% celle du béton de référence à 90 jours. Pour un taux de LHF de 80%, la résistance mesurée est 12,5% moins que celle du $BUHP_1$.

# 1. Introduction

The main feature of UHPC is its extremely high mechanical performance as it contains fine particles which are optimized in order to obtain compact material with high compressive strength. This section aims at assessing the mechanical properties of optimized UHPC (chapter5), and correlating them with microstructural ones (chapter6). Compressive and flexure strengths are measured for all studied UHPCs at 3, 7, 28 and 90 days. Splitting tensile one is measured at 3 and 28 days. Three parameters are considered in this chapter:

- The BFS content: three cement substitution-volumes are considered (30, 50 and 80%), and their effects on early age and later mechanical properties of UHPCs are investigated;
- The effect of chemical activation on mechanical properties: the chemical activator, KOH, is added to compensate for the lack of alkalis in blended UHPCs particularly for high BFS content;
- The effect of thermal activation, for 30% and 50% of BFS, on mechanical performance of blended UHPCs compared to that of reference concrete at 90 days.

# 2. Results and discussion

In this section, the flexure, compressive and splitting tensile strengths are explored for different studied UHPCs. The cited parameters are analysed regardless of BFS content and activation methods as the mechanical properties of UHPC depend on the curing regime [Yang et al., 2009].

## 2.1. Effect of slag content

The incorporation of different amounts of slag in blended mixtures of UHPC results in different flexure and compressive strengths as illustrated by Fig. 1 and Fig. 2 respectively.
According to Figs 1 and 2, the strength gain ratios of $UHPC_2$ in flexion are of 6%, 4%, 13% and 4% whereas the gain ratios in compression are of 2.8%, 6%, 1.4% and 1.2% for 3, 7, 28 and 90 days respectively. When focussing on compressive strength progress, it was noted that the substitution of 30% of cement with BFS induces an important increase at early ages (3 and 7 days) compared to those at 28 and 90 days. Two reasons could explain this result: i) the high superplasticizer dosage of $UHPC_1$, compared to $UHPC_2$, which restricts the hydration reaction of cement particles and delays the hydrates formation. This results in decreasing compressive strength particularly at early age (3 days). ii) The beneficial effect of BFS particles on concrete hydration and hardening due to the high specific area of BFS. This effect is coupled; physical, by improving the packing density of UHPC and chemical by activating the cement hydration.

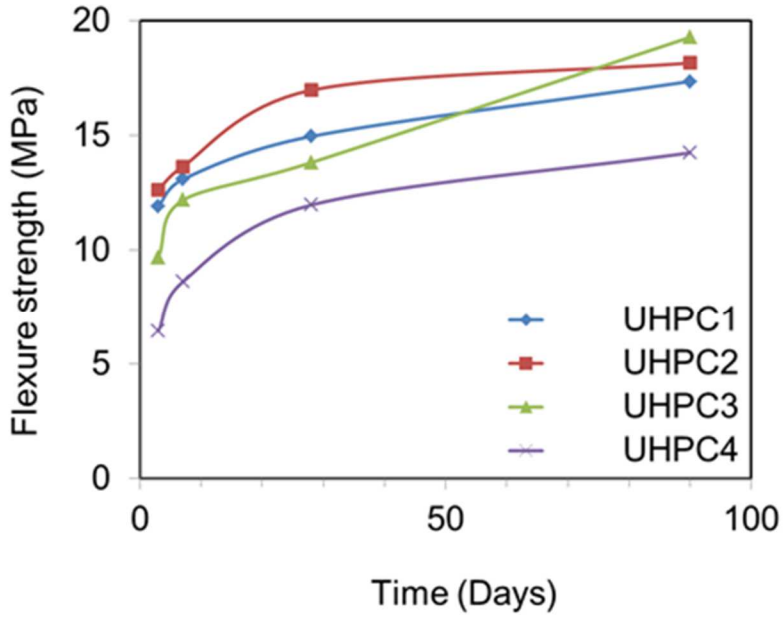


***Figure 1: Flexure strengths of UHPC specimens***

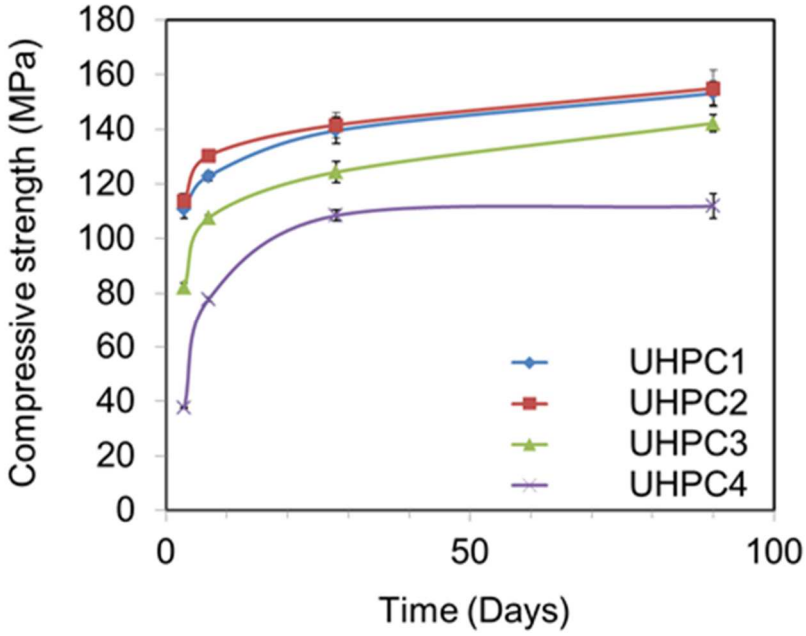


***Figure 2: Compressive strengths of UHPC specimens***

Thanks to fineness of the BFS particles that fill voids between cement grains themselves and those between cement grains and quartz sand ones, the bond strength between the components of matrix skeleton is enhanced [Siddique, 2008; Yazıcı et al., 2009], and the ITZ of the aggregate-cement paste is intensified. In addition, BFS particles, like SF ones, act as heterogeneous nucleation sites. Thereby, they accelerate the hydration of cement [Abdulkareem et al., 2018], and the formation of hydrates required for strength development.

The obtained results are compatible with those of thermogravimetric analysis, showing the slight increase of C-S-H peak of $UHPC_2$, compared to $UHPC_1$. These formed hydrates (C-S-H gel with low density) fill the capillary pores, and then decrease the total porosity of $UHPC_2$ by 18% at 3 days, as shown in chapter6.

At later ages (28 and 90 days) the difference between $UHPC_1$ and $UHPC_2$ is reduced, and the compressive strength of the second exceeds slightly that of the former. This trend could be explained by the low water content of UHPC, which restricts the reactions of SF and BFS in long term. Indeed, unlike ordinary and high performance concretes, the formed portlandite in UHPC is reduced. The portlandite is needed for the pozzolanic reaction of SF and BFS, and its scarcity decreases their reactivity.

In order to show the filler effect of slag in improving packing density and then compressive strength of concrete, limestone filler is incorporated as partial substitution of cement by 30% in the UHPC mixture which is compared with slag in the $UHPC_2$. Figs. 3 and 4 exhibit the comparison of flexure and compressive strengths of $UHPC_2$ (with slag) and that based on limestone filler.

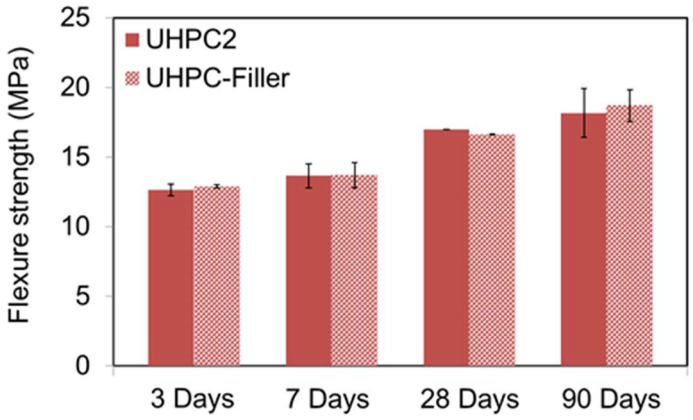


***Figure 3: Flexure strengths of $UHPC_2$ with slag and UHPC mixture with limestone filler***

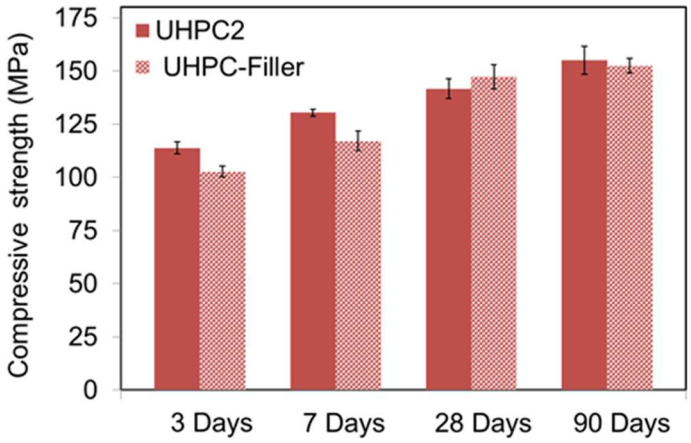


***Figure 4: Compressive strengths of $UHPC_2$ with slag and UHPC mixture with limestone filler***

Despite its lower specific area, compared to limestone filler, slag confers more compressive strength at all curing ages. This result highlights the slight reactivity of slag at early age, which compensates for the loss of strength that should occur because of the decreased specific area. Indeed, limestone filler, and despite its high specific area, has lower chemical activity. The chemical activity of limestone filler is 0.79 while it is around 0.9 for the slag. The limestone powder effect consists of increasing the compressive strength at early age by heterogeneous nucleation while slag could play a complex role consisting on filling voids between cement particles and improving compressive strength by heterogeneous nucleation in addition to its chemical effect through its latent reactivity at early age.

With high BFS content, the decrease of flexure and compressive strengths is important, particularly at early age. As shown in Fig. 2, the drop amounts of compressive strength of $UHPC_3$ are 26%, 12%, 11% and 7% whereas for $UHPC_4$ are 66%, 37%, 22% and 27% at 3,7, 28 and 90 days, sequentially. As explained in our recent study [Abdulkareem et al., 2018], at early age, the dilution effect of BFS particles prevails on the heterogeneous nucleation one. This results in high liquid-solid ratio, leading to delay the hardening of UHPC and its strength development. According to thermogravimetric analysis, at 3 days, the rates of formed hydrates and portlandite are very low, denoting the delay of cement hydration and the latent reaction of slag. Thereby, UHPC microstructure is more porous and the compressive strength is decreased. At later ages (28 and 90 days) the difference between $UHPC_1$ and $UHPC_3$ decreases, denoting the progress of pozzolanic reaction of SF and BFS. For $UHPC_4$, the compressive strength, and despite its rapid increase between 3 and 7 days, is quite the same at 28 and 90 days. This trend shows that the hydration reaction of solid components is postponed after 28 days and the rate of formed hydrates is low. Indeed, with high BFS content and low water one, the produced portlandite is restricted and not enough for pozzolanic reaction of SF and BFS, which reduces C-S-H content and decreases the compressive strength despite the refinement of the microstructure [Schuldyakov et al., 2016].

Fig. 5 shows the splitting tensile strength of different UHPCs at 3 and 28 days. At first glance, all manufactured UHPC have a splitting tensile strength at 28 days exceeding 8 MPa in spite of absence of fibres. This result is very interesting, as the tensile strength is a key parameter in UHPC mixture design. Even if a low BFS content does not affect greatly the concrete tensile strength, the high BFS content of 50% decreases the strength by 10% and 13% at 3 and 28 days respectively. The drop of splitting tensile strength of $UHPC_4$ with 80% of BFS is 68% at 3 days. This important result agrees with that of compressive strength. The same factors influencing the compressive strength of tested UHPCs could be presented to explain the effect of BFS content on the splitting tensile strength even if the latter seems to be less sensitive than the former.

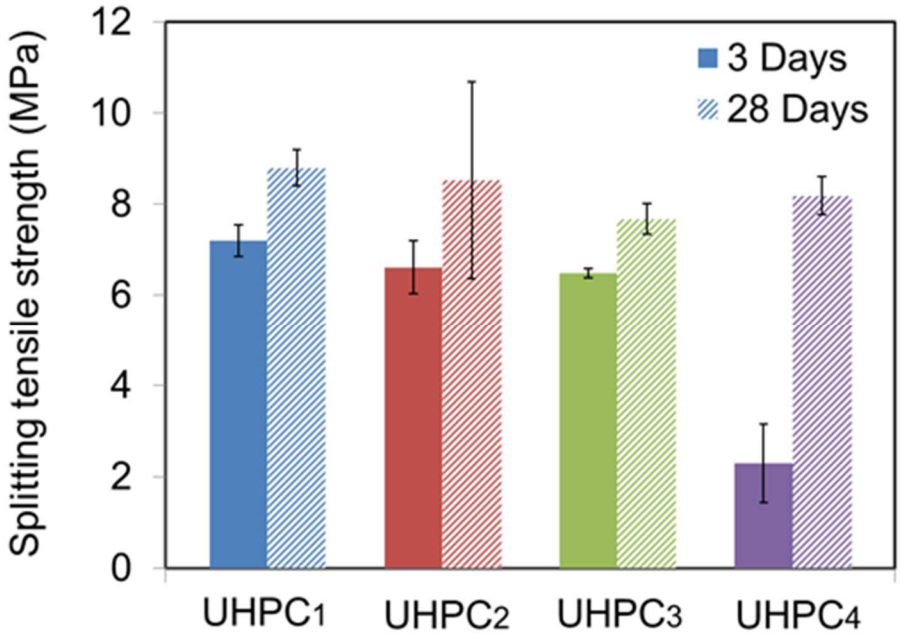


***Figure 5: Splitting tensile strengths of UHPC specimens***

## 2.2. Effect of chemical activation

As aforementioned earlier, the original concentration of the used alkaline activator, $[KOH]_1$, is calculated to compensate for the lack of alkalis caused by the substitution of cement. The concentration of KOH should be high to improve the early age properties of blended UHPCs [Abdulkareem et al., 2018]. Therefore, we will focus on $UHPC_4$, where the rate of cement substitution is important. Thus, an important quantity of KOH (proportional to the BFS content) can be added. To ensure the required compressive strength of $UHPC_4$, the concentration of $[KOH]_1$ was increased up three times ($[KOH]_3 = 3 \times [KOH]_1$). The latter is considered as the optimal concentration even if more potassium hydroxide is needed to improve the early compressive strength of $UHPC_4$ in order to reach that of reference $UHPC_1$. Indeed, more KOH affects greatly the workability of concrete and has a negative effect on its implementation and then on its compressive strength [Abdulkareem et al., 2018]. Figs. 6 and 7 depict the variation of both flexure and compressive strengths of $UHPC_4$-$[KOH]_3$ at all ages. As shown in Fig. 6, the flexure strength increases proportionally to activator's concentration, denoting the regularity and the high density of interfacial transition zone between the binder and the aggregate in the alkali activated slag mixtures [Sajedi and Abdul Razak, 2010]. This was helpful for raising the bond strength of alkali-activated concretes. Indeed, in presence of alkalis, BFS particles react rapidly, promoting hydrates formation, which explains the high consumption of portlandite for $UHPC_4$-$[KOH]_3$. The formed hydrates fill porosity and improve the properties of the transition zone in $[KOH]_3$-activated UHPCs. This results in flexure strength increase.

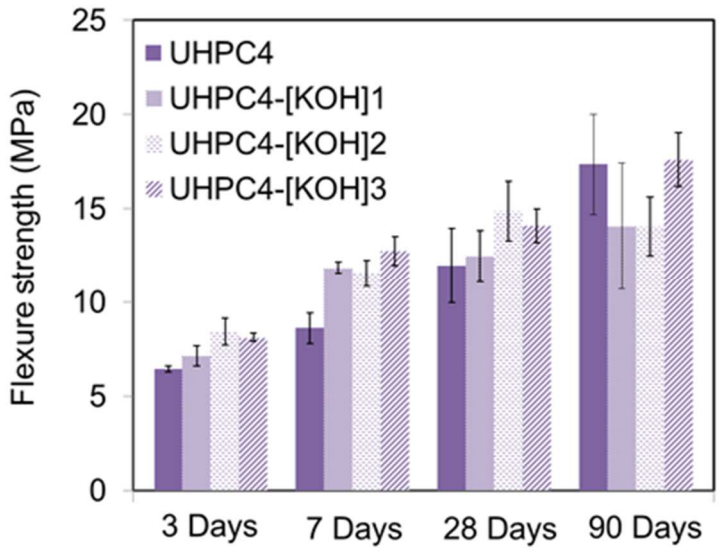


***Figure 6: Flexure strengths of [KOH]$_3$-activated UHPC$_4$ at all ages***

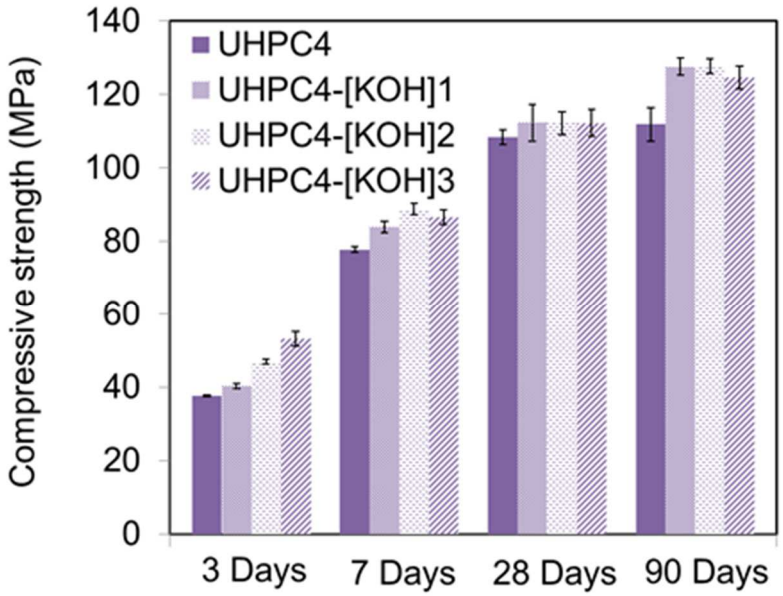


***Figure 7: Compressive strengths of KOH-activated UHPC$_4$ at all ages***

Like flexure strength, the compressive one is improved by chemical activation particularly at early age and with high concentration of alkaline activator. The measured growth of compressive strength is nearby 42% at 3 days whereas at 7, 28 and 90 days, the strength gain reached about 14%, 3% and 14% respectively as shown in Fig. 7. This trend is in accordance with those of previous studies, emphasizing on the dosage of activating agent as a paramount factor for improving the early age performance of blended mixtures [Gruskovnjak et al., 2006; Bilim and Atiş, 2012; Heikal et al., 2014; Gebregziabiher et al., 2016].

The presence of KOH with high concentration increases the solution's pH (i.e. higher alkalinity and correspondingly higher concentration of $OH^-$ ions), which rises the ability of dissolution of both Si and Al ions through destroying the Si-O and Al-O bonds in the slag glass matrix. This is followed by precipitation of hydrated products with low solubility such as calcium silicates, calcium aluminates, and magnesium aluminate. Then, steady ettringite is formed as a result of the interaction between Ca and Al. As a combined result of rising pH and generating ettringite, the hydration quickens [Abdulkareem et al., 2018], increasing hydrates formation and improving the compressive strength of concrete at early age [Ravikumar and Neithalath, 2012]. The obtained result agreed with those of thermogravimetric analysis and porosity. DTG curves showed clearly the great increase of C-S-H amount at 3 days when KOH is added leading to decrease the total porosity of $UHPC_4$ by 39%.

### 2.3. Effect of thermal activation

In order to reach the required compressive strength of reference concrete at 90 days, $UHPC_3$ and $UHPC_4$ are thermally-activated. The results of flexure and compressive strengths in comparative with $UHPC_1$ at 90 days are shown -in Figs. 8 and 9 respectively.

Compared to non-activated UHPCs (i.e. $UHPC_3$ and $UHPC_4$), both $UHPC_3$-T and $UHPC_4$-T have a great increase of their flexure and compressive strengths. This result shows the important role of thermal activation in accelerating the hydration process and producing hydrates [Habel et al., 2006] particularly in presence of BFS and SF, which improves the packing density and decreases the concrete's porosity. This results in increasing the mechanical properties of UHPC.

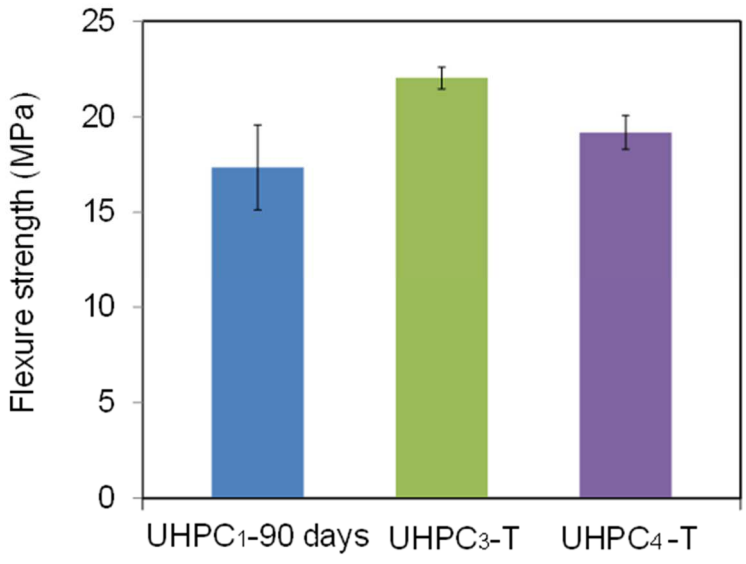


***Figure 8: Comparison of flexure strengths of thermally-activated $UHPC_3$ and $UHPC_4$ with $UHPC_1$***

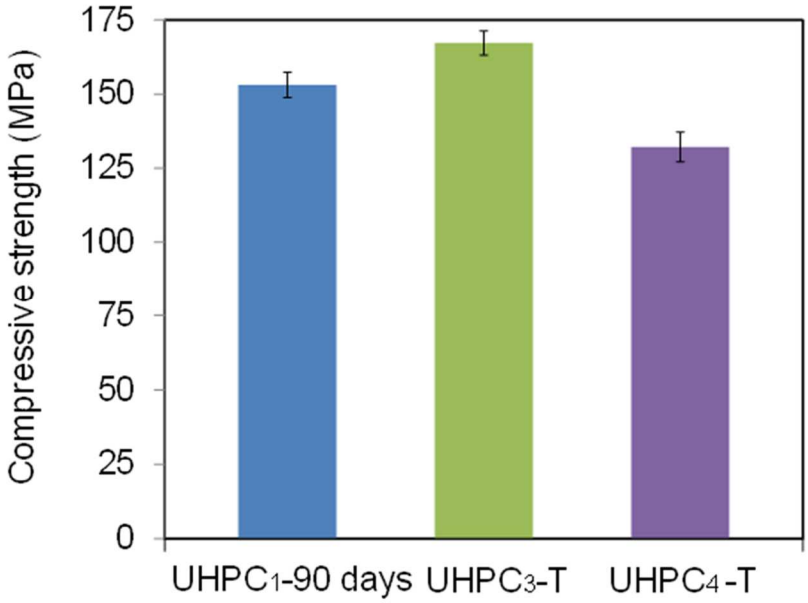


***Figure 9: Comparison of compressive strengths of thermally-activated $UHPC_3$ and $UHPC_4$ with $UHPC_1$***

As observed -in Fig. 9, the thermal activation increases the compressive strength of $UHPC_3$ and $UHPC_4$ by 1.7 and 3 times at 3 days respectively. The temperature accelerates the reaction process of solid components of concrete particularly BFS. Thereby, the higher slag amount, the higher apparent hydration activation energy [Habel et al., 2006; Kamen et al., 2007; Sajedi and Abdul Razak, 2010; Sajedi and Abdul Razak, 2011]. At 90 days, the compressive strength increase is of circa 16% and 20% for $UHPC_3$ and $UHPC_4$ sequentially. This result shows that contrary to ordinary and high performance concretes, the thermal activation improves the mechanical properties of UHPC at later age. For the formers and with thermal activation, there is not enough time for hydrated products to be regularly arranged inside the pores of the hardened paste, so the capillary pores are enlarged and the later strength is decreased. This phenomenon is known as crossover impact [Sadrekarimi, 2004; Castellano et al., 2016]. For UHPC, there is not enough water for totally concrete hydration, which disables the compressive strength development at later age. Therefore, the high temperature compensates for the lack of water by activating the solid components particularly the more sensitive one (BFS). This results in high consumption of portlandite by mineral admixtures (0% for thermally-activated UHPC) [Yazıcı et al., 2010], inducing a high production of hydrates. The latter will fill pores and improve the packing density of UHPC. Thereby, the porosity drops and the compressive strength increases.

As aforementioned, the objective of thermal activation is to reach the compressive strength of $UHPC_1$ at 90 days. This objective is reached for $UHPC_3$ and its compressive strength exceeds that of reference concrete by 7%, denoting the effectiveness of applied activation

scenario (temperature and duration). For $UHPC_4$, the thermal activation improves the compressive strength without reaching that of reference concrete (-12.5%). Indeed, the low cement content accompanied with the high water absorption of SF and BFS affect greatly the compressive strength. The thermal activation at 90°C for 48 hours does not counterbalance this drop. Thereby, the temperature should be increased or the duration should be extended to compensate for the decrease of compressive strength in presence of high BFS content.

## 2.4. Effect of combined chemical and thermal activation

The combined activation scenario consists of using chemical and thermal activation jointly. In this case, $UHPC_4$-$[KOH]_3$ is demoulded after 24 hours and thermally-activated for 48 hours as explained previously. The results of flexure and compressive strengths at 3, 28 and 90 days are shown -in Figs. 10 and 11 respectively.

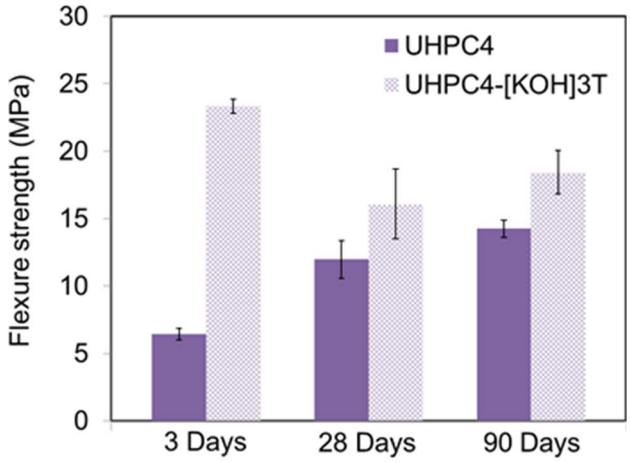


***Figure 10: Flexure strength of chemically and thermally-activated $UHPC_4$ mixtures***

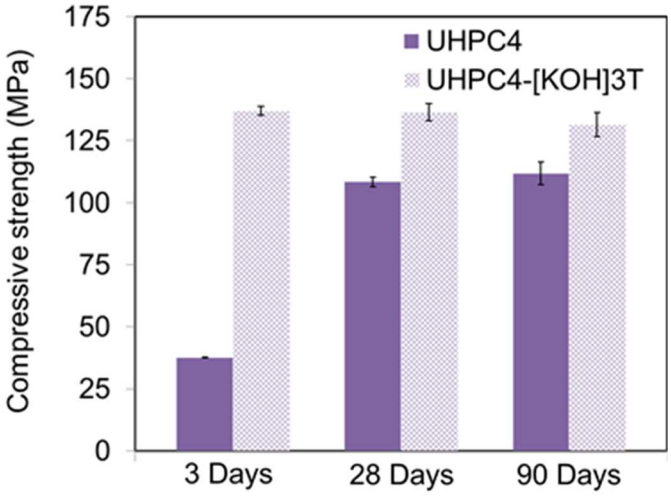


***Figure 11: Compressive strength of chemically and thermally-activated $UHPC_4$ mixtures***

Figs. 10 and 11 show clearly that the effect of chemical activation with $[KOH]_3$ is negligible as the measured compressive strength does not exceed that of $UHPC_4$-T. This result highlights two interesting ideas; i) even if $[KOH]_3$ improves the compressive strength of $UHPC_4$ at 3 days, this improvement has to be nuanced at 1 day, as the concrete has high superplasticizer content, which postpones the hydration reaction of cement and then that of activated slag. ii) the thermal activation, applied at 1 day, ensures an activation of all silicon solid components, which accelerates their hydration reaction, and induces an important increase of developed strength. In addition, the formed hydrates for thermally-activated UHPC are more densified than that formed by the chemical activation. Therefore, in this case study, it is not interesting to combine chemical and thermal activation.

## 3. Conclusions

The work carried out, allows us to withdraws the following conclusions:

- With 30% of slag, the heterogeneous nucleation effect of BFS particles prevails on dilution one. This results in acceleration of cement hydration reaction and consequently that of mineral admixtures (SF and BFS), which increases the amount of produced hydrates. The latter improve the packing density of concrete and decrease its porosity. Therefore, the compressive strength increases.

In addition to compressive strength enhancement, BFS particles improve the UHPC workability by their filling and lubrication roles which decrease the superplasticizer content. This reduces the environmental impacts and the cost of $UHPC_2$, compared $UHPC_1$.

-For high BFS contents (50% and 80%), the dilution effect prevails on heterogeneous one. The compressive strength of $UHPC_3$ and $UHPC_4$ developed slightly, denoting the low portlandite content, which results in less formed hydrates. Despite the physical effect (filling pores and improving the packing density) of BFS, the lack of water and portlandite restricts the pozzolanic reaction of SF and BFS, which decreases the mechanical performance of blended UHPC, compared to reference one.

- Alkaline activation with $[KOH]_3$ raises the dissolution of Si and Al ions by breaking the bonds of Si-O and Al-O in the slag glass, which promotes BFS reaction. This results in increasing C-S-H amount, decreasing porosity and improving the compressive strength of $UHPC_4$ at early age.

- Thermal activation increases the reaction of solid components and accelerates their hydration, which increases the portlandite consumption. Therefore, more hydrates are formed, filling the porosity, improving the packing density of UHPC and enhancing its mechanical performance. For $UHPC_3$-T, the chosen parameters of thermal activation ensure the required compressive strength. However, at 90°C and for 48 hours of activation duration, the compressive strength of $UHPC_4$-T is less than that of $UHPC_1$ at 90 days by 12.5%. The

lack of water and the high content of BFS explains this result. In order to improve the compressive strength of $UHPC_4$, higher temperature or longer duration have to be applied, as the combined chemical and thermal activation was not enough to compensate for the drop of strength.

## 4. References

[Abdulkareem et al., 2018] O. M. Abdulkareem, A. Ben Fraj, M. Bouasker, A. Khelidj, Mixture design and early age investigations of an environmentally friendly UHPC. Constr. Build. Mater. 163 (2018) 235-246.

[Bilim and Atiş, 2012] C. Bilim, C.D. Atiş, Alkali activation of mortars containing different replacement levels of ground granulated blast furnace slag. Constr. Build. Mater. 28 (2012) 708-712.

[Castellano et al., 2016] C.C. Castellano, V.L. Bonavetti, H.A. Donza, E.F. Irassar, The effect of w/b and temperature on the hydration and strength of blast furnace slag cements. Constr. Build. Mater. 111 (2016) 679-688.

[Gebregziabiher et al., 2016] B.S. Gebregziabiher, R. Thomas, S. Peethamparan, Temperature and activator effect on early-age reaction kinetics of alkali-activated slag binders. Constr. Build. Mater. 113 (2016) 783-793.

[Gruskovnjak et al., 2006] A. Gruskovnjak, B. Lothenbach, L. Holzer, R. Figi, F. Winnefeld, Hydration of alkali-activated slag: comparison with ordinary Portland cement. Adv. in Cem. Res. 18 (3) (2006) 119-128.

[Habel et al., 2006] K. Habel, M. Viviani, E. Denarié, E. Brühwiler, Development of the mechanical properties of an ultra high performance fiber reinforced concrete (UHPFRC). Cem. Concr. Res. 36 (7) (2006) 1362-1370.

[Heikal et al., 2014] M. Heikal, M.Y. Nassar, G. El-Sayed, S.M. Ibrahim, Physico-chemical, mechanical, microstructure and durability characteristics of alkali activated Egyptian slag. Constr. Build. Mater. 69 (2014) 60-72.

[Kamen et al., 2007] A. Kamen, E. Denarié, E. Brühwiler, Thermal effects on physico-mechanical properties of UHPFRC. ACI. Mater. Jour. 104 (4) (2007) 415-423.

[Ravikumar and Neithalath, 2012] D. Ravikumar, N. Neithalath, Effects of activator characteristics on the reaction product formation in slag binders activated using alkali silicate powder and NaOH. Cem. Concr. Compos. 34 (2012) 809-818.

[Sadrekarimi, 2004] A. Sadrekarimi, Development of a light weight reactive powder concrete. Jour. of Adv. Concr. Techn. 2 (3) (2004) 409-417.

[Sajedi and Abdul Razak, 2010] F. Sajedi, H. Abdul Razak, The effect of chemical activators on early strength of ordinary Portland cement-slag mortars. Constr. Build. Mater. 24 (2010) 1944-1951.

[Sajedi and Abdul Razak, 2010] F. Sajedi, H. Abdul Razak, Thermal activation of ordinary Portland cement–slag mortars. Mater. and Des. 31 (2010) 4522-4527.

[Sajedi and Abdul Razak, 2011] F. Sajedi, H. Abdul Razak, Effect of thermal and mechanical activation methods on compressive strength of ordinary Portland cement-slag. Mater. and Des. 32 (2011) 984-995.

[Schuldyakov et al., 2016] K.V. Schuldyakov, L.Ya. Kramar, B.Ya. Trofimov, The properties of slag cement and its influence on the structure of the hardened cement paste. Proc. Eng. 150 (2016) 1433-1439.

[Siddique, 2008] R. Siddique, Waste Materials and By-Products in Concrete, Springer-Verlag Berlin Heidelberg, 2008.

[Yang et al., 2009] S.L. Yang, S.G. Millard, M.N. Soutsos, S.J. Barnett, T.T. Le, Influence of aggregate and curing regime on the mechanical properties of ultra-high performance fibre reinforced concrete (UHPFRC). Constr. Build. Mater. 23 (2009) 2291-2298.

[Yazıcı et al., 2009] H. Yazıcı, M.Y. Yardımcı, S. Aydın, A.S. Karabulut, Mechanical properties of reactive powder concrete containing mineral admixtures under different curing regimes. Constr. Build. Mater. 23 (2009) 1223-1231.

[Yazıcı et al., 2010] H. Yazıcı, M.Y. Yardımcı, H. Yiğiter, S. Aydın, S. Türkel, Mechanical properties of reactive powder concrete containing high volumes of ground granulated blast furnace slag. Cem. Concr. Compos. 32 (2010) 639-648.

# Part 2. Experimental program

# Chapter 8. Durability properties of UHPCs

## Table of Contents



## List of figures



## List of tables

## Résumé

Dans ce chapitre, nous nous intéressons à l'évolution des propriétés de durabilité des BUHP en fonction de la teneur en laitiers des hauts fourneaux (LHF). Il s'agit de quantifier et d'étudier la perméabilité au gaz, la diffusion des ions chlore, la carbonatation et la résistance aux cycles gel/dégel des BUHP.

De nos résultats, nous pouvons tirer les conclusions suivantes :

- Avec un rapport eau/liant très faible, les BUHP étudiés présentent des propriétés de durabilité très élevées. Afin de les quantifier certaines modifications/ adaptations de methodes d'essais actuelles ont été nécessaires : (i) pour la perméabilité au gaz, nous avons opté pour un débitmètre de haute précision et la pression de confinement a été augmentée afin de pouvoir appliquer une pression d'injection plus élevée. (ii) Afin de s'assurer de la saturation des BUHPs, des échantillons de 2,5 cm d'épaisseur ont été mis en contact avec une solution basique pendant une semaine. Ensuite le béton a été placé entre les deux compartiments d'une cellule de diffusion et un champ électrique de 30 V a été appliqué pendant 1 mois, avant de mesurer la profondeur de diffusion. (iii) pour la carbonatation, les échantillons ont été exposés à une ambiance riche en $CO_2$ (à 50%) pendant 6 mois et 1 an. (iv) 1000 cycles de gel/dégel ont été appliqués sur les BUHPs.
- Les résultats ont montré l'effet bénéfique des LHF sur les propriétés de durabilité des BUHPs et c'est quel que soit le taux de substitution. Les particules de LHF diminuent la porosité et densifient la microstructure en diminuant la porosité capillaire et en augmentant le volume des nano-pores. A long terme, les LHF consomment la portlandite et génèrent des hydrates. Ces dernières remplissent les pores capillaires, déconnectent les pores et rendent le milieu plus tortueux. Cela augmente les propriétés de durabilité des BUHP à base de LHF. Pour les chlorures, la présence des LHF augmente également la capacité de fixation, ce qui diminue considérablement le coefficient de diffusion du BUHP. Au contraire, les LHF engendrent une diminution du pH de béton, ce qui favorise sa carbonatation. Toutefois, cet effet est contrebalancé par l'effet de remplissage due à la finesse. Le dernier prévaut en obstruant les chemins préférentiels de diffusion de $CO_2$.
- A l'exception de la diffusion des ions chlore, l'activation chimique de $BUHP_4$ avec $[KOH]_3$, améliore les propriétés de durabilité. La solution alcaline augmente le pH, ce qui diminue la profondeur de carbonatation dans les bétons activés chimiquement.
- L'activation thermique des $BUHP_3$ (50% LHF) et $BUHP_4$ (80% LHF) assure une meilleure durabilité. Avec 90°C, le taux d'hydrates augmente rapidement et la microstructure devient plus fine avec une tortuosité élevée. L'effet *filler* des LHF et leur activation thermique induisent une matrice plus compacte, avec une faible perméabilité au gaz, une faible profondeur de carbonatation et une résistance élevée au gel/dégel.

# 1. Introduction

UHPC is the ideal material in aggressive environment, thanks to its fine pores and dense microstructure. To characterize its durability, some properties should be assessed; gas permeability, chloride diffusion, carbonation and freezing-thawing cycles. In order to reduce the environmental footprints of developed UHPC, BFS is incorporated as partial substitution of cement. This industrial co-product is known by its fineness and binding capacity of aggressive agents.

This chapter is dedicated to durability properties assessment considering the BFS content, and the effect of chemical activation and that of thermal one. Results are correlated with microstructural observations in order to explain deeply the behaviour of different UHPCs in presence of BFS.

# 2. Results and discussion

## 2.1. Gas permeability

It has great interest to remind that one day is necessary to carry out all measurements before evaluating the permeability of UHPC. Indeed, we waited few hours before obtaining constant flow for every applied pressure despite the lower thickness of UHPC specimen (2.5 cm).

Table 1 exhibits the coefficients of gas permeability for reference UHPC mixture and the blended mixtures with and without activation.

***Table 1: Gas permeability coefficients of UHPC specimens with and without activation***

| Mix designation | Gas permeability coefficients-$k_V$ ($m^2$) |
|---|---|
| $UHPC_1$ | $28.0x10^{-19}$ |
| $UHPC_2$ | $10.1x10^{-19}$ |
| $UHPC_3$ | $20.0x10^{-19}$ |
| $UHPC_4$ | $4.9x10^{-19}$ |
| $UHPC_4$-$[KOH]_3$ | n.d |
| $UHPC_3$-T | $6.6x10^{-19}$ |
| $UHPC_4$-T | $0.43x10^{-19}$ |

Firstly, it should be noted that the lower values of gas permeability coefficients for all UHPCs exceed slightly those reported in the literature [Lafarge, 2003; Carcasses, 2009; Mounanga et al., 2012], where the permeability of UHPC is about $10^{-19}$-$10^{-20}$ m². This could be attributed to the utilization of the new experimental set up that provides precise assessment of UHPC permeability. Furthermore, it could be attributed to the high drying temperature of 105°C. Contrary, the obtained results agree with that of Roux [Roux et al., 1995]. The latter tested non treated Reactive Powder Concrete (RPC) and measured 2.5 x $10^{-18}$ m². The extremely low permeability coefficient of $28x10^{-19}$ $m^2$ for $UHPC_1$ is due to the presence of the diminutive

and incoherent pores in the tightly packed and dense pore structure. As hydration proceeds, the capillary pores converted to be tortuous increasingly as interrelated pores were closed due to the production of C-S-H. So the enhancement in C-S-H thickness between capillaries composes an impermeable area in $UHPC_1$ and gives rise to continual decrease in permeability coefficient [Wang et al., 2015].

Likewise, there is an obvious reduction of permeability coefficients by 2.5 times and 1.5 times for $UHPC_2$ and $UHPC_3$ respectively while for $UHPC_4$ the intrinsic permeability lowers by 6 times compared to that of reference UHPC. Two parameters explain these results; concrete porosity and its pore size distribution. In this study, the total porosities are quite the same and not proportional to the reduction of permeability. According to the flow theories, the narrower pores reduce the flow rate even if the total porosity is the same. As shown in chapter6, no capillary pores were shown in presence of slag, so the microstructure is refined and the volume of nano-pores is increased. This was explained by filling role of BFS particles and the production of denser C-S-H in long term (pozzolanic reaction). These hydrates fill pores, making them narrower, and leading to tortuous and less permeable medium [Alamri, 1988].

When the thermal activation is applied, the permeability of $UHPC_3$ and $UHPC_4$ decreases by 3 and 10 times sequentially in spite of their closed total porosities (i.e. with and without thermal activation). As explained above, the key parameter in gas permeability is the pore size distribution and the application of thermal activation makes the porous network discontinuous which obstruct paths and decreases the permeability [Reddy and Tilak, 2015]. Indeed, in presence of temperature, the reaction of solid components is quickened and the C-S-H content increases. The latter fill the pores and makes the microstructure denser, with finer porous network, and subsequently the permeability reduces [Çakır and Aköz, 2008].

## 2.2. Chloride Diffusion

Table 2 exhibits the apparent chloride diffusion coefficients for all mixtures of UHPC after 1 month of chloride exposure with 30-V potential difference. The measured coefficients agree with those of bibliography [Roux et al., 1995; Delagrave et al., 1997; Vernet, 2002; Lafarge, 2003; Resplendino and Petitjean, 2003].

The apparent diffusion coefficients for blended mixtures of UHPC are lower than that of $UHPC_1$, and the larger slag amount tends to decrease diffusion coefficient as observed in Table 2. The incorporation of slag decreases the total porosity and the pores interconnectivity accompanied with enhancing its binding and then its resistance to chloride ingress [Ben Fraj et al., 2012].

***Table 2: Apparent chloride diffusion coefficients of UHPC specimens with and without activation***

| Mix designation | Apparent chloride diffusion coefficients- $D_{app}$ ($m^2/s$) |
|---|---|
| $UHPC_1$ | $14.6x10^{-14}$ |
| $UHPC_2$ | $4.18\ x10^{-14}$ |
| $UHPC_3$ | $5.64x10^{-14}$ |
| $UHPC_4$ | $3.56x10^{-14}$ |
| $UHPC_4$-$[KOH]_3$ | $4.36x10^{-14}$ |
| $UHPC_3$-T | $2.16x10^{-14}$ |
| $UHPC_4$-T | $0.92x10^{-14}$ |

The first factor that governs the chloride diffusion in UHPC is pores diameter distribution. As mentioned before, the variation of chloride diffusion coefficient is ascribed to the pore system geometry like tortuosity and constrictivity, which may be various even if the porosity is quite the same. Saeki [Saeki et al., 2006] reported that specific surface area could be used as an index of geometric characteristics of pores (i.e. tortuosity and constrictivity). In case of identical total porosity, the specific surface area of pore system enhances when the complexity of pore geometry enhances and the amount of fine pores grows. Ions in these fine pores attempt to be impacted by pore surface-charge impact on account of the limited distance between ions and pore surface. Furthermore, during hydration slag will bind the portlandite and generate secondary C-S-H gel. The higher slag content, the lower portlandite, and the higher C-S-H gel after hydration. Indeed, the potential slag reactivity decreases the total porosity by generation of slag reaction products that can fill large capillary voids and decrease the critical pore diameter which is regarded as an index for the porosity. Thus, it can be seen that the critical pore diameter in the blended slag mixtures of UHPC diminishes with a rise of slag quantity as shown in chapter6. The diversity in slag replacement rate modifies the pore structure and the mineral composition of cement paste. As a result, the pore diameter distribution is finer despite the similarity of total porosity [Saeki et al., 2006; Park et al., 2017].

The second factor is the chloride binding particularly in presence of BFS. The great amount of aluminates in slag promotes its binding capacity [Newman and Choo, 2003; Vejmelková et al., 2009; Ben Fraj et al., 2012; Takahashi and Ishida, 2016; Van Noort et al., 2016; Park et al., 2017;]. Therefore, the apparent chloride diffusion coefficient significantly reduces. This explains the low diffusion coefficient of $UHPC_4$, compared to $UHPC_3$. In fact, despite the higher total porosity of $UHPC_4$, it has great binding capacity and a high proportion of nano-pores with diameter lower than 10 nm. The latter is considered as threshold diameter for chloride diffusion [Takahachi and Ishida, 2016]

Table 5 shows the slight difference between the chloride diffusion coefficients of $UHPC_4$-$[KOH]_3$ and $UHPC_4$. This result confirms the rule that the effect of chemical activation is

remarkable in the early ages and marginal in the later ages. As shown through curves of pore size distribution at later ages, in chapter 6, $UHPC_4$ and $UHPC_4$-$[KOH]_3$ are similar, excepting that the second contains more pores with 6 nm. This difference explains the increase by 22% of chloride diffusion coefficient of $UHPC_4$ in presence of KOH.

As demonstrated in Table 2, the thermal activation is effective in reducing the chloride diffusion coefficients of the blended UHPC mixtures, compared to non-activated mixtures in particular with the high proportion of slag ($UHPC_4$). The thermally-activated mixtures are provided by a least porosity, miniature pore size distribution, and incoherent pore structure (in terms of the connectivity degree and the size of capillary pores) because of enhanced reactivity degree. The hydrates of the thermally-activated mixtures close tightly the nano-pores by C-S-H. For $UHPC_4$, BFS particles improve the packing density and obstruct different pores as exhibited in chapter6. Moreover, the high BFS content enhances the binding capacity of UHPC, and hence the chloride ingress notably reduces. Riding et al. [Riding et al., 2013] mentioned that high substitution rate of cement with 65% of slag was quite sensitive to curing temperature. In consequence, the arbitrary mobility of chloride ions in the thermally-activated mixtures is slowed and restricted, and hence the rate of ingress is decreased.

### 2.3. Carbonation

After 6 months and 1 year of exposure, specimen are sprayed with Phenolphthalein solution. Fig. 1 (right) highlights the difficulty to distinguish the carbonated depth which is not uncoloured like that for ordinary or high performance concretes. It is easier to measure this depth on broken specimen before spraying Phenolphthalein as shown in Fig. 1 (left). In addition, Fig. 1 shows the presence of some air bubbles due to the casting method. The specimens are compacted handily. This observation indicates that the measured carbonation depth should not be analysed only versus UHPC composition.


***Figure 1: $UHPC_3$ specimen with 50% $CO_2$ at 1 year, before and after spraying phenolphthalein solution***

The carbonation depths for high concentration of $CO_2$ (50%) in all studied UHPCs are summarized in Table 3. For 1% of $CO_2$, the carbonation depth is zero.

***Table 3: Carbonation depths for activated and non-activated UHPCs after 6 months and 1 year of exposure***

| Mix designation | Carbonation depth at 6 months (mm) | Carbonation depth at 1 year (mm) |
|---|---|---|
| $UHPC_1$ | 1.0 | 2.0 |
| $UHPC_2$ | 1.0 | 2.0 |
| $UHPC_3$ | 2.0 | 2.0 |
| $UHPC_4$ | 0.7 | 2.2 |
| $UHPC_4$-$[KOH]_3$ | 0.27 | 0.46 |
| $UHPC_3$-T | 0 | 1.04 |
| $UHPC_4$-T | 0 | 0.92 |

For all UHPCs, the measured depths of carbonation are lower after 6 months of exposure, compared to those of 1 year.

Focusing on carbonation depths measured after one year, some reasons could be stated to explain the slight difference between characterized UHPCs. However, these explanations have to be relativized, as the carbonation depth is very low and depends on casting energy.

- *Effect of BFS content*: as detailed in chapter6, the substitution of cement with BFS makes the microstructure dense and enhances the tortuosity by refining the porous network. The fine BFS particles fill spaces between cement particles (physical role) and their reaction generates dense C-S-H in the long term. The C-S-H fill the capillary pores and decrease the porosity of UHPC. However, this beneficial effect of BFS is counterbalanced by decrease of pH, caused by the consumption of portlandite for pozzolanic reaction. As a result, the carbonation reaction is promoted and the carbonation depth increases. This result agrees with that of Holthuizen [Holthuizen, 2016], who observed an increase of carbonation depth by 2 and 3 times in mortars with 55% and 70% of BFS contents respectively. Specimens were exposed to 3%-$CO_2$ ambiance for 160 days.

- *Effect of chemical activation*: in presence of KOH, pH increases, which promotes the reaction of BFS. Therefore, the microstructure is refined by the physical role of BFS particles and diffusion paths are obstructed. In addition, the pozzolanic reaction is boosted and the formed C-S-H enhances the concrete tortuosity. This interesting result highlights the beneficial effect of chemical activation in carbonation resistance of UHPC, compared to normal strength concretes. For these mixtures, the chemical activation increases the volume of capillary pores and promotes the carbonation phenomenon [Hossain et al., 2015].

Furthermore, this result confirms the suitability of used chemical activator and its concentration [Bilim and Atiş, 2012].

- *Effect of thermal activation*: the thermal activation decreases the carbonation depths in $UHPC_3$ and $UHPC_4$ by circa two times. As demonstrated in chapter6, temperature boosts the reaction of all components, accelerates the formation of hydrates and then the densification of UHPC microstructure. In the thermally-activated UHPC, diffusion paths are more tortuous, finer and obstructed. This effect prevails on that of BFS in decreasing pH. Thus, the carbonation resistance of activated-UHPCs is increased.

### 2.4. Freezing and thawing cycles

The effect of freezing-thawing cycles on the UHPC mixtures is measured through the variation of mass and length. Fig. 2 shows the variation of mass for the reference mixture ($UHPC_1$) and the rest blended mixtures with slag while Fig. 3 shows the length change of the specimens under the effect of 1000 cycles of freezing and thawing.

As known, the elongation of specimen was an index of micro-cracks that provide void spaces in the specimen, and the reduction in mass was an indicator of spalling or degradation of substance [Ahlborn et al., 2008]. From Fig. 2, it was demonstrated that there is slight increase of the mass for all UHPC mixtures and this increase is rapid up to 300 cycles of freezing and thawing and thereafter it becomes stable. Moreover, the small enhancement of the mass in both $UHPC_1$ and $UHPC_3$ was higher than that in $UHPC_2$ and $UHPC_4$ respectively. However, this mass variation between these mixtures remains modest. In addition, the length change of whole UHPC mixtures is quite little and negligible as observed in Fig. 3 despite that it was lower in $UHPC_1$ than the other blended slag mixtures. This can be explained through that the restricted expansion forces which are supported by the capillary pores as an effect of freezing cycles. The handle compaction of whole UHPC mixtures led to generation of few entrained air bubbles that could in turn liberate feeble forces of expansion. Furthermore, the smaller capillary pore volume of the UHPC mixtures is essential for enhancing the resistance of freezing and thawing damage. The interaction of slag and silica fume in the blended mixtures of UHPCs makes them further stabilized due to a lower cumulative pore volume which lessens as much with the increment of slag replacement level as explicated earlier, and generates weak expansion forces during freezing and thawing cycles [Lee et al., 2016]. So the amounts of specimens' elongation are very limited and may be ignored.

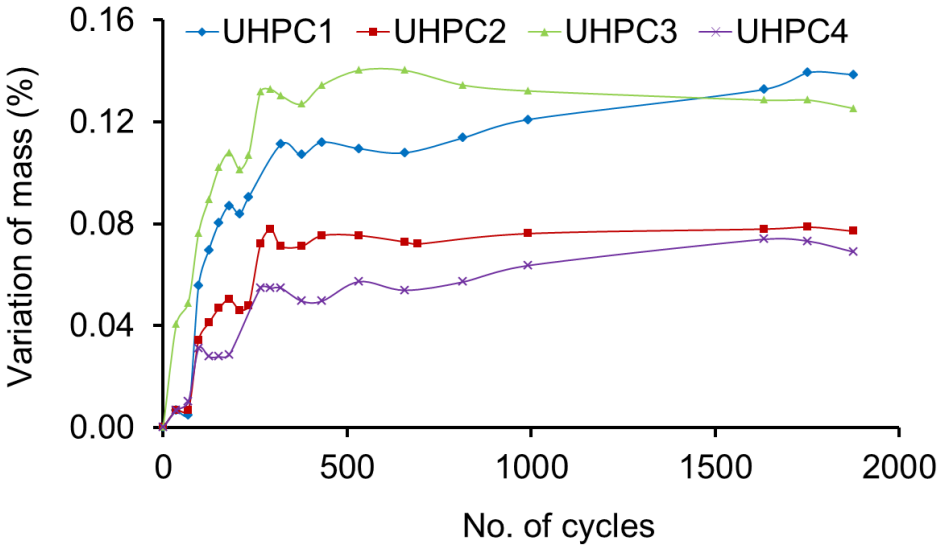


***Figure 2: Variation of mass of UHPC mixtures under effect of freezing-thawing cycles***

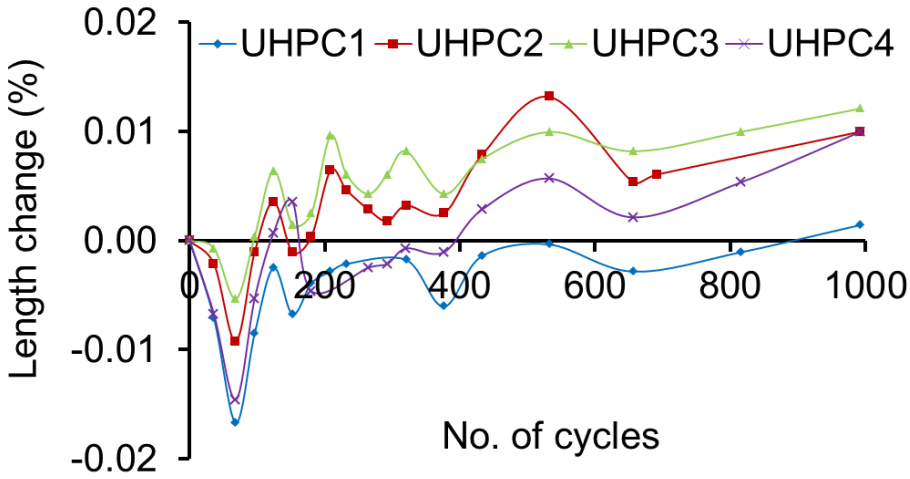


***Figure 3: Length change of UHPC mixtures under effect of freezing-thawing cycles***

Fig. 4 demonstrates the mass variation of both $UHPC_3$ and $UHPC_4$ with and without activation whereas Fig. 5 exhibits the length change of these mixtures after 1000 cycles of freezing and thawing.

The chemical activation used in $UHPC_4$-$[KOH]_3$ is efficient through a decreasing in mass increment of the $UHPC_4$ in addition to the ignored length change as demonstrated in Figs. 4 and 5 sequentially. This can be explained by the distinctive advantages of the $UHPC_4$-$[KOH]_3$ in terms of the hydration products that are dense and regular as well as the refined pore structure as seen in chapter6. Hence, the temperature of ice generation in the alkali-activated slag concrete is transferred to the zone of the least temperatures because the quantities of fine pores in the $UHPC_4$-$[KOH]_3$ are slightly more compared to that in the

$UHPC_4$ [Krivenko et al., 2014]. The pore structure of this chemically-activated mixture is effective in hindering the air breakthrough.

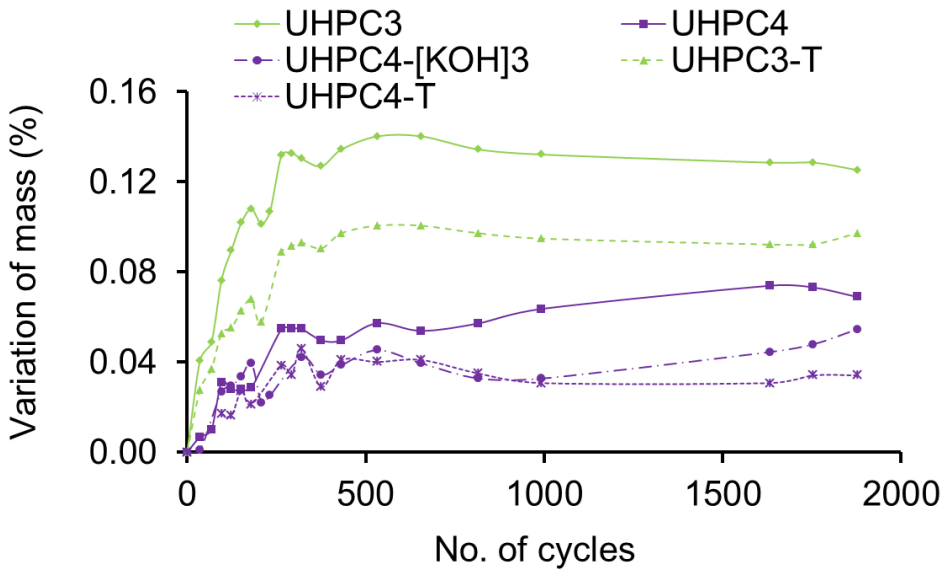


***Figure 4: Variation of mass of $UHPC_3$ and $UHPC_4$ mixtures with and without activation under effect of freezing-thawing cycles***

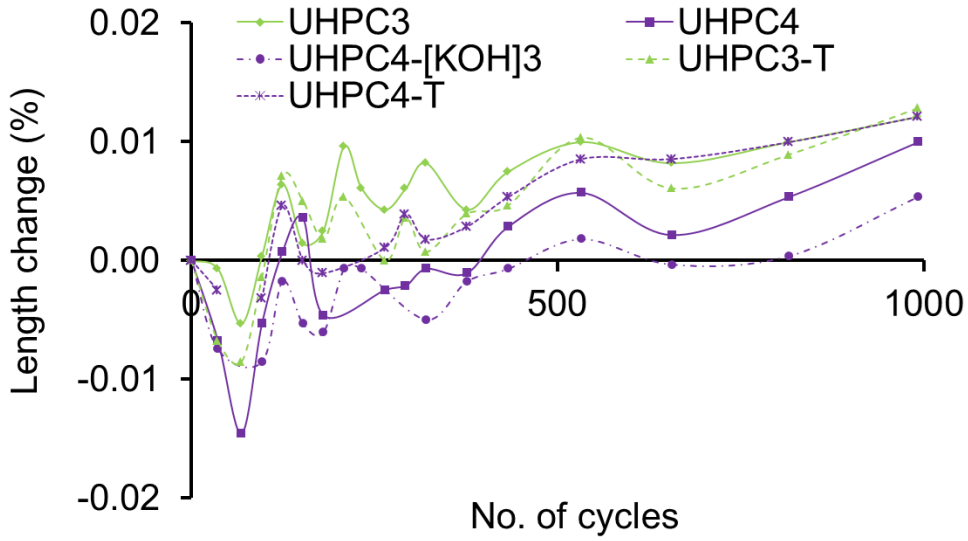


***Figure 5: Length changes of $UHPC_3$ and $UHPC_4$ mixtures with and without activation under effect of freezing-thawing cycles***

The application of thermal activation refines the porosity as observed in chapter6. Thereby, the mass and length variations are extremely low for both $UHPC_3$-T and $UHPC_4$-T. Through a minimal w/b and in presence of silica fume and slag, the internal relative humidity is very low. The limited air absorption into the external layer of specimens and freezing of the air could not rise the relative humidity in these layers. So, the tensional forces become lower and the variations of both mass and length are restricted.

## 3. Conclusions

The following conclusions can be drawn:

- With the low w/b of UHPC, the studied mixtures exhibit extraordinary durability properties. To assess these properties, several modifications/ accommodations of standards were applied: (i) For gas permeability, high precision flowmeter was used and the confinement pressure was increased in order to achieve high injection pressure; (ii) To saturate the UHPCs completely, a 2.5 cm-specimen was exposed to basic solution for one week. Then, the specimen was placed in diffusion cell and a 30V-potential difference was applied for one month before measuring the chloride depth; (iii) For carbonation test, specimens were exposed for 6 months and one year to 50%$CO_2$ ambiance; (iv) A 1000 cycles of freezing and thawing were applied.

- The beneficial effect of the BFS incorporation by various rates on the durability performance has been demonstrated. BFS lowers UHPC porosity and refines the microstructure by decreasing the capillary pores and increasing the volume of nano-pores. In long term, BFS consumes portlandite and generates plentiful quantities of hydration products (mainly C-S-H). The latter fill the capillary pores and make the porous network discontinuous and less interconnected, leading to form a tortuous and compact matrix. This results in enhancing the durability performance of blended UHPC. For chloride diffusion, the presence of slag, increases also the binding capacity of UHPC, leading to decrease its diffusion coefficient greatly, compared to reference one. Contrary, BFS decreases the pH in concrete and promotes its carbonation. However, this negative effect of BFS is counterbalanced by the filling one. The latter prevails by obstructing the paths of $CO_2$ diffusion.

- Except for chloride diffusion, the chemical activation of $UHPC_4$ by $[KOH]_3$ solution seems improving its durability properties. The alkaline solution increases pH, which decreases the carbonation depth of chemically-activated $UHPC_4$.

- The thermal activation of $UHPC_3$ (50% BFS) and $UHPC_4$ (80% BFS) ensures their high durability performances. At 90°C, the hydrates content increases greatly and the microstructure is refined, inducing more tortuous material. The filler effect of BFS and its thermal activation result in compact matrix, with low gas permeability, low carbonation depth and with high resistance to freezing/thawing cycles.

## 4. References

[Ahlborn et al., 2008] T.M. Ahlborn, E.J. Peuse, D.L. Misson, Ultra-High-Performance-Concrete for Michigan Bridges Material Performance – Phase I. Research report RC-1525, Center for Structural Durability Michigan Technological University, 2008, pp.1-181.

[Alamri, 1988] A.M. Alamri, Influence on curing on the properties of concretes and mortars in hot climates, Department of Civil Engineering, The University of Leeds, UK, Doctoral Thesis, 1988.

[Ben Fraj et al., 2012] A. Ben Fraj, S. Bonnet, A. Khelidj, New approach for coupled chloride/moisture transport in non-saturated concrete with and without slag. Constr. Build. Mater. 35 (2012) 761-771.

[Bilim and Atiş, 2012] C. Bilim, C.D. Atiş, Alkali activation of mortars containing different replacement levels of ground granulated blast furnace slag. Constr. Build. Mater. 28 (2012) 708-712.

[Çakır and Aköz, 2008] Ö. Çakır, F. Aköz, Effect of curing conditions on the mortars with and without GGBFS. Constr Build Mat. 22 (2008) 308-314.

[Carcasses, 2009] M. Carcassès, Bétons Fibrés Ultra Performant (BFUP). Les nouvelles recommandations AFGC chapitre 3 durabilité des BFUP", UHPFRC, Marseille, France.

[Delagrave et al., 1997] A. Delagrave, J. Marchand, J-P. Ollivier, S. Julien et K. Hazrati, Chloride binding capacity of various hydrated cement paste systems", Adv. Cem. Bas. Mater. 6 (1997) 28-35.

[Holthuizen, 2016] P. E. Holthuizen, Chloride ingress of carbonated blast furnace slag cement mortars, Section of Materials and Environment, Delft University of Technology, Netherlands, Master Thesis, 2016.

[Hossain et al., 2015] M.M. Hossain, M.R. Karim, M.K. Hossain, M.N. Islam, M.F.M. Zain, Durability of mortar and concrete containing alkali-activated binder with pozzolans: A review. Constr. Build. Mater. 93 (2015) 95-109.

[Krivenko et al., 2014] P.V. Krivenko, H.L. Cao, L.Q. Weng, O.N. Petropavlovskii, High-performance alkali-activated cement concretes for marine engineering applications, INTECH, http://dx.doi.org/10.5772/64525, 2014.

[Lafarge, 2003], Ductal: presentation du pont en Ductal de Saint Pierre Lacour.

[Lee et al., 2016] B. Lee, G. Kim, J. Nam, B. Cho, Y. Hamad, R. Kim, Compressive strength, resistance to chloride-ion penetration and freezing/thawing of slag-replaced concrete and cementless slag concrete containing desulfurization slag activator. Constr. Build. Mater. 128 (2016) 341-348.

[Mounanga et al., 2012] P. Mounanga, K. Cherkaoui, A. Khelidj, M. Courtial, M.-N.D. Noirfontaine, F. Dunstetter, Extrudable reactive powder concretes hydration, shrinkage and transfer properties. Europ. Jour. Env. Civ. Eng. 16 (2012) 99-114.

[Newman and Choo, 2003] J. Newman, B. S. Choo, Advanced Concrete Technology: Constituent Materials, Linacre House, Jordan Hill, Oxford OX2 8DP, Elsevier Ltd. UK, 2003.

[Park et al., 2017] K.-B. Park, H.-S. Lee, X.-Y. Wang, Prediction of Time-dependent chloride diffusion coefficients for slag-blended concrete. Advances in Materials Science and Engineering. 2017 (2017) 1-10.

[Reddy and Tilak, 2015] A.N. Reddy, U.V. Tilak, Drying shrinkage and durability studies on alkali activated slag concrete using different activators. Ijirset. 4 (11) (2015) 11483-11492.

[Resplendino and Petitjean, 2003] J. Resplendino et J. Petitjean, French recommendations for ultra-high performance fiber-reinforced concretes. International RILEM Workshop on Test and Design Methods for Steelfibre Reinforced Concrete, Bagneux (2003) 91-103.

[Riding et al., 2013] K. A. Riding, M. D. A. Thomas, K. J. Folliard, Apparent diffusivity model for concrete containing supplementary cementitious materials. ACI Mater Jour. 11 (6) (2013) 705-714.

[Roux et al., 1995] N. Roux, C. Andrade et M. A. Sanjuan, M. A., Etude expérimentale sur la durabilité des bétons de poudres réactives, Les Bétons de Poudres Réactives (BPR) à ultra haute résistance (200 à 800 MPa)", Annales de l'Institut Technique du Bâtiment et des Travaux Publics, 532 (1995) 133-141.

[Saeki et al., 2006] T. Saeki, K. Shinada, K. Sasaki, Chloride ions diffusivity and micro-structure of concrete madewith mineral admixtures. Proceedings of the Concrete Life-International RILEM-JCI Seminar on Concrete Durability and Service Life, 2006.

[Takahashi and Ishida, 2016] Y. Takahashi, T. Ishida, Modeling of chloride transport resistance in cement hydrates by focusing on nanopores. Jour Adv Concr Technol. 14 (2016) 728-738.

[van Noort et al., 2016] R. van Noort, M. Hunger, P. Spiesz, Long-term chloride migration coefficient in slag cement-based concrete and resistivity as an alternative test method. Constr. Build. Mater. 115 (2016) 746-759.

[Vejmelková et al., 2009] E. Vejmelková, M. Pavlíková, Z. Keršner, P. Rovnaníková, M. Ondráček, M. Sedlmajer, R. Černý, High performance concrete containing lower slag amount: A complex view of mechanical and durability properties. Constr. Build. Mater. 23 (2009) 2237-2245.

[Vernet, 2002] C. Vernet, Enseignements tirés des recherches sur les BFUP, Chapitre ACI de Paris. Journées d'étude « Durabilité des ouvrages en béton », 2002.

[Wang et al., 2015] D. Wang, C. Shi, Z. Wu, J. Xiao, Z. Huang, Z. Fang, A review on ultra high performance concrete: Part II. Hydration, microstructure and properties. Constr. Build. Mat. 96 (2015) 368-377.

# Part 2. Experimental program

# Chapter 9. Life cycle assessment of UHPCs

## Table of Contents



## List of figures



## List of tables

## Résumé

Dans ce chapitre nous nous intéressons aux impacts envrionnementaux des bétons Ultra-Haute Performance (BUHP), en considérant le taux de substitution du ciment par des laitiers des hauts fourneaux (LHF) et l'effet de l'activation, appliquée dans le but d'atteindre une performance donnée.

L'étude environnementale a été réalisée à partir d'une Analyse de Cycle de Vie (ACV) des bétons mis en oeuvre en considérant trois unités fonctionnelles: (i) la fabrication d'un $m^3$ de BUHP de classe C150, (ii) le fabrication d'un BUHP avec une durabilité (porosité) donnée et (iii) la mise en oeuvre d'un ouvrage dans l'est de la France.

- Pour la première unite fonctionnelle, nous avons comparé $BUHP_1$, $BUHP_2$ et $BUHP_3$-T, ayant une résistance à la compression dépassant 150 MPa à 90 jours. Nous avons démontré que même en absence d'activation, la substitution de 30% de ciment par des LHF diminue tous les impacts environnementaux du BUHP. En substituant 50% du ciment par des LHF, une activation thermique s'impose afin de compenser la diminution de la résitance, sans pour autant augmenter les impacts environnementaux du BUHP.
- Pour la deuxième unite fonctionnelle, les résultats ont démontré qu'on pouvait substituer jusqu'à 80% de ciment par des LHF, tout en gardant la même porosité. L'empreinte écologique des BUHP à base des LHF est beaucoup plus faible que celle du béton de référence (sans LHF).
- L'utilisation d'une poutre en BUHP à la place d'une poutre en acier réduit les quantités de béton ordinaire dans les différents éléments de structure, ainsi que les armatures. Toutefois, les impacts environnementaux de l'ouvrage restent supérieurs à ceux de la solution de base (pouter en acier et dalle en béton armé). Pour ce qui concerne le dégagement de $CO_2$, la difference entre les deux variantes reste faible. Le remplacement de la poutre en béton armé par une poutre en BUHP et la prise en compte des impacts des operations de réhabilitation pour la solution de base, devraient permettre de réduire les émissions de $CO_2$ de la variante BUHP.

# 1. Introduction

The building materials sector concentrates 5-10% of the total anthropogenic $CO_2$ emissions, most of which are related to concrete manufacturing. It is also the main contributor to natural resource consumption. To make this sector more sustainable, one option is to replace cement with other binders. Another option is to reduce the concrete volume needed by enhancing the concrete performance. Otherwise, life cycle assessment (LCA) is a manner allowing the assessment of the potential environmental impacts of a product over its life cycle, taking into account all the steps in its production from the extraction of resources to the allocation of the prepared product or to the treatment of the definitive generated wastes. This comprises distinguishing and quantifying energy and constituents utilized and wastes liberated in the environment, estimating their environmental effect and valuating opportunities for amelioration.

In this context, this research work aimed at designing UHPC with high BFS content in order to reduce the amount of emitted $CO_2$ relating to clinker transformation and then cement production. Designed UHPC have to reach required performance in terms of compressive strength and durability properties. In this chapter, the environmental impacts of different UHPCs are assessed for the same functional unit.

# 2. Environmental analysis

## 2.1. Functional units

The studied functional units are the following:

i) Manufacture 1 $m^3$ of C150-UHPC (FU 1): Three studied UHPCs, owning compressive strength of circa 150 MPa, have to be compared and environmentally assessed; $UHPC_1$ at 90 days, $UHPC_2$ and $UHPC_3$-T (thermally-activated $UHPC_3$);

ii) Manufacture 1 $m^3$ of UHPC with required durability (porosity) (FU 2): Four studied UHPCs including $UHPC_1$, compared to blended mixtures $UHPC_2$, $UHPC_3$ and $UHPC_4$;

iii) The construction of Buthaumont bridge (FU 3): This Buthaumont bridge in Boncourt, Meurthe-et-Moselle in France, is a structure of modest length enabling the road of RD 603 to cross Orne river as shown in Fig.1. The existed triple-arch masonry bridge was built in the mid-19$^{th}$ century [Hajar et al., 2017].


***Figure 1: Overview of the structure (old and new bridges)***
***[Hajar et al., 2017]***

To build the new structure, two solutions were considered:

- **Basic solution: Twin girders**

The project aims to rebuild the structure about 10m downstream from the existing bridge, and has to comply with the hydraulic requirements of piers absence in the minor bed of the river, and that the underside of the deck had to be above the 100-year flood level at least by 1 m. The new constructed bridge is a structure with a single span of 31.69 m that crosses the river with a scew angle of 70 grades as demonstrated in Fig. 2.

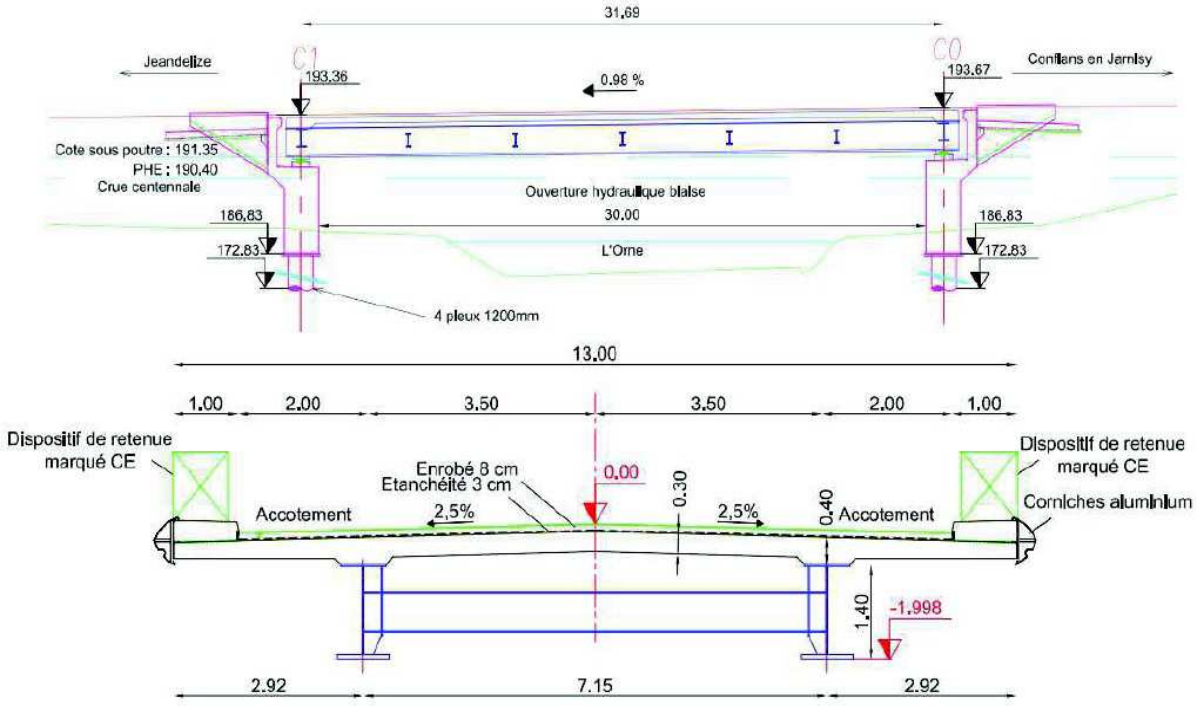


***Figure 2: Basic solution-longitudinal and cross sections [Hajar et al., 2017]***

As shown in Fig. 2 (lower), the deck has 13 m width, It carries about 11 m carriageway having two traffic lanes with 3.50 m width of each lane, and it is framed on each side by two

shoulders at the same level with 2 m width of each one. The deck in the basic solution is a composite structure with two steel beams having 1.4 m height and a distance of 7.0 m between their centre lines. The main beams carry a reinforced concrete slab having 13 m width and 30 cm thickness. The full-retaining type abutments sit on four drilled tube piles with a diameter of 1.2 m [Hajar et al., 2017]**.**

- **Alternative solution**: **Full integral bridge**

The alternative solution, proposed by Eiffage, is an integral bridge with ITE beams. The propositions in this solution include [Hajar et al., 2017]:

(i) The structural height of the composite deck in the basic solution was decreased from 1.9 m to 1.25 m due to usage of a prestressed girder deck with ITE (I-beam having an enlarged bottom flange) in UHPC as seen in Fig. 3;

(ii) The shape of ITE beams as appeared in Fig. 4 and the high strength of UHPC made that it is possible to obtain the best utilization out of the prestressed concrete and achieve competitive length/height ratio;

(iii) The diameters of the piles were optimized to fulfil the best potential flexibility in the foundations, and capitalize from a further appropriate redistribution of the stresses in the resultant frame;

(iv) Beside the quantity saving, there are more advantages of integral bridges including the maintenance cost for the bearings and expansion joints, and the high durability of UHPC;

(v) The deck is constituted of 12 prefabricated ITE beams, having 30.60 m long and 90 cm height in addition to the slab poured in situ, that made by conventional concrete (C35/45) and has a thickness of 22 cm.

The ITE beams comprise the following [Hajar et al., 2017]:

- A board of 107 cm lower flange, 15 cm thick, housing class 1860 T15s, and progressively anchoring thanks to sheathing of the strands end. Four lengths of sheathing have been selected;
- A constant width of 12 cm web,
- A 34 cm upper flange, on which the rebars of steel connectors are placed to connect the prefabricated beams with the upper slab poured in situ.

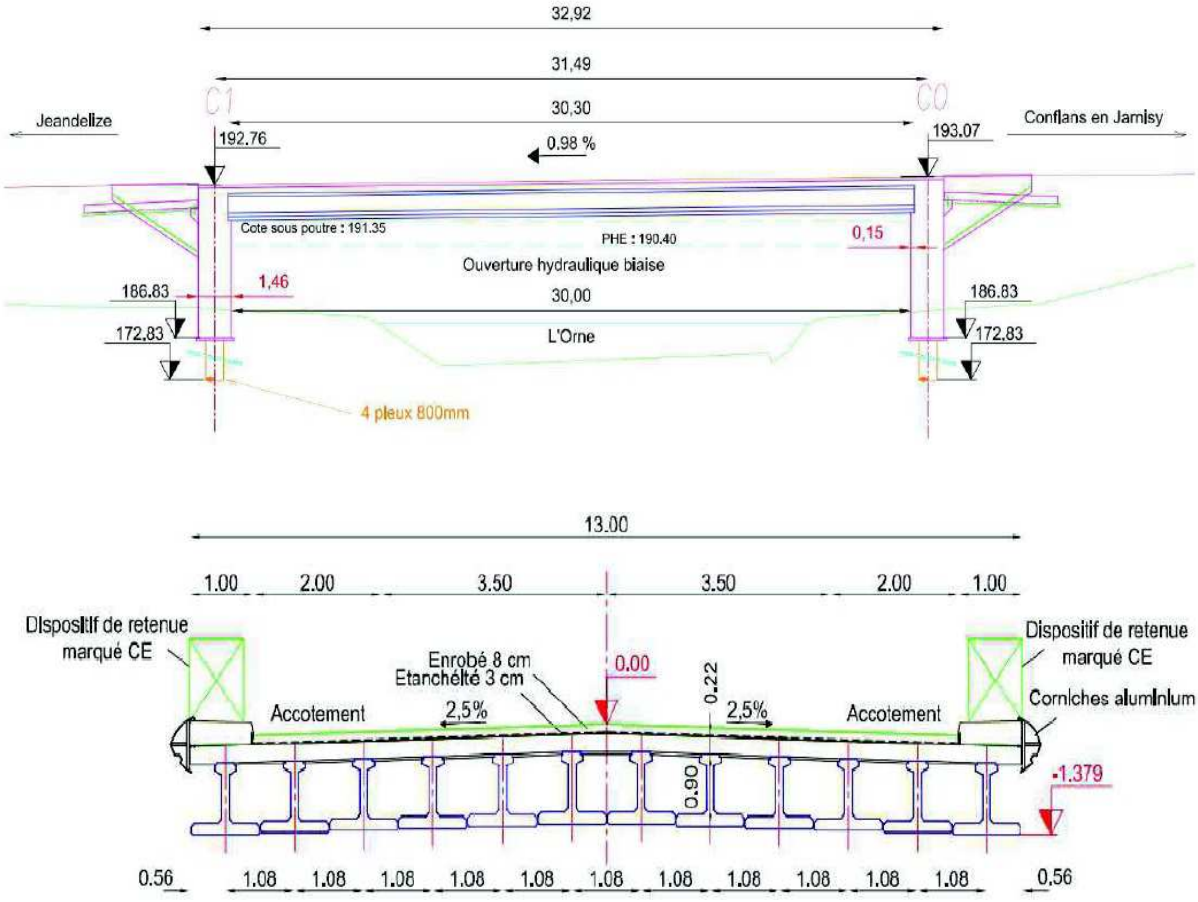


***Figure 3: Alternative solution-longitudinal and cross sections [Hajar et al., 2017]***

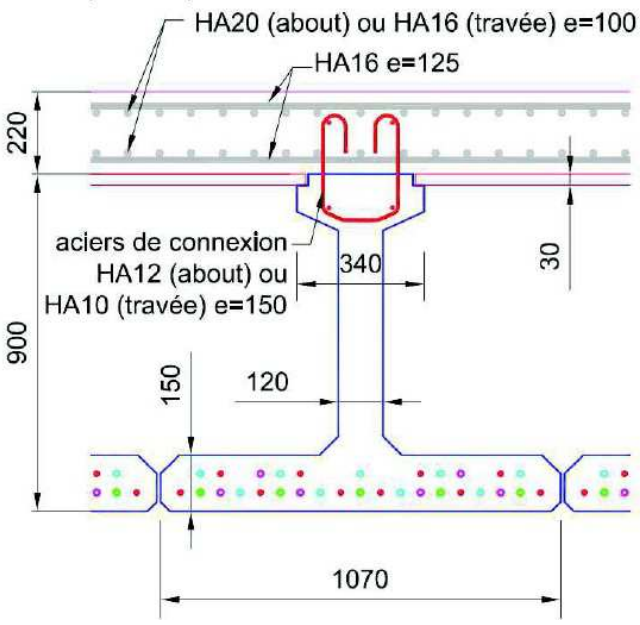


***Figure 4: Cross section and details of strands (dimensions in mm) [Hajar et al., 2017]***

## 2.2. System's boundaries

For the first and second functional units, it can be seen that an attention is paid to the production of constituents (cement, silica fume, slag, crushed quartz, quartz sand, water, and superplasticizer) without taking in consideration the energy of mixer for these constituents during the manufacture operation nor the transport of these constituents. In contrast, for the third functional unit relating to Buthaumont bridge construction, it is taken into account both production of constituents and concrete use while production of concrete and demolition are not counted as exhibited in Fig. 5.

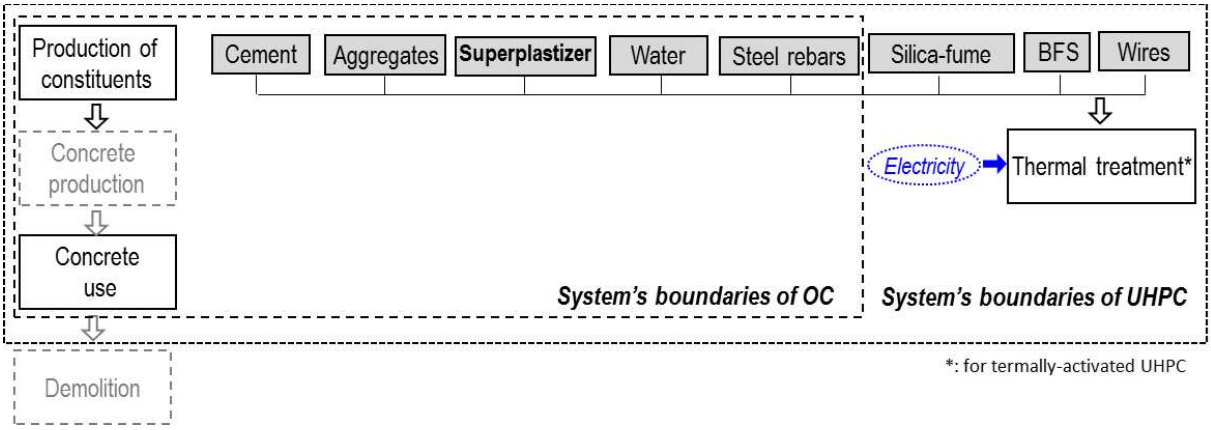


***Figure 5: System's boundaries for different functional units***

## 2.3. Inventory data

The modelling of scenarios is performed thanks to SimaPro v82.3 software program associated to environmental database. The inventory data depends on Ecoinvent version 2.2 (2010) and to bibliographical and industrial data [Frischknecht et al., 2005]. For the prestressed steel used in the bridge, the informations are taken from the data base, assuming that the prestressed steel is considered as steel. The latter concentrates the major environmental impacts [Périer and Pacitti, 2012]. Concerning the slag, all the informations are provided by Diogène (. The CML method, complying the standard NF P01-010 [NF P01-010, 2004], is used to evaluate different indicators of environmental impact: energy consumption (MJ), abiotic depletion (kg Sb eq), water usage (L), wastes (kg), global warming (kg $CO_2$ eq), acidification (kg$SO_2$eq), air pollution ($m^3$), water pollution ($m^3$), ozone layer depletion (kgCFC11 eq), photochemical oxidation (kg $C_2H_4$ eq) and eutrophication ($PO_4$eq).
The informations on the exploited data and the used moduli for different processes of constituents' production are summarized in Table 1.

***Table 1: Informations relative to data used in this study***

| Process | Used modulus | Data sources | Geographical scale | Time scale |
|---|---|---|---|---|
| Production of quartz sand and crushed quartz | Sand, at mine/CH S | Ecoinvent©[1] | Switzerland | 2010 |
| Production of natural aggregates | Coarse aggregates, crushed at mine/ CH S | Ecoinvent©[1] | Switzerland | 2010 |
| Production of admixtures | / | Industrial data | / | 2012 |
| Production of cement | Cement, alternative constituents 21-35%, S | Ecoinvent©[1] | Europe without Switzerland | 2004 |
| | Cement, blast furnace slag 36-65%, non-US | Ecoinvent©[1] | Europe without Switzerland | 2014 |
| | Portland slag sand cement, at plant/CH S | Ecoinvent©[1] | / | Undefined |
| | Portland cement, strength class Z 52.5, at plant/CH S | Ecoinvent©[1] | / | Undefined |
| Production of steel rebars | Steel rebar, blast furnace and electric arc furnace route, production mix, S | Ecoinvent©[1] | World | 2007/ 2008 |
| Production of wires | Reinforcing steel (RER), S | Ecoinvent©[2] | / | 2014 |
| Production of silica fume | Silica fume, densified, S | Ecoinvent©[1] | World | 2014 |
| Production of blast furnace slag | / | Industrial data[3] | / | 2011 |
| Painting production | Alkalyd paint, white, 60% in solvent, at plant/RER S | Ecoinvent©[1] | / | Undefined |
| Production of water | Tap water, at user/CH S | Ecoinvent©[1] | Switzerland | 2005 |

[1] Database;
[2] The most impacting component in wires' production is steel. Hence wires are considered as steel [Périer and Pacitti, 2012];
[3] The informations concerning the slag production are established by Diogène

## 2.4. Results and discussion

### 2.4.1. Comparison of environmental impacts for FU 1

For this functional unit, only UHPCs owning the required compressive strength of 150 MPa are considered. Thereby, the comparison concerns $UHPC_1$ at 90 days**,** $UHPC_2$ at 90 days and $UHPC_3$-T. The comparison was carried out through different indicators of NF P01-010 standard as shown in Fig. 6.

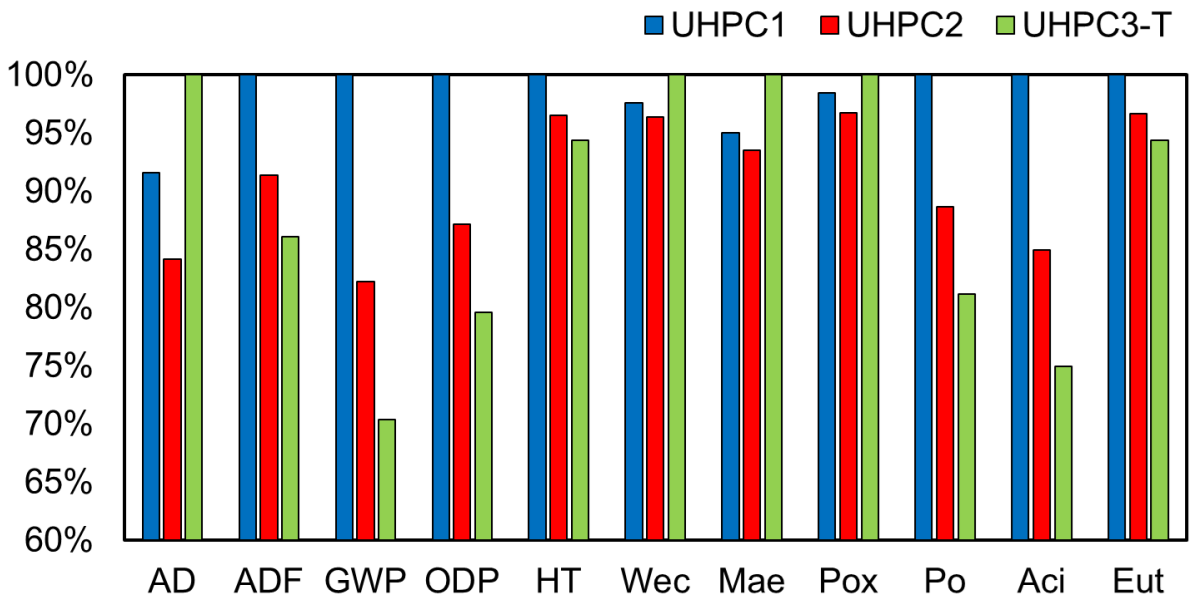


***Figure 6: Environmental impacts of 1 m³ of C150-UHPC***

From Fig. 6, it was revealed that the indicator of abiotic depletion (AD) of both $UHPC_1$ and blended mixture $UHPC_2$ was lower than that of $UHPC_3$-T. Abiotic depletion in LCA deals with environmental interests because of the utilization of resources. One of these resources is the energy [Hauschild and Huijbregts, 2015]. The study of the consumption of energy complies with the procedure mentioned in ISO 14042:2000 that guides to consider the energy consumption as one of the key factors for checking the precision of inventories utilized in product or process of LCA. Generally, the consumed gross energy can be classified to thermal energy and electrical energy [Josa et al., 2004]. In the case of $UHPC_3$-T, the thermal activation increases the abiotic depletion in terms of electrical energy, making this concrete more impacted than $UHPC_1$ and $UHPC_2$. The substitution of 30% of cement with slag in $UHPC_2$ decreases the abiotic depletion of UHPC by 9%, denoting of the high consumed electrical and thermal energies of $UHPC_1$. Indeed, these energies are consumed through the plant operations in the cement industry. Usually, the electricity is consumed in the cement industry for every equipment like grinding mills, preheater and kiln. Moreover, the clinker kiln is the major consumer of thermal energy. Nearly 90% of the gross energy consumed by the system is attributed to the clinker manufacture and for this reason, cement with lower clinker amounts consumes lower energy [Josa et al., 2004]. Accordingly, $UHPC_1$ owning full cement content has higher energy consumption and higher abiotic depletion than $UHPC_2$. The partial replacement of cement with lower energy intensive ingredients like slag decreases efficiently the ecological overload. In fact, the cement is a major component and influences greatly the environmental footprints of concrete [Kim et al., 2016]. Nevertheless, slag is no longer

deemed as solely waste but as beneficial by-products [Van den Heede and N. De Belie, 2012].

The indicator of abiotic depletion (fossil fuels) can be considered as a salutary checking indicator which supplies proportionate results when LCA concerns the fossil fuel consumption through the life cycle of products [Hauschild and Huijbregts, 2015]. As known, the cement industry utilizes fossil fuels in the burning or incineration operation. Therefore, the abiotic depletion in terms of fossil fuel consumption decreases by 9% and 14% for 30 and 50% of cement substitutions with BFS respectively.

The carried out comparison concerns also global warming potential indicator of NF P01-010 standard, that acts as a strong and authoritative indicator. Fig. 6 presents the evolution of global warming (kg eq $CO_2$) indicator versus UHPC mixture. Generally, the cubic meter of UHPC liberates around 5–7 times of $CO_2$ than a cubic meter of the conventional concrete (3000 kg compared to 450 kg $CO_2$ eq.) [Habert et al., 2013]. From Fig. 6, it was observed that $UHPC_1$ has a largest GWP compared to $UHPC_2$ and $UHPC_3$-T regardless of usage of the thermal activation of slag in the last mixture. As known, the major $CO_2$ releases are caused by the chemical reactions in the clinker kiln, the fuel burning through clinker manufacture and the energy consumed over the total manufacture operation. The liberated $CO_2$ quantity relies on the cement's clinker amount in the UHPC mixture. Thereby, the substitutions of cement by 30% ($UHPC_2$) and 50% ($UHPC_3$-T) decrease the $CO_2$ emissions by 18% and 30%respetively. The utilization of these coproducts can efficiently decrease the environmental loads related to cement fabrication [Josa et al., 2004].

The ecotoxicity indicators (fresh water aquatic, marine aquatic, and terrestrial) cover the rate of whole classes in the environment living under toxic stress. It was shown from Fig. 6 that $UHPC_3$-T has ultimate limits compared to $UHPC_1$ and $UHPC_2$ due to the application of thermal activation procedure. It should be remembered that the demolition and waste phase are likewise not taken into consideration. Thereby, it may ignore the effects of heavy metal leaching from industrial byproducts, that contribute to human toxicity and ecotoxicity [Van den Heede and N. De Belie, 2012].

Relating to acidification potential and eutrophication potential indicators, it was noticed from Fig. 6 that the $UHPC_1$ attained largest limits of both acidification and eutrophication potentials, compared to $UHPC_2$ and $UHPC_3$-T. Indeed, nitrogen and sulphur are underlying the deterioration of ecosystem. The contribution to acidification and eutrophication on a regional level was a main reason for the nitrogen while the contribution to acidification on a regional level was a main reason for the sulphur [Josa et al., 2004; Hauschild and Huijbregts, 2015]. $NO_2$ and NO released in the air are major results from fuel utilization through clinker manufacture and energy consumption over the full operation. These releases are not resulted from the chemical reactions; but from the burning of fuel. In contrast, the essential

helpers of $SO_2$ releases are the chemical reactions in the clinker kiln (due to the sulphur amount in the clay and another raw materials), the burning of sulphur contained in the fossil fuels that utilized in the clinker manufacture, and the burning of sulphur through the production of energy consumed by the full operation. A larger level of cement replacement (by slag) decreases $NO_x$ liberation [Josa et al., 2004].

### 2.4.2. Comparison of environmental effects for FU 2

The environmental impacts of different UHPCs are compared in accordance to FU 2. The latter considers the same durability. To facilitate the comparison, total porosity was considered as quite the same for all studied concretes. Therefore, $UHPC_1$ is compared with $UHPC_2$, $UHPC_3$ and $UHPC_4$ (Fig. 7). According to the environmental performance evaluation, the partial substitution of cement with slag appears a clear dwindling for all environmental categories, and this dwindling grows with a slag content in the UHPC mixtures. However, the improvement of GWP is outstanding. The latter decreases proportionally to BFS content, by 18%, 30%, and 47% for $UHPC_2$, $UHPC_3$ and $UHPC_4$ respectively, compared to $UHPC_1$.

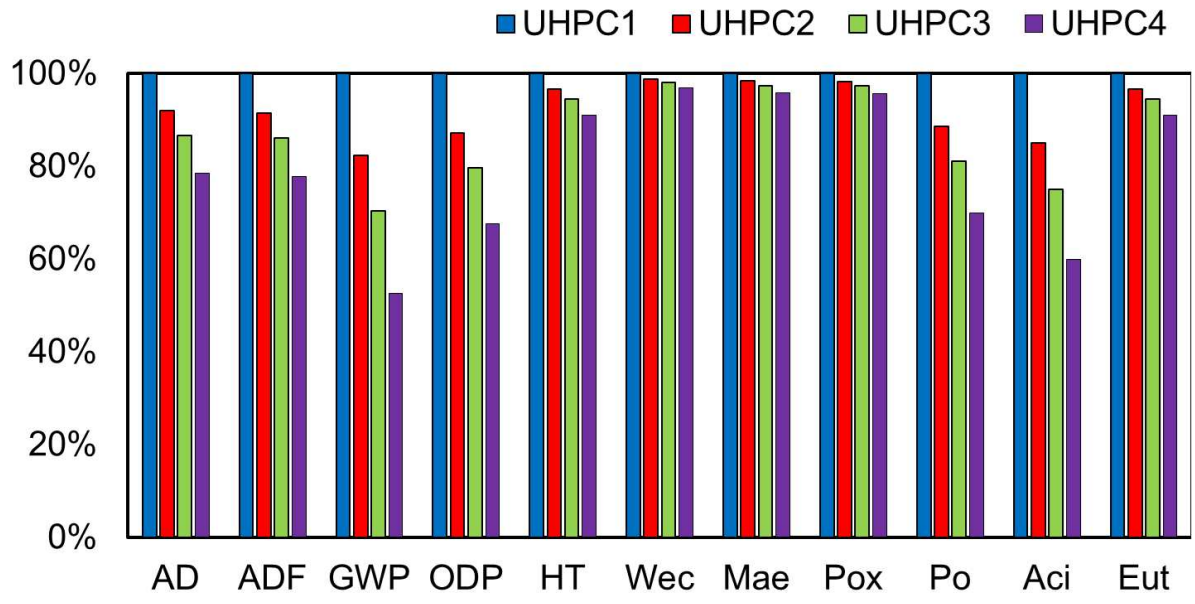


***Figure 7: Environmental impacts of 1 $m^3$ of UHPC with required durability***

Theses interested results highlight the beneficial effect of slag in decreasing the environmental footprint of UHPC without affecting its durability. Nevertheless, this environmental evaluation is not realistic in the actual context. For UHPC structure design, the considered parameter is the mechanical strength of concrete, which governs the cross sectional areas and then the required concrete quantity for the project. Thereby, for UHPC with lower compressive strength, the cross sectional area should be increased in spite of its high durability performance.

### 2.4.3. Comparison of environmental impacts for FU 3

The analysis of LCA was performed on Buthaumont bridge where ITE beams were made by different UHPC mixtures as an alternative solution (Var-UHPC), compared to the basic solution (Var-0) as shown in Fig. 8. The goal of this analysis is to show if the use of UHPC in optimized shape of ITE beam can contribute to the reduction of environmental impacts. In the first, by benefiting from the superior mechanical strength of the UHPC, the ultra-thin bridge decks can be constructed which acclimate to high geometric and construction constrains (decrease in size, watercourses or roads in service), and quick and safe installation of the deck. Moreover, this alternative solution of integral bridge type using UHPC minimizes the global cost of the structure by reducing the quantities of required concrete amount for casting the slab, columns and pious (Table 2) in addition to the decreased maintenance costs (no bearing or expansion joints and no painting) [Hajar et al., 2017].

***Table 2: Comparison between basic and alternative solutions in term of materials consumption***

| | Materials | Basic solution-Var-0 | Alternative solution-Var-UHPC |
|---|---|---|---|
| Reinforced concrete pious | Concrete ($m^3$) | 126.7 | 94.2 |
| | Steel reinforcement (ton) | 17.7 | 14.7 |
| Reinforced concrete column | Concrete ($m^3$) | 225.0 | 165.4 |
| | Steel reinforcement (ton) | 32.6 | 27.1 |
| Reinforced concrete slab | Concrete ($m^3$) | 158.0 | 144.0 |
| | Steel reinforcement (ton) | 46.6 | 44.3 |
| UHPC | Concrete ($m^3$) | - | 101.2 |
| | Fibres (ton) | - | 19.7 |
| | Wires (ton) | - | 12.6 |
| Steel beam | Steel reinforcement (ton) | 66.1 | - |
| Painting | Surface ($m^2$) | 550.9 | - |

From Table 2, it was indicated that the alternative solution ensures a reduction in consumed ordinary concrete and steel reinforcement by 39% and 47% sequentially. It should be remarked that there is no needing for painting when ITE beam is replaced with the steel one in the basic solution. Nevertheless, fibers, wires and UHPC are necessary for the alternative solution (Var-UHPC).

The different assessed indicators of bridge with Var-UHPC are presented in Fig. 8 in comparative with that of basic solution (Var-0). Except for photochemical oxidation indicator, Var-UHPC has more environmental impacts than basic one despite the reduction of ordinary concrete quantity in pious, columns and slab. This reduction is not enough to counterbalance the negative impact of fibres, wires and the high cement content of UHPC. The absence of painting explains the decrease of photochemical oxidation indicator for the alternative solution.

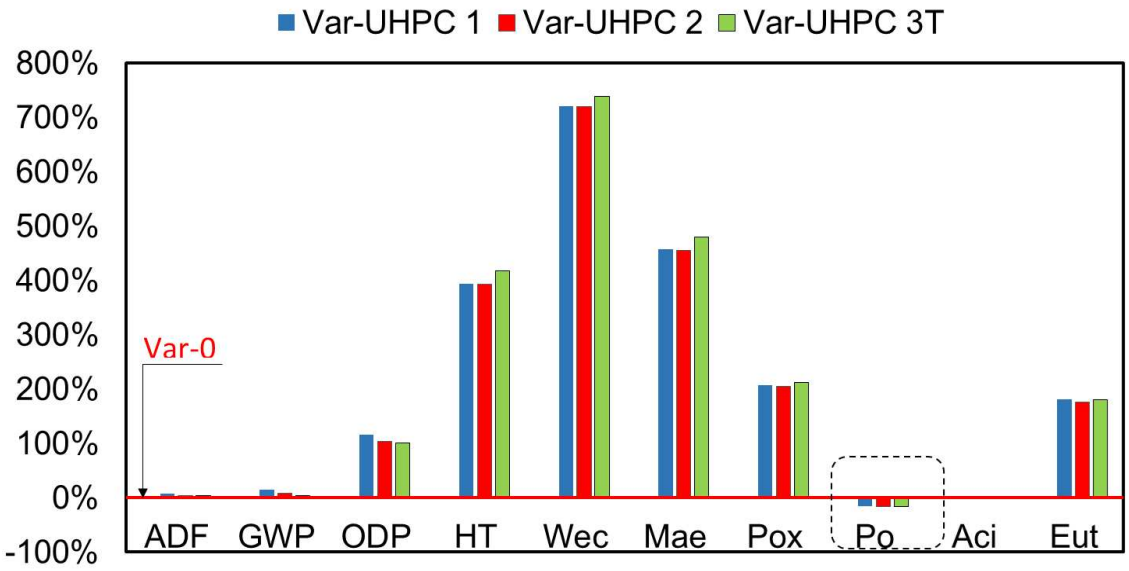


***Figure 8: Environmental impacts of bridge with basic solution (Var-0) and alternative solution (Var-UHPC)***

Even if the difference between basic solution (Var-0) and alternative solution (Var-UHPC) is slight from where GWP indicator, Fig. 9 shows that the replacement of steel beam with UHPC-ITE one has negative environmental effect. This effect is subdued when 50% of cement is substituted with slag in spite of the thermal activation ($UHPC_3$-T). This result is very encouraging, as the difference to compensate for is only about 4.6%. Using UHPC for slab casting in place of ordinary concrete, and considering the impacts of rehabilitation operation could decrease the GWP indicator of the alternative solution (Var-UHPC) in comparative with that in the basic solution (Var-0).

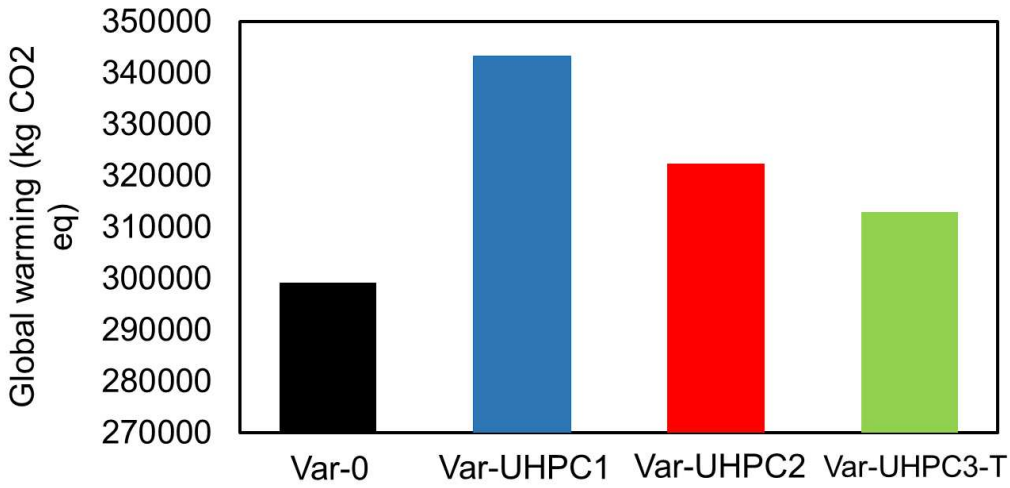


***Figure 9: Global warming potential (GWP) of basic solution (Var-0) and alternative solution (Var-UHPCs)***

## 3. Conclusions

- The partial substitution of cement with BFS improves the sustainability of UHPC from an ecological standpoint. With low BFS content ($UHPC_2$), all environmental impacts are decreased regardless of the functional unit and even in the absence of any activation. Considering durability performance, cement could be substituted up to 80%, which decreases greatly the environmental impacts of UHPC.
- Regardless of its BFS content and applied activation, the use of UHPC in beam casting does not improve the environmental footprint of bridge, compared to the steel one. Nevertheless, in term of global warming potential indicator, which represents the amount of emitted $CO_2$, a slight difference is observed between basic and alternative solutions. This difference could be reduced or inversed by using UHPC in slab and by considering the impact of rehabilitation operation in the case of basic solution.

## 4. References

[Frischknecht et al., 2005] R. Frischknecht, N. Jungbluth, H.J. Althaus, G. Doka, R. Dones, T. Heck, S. Hellweg, R. Hischier, T. Nemecek, G. Rebitzer, M. Spielmann, The ecoinvent database: overview and methodological framework, Intern. J. LCA. 10 (2005) 3–9.

[Habert et al., 2013] G. Habert, E. Denarié, A. Šajna, P. Rossi, Lowering the global warming impact of bridge rehabilitations by using Ultra High Performance Fibre Reinforced Concretes. Cem. Concr. Compos. 38 (2013) 1-13.

[Hajar et al., 2017] Z. Hajar, F. Pastor, L. Picard, D. Champenoy, L. Loutte, Buthaumont bridge on the orne river in boncourt. Proceedings of the AFGC-ACI-*fib*-RILEM International Conference on Ultra High Performance Fibre-Reinforced Concrete, Montpellier, France, 2017, pp.777-786.

[Hauschild and Huijbregts, 2015] Hauschild M.Z., Huijbregts M.A.J., "Life cycle impact assessment", LCA Compendium – The Complete World of Life Cycle Assessment, Springer Science+Business Media Dordrecht, 2015.

[Josa et al., 2004] A. Josa, A. Aguado, A. Heino, E. Byars, A. Cardim, Comparative analysis of available life cycle inventories of cement in the EU. Cem. Concr. Compos. 34 (2004) 1313-1320.

[Kim et al., 2016] H. Kim, T. Koh, S. Pyo, Enhancing flowability and sustainability of ultra high performance concrete incorporating high replacement levels of industrial slags. Constr. Build. Mater. 123 (2016) 153-160.

[NF P01-010, 2004] NF P01-010, Environmental quality of construction products, environmental and sanitary declaration of construction products in French, French standard, 2004.

[Périer and Pacitti, 2012] V. Périer, A. Pacitti, Evaluation des impacts environnementaux des torons de précontrainte. Journées Câbles, Nantes, France, 2012.

[Van den Heede and De Belie, 2012] P. Van den Heede, N. De Belie, Environmental impact and life cycle assessment (LCA) of traditional and ‘green’ concretes: Literature review and theoretical calculations. Cem. Concr. Compos. 34 (2012) 431-442.

# Conclusion et perspectives

L'objectif de cette thèse était de produire un BUHP à faible empreinte environnementale, en remplaçant partiellement le ciment par des laitiers des hauts fourneaux (LHF). La première partie du travail a porté sur l'optimisation des mélanges BUHP, avec différentes teneurs de LHF et l'étude de leurs propriétés à l'état frais et au jeune âge. Ensuite, les bétons ont été étudiés à différentes échelles afin de corréler leurs propriétés mécaniques et de durabilité avec l'état de la microstructure. Les travaux ont été réalisés sur des BUHP à base de LHF, en comparaison avec la composition de référence 1 (sans LHF) et en considérant trois paramètres ; la teneur en LHF, l'activation chimique et l'activation thermique.

Les conclusions suivantes peuvent être tirées :

- Du point de vue de la conception du mélange : l'utilisation d'un malaxeur à haute énergie, avec une pale en étoile et une vitesse de malaxage élevée, assure un mélange homogène au bout de 3,5 minutes seulement. Ce mélange, avec un faible rapport eau/liant (0,14), a une maniabilité optimale lorsqu'un superplastifiant polycarboxylate (ACP1) est utilisé avec un dosage de 1,8%. Ce dernier affecte largement l'hydratation au jeune âge et donc la résistance à la compression. De ce fait, l'utilisation de la fumée de silice grise, à forte teneur en carbone et à forte réactivité, est recommandée par rapport à la fumée de silice blanche ;

Pour évaluer l'effet de la teneur en LHF et de l'activation chimique sur les propriétés à l'état frais et au jeune âge, une étude expérimentale a été menée sur un BUHP de référence optimisé et ceux ayant une teneur en LHF de 30%, 50% et 80%. Les résultats ont montré que :

- Pour une faible teneur en LHF (30%), l'effet de dilution se produit avec une nucléation hétérogène. Le premier rend l'eau plus disponible pour la réaction du ciment (plus d'affaissement ou moins de superplastifiant pour une même maniabilité) et le second accélère la réaction du ciment, ce qui réduit le temps de prise de $BUHP_2$, par rapport à $BUHP_1$. La chaleur de réaction produite est la même pour les deux BUHP ;
- Pour une teneur élevée en LHF, l'effet de dilution prévaut malgré la forte absorption d'eau des particules de LHF. Cela entraîne une augmentation du temps de prise et ralentit la réaction d'hydratation. Pour $BUHP_3$ et $BUHP_4$, la réaction thermique et les pics de flux de chaleur diminuent fortement par rapport à ceux de $BUHP_1$. Pour accélérer la réaction d'hydratation, une solution de KOH a été ajoutée, avec un dosage élevé, ce qui augmente le pH et favorise la réaction du LHF. En conséquence, le temps de prise diminue.

Dans la deuxième partie du travail, les propriétés mécaniques et de durabilité sont corrélées avec la microstrure et les conclusions suivantes peuvent être tirées :

- Avec 30% de LHF, l'effet de nucléation des particules de laitier prévaut sur l'effet de dilution. Il en résulte une accélération de la réaction d'hydratation du ciment et par conséquent celle des additions minérales (FS et LHF), ce qui augmente la quantité d'hydrates formées. Ces dernières améliorent la densité du béton et diminuent sa porosité. Par conséquent, la résistance à la compression augmente et les propriétés de durabilité sont améliorées.
- Pour une teneur élevée en LHF (50% et 80%), l'effet de dilution prévaut sur l'effet de nucléation hétérogène. La résistance à la compression de $BUHP_3$ et $BUHP_4$ sont légèrement diminuées, dénotant la faible teneur en portlandite, ce qui diminue le taux d'hydrates fromées. En dépit de l'effet physique (remplissage des pores et amélioration de l'empilement) du LHF, le manque d'eau et de portlandite limitent la réaction pouzzolanique de la FS et du LHF, ce qui diminue les performances mécaniques des mélanges. Néanmoins, plus de laitier affine le réseau poreux et obstrue les chemins de diffusion, ce qui améliore la résistance des BUHPs aux chlorures et au $CO_2$. Leur perméabilité intrinsèque est également abaissée.

L'activation alcaline au $[KOH]_3$ augmente la dissolution des ions Si et Al par rupture des liaisons Si-O et Al-O du laitier, ce qui favorise sa réaction. Ceci entraîne l'augmentation de la quantité des C-S-H, la reduction de la porosité et l'amélioration de la résistance à la compression de $BUHP_4$ au jeune âge. A long terme, l'effet de l'activation chimique sur les propriétés mécaniques et de durabilité n'est pas remarquable.

- L'activation thermique augmente la réaction des composants solides et accélère leur hydratation, ce qui augmente la consommation de portlandite. Par conséquent, plus d'hydrates sont formées, remplissant ainsi la porosité, ce qui densifie la structure et améliore ses performances mécaniques et de durabilité. Pour $BUHP_3$-T, les paramètres d'activation thermique choisis permettent d'atteindre la résistance à la compression visée. Cependant, pour une durée d'activation de 48h à 90°C, la résistance à la compression de $BUHP_4$-T est de 12,5% inférieure à celle de $BUHP_1$ à 90 jours. Le manque d'eau et la teneur élevée de LHF expliquent ce résultat. Afin d'améliorer la résistance à la compression de $BUHP_4$, une température plus élevée ou une durée plus longue doivent être étudiées, la combinaison de l'activation chimique et thermique n'étant pas suffisante pour compenser la perte de résistance.

Néanmoins, aucune activation n'est nécessaire pour améliorer les propriétés de durabilité des BUHPs à forte teneur en LHF. Ces derniers ont un réseau poreux plus fin et une forte capacité de fixation, ce qui diminue leurs propriétés de transfert.

D'un point de vue environnemental, la comparaison des différents indicateurs, à travers l'analyse de cycle de vie, pour différentes unités fonctionnelles, a montré que :

- Pour 1 $m^3$ de C150-BUHP, la substitution de 30% de ciment par du LHF diminue tous les impacts environnementaux, rendant $BUHP_2$ moins impactant que $BUHP_1$. Pour l'indicateur réchauffement climatique, (émissions de CO2), $BUHP_1$ est le plus impactant des BUHPs, malgré l'activation thermique appliquée au $BUHP_3$.
- Pour 1 $m^3$ de BUHP avec une durabilité donnée (porosité), tous les BUHPs ont moins d'impacts environnementaux que le béton de référence. Une substitution jusqu'à 80% du ciment par du LHF est bénéfique pour l'environnement.

Nous pouvons conclure que les BUHPs développés sont moins impactants pour l'environnement, lorsque le ciment est partiellement substitué par du LHF. Le taux de substitution optimal dépend de l'unité fonctionnelle (résistance à la compression donnée ou durabilité donnée)

Pour la dernière unité fonctionnelle, une structure réelle (pont) a été considérée pour évaluer, d'un point de vue environnemental, l'intérêt ou non d'utiliser des BUHPs. L'utilisation d'une poutre en BUHP, remplaçant celle en acier, a entrainé un gain en terme de quantité de béton ordinaire nécessaire pour la dalle, les piles et les pieux. Néanmoins, les impacts environnementaux n'ont pas été réduits, même si les émissions de $CO_2$ sont légèrement différentes pour les deux variantes (variante de base et variante BUHP). Pour améliorer la performance environnementale du pont, avec la variante BUHP, nous devrions considérer dans l'analyse de cycle de vie, l'absence de réhabilitation et le remplacement de la dalle en béton ordinaire par une dalle en BUHP.

En perspectives :
i) Explorer les déformations au jeune âge : retrait chimique, retrait endogène et retrait empêché des BUHP ;
ii) Etudier la résistance à l'acide des BUHPs à base des LHF ;
iii) Investiguer la microstructure et les propriétés de durabilité de BFUHP (2% vol. fibres) avec 30% de LHF ;
iv) Comparer les impacts environnementaux des structures à base de BFUHP en BO/BHP.

# Conclusion and prospects

The objective of this thesis was to produce an UHPC with low environmental footprint by substituting cement with BFS partially. The first part of this research work dealt with optimizing UHPC mixtures with different BFS contents and investigating their fresh and early age properties. Then, the manufactured concretes were explored at different scales to correlate their mechanical and durability properties with the state of the microstructure. The research work was carried out on blended mixtures of UHPCs, compared to reference one and considering three parameters; BFS content, chemical activation and thermal one.

The following conclusions can be drawn:

- From mixture design standpoint, the use of high energy mixer with star blade and high mixt speed ensures homogeneous mixture after only 3.5 min. This mixture with low w/b of 0.14 has the required workability of 30 cm when polycarboxylate superplasticizer ($ACP_1$) is used with a dosage of 1.8%. The use of grey silica fume with high reactivity is recommended, compared to white one;

To assess the effect of BFS content and chemical activation on fresh and early age properties, an experimental study was carried out on optimized reference UHPC and those with BFS content of 30%, 50% and 80%. Results showed that:

- For low BFS content (30%), dilution occurs with heterogeneous nucleation. The first, makes more water available for cement reaction (more slump flow or less superplasticizer dosage for the same workability), and the second accelerates the cement reaction, which reduces the setting time of $UHPC_2$ compared to $UHPC_1$. The produced reaction heat is quite the same for both UHPCs;
- For high BFS contents (50 and 80%), dilution effect prevails despite the high water absorption of BFS particles. This results in increasing setting time and decelerating the hydration reaction. For $UHPC_3$ and $UHPC_4$, the heat reaction and the heat flow peaks decrease greatly, compared to those of $UHPC_1$. To accelerate the hydration reaction, KOH solution was added with high dosage, which increases pH and promotes BFS reaction. As result, the setting duration reduces.

In the second part of this research work, mechanical and durability properties were correlated with microstructural ones and the following conclusions can be drawn:

- With 30% of slag, the heterogeneous nucleation effect of BFS particles prevails on dilution one. This results in acceleration of cement hydration reaction, and consequently that of mineral admixtures (SF and BFS), which increases the amount of produced hydrates. The latter improve the packing density of concrete and

decrease its porosity. Therefore, the compressive strength increases and durability properties are enhanced.

- For high BFS content (50% and 80%), the dilution effect prevails on heterogeneous one. The compressive strength of $UHPC_3$ and $UHPC_4$ develops slightly, denoting the low portlandite content, which results in less formed hydrates. Despite the physical effect of BFS (filling pores and improving the packing density), the lack of both water and portlandite restricts the pozzolanic reaction of SF and BFS, which decreases the mechanical performance of blended UHPCs, compared to reference one. Nevertheless, more BFS refines porous network and obstructs diffusion paths, which improves the resistance of blended UHPCs against chlorides and $CO_2$. Their intrinsic permeability is also lowered.
- Alkaline activation with $[KOH]_3$ raises the dissolution of Si and Al ions by breaking the bonds of Si-O and Al-O in the slag glass, which promotes BFS reaction. This results in increasing C-S-H amount, decreasing porosity and improving the compressive strength of $UHPC_4$ at early age. At later age there is no remarkable effect of chemical activation on mechanical and durability properties.
- Thermal activation increases the reaction of solid components and accelerates their hydration, which increases the portlandite consumption. Therefore, more hydrates are formed, filling the porosity, improving the packing density of UHPC and enhancing its mechanical and durability performances. For $UHPC_3$-T, the chosen parameters of thermal activation ensure the required compressive strength. However, with 90°C and 48 hours of activation duration, the compressive strength of $UHPC_4$-T is 12.5% less than that of $UHPC_1$ at 90 days. The lack of water and the high content of BFS explain this result. In order to improve the compressive strength of $UHPC_4$, higher temperature or longer duration have to be explored. The combined chemical and thermal activation was not effective to compensate for the drop of strength.
- However, any activation is needed to improve the durability properties of UHPCs with high BFS contents. The latter have finer porous network and high binding capacity, which decrease their transfer properties.

From an environmental viewpoint, the comparison of different indicators through LCA analysis for different functional units showed that:

- For 1 $m^3$ of C150-UHPC, the substitution of 30% of cement with BFS decreases all environmental impacts, making $UHPC_2$ more sustainable than $UHPC_1$. For Global Warming Potential ($CO_2$ emissions), $UHPC_1$ is the more impacting UHPC, compared to $UHPC_2$ and $UHPC_3$-T, despite the applied thermal activation on the latter.

- For 1 $m^3$ of UHPC with required durability (porosity), all blended UHPCs have less environmental impacts than reference one. The substitution of cement with BFS (up to 80%) is environmentally beneficial.

We can conclude that developed UHPCs are more sustainable when cement is partially substituted with BFS. The optimal substitution rate depends on the functional unit (required compressive strength or required durability)

For the last functional unit, a real bridge was considered to assess its environmental footprint when using UHPC instead of ordinary concrete. The use of UHPC beams (as an alternative solution) replacing steel ones (basic solution), induced a gain in the quantity of ordinary concrete required for casting each of slab, columns and pious. Nonetheless, the environmental impacts were not reduced, even if $CO_2$ emissions are slight different for both solutions (basic and alternative solutions). To improve the environmental performance of the bridge with UHPC, the absence of rehabilitation and replacement of the ordinary concrete slab with UHPC one should be taken into consideration.

The prospects are the following:

i) Investigation of the early age deformations: Chemical, autogenous and restrained shrinkages of the UHPC;

ii) Investigation of the acid resistance of environmentally friendly UHPC;

iii) Investigation of microstructure and durability properties of UHPFRC (2% vol. of fibres) incorporating 30% GGBFS;

iv) Comparison of the environmental impacts of structures with UHPFRC and OC/HPC.

# Appendix

## Appendix 1_Cement_CEM I 52.5 PM ES

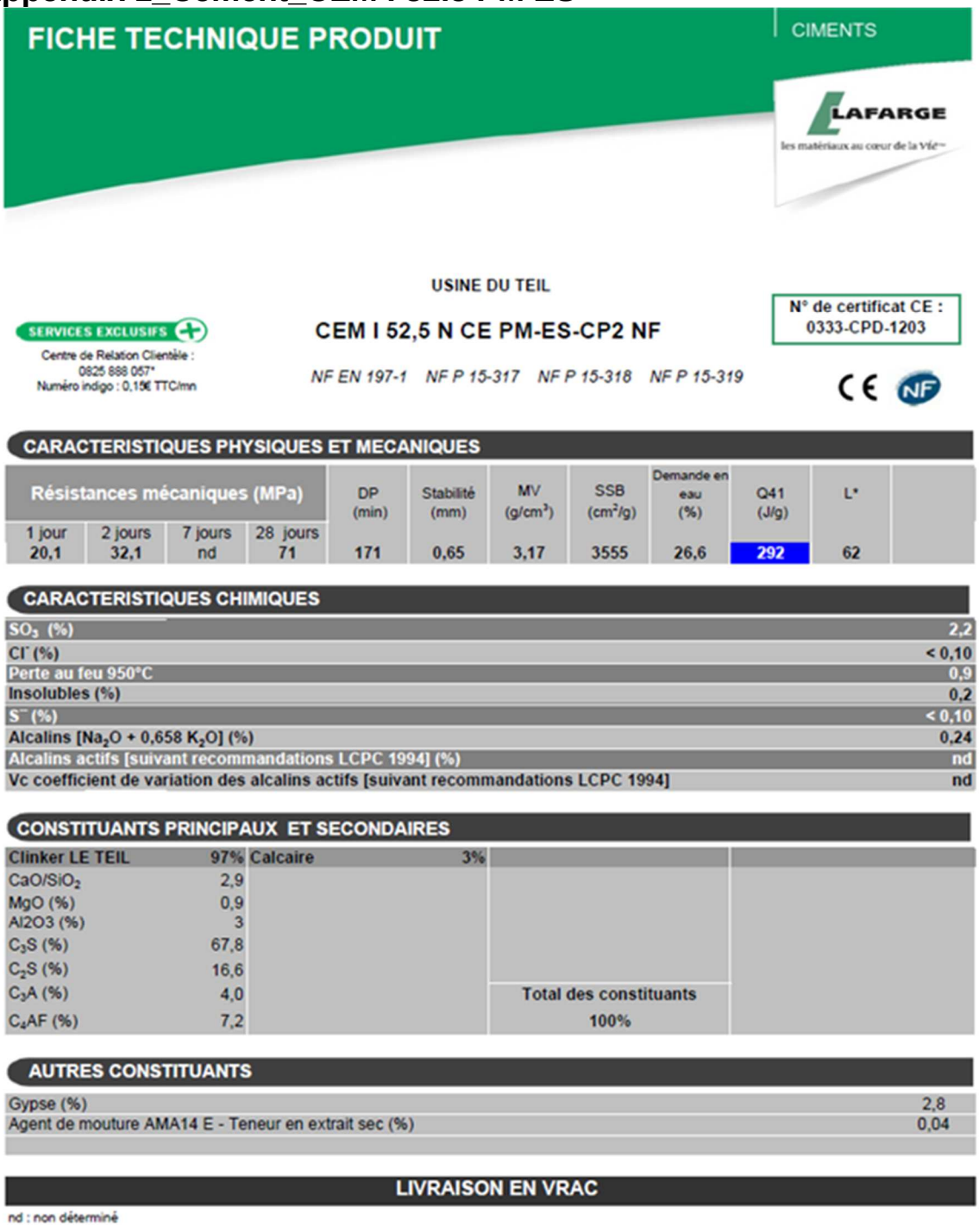

FICHE TECHNIQUE PRODUIT

CIMENTS

LAFARGE

les matériaux au cœur de la Vie

USINE DU TEIL

SERVICES EXCLUSIFS

Centre de Relation Clientèle :
0825 888 057*
Numéro indigo : 0,15€ TTC/mn

CEM I 52,5 N CE PM-ES-CP2 NF

*NF EN 197-1 NF P 15-317 NF P 15-318 NF P 15-319*

N° de certificat CE :
0333-CPD-1203

CE NF

**CARACTERISTIQUES PHYSIQUES ET MECANIQUES**

| Résistances mécaniques (MPa) | | | | DP (min) | Stabilité (mm) | MV (g/cm³) | SSB (cm²/g) | Demande en eau (%) | Q41 (J/g) | L* | |
|---|---|---|---|---|---|---|---|---|---|---|---|
| 1 jour | 2 jours | 7 jours | 28 jours | | | | | | | | |
| 20,1 | 32,1 | nd | 71 | 171 | 0,65 | 3,17 | 3555 | 26,6 | 292 | 62 | |

**CARACTERISTIQUES CHIMIQUES**

| | |
|---|---|
| $SO_3$ (%) | 2,2 |
| $Cl^-$ (%) | < 0,10 |
| Perte au feu 950°C | 0,9 |
| Insolubles (%) | 0,2 |
| $S^=$ (%) | < 0,10 |
| Alcalins [$Na_2O$ + 0,658 $K_2O$] (%) | 0,24 |
| Alcalins actifs [suivant recommandations LCPC 1994] (%) | nd |
| Vc coefficient de variation des alcalins actifs [suivant recommandations LCPC 1994] | nd |

**CONSTITUANTS PRINCIPAUX ET SECONDAIRES**

| Clinker LE TEIL | 97% | Calcaire | 3% | | |
|---|---|---|---|---|---|
| $CaO/SiO_2$ | 2,9 | | | | |
| MgO (%) | 0,9 | | | | |
| Al2O3 (%) | 3 | | | | |
| $C_3S$ (%) | 67,8 | | | | |
| $C_2S$ (%) | 16,6 | | | | |
| $C_3A$ (%) | 4,0 | | | Total des constituants | |
| $C_4AF$ (%) | 7,2 | | | 100% | |

**AUTRES CONSTITUANTS**

| | |
|---|---|
| Gypse (%) | 2,8 |
| Agent de mouture AMA14 E - Teneur en extrait sec (%) | 0,04 |

**LIVRAISON EN VRAC**

nd : non déterminé

## Appendix 2_Silica Fume_S95 B DM

**Notice technique**
**Edition 01.2014**
CONDENSIL® S95 B DM

# CONDENSIL® S95 B DM

Fumée de silice claire densifiée, addition pour bétons haute durabilité et hautes, très hautes et ultra hautes performances

**Conforme à la Norme NF EN 13263-1, Marquage CE**

**N° d'enregistrement REACH 01-2119486866-17-0005**

**Code CAS 69012-64-2**

**Code EINECS 273-761-1**

| CARACTERISTIQUES GENERALES | |
|---|---|
| **Présentation** | **CONDENSIL® S95 B DM** est une fumée de silice ultrafine obtenue lors de la fabrication du silicium. |
| **Domaines d'application** | La fumée de silice **CONDENSIL® S95 B DM** permet de fabriquer des :<br>■ Bétons à haute durabilité résistants en milieux agressifs :<br>■ Bétons à hautes résistances (BHP, BTHP et BUHP) |
| **Caractères généraux** | **CONDENSIL® S95 B DM** confère aux bétons les propriétés suivantes :<br>■ permet la réalisation de bétons blancs ou colorés<br>■ améliore les performances mécaniques à long terme : résistances en compression, flexion et traction<br>■ augmente le module d'élasticité<br>■ réduit le fluage<br>■ améliore la résistance à l'abrasion et à l'érosion<br>■ améliore la durabilité en milieux agressifs<br>■ diminue les risques d'expansion dus aux phénomènes d'alcali-réaction et de la réaction sulfatique interne (RSI)<br>■ diminue la perméabilité aux gaz et aux liquides<br>■ facilite le pompage de tous les bétons même peu dosés en ciment<br>■ réduit le risque de ségrégation du béton |
| **CARACTERISTIQUES TECHNIQUES** | |
| **Coloris** | Gris clair |
| **Conditionnement** | ■ Big bag 500 kg<br>■ Sac 20 kg (palette 50 sacs) |
| **Stockage** | ■ Big bag et sacs dans un local à l'abri de l'humidité. |
| **Conservation** | Dans son emballage d'origine intact, le produit se conserve 3 ans. |

## DONNEES TECHNIQUES

| | EN 13263 – 1,2 : 2009* | Valeurs observées** |
|---|---|---|
| Densité apparente | ≈ 0.35 ± 0.1 | 0.37 ± 0.05 |
| Densité réelle | 2.24 | |
| Surface spécifique BET ($m^2/g$) | Entre 15 et 35 | 25 ± 5 |
| Teneur en $SiO_2$ | ≥ 85 % | 95 % ± 3 |
| Teneur en Si élémentaire | ≤ 0.4 % | 0.3 % ± 0.1 |
| Teneur en $Na_2O$ équivalent | ≤ 1.0 % | 0.08 % ± 0.04 |
| Teneur en $SO_3$ | ≤ 2.0 % | 0.06 % ± 0.03 |
| Teneur en $Cl^-$ | ≤ 0.1 % | 0.02 % ± 0.01 |
| Indice d'activité à 28 j | ≥ 100 | |
| Perte au feu | ≤ 4.0 % | 0.6 % ± 0.02 |
| Teneur CaO | ≤ 1.0 % | 0.3 % ± 0.1 |
| | ** Valeurs contractuelles* | *** Valeurs non contractuelles* |

## CONDITIONS D'UTILISATION

| | |
|---|---|
| **Consommation / Dosage** | Le dosage peut être compris entre 5 à 10 % du poids du ciment. Le dosage le plus courant est de 8 % du poids du ciment. |
| **Mise en œuvre** | ■ **CONDENSIL® S95 B DM** doit être introduit avec le ciment.<br>■ Afin d'obtenir toutes les performances de **CONDENSIL® S95 B DM**, il est indispensable de défloculer complètement les micro-particules de silice. Pour cela, **CONDENSIL® S95 B DM** doit être systématiquement associé avec un superplastifiant, haut réducteur d'eau. |
| **Précautions d'emploi** | ■ L'emploi d'un masque est obligatoire lors de son utilisation<br>■ Fiche de données de sécurité fournie sur demande. |
| **Mentions légales** | **Produit réservé à un usage strictement professionnel. Nos produits bénéficient d'une assurance de responsabilité civile.**<br>«Les informations sur la présente notice et, en particulier, les recommandations relatives à l'utilisation finale des produits sont fournies en toute bonne foi et se fondent sur la connaissance et l'expérience que la Société CONDENSIL a acquises à ce jour de ses produits lorsqu'ils ont été convenablement stockés, manipulés et utilisés dans des conditions normales. En pratique, les différences entre matériaux et conditions spécifiques sur site sont telles que ces informations ou toute recommandation écrite ou conseil donné n'impliquent aucune garantie de qualité marchande autre que la garantie légale contre les vices cachés. Nous sommes à votre disposition pour toute précision complémentaire. Notre responsabilité ne saurait d'aucune manière être engagée dans l'hypothèse d'une utilisation non conforme à nos renseignements. Toutes les commandes sont acceptées sous réserve de nos Conditions de Vente et de Livraison en vigueur. Les utilisateurs doivent impérativement consulter la version la plus récente de la fiche technique correspondant au produit concerné, qui leur sera remise sur demande». |

## Appendix 3_Crused Quartz_C500

**C500**

**Fiche Technique Type**

| Analyse chimique type | | |
|---|---|---|
| SiO2 | sup. à | 99,1 % |
| Fe2O3 | inf. à | 487 ppm |
| Al2O3 | inf. à | 4587 ppm |
| TiO2 | inf. à | 233 ppm |
| CaO | inf. à | 297 ppm |
| K2O | inf. à | 3054 ppm |

| Caractéristiques physiques type | | |
|---|---|---|
| Densité réelle | (Pycnomètres) | 2,65 |
| Dureté | (Mohs) | 7 |
| Indice de réfraction | | 1,54 à 1,55 |
| Densité | | #0,50 |
| Surface spécifique BLAINE (cm2/g) | | 10435 |
| Absorption d'huile (ISO 787/5-1980 en g/100 g) | | #32 |
| Humidité sortie usine | (%) | maxi 0,1 |
| Perte au feu | (%) | maxi 0,2 |
| pH | | 7 à 8,5 |
| Couleur L* | | 92,62 |
| Couleur a* | | 0,54 |
| Couleur b* | | 2,55 |

**Granulométrie moyenne statistique (valeurs indicatives )**

Instrument Laser MALVERN 2000

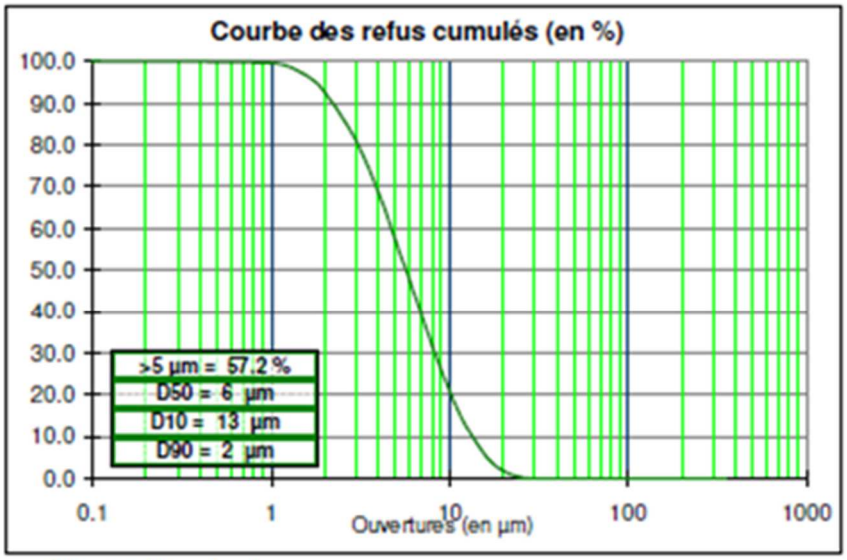


D10 = 10% de la courbe > à ..... µm
D90 = 90% de la courbe > à ..... µm

SIBELCO FRANCE

CENTRE DE PRODUCTION DE COMPIEGNE
2 Avenue Louis Barbillon BP 10421
60204 Compiègne Cedex
Tel : +33 (0)3 44 38 62 00 Fax : +33 (0)3 44 40 11 66

SIEGE SOCIAL ET DIRECTION COMMERCIALE
141 Avenue de CLICHY 75848 PARIS Cedex 17
Tel : +33 (0)1 53 76 82 00 Fax : +33 (0)1 42 25 32 23
site web : www.Sibelco.fr

# Appendix 4_Blast Furnace Slag

Fiche Technique Produit d'Ecocem,

LAITIER GRANULE DE HAUT-FOURNEAU MOULU CE

Révision : 05/01/2015

ECOCEM FRANCE SAS

## 1. DEFINITION

Ecocem, le laitier granulé de haut fourneau moulu CE produit par ECOCEM France à Fos sur Mer (13), répond à la norme européenne **NF EN 15167-1**, 2006 : Laitier granulé de haut-fourneau moulu pour utilisation dans le béton, mortier et coulis - Partie 1 : définitions, exigences et critères de conformité.
Le certificat CE de constance des performances 1164-CPR-LGM001, a été renouvelé le 10 Janvier 2014, par le CERIB, organisme notifié n°1164.
Ecocem est un laitier moulu de classe A, suivant les distinctions faites dans la norme NF EN 206-1/CN décembre 2012, classe confirmée, en date du 28 Juin 2013, par le CERIB.

## 2. FABRICATION

Ecocem est produit par le séchage et le broyage du laitier granulé de haut-fourneau.
Le laitier granulé est obtenu par trempe à l'eau du laitier à la sortie des hauts-fourneaux de Fos sur Mer, au moyen de granulateur de nouvelle génération (INBA®).
Le taux de vitrification moyen obtenu est supérieur à 90% (mesure par diffraction de rayons X).
Ecocem est livré en vrac.

## 3. COMPOSITION CHIMIQUE (centésimale moyenne)

| | | | | | |
|---|---|---|---|---|---|
| **CaO** | 43,9 | **$Fe_2O_3$** | 0,7 | **$Na_2O$** | 0,34 |
| **$SiO_2$** | 37,4 | **$TiO_2$** | 0,5 | **$K_2O$** | 0,24 |
| **$Al_2O_3$** | 10,9 | **$SO_3$** | 0,1 | **$Na_2O$ éq.** | 0,46 |
| **MgO** | 6,5 | **$S^{2-}$** | 0,8 | **$Cl^-$** | 0,01 |

Module chimique $(CaO+MgO)/SiO_2$ : > 1,25 *(≥ 1,2 : classe A selon NF EN 206-1/CN)*

## 4. CARACTERISTIQUES PHYSIQUES (valeurs indicatives représentatives)

| **FORMULATION** | | **Résistances en Compression (MPa)** | | | **Indice d'activité** | | | **Temps de prise initial** (min) |
|---|---|---|---|---|---|---|---|---|
| **Ecocem** | **Ciment référence** | 7 jrs | 28 jrs | 90 jrs | 7 jrs | 28 jrs | 90 jrs | |
| **0%** | **100%** | 45 | 56 | 64,5 | - | | | 140 |
| **50%** | **50%** | 32,5 | 58,5 | 73 | 73% | 104% | 113% | 170 |
| *Limites de la Norme produit NF EN 15167-1* | | | | | *≥ 45%* | *≥ 70%* | - | *< 2× Tps Ciment* |
| *Limites Classe A selon Norme NF EN 206-1/CN* | | | | | *≥ 65%* | *≥ 85%* | - | - |

## 5. AUTRES CARACTERISTIQUES

Surface spécifique Blaine : 4450 ± 250 $cm^2/g$
*≥ 2750 cm2/g : NF EN 15167-1*
*≥ 4200 cm2/g : classe A selon NF EN206-1/CN*

Passant à 32 µm : ≥ 95%
Diamètre médian indicatif (d50) : 12µm

Indice [CIE L*ab] avec CR410: 89 ± 2
Perte au feu (950°C): < 1,5 %
Humidité (100°C): < 0,5%
Masse volumique ($g/cm^3$) : 2,90 ± 0,03
Densité apparente : 0,8 ± 0,1

# Appendix 5_Filler

## Betocarb® HP - OG

| | | | |
|---|---|---|---|
| SITE: | ORGON, France (certifié ISO 9001) | | |
| DESCRIPTION DU PRODUIT: | Addition calcaire sélectionnée pour bétons hydrauliques et filler pour bétons hydrauliques hautes performances (EN 12620).<br>Produit particulièrement adapté aux bétons de parement et architectoniques (essai LG_007).<br>Ce produit est de catégorie A selon la norme NF P 18-508. | | |
| COMPOSITION TYPE DE LA ROCHE: | $CaCO_3$ | 98.8 | % |
| | Carbonates totaux | 99.1 | % |
| | Chlorures | 0.001 | % |
| | Sulfates | 0.001 | % |
| | Soufre total | 0.005 | % |
| | Matières organiques | 0.01 | % |
| | Essai au bleu de méthylène | 0.3 | g/kg |
| | Alcalins équivalents | 0.005 | % |
| | Silice totale | 0.1 | % |
| | Réactivité aux alcalins | NR | |
| CARACTERISTIQUES TYPES DU PRODUIT: | Granulométrie: | | |
| | · Particules < 2 mm | 100 | % |
| | · Particules < 0.125 mm | 100 | % |
| | · Particules < 0.063 mm | 97 | % |
| | · Surface spécifique Blaine | 462 | $m^2/kg$ |
| | Blancheur CIE L* | 95 | |
| | Indice d'activité à 28 jours | 0.79 | |
| | Taux d'humidité départ usine | 0.2 | % |
| CARACTERISTIQUES GENERALES DU PRODUIT: | Densité | 2.7 | g/ml |
| | Densité apparente tassée | 1.5 | g/ml |

APPLICATIONS PRINCIPALES:

Béton auto-plaçant
Béton prêt à l'emploi
Eléments préfabriqués architectoniques
Applications spéciales
- Béton projeté

REPARTITION GRANULOMETRIQUE (Malvern Mastersizer 2000):

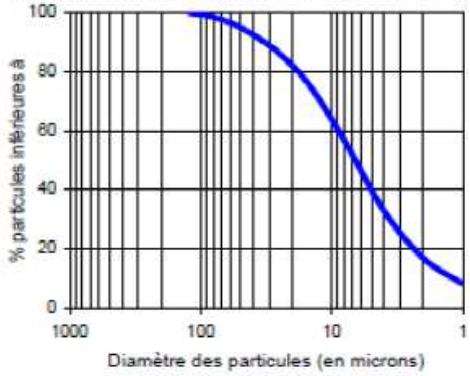


CONDITIONNEMENT STANDARD:

- VRAC
- SAC (papier) de 25 kg sur palette



édition : 29.03.2012
Product information :
608.03.01_FR_CORP.FROG
I03200_14_F
version : 9

## Appendix 6_Quartz Sand_CV32

# CV32

Fiche Technique Type

### Composition chimique type

| | | |
|---|---|---|
| $SiO_2$ ..... sup. à | 99.00 | % |
| $Fe_2O_3$ .... moy. à | 0.026 | % |
| $Al_2O_3$ .... moy. à | 0.494 | % |
| $TiO_2$ ..... moy. à | 0.017 | % |
| CaO ..... moy. à | 0.013 | % |
| $K_2O$ ..... moy. à | 0.347 | % |

### Caractéristiques physiques types

| | |
|---|---|
| densité réelle (Pycnomètre) ..... | 2.65 |
| dureté (Mohs) ..... | 7 |
| pH ..... | # 7 |
| densité apparente sable sec ("Prolabo") ..... | 1.5 |
| surface spécifique ("G F") ..... | # 124 cm²/g |
| coefficient d'angulosité ("G F") ..... | 1.1 |
| perte au feu (à 1000°C) ..... | Maxi 0.20% |
| résistance pyroscopique (SFC ISO R528) .. | 1750 °C |

### GRANULOMETRIE MOYENNE STATISTIQUE

(% en masse - Valeurs indicatives)

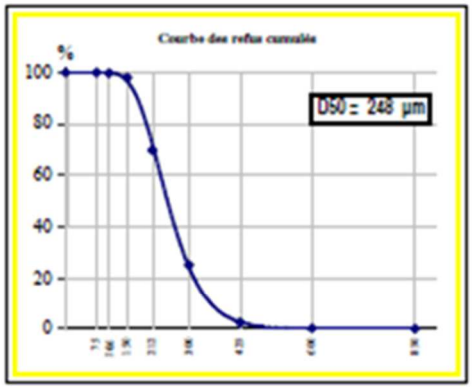


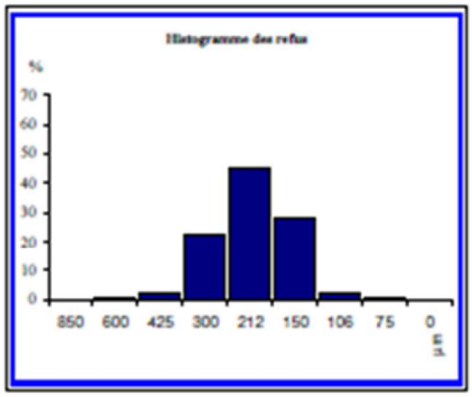


**TAMISAGE ASTM E.11/70**

| ouverture des mailles µm | refus cumulés % |
|---|---|
| > 850 µm | 0.0 |
| > 600 µm | 0.1 |
| > 425 µm | 2.4 |
| > 300 µm | 25.0 |
| > 212 µm | 69.8 |
| > 150 µm | 98.0 |
| > 106 µm | 99.9 |
| > 75 µm | 100.0 |
| > 0 µm | 100.0 |
| AFA = | 54.0 |

**CORRESPONDANCE Série R20 ISO 565**

| ouverture des mailles µm | refus cumulés % |
|---|---|
| > 2000 µm | 0.0 |
| > 1400 µm | 0.0 |
| > 1000 µm | 0.0 |
| > 630 µm | 0.0 |
| > 500 µm | 0.5 |
| > 315 µm | 19.2 |
| > 250 µm | 48.9 |
| > 180 µm | 87.8 |
| > 125 µm | 99.4 |
| > 63 µm | 100.0 |
| passe | 0.0 |

| Classe µm | refus par tamis % |
|---|---|
| > 850 µm | 0.0 |
| 850-600 µm | 0.1 |
| 600-425 µm | 2.3 |
| 425-300 µm | 22.5 |
| 300-212 µm | 44.8 |
| 212-150 µm | 28.2 |
| 150-106 µm | 1.9 |
| 106-75 µm | 0.1 |
| Passant | 0.0 |

| Classe µm | refus par tamis % |
|---|---|
| > 2000 µm | 0.0 |
| 2000-1400µm | 0.0 |
| 1400-1000µm | 0.0 |
| 1000 - 630µm | 0.0 |
| 630 - 500 µm | 0.5 |
| 500-315 µm | 18.7 |
| 315 - 250 µm | 29.6 |
| 250 - 180 µm | 39.0 |
| 180 - 125 µm | 11.5 |
| 125 - 63 µm | 0.6 |
| < 63 µm | 0.0 |

particules < 20 µm : maxi 0.06 % sur sable lavé

SIBELCO FRANCE

SITE DE PRODUCTION DE CREPY
La Pierre aux Corbeaux - BP 70314

SIEGE SOCIAL ET DIRECTION COMMERCIALE
141 Avenue de CLICHY 75848 PARIS Cedex 17

## Appendix 7_KOH

| GACHES CHIMIE | SPECIFICATIONS DE VENTE ST 050201 | Réf : HYDPOPUR |
|---|---|---|
| | Edition du n°6 du 05/02/2014 | Page : 1/1 |

# POTASSIUM HYDROXIDE 90% ECAILLES

Fournisseurs retenus : 405020 - 404009

| | |
|---|---|
| ➢ Hydroxide de potassium (% p/p) | 89,5 % mini |
| ➢ Soude (NaOH) (% p/p) | 1 % maxi |
| ➢ Carbonate de potassium ($K_2CO_3$) (% p/p) | 0,5 % maxi |
| ➢ Chlorures (Cl) | 80 ppm maxi |
| ➢ Fer (Fe) | 5 ppm maxi |
| ➢ Nickel (Ni) | 5 ppm maxi |

| | |
|---|---|
| Vérifié par : B. LAFFORGUE<br>Date : 4/02/2014<br>Visa : | Approuvé par : S. MOLINS<br>Date : 04/02/2014<br>Visa : |

# Appendix 8_Superplasticizer_SIKA Viscocrete Krono 20 HE

Construction

| | |
|---|---|
| **Stockage** | A l' abri du gel.<br>En cas de gel accidentel, le produit retrouve ses qualités d'origine une fois dégelé lentement et réhomogénéisé. |
| **Conservation** | 12 mois dans son emballage intact. |
| **Données techniques** | |
| **densité** | 1,085 ± 0,020 |
| **pH** | 4,5 ± 1,0 |
| **Teneur en $Cl^-$** | ≤ 0,1 % |
| **Teneur en $Na_2O_{éq}$** | ≤ 1 % |
| **Extrait sec** | 41,0 ± 1,5% (NF EN 480-8)<br>41,0 ± 2,0% (méthode halogène selon NF 085) |
| **Conditions d'application** | |
| **Dosage** | **Plage de dosage** : 0,1 à 5,0% du poids du liant ou du ciment selon la fluidité et les performances recherchées. |
| **Mise en œuvre** | |
| **Préparation du mélange** | SIKA VISCOCRETE® KRONO 20 HE est ajouté, soit, en même temps que l'eau de gâchage, soit en différé dans le béton préalablement mouillé avec une fraction de l'eau de gâchage. |
| **Précautions d'emploi** | En cas de contact avec la peau, laver abondamment à l'eau.<br>Consulter la fiche de données de sécurité sur Internet www.sika.fr |
| **Mentions légales** | Produit réservé à un usage strictement professionnel<br>Nos produits bénéficient d'une assurance de responsabilité civile.<br>«Les informations sur la présente notice, et en particulier les recommandations relatives à l'application et à l'utilisation finale des produits SIKA, sont fournies en toute bonne foi et se fondent sur la connaissance et l'expérience que la Société SIKA a acquises à ce jour de ses produits lorsqu'ils ont été convenablement stockés, manipulés et appliqués dans des conditions normales. En pratique, les différences entre matériaux, substrats et conditions spécifiques sur site sont telles que ces informations ou toute recommandation écrite ou conseil donné n'impliquent aucune garantie de qualité marchande autre que la garantie légale contre les vices cachés. Nos agences sont à votre disposition pour toute précision complémentaire. Notre responsabilité ne saurait d'aucune manière être engagée dans l'hypothèse d'une application non conforme à nos renseignements. Les droits de propriété détenus par des tiers doivent impérativement être respectés. Toutes les commandes sont acceptées sous réserve de nos Conditions de Vente et de Livraison en vigueur. Les utilisateurs doivent impérativement consulter la version la plus récente de la notice correspondant au produit concerné, qui leur sera remise sur demande.» |

UNIVERSITE BRETAGNE LOIRE

UNIVERSITÉ DE NANTES

# Thèse de Doctorat

Omar Mohammed ABDULKAREEM

# Microstructure et Propriétés de Durabilité des Bétons Ultra-Haute Performance à Faible Impact Environnemental

# Microstructure and Durability Properties of Environmentally Friendly Ultra High Performance Concrete (UHPC)


## Résumé

Cette thèse traite de l'effet de l'incorporation des laitiers des hauts fourneaux (LHF) sur la microstructure et la durabilité des bétons à Ultra Haute Performance (BUHP) avec et sans activation. Trois taux de substitution du ciment par des LHF sont explorés (30%, 50% et 80%). Les résultats montrent qu'une teneur de 30% de laitier améliore légèrement la résistance à la compression, alors qu'avec 50% et 80% de LHF, la résistance à la compression chute significativement. A 3 jours, lorsque la teneur en LHF augmente, la porosité du béton augmente. A 90 jours, la réaction des LHF induit une diminution de la porosité capillaire et le réseau poreux devient plus fin. Ainsi, la perméabilité au gaz et la diffusion des ions chlore diminuent significativement. Les résultats montrent aussi que tous les bétons testés ont une profondeur de carbonatation similaire, après une année d'exposition au $CO_2$. En effet, la diminution de la porosité, due à l'ajout des LHF est équilibrée par la diminution du pH, qui favorise la diffusion de $CO_2$. Pour ce qui concerne l'activation, les résultats montrent que l'activation chimique/thermique des BUHP à fort dosage en LHF améliore les propriétés microstructurales, mécaniques et de durabilité du béton. D'un point de vue environnemental et en considérant l'unité fonctionnelle « 1 $m^3$ d'un BUHP à 150 MPa », la substitution partielle du ciment par des LHF diminue les impacts environnementaux du BUHP et c'est malgré l'activation thermique.



## Mots clés

**BUHP, LHF, Activation chimique, Activation thermique, Microstructure, Propriétés mécaniques, Propriétés de durabilité, Analyse de cycle de vie.**



## Abstract

This thesis deals with microstructural and durability performances of environmentally friendly Ultra-High Performance Concrete (UHPC) by integrating high volumes of Blast Furnace Slag (BFS) with and without activation. Three substitution rates of cement by slag are used (30%, 50% and 80%). Results show that a slag content of 30% improves slightly the compressive strength of UHPC whereas the strength of UHPCs containing 50% and 80% of slag are significantly reduced particularly at early age. At 3 days when the slag content increases, the porosity of UHPC mixtures with high slag contents increases. In contrast, at 90 days the volume of capillary pores decreases greatly and the global pores network becomes finer when cement is substituted by BFS. This results in decreasing gas permeability coefficients around (30-61%) and chloride diffusion (up to 4 times). Results show also that all tested UHPCs have quite the same $CO_2$ depths after exposure of 1 year. Indeed, the decrease of porosity due to slag incorporation, is balanced by the decrease of pH which promotes $CO_2$ diffusion. The chemical/thermal activation improves the packing density and the mechanical and durability properties of UHPC. From an environmental standpoint and considering the functional unit "1 $m^3$ of UHPC with 150 MPa", the partial substitution of cement with BFS decreases the environmental impacts of UHPC, even for thermally activated blended UHPCs.



## Key words

**UHPC, BFS, Chemical activation, Thermal activation, Microstructure, Mechanical properties, Durability properties, Life cycle assessment.**


L'Université Bretagne Loire